PARAMETER ESTIMATION BASED MODELS OF WATER SOURCE HEAT PUMPS

By

HUI JIN

Bachelor of Science
Shanghai Jiaotong University
Shanghai, China
1992

Master of Science
Shanghai Jiaotong University
Shanghai, China
1995

Submitted to the Faculty of the
Graduate College of the
Oklahoma State University
in partial fulfillment for
the requirements for
the degree of
DOCTOR OF PHILOSOPHY
December 2002

PARAMETER ESTIMATION BASED MODELS
OF WATER SOURCE HEAT PUMPS

Thesis Approved:

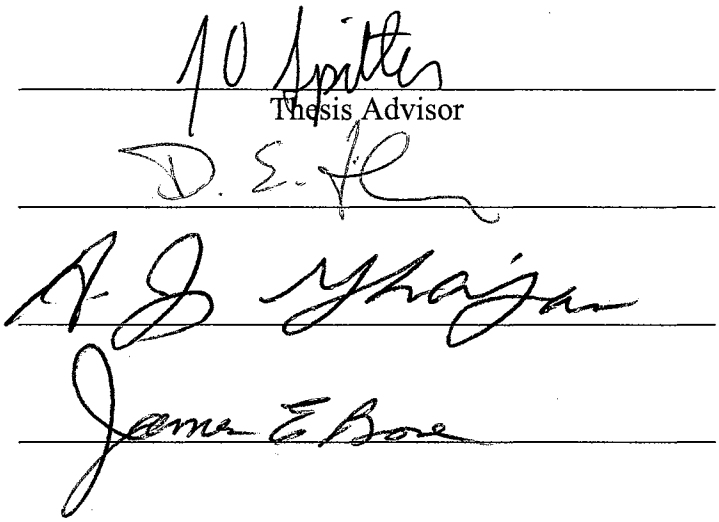

Thesis Advisor

Dean of the Graduate College

ACKNOWLEDGEMENTS

I wish to express my sincere appreciation to all of the people who helped me to accomplish this dissertation.

First and foremost, I wish to thank my advisor, Dr. Jeffrey D. Spitler. His expertise and respected reputation in the HVAC field allowed for the funding of many projects and the opportunity for me to adopt knowledge and experience in modeling of building thermal systems. I am grateful for your constructive guidance and leadership.

I would like to extend my gratitude to the members of my doctoral committee, Dr. D. E. Fisher, Dr. A. J. Ghajar and Dr. Jim Bose for their committed service and support, ideas and suggestions that helped improve my work significantly.

Thanks also to Dr. Marvin Smith who provided input and experimental data regarding the water-to-water heat pump model validation. Fred Schroeder, Development Engineer, with the Division of Engineering Technology also provided valuable information and help on the portions of the water-to-water heat pump experimental data.

I wish to deliver special credit to Dr. Fisher and David Eldridge for their generous assistance on the experimental validation of the water-to-air heat pump model.

It's hard to find any words to express the thanks to my parents, Zhixue Jin and Lingdi Jiang and my wife, Pony for their love and understanding along the way.

Last, but not least, I would like to thank my colleagues in B-10, ATRC, MAE Research Lab and Electronics Lab, both here and gone, namely, Dr. Cenk Yavuzturk,

Andrew Chiasson, Mahadevan Ramamoorthy, Xiaobing Liu, Dongyi Xiao and Chanvit, for their ideas and precious help in a direct or indirect way.

Support of the U.S. Department of Energy under the grant numbers DE-FG48-97R810627 and DE-FG48-94R689416, and of the Federal Highway Administration under grant number DTFH61-99-X-00067 is gratefully acknowledged.

TABLE OF CONTENTS

Chapter *Page*

LIST OF TABLES

Table *Page*

Table *Page*

LIST OF FIGURES

Figure *Page*

Figure *Page*

Figure *Page*

Figure *Page*

Figure *Page*

NOMENCLATURE

Symbols

A_w	=	wetted airside surface area on which moisture is condensing, m^2 or ft^2
C	=	clearance factor
C_s	=	specific heat of saturated air, J/(kg-K) or Btu/(lbm-F)
C_p	=	specific heat, J/(kg-K) or Btu/(lbm-F)
f_g	=	sensible heat transfer coefficient through air film, W/(m^2-K) or Btu/(hr-°F-ft^2)
h	=	enthalpy of air vapor mixture per pound of dry air evaluated at the main stream temperature, kJ/kg or Btu/lbm
$h_{c,o}A_o$	=	outside surface heat transfer coefficient, kW/K or Btu/(hr-F)
h	=	enthalpy, J/kg or Btu/lbm
h_s	=	enthalpy of air vapor mixture per pound of dry air evaluated at the surface temperature, kJ/kg or Btu/lbm
H_T	=	total heat loss by total weight of air flowing over wetted surface, kW or Btu/hr
$\dot{m}$	=	mass flow rate, kg/s or lbm/hr
NTU	=	number of transfer units
P	=	pressure, Pa or psia
PD	=	piston displacement, m^3/s or CFM
$\dot{Q}$	=	heat transfer rate, W or Btu/hr
s	=	humid specific heat of air vapor mixture, kJ/(kg dry air - °C) or Btu/(lbm dry air - °F)
S	=	thermostat signal
T	=	temperature, °C , °F or °K
UA	=	heat transfer coefficient, W/K or Btu/(hr-F)
$(UA)_i$	=	inside surface heat transfer coefficient, kW/K or Btu/(hr-F)
V	=	specific volume, m^3/kg or ft^3/lbm
w	=	humidity ratio, kg/kg dry air

$\dot{W}$	=	compressor power input, W or Btu/hr
γ	=	isentropic exponent
η	=	loss factor used to define the electro-mechanical loss that is supposed to be proportional to the theoretical power
ε	=	thermal effectiveness of heat exchanger
ΔT_{sh}	=	superheat, °C or °F
ΔP	=	pressure drop across suction or discharge valve, Pa or psia

Subscripts

a	=	air
A	=	A state point in refrigeration cycle
B	=	B state point in refrigeration cycle
c	=	condensing state
com	=	compressor
cat	=	catalog data
dis	=	discharge state
dry	=	dry condition
e	=	evaporating state
hi	=	high pressure cut-off
i	=	inlet condition, *i*th calculated result or inside surface
in	=	compressor inlet state
L	=	load side
lo	=	low pressure cut-off
loss	=	constant part of the electro-mechanical power losses
o	=	outlet condition or outside surface

out	=	compressor outlet state
r	=	refrigerant
s	=	saturated state or outside surface
S	=	source side
sen	=	sensible
t	=	Theoretical power
suc	=	suction state
w	=	water
wet	=	wet condition

1. Introduction

Reciprocating vapor compression heat pumps and chillers have been the target of a number of simulation models. Hamilton and Miller (1990) presented a classification scheme for air conditioning equipment with two extremes. At one end of the spectrum are equation-fit models, called "functional fit" models by Hamilton and Miller, which treat the system as a black box and fit the system performance to one or a few large equations. At the other end are deterministic models, called "first principle" models by Hamilton and Miller, which are detailed models based on applying thermodynamic laws and fundamental heat and mass transfer relations to individual components.

Many of the models found in the literature might actually fall between the two extremes, although the detailed deterministic models often apply equation-fitting for some of the components. For example, in the reciprocating chiller model proposed by Bourdouxhe, et al. (1994), the chiller was modeled as an assembly of several simplified components. Each component (e.g., compressor, evaporator, condenser, expansion device) is modeled with a detailed deterministic approach. The parameters describing the detailed physical geometry and operation of each component are then adjusted (i.e., in an equation-fit procedure) to reproduce the behavior of the actual unit as accurately as possible. The model of Bourdouxhe, et al. requires more details for each component than what is usually available from the manufacturers' catalogs. This type of model is most suitable for users that have access to internally measured data (e.g., in Bourdouhxe's

model, condensing and evaporating temperatures and subcooling and superheating temperature differences) from the chiller or heat pump.

The alternative approach, equation-fitting, alleviates the need for internally measured data and usually maintains better fidelity to the catalog data. It also usually requires less computational time. These models are most suitable for users that only have access to catalog data. These models would not be useful for someone attempting to design a heat pump or chiller by modifying or replacing internal components. Especially troublesome for some applications, extrapolation of the model may lead to unrealistic results.

It is desirable to have a model that only requires catalog data, but allows extrapolation beyond the catalog data. In the authors' experience, this model has been extremely useful for modeling of ground source heat pumps in novel applications where the fluid temperatures occasionally go beyond the catalog data. It is also useful in simulations that are part of a ground loop sizing procedure. In this application, it often happens that the temperatures are well beyond the catalog data. Even though the ultimate outcome is that the ground loop heat exchanger size will be adjusted to bring the temperatures within reasonable limits, it is helpful to have a model that does not catastrophically fail when the temperatures are too high or too low.

The model presented in this report uses deterministic models of each heat pump component. Each of the fundamental equations describing the system components may

have one or more parameters, which are estimated simultaneously using catalog data only; no other experimental data are required. The parameter estimation is done with a multi-variable optimization method. Once the parameters have been estimated, the heat pump model may be used as part of a multi-component system simulation.

This modeling approach has the advantage of not requiring experimental data beyond what are published in the manufacturer's catalog. Yet, its predictions are of similar or better accuracy than previously published deterministic models that required additional experimental data. Unlike the equation-fit models, the model domain may be extended beyond the catalog data without catastrophic failure in the prediction.

2. Literature Review

2.1. Heat Pump and Chiller Models

Simulation models of vapor-compression refrigeration and air-conditioning systems such as heat pumps and chillers have been the topic of numerous papers. The models can generally be classified in terms of the degree of complexity and empiricism. A review of the literature reveals a few limitations on existing models. For the more deterministic models, there is a gap between what data are provided by manufacturers' catalogs and what data the simulation models require. For equation-fit models, the valid application is limited to the manufacturer-supplied data range and conditions.

2.1.1. Equation-fit Models

2.1.1.1. Allen and Hamilton Model

Allen and Hamilton (1983) proposed a steady state reciprocating water chiller model which can be used for full and part load performance evaluation. This model is a typical equation-fit model. Other modeling algorithms employing the equation-fit approach are similar to this method. This water chiller model was a model of the complete system and did not consist of individual component models or involve internal pressures and temperatures. Although basic equations governing the steady state water chiller operation can be obtained by applying basic physical laws to the systems, the author eliminated the internal variables by utilizing the functional relationships among variables and examing typical water chiller performance data. For example, evaporator

cooling load was expressed by a polynomial in terms of evaporator water and condenser water temperatures in which several constant coefficients were actually fitted by a regression approach:

$$QE = B_1 \cdot TE_2 + B_2 \cdot TC_2 + B_3 \cdot TE_2 \cdot TC_2 + B_4 \cdot TE_2^{\,2} + B_5 \cdot TC_2^{\,2} + B_6 \quad (2.1)$$

where QE = evaporator cooling load, kW or Btu/hr

TE_2 = evaporator leaving water temperature, °C or °F

TC_2 = condenser leaving water temperature. °C or °F

Similarly, the compressor energy balance can also be expressed by the following polynomial equation,

$$P = B_7 \cdot TE_2 + B_8 \cdot TC_2 + B_9 \cdot TE_2 \cdot TC_2 + B_{10} \cdot TE_2^{\,2} + B_{11} \cdot TC_2^{\,2} + B_{12} \quad (2.2)$$

where P = compressor power, kW or Btu/hr

TE_2 = evaporator leaving water temperature, °C or °F

TC_2 = condenser leaving water temperature, °C or °F

The evaporator water energy balance, condenser water energy balance and the simple thermal balance for the whole system are expressed respectively as:

$$QE = ME \cdot C_p \cdot (TE_1 - TE_2) \quad (2.3)$$

$$QC = MC \cdot C_p \cdot (TC_2 - TC_1) \quad (2.4)$$

$$QC = QE + P \tag{2.5}$$

where ME = evaporator water mass flow rate, kg/s or lbm/hr

C_p = water specific heat, kJ/(kg-K) or Btu/(lbm-°F)

QC = condenser heat rejection rate, kW or Btu/hr

MC = condenser water mass flow rate, kg/s or lbm/hr

TC_1 = condenser entering water temperature, °C or °F

TE_1 = evaporator entering water temperature, °C or °F

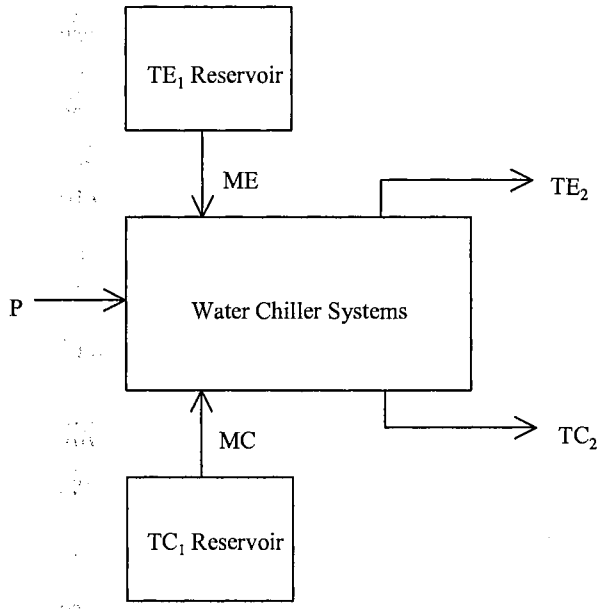

Figure 2.1. Water chiller conceptual experiment

The constant coefficients in above equations B_1-B_{12} are to be determined. The physical significance of the model, consisting of five equations and nine variables, can be envisioned in a conceptual experiment which is described in the paper. Given a water chiller, Figure 2.1, a reservoir of chilled water at TE_1 with a mass flow rate of ME, and a

reservoir of cooling water at TC_1 with a mass flow rate of MC, then the five system equations can be solved for energy rates QE, P and QC and leaving temperatures TE_2 and TC_2.

2.1.1.2. Hamilton and Miller Model

The Allen and Hamilton (1983) model utilizes overall system data, e.g. entering and leaving water temperatures and flow rates. In contrast, the model of Hamilton and Miller (1990) requires more detailed data, such as internal refrigerant pressures and temperatures. Hamilton and Miller (1990) developed this general steady state model by equation-fitting manufacturers' catalog data of the individual components, along with thermodynamic relationships. The model is capable of simulating the response of an air-conditioning system configuration for a variety of ambient and inside conditions. According to the author, any air conditioning system can be divided into components such as heat exchangers, fans, etc. It permits modeling a particular air conditioning system with the general usefulness of the simulation program. Several models of each component can be made and combined into a broad range of air conditioning systems using the concepts of mass and energy flow continuity and pressure-temperature compatibility at each component connection. The conceptual model of each component consists of an energy balance and a mass balance at steady state conditions yielding two rate equations for each component. Figure 2.2 illustrates the conceptual model for a general component operating at steady state conditions.

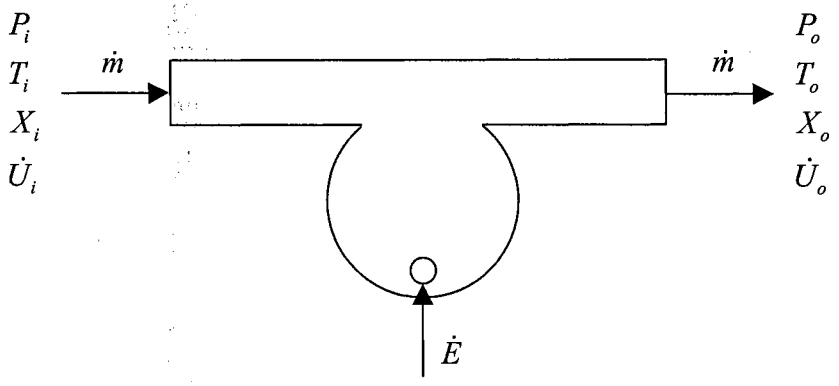

$$\dot{E} = f_1(P_i, T_i, X_i, P_o, T_o, X_o)$$
$$\dot{m} = f_2(P_i, T_i, X_i, P_o, T_o, X_o)$$

where, $\dot{E}$ = energy rate, kW or Btu/hr

$\dot{m}$ = mass flow rare, kg/s or lbm/hr

P = pressure, kPa or psig

T = temperature, °C or °F

X = refrigerant quality

$\dot{U}$ = energy flow rate, kW or Btu/hr

Figure 2.2. Inlet and outlet variables of a single fluid general component at steady-state conditions

The authors defined the model as a simulation tool for 'air conditioning system'. Since air is the secondary working fluid in both evaporator and condenser, the equipment might be an air-to-air unit or split type air conditioner. The evaporator and condenser models include the air mass flow rates and the evaporator model accounts for the mass flow rate of the water condensing on the coil. Obviously, the mass flow rate of the water on condenser coils is zero.

The functional fit equations describing the individual component characteristics form a set of simultaneous algebraic rate equations describing the system performance. This model is actually a equation-fit model, but it established a model for each component individually by internal operating conditions, instead of treating the whole system as a black box. According to the author, in the general simulation developed in this work, each component model is primarily based on data available in manufacturers' catalogs. Similar to the deterministic model, those detailed component performance data are usually not readily available.

2.1.1.3. Stoecker and Jones Model

Stoecker and Jones (1982) present a vapor compression system simulation analysis. The purpose of the analysis is to predict the performance of the entire system when the characteristics of the individual components are known.

- *Reciprocating compressor*

The mathematical equations that represent the performance data is:

$$q_e = c_1 + c_2 t_e + c_3 t_e^2 + c_4 t_c + c_5 t_c^2 + c_6 t_e t_c + c_7 t_e^2 t_c + c_8 t_e t_c^2 + c_9 t_e^2 t_c^2 \qquad (2.6)$$

and

$$P = d_1 + d_2 t_e + d_3 t_e^2 + d_4 t_c + d_5 t_c^2 + d_6 t_e t_c + d_7 t_e^2 t_c + d_8 t_e t_c^2 + d_9 t_e^2 t_c^2 \qquad (2.7)$$

where q_e = refrigeration capacity, kW or Btu/hr

P = power required by compressor, kW or Btu/hr

t_e = evaporating temperature, °C or °F

t_c = condensing temperature, °C or °F

The constants applicable to Equations (2.6) and (2.7) for the compressor are determined by equation-fit procedures (i.e. the method of least squares). In addition to the refrigerating capacity and the power requirement of the compressor, another quantity of interest is the rate of heat rejection required at the condenser. The compressor catalogs show this quantity and usually it is simply the sum of the refrigerating and condensing temperatures.

$$q_c = q_e + P \tag{2.8}$$

where q_c is the rate of heat rejection at the condenser in kilowatts or Btu/hr.

- *Condenser performance*

The precise representation of the heat-transfer performance of a condenser can be quite complex, because the refrigerant vapor enters the condenser superheated and following the onset of condensation in the tube the fraction of liquid and vapor changes consequently through the condenser. A satisfactory representation of air-cooled condenser performance for most engineering calculations is available, however, through an assumption of a constant heat-exchanger effectiveness for the condenser, namely

$$q_c = F(t_c - t_{amb}) \tag{2.9}$$

where F = capacity per unit temperature difference, kW/K or Btu/(hr-°F)

t_{amb} = ambient temperature, °C or °F

- *Evaporator performance*

For subsequent mathematical simulation, an equation is needed to express the evaporator capacity. An adequate equation could originate from:

$$q_e = G(t_{wi} - t_e) \tag{2.10}$$

where t_{wi} = entering water temperature, °C or °F

G = proportionally factor, kW/K or Btu/(hr-°F)

The G value may be constant, or if the G value is not constant, as an approximation G can be proposed as a linear function of the temperature difference. For a particular case:

$$G = 6.0[1 + 0.046(t_{wi} - t_e)] \tag{2.11}$$

Thus,

$$q_e = 6.0[1 + 0.046(t_{wi} - t_e)](t_{wi} - t_e) \tag{2.12}$$

- *Simulation of complete system*

In the mathematical simulation, the three components can be simulated simultaneously. The sequence of the calculation is shown by the information-flow diagram in Figure 2.3.

Similar to the model of Hamilton and Miller (1990), this model also requires more detailed data, such as internal refrigerant pressures and temperatures.

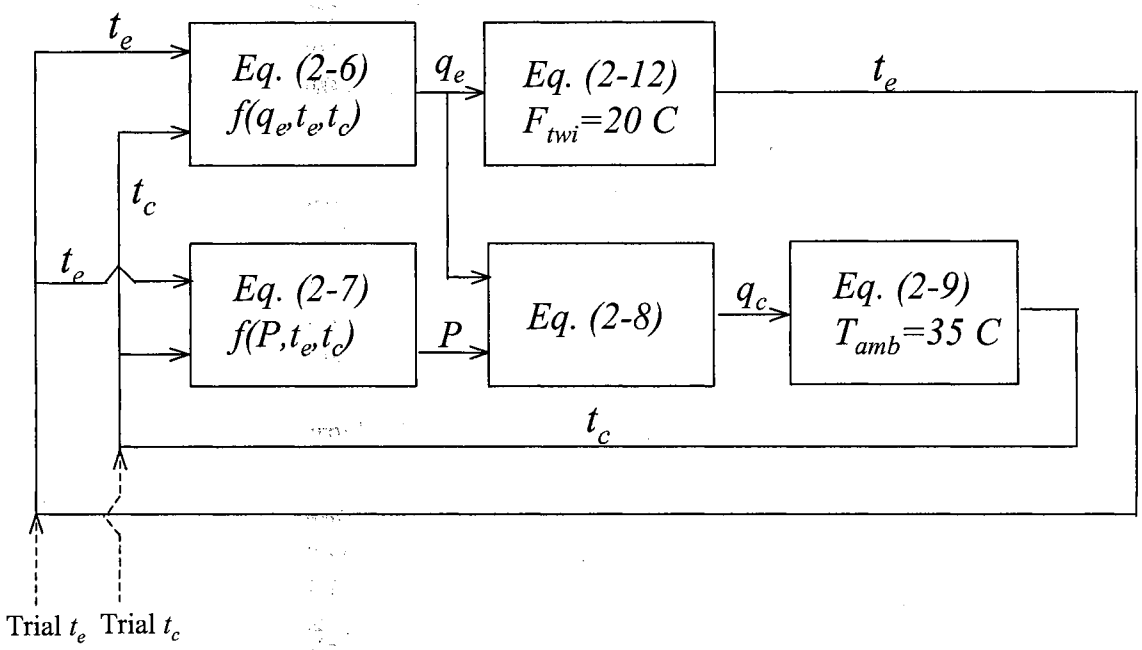

Figure 2.3. Information-flow diagram for simulation the complete vapor-compression system

2.1.2. Models Falling Between the Two Extremes

2.1.2.1. Stefanuk et al. Model

The superheat–controlled water-to-water heat pump model developed by Stefanuk, et al. (1992) may be the most detailed model presented to date. The authors claim "The model is derived entirely from the basic conservative laws of mass, energy, momentum and equations of state as well as fundamental correlations of heat transfer." Each component is modeled to a very detailed level. For example, to simulate the real heat

transfer process in the condenser, the condenser itself is analyzed as three heat exchangers connected in series corresponding to the three phases of the refrigerant.

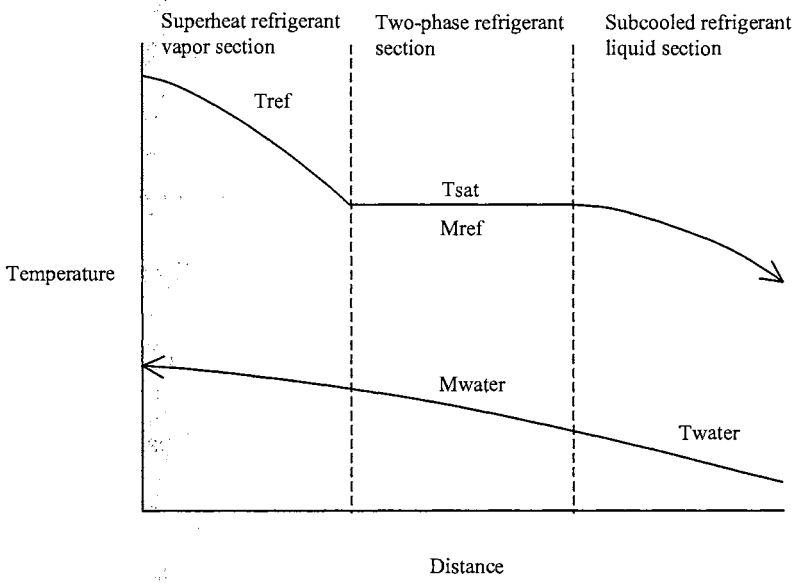

Figure 2.4. Temperature profile of the counter-flow concentric tube condenser

Values of the parameters that describe the behavior of the individual components are assumed to be available. For example, the parameters of the compressor are selected by "fitting the model to manufacturer-supplied performance curves that related mass flow rate and input electrical power to evaporation temperature and the compressor discharge pressure." However, they are not normally available in the heat pump manufacturers' catalogs. Comparisons between the experimental measurements and model predictions for the evaporating and condensing pressures, the heat transfer rates in the evaporator and the condenser, and the *COP* of the heat pump are given. Except a few points with errors beyond ±10%, most of the results are generally acceptable. The predictions of the heat transfer rates in both heat exchangers are consistently too high. The authors explain that

the cause for this phenomenon is the overestimated predictions of heat transfer coefficients since heat transfer coefficients used in the model are only known to within ±20%.

2.1.2.2. Domanski and Didion Model

Domanski and Didion (1984) developed a steady state model of an air-to-air heat pump having air to air heat exchangers, a capillary tube, and a reciprocating compressor. The basic assumption for the compressor simulation is that the highly dynamic compression process results in steady vapor flow condition through the compressor. Four internal locations are defined and refrigerant is considered to have uniform thermodynamic properties throughout the space assigned at the particular location. Heat transfer between these locations is governed by forced convection and is evaluated by expression based on the equation:

$$Nu \propto \mathrm{Re}^{0.8}\ \mathrm{Pr}^{0.333} \tag{2.13}$$

The refrigerant pressure drop within the compressor due to dynamic or friction effects is considered and evaluated based on the following expression respectively,

$$\Delta P \propto \frac{m^2}{\rho} \tag{2.14}$$

$$\Delta P \propto \mu^{0.2} \frac{m^{0.8}}{\rho} \tag{2.15}$$

where P = pressure, kPa or psia

m = refrigerant mass flow rate, kg/s or lbm/hr

ρ = density, kg/m^3, or lbm/ft^3

μ = dynamic viscosity, N-s/m^2 or centipoise

The process in the compressor is assumed to be polytropic for both compression and re-expansion, with the same polytropic index. The refrigerant enthalpy increment during polytropic compression is evaluated by the equation derived from the expression for isentropic and polytropic work of compression at the same compression pressure ratio,

$$\Delta i = \Delta i_s \frac{1}{\eta_p} \frac{R^{n-1/n} - 1}{R^{\gamma-1/\gamma} - 1} \tag{2.16}$$

where i = enthalpy, kJ/kg or Btu/lbm

$\eta_p = \dfrac{\dfrac{\gamma - 1}{\gamma}}{\dfrac{n-1}{n}}$ polytropic efficiency

R = compression pressure ratio

n = polytropic index

γ = isentropic index

subscript s = isentropic

Compressor energy balance is found iteratively by solving the equation,

$$E + m(i_3 - i_4) - Q_{can} = 0 \tag{2.17}$$

where E = electrical energy input rate to the compressor, kW or Btu/hr

m = refrigerant mass flow rate, kg/s or lbm/hr

i_3 = refrigerant enthalpy at compressor suction state, kJ/kg or Btu/lbm

i_4 = refrigerant enthalpy at compressor exhausting state, kJ/kg or Btu/lbm

Q_{can} = heat rejection rate from a compressor to ambient air, kW or Btu/hr

This model requires a variety of design parameters of the compressor and retains in some degree the complexity of the physical processes involved in describing the performance of a compressor, such as motor and mechanical efficiencies. The motor and mechanical efficiencies are related to the compressor motor and its interaction with the compressor. The polytropic and volumetric efficiencies are related to the processes occurring in the compressor cylinder. However, all of these parameters are based on the compressor manufacturer's one bench test.

Condenser and evaporator models are set up by a tube-by-tube simulation method which is based on an imaginary isolation of each finned tube from the coil assembly. The air to refrigerant heat transfer and refrigerant enthalpy change calculation are made on each tube independently. Heat transfer to/from each individual tube is calculated with the aid of the heat exchanger cross flow theory. Derived equations allow for consideration of two encountered cases: heat exchange between air and single-phase refrigeration

(temperature of both fluids change) and heat exchange between air and two-phase refrigerant (temperature of refrigerant is constant). For a tube in which change from one flow mode into another occurs, length of the tube with two-phase and single-phase is evaluated and heat transfer and pressure drop are evaluated accordingly. Overall heat transfer coefficient is calculated by the following equation,

$$U = \left[\frac{A_o}{h_i A_{p,i}} + \frac{A_o x_p}{A_{p,m} k_p} + \frac{1}{\frac{k}{\delta}} + \frac{1}{h_o \left(1 - \frac{A_f}{A_o}(1-\phi) \right)} \right]^{-1} \tag{2.18}$$

where $h_o = h_c \cdot \left[1 + \frac{i_{fg,w}(w_a - w_w)}{C_{p,a}(T_a - T_w)} \right]$

U = overall heat transfer coefficient, kW/(m^2-K) or Btu/(hr-ft^2-°F)

A_o = pipe total outside surface area, m^2 or ft^2

h_i = forced convection inside tube heat transfer coefficient,

kW/(m^2-K) or Btu/(hr-ft^2-°F)

$A_{p,i}$ = pipe inside surface area, m^2 or ft^2

x_p = pipe wall thickness, m or ft

$A_{p,m}$ = pipe mean surface area, m^2 or ft^2

k_p = thermal conductivity of pipe material, kW/(m-K) or Btu/(hr-ft-°F)

k = thermal conductivity of frost or water, kW/(m-K) or Btu/(hr-ft-°F)

δ = condensate (frost) layer thickness, m or ft

h_o = forced convection air side tube heat transfer coefficient modified for

the latent heat, kW/(m^2-K) or Btu/(hr-ft^2-°F)

A_f = fin surface area, m^2 or ft^2

ϕ = fin efficiency

h_c = forced convection air side heat transfer coefficient, kW/(m^2-K) or Btu/(hr-ft^2-°F)

$i_{fg,w}$ = latent heat of condensate of water, kJ/kg or Btu/lbm

w_a = air humidity ratio, kgv/kga, lbmv/lbma

w_w = humidity ratio of saturated air at water (frost) temperature, kgv/kga, lbmv/lbma

$C_{p,a}$ = air specific heat at constant pressure, kJ/(kg-K) or Btu/(lbm-°F)

T_a = air temperature, °C or °F

T_w = temperature of water (frost) on a fin, °C or °F

2.1.2.3. Cecchini and Marchal Model

Cecchini and Marchal (1991) proposed a computer program for simulating refrigeration and air conditioning equipment of all types: air-to-air, air-to-water, water-to-water and water-to-air. The model presented did not describe in detail the operation of equipment but characterized it with a small number of parameters determined from the results of a few testing points. The author divided the simulation of a piece of equipment into two steps: evaluation of the characteristic parameters of the equipment; prediction of equipment performance at any operation conditions. The paper is presented by two parts.

In the first part the simulation model is described focusing on the refrigerant thermodynamic cycle, which is the same for all types of equipment. The heat exchanger laws for external fluids (water, air) at the evaporator and at the condenser, adapted to each type of equipment are also described. The second part deals with the comparison between computed results and experimental data.

The following simplifying assumptions are made:

- Steady-state operation (same mass flow of refrigerant in any part of the loop)
- Pressure drops neglected, except at the expansion valve
- Constant subcooling at the condenser outlet
- Constant superheating at the evaporator outlet

The thermodynamic cycle is presented in Figure 2.5.

Different components are simulated with the following set of equations:

- Compressor:
  - Enthalpy balance:

$$h_1 - h_3 = \frac{k}{k-1}\frac{P_v}{\rho_v}\left[\left(\frac{P_c}{P_v}\right)^{\frac{k-1}{k}} - 1\right] \tag{2.19}$$

Where h_1 = compressor outlet refrigerant specific enthalpy, kJ/kg or Btu/lbm

h_3 = evaporator outlet refrigerant specific enthalpy, kJ/kg or Btu/lbm

k = polytropic exponent

P_v = refrigerant saturation pressure for evaporator, kPa or psia

P_c = refrigerant saturation pressure for condenser, kPa or psia

ρ_v = refrigerant saturation specific mass for evaporator, kg/m^3 or lbm/ft^3

- Volumetric balance:

$$q = \rho_v Q\left[1-\tau\left(\left(\frac{P_c}{P_v}\right)^{1/k}-1\right)\right] \tag{2.20}$$

Where q = refrigerant mass flow rate, kg/s or lbm/hr

Q = swept volume, m^3/s or CFM

τ = built-in volume ratio

These parameters (k, Q, τ) characterize the compressor size and compression irreversibility.

- Condenser
  - Thermal balance:

$$q(h_1-h_2)=U_c(\vartheta_c-T_c) \tag{2.21}$$

Where U_c = thermal conductance on the refrigerant side, kW/K or Btu/(hr-°F)

q = refrigerant mass flow rate, kg/s or lbm/hr

h_1 = compressor outlet refrigerant specific enthalpy, kJ/kg or Btu/lbm

h_2 = condenser outlet refrigerant specific enthalpy, kJ/kg or Btu/lbm

ϑ_c = refrigerant saturation temperature for condenser, °C or °F

T_c = condenser mean surface temperature, °C or °F

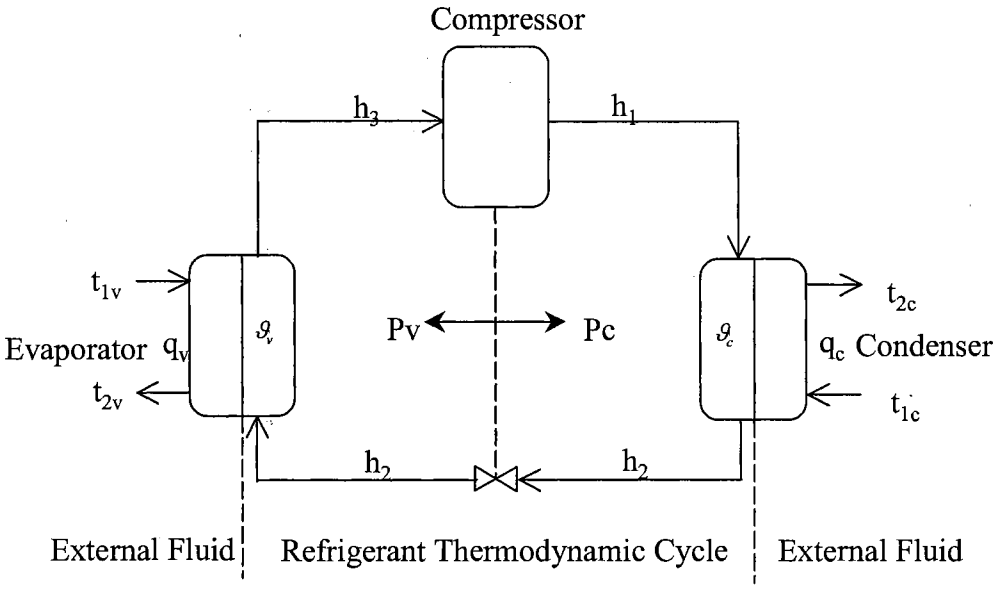

Figure 2.5. Thermodynamic compression cycle

- Evaporator
  - Thermal balance:

$$q(h_3 - h_2) = U_v(T_v - \vartheta_v) \tag{2.22}$$

Where U_v = thermal conductance on the refrigerant side, kW/K or Btu/(hr-°F)

q = refrigerant mass flow rate, kg/s or lbm/hr

h_3 = evaporator outlet refrigerant specific enthalpy, kJ/kg or Btu/lbm

h_2 = condenser outlet refrigerant specific enthalpy, kJ/kg or Btu/lbm

ϑ_v = refrigerant saturation temperature for evaporator, °C or °F

T_v = condenser mean surface temperature for evaporator, °C or °F

The author provided some correlations for thermal conductance on the refrigerant side. However, this model still requires detailed performance data for each component. The same disadvantages previously discussed appear again.

The model was first tested on three water-to-water heat pumps, ranging between 5 kW and 20 kW heat output. Predicted and measured capacities are compared on one piece of equipment. The uncertainty on capacity is about ±5%. The results obtained with three air-to-air conditioners and one water-cooled air conditioner have an uncertainty of slightly higher than ±10%.

2.1.2.4. Bourdouxhe, et al. Model

The quasi-static reciprocating chiller model developed by Bourdouxhe, et al. (1994) are characterized by the authors as being part of a toolkit "oriented towards simple solutions with a minimum number of parameters" and being somewhere between "curve-fitting, the traditional way to describe the input-output relationships, and deterministic modeling, which is an exhaustive description of the physical phenomena". Their approach is to utilize a "conceptual schema" as a modeling technique to represent the unit as an assembly of classical and elementary components. The behavior of the each component is then modeled by a deterministic approach. This approach requires fewer

parameters and experimental data compared with the models developed previously. In the parameter identification procedure, the "available experimental data" such as the condensing and evaporating temperatures, the possible subcooling and superheating are required. Based on these experimental results, the parameters of the compressor are identified. Then the whole chiller is considered to identify the evaporator and condenser heat transfer coefficients. However, those experimental data are normally not available from manufacturers' catalogs.

Both the condenser and the evaporator are represented as classical heat exchangers with water as secondary working fluid. No pressure drop is considered on the refrigerant side, and the refrigerant side is considered to be isothermal. The effectiveness model of such a heat exchanger is defined by the following relationship,

$$\varepsilon = 1 - e^{-NTU} \tag{2.23}$$

$$NTU = \frac{UA}{\dot{m}_w C_w} \tag{2.23a}$$

where ε = thermal effectiveness of heat exchanger

NTU = number of transfer units

UA = heat transfer coefficient, kW/K or Btu/(hr-°F)

$\dot{m}_w$ = water mass flow rate, kg/s or lbm/hr

C_w = water specific heat, kJ/(kg-K) or Btu/(lbm-°F)

The heat transfer coefficient (UA) is prescribed to be independent of water flow rate thus remains constant during the simulation.

This is based on some idealized assumptions as follows:

- Isobaric aspiration of refrigerant into the cylinders,
- Isentropic compression,
- Isobaric expulsion of refrigerant from the cylinders, and
- Isentropic re-expansion of the refrigerant that remains in the clearance volume at the end of the expulsion process.

The refrigerant flow rate due to the re-expansion of the clearance volume is expressed by the following widely used equation,

$$\dot{V} = \dot{V}_s \left[1 + C_f - C_f \left(\frac{p_2}{p_1} \right)^{\frac{1}{\gamma}} \right] \tag{2.24}$$

where $\dot{V}$ = volume flow rate, m^3/s or CFM

$\dot{V}_s$ = piston displacement of the compressor, m^3/s or CFM

C_f = clearance factor

P_2 = compressor exhausting pressure, kPa or psia

P_1 = evaporator exhausting pressure, kPa or psia

γ = isentropic coefficient

The author describes the energy calculation of reciprocating chiller model in two parts: a parameter identification procedure and a simulation procedure. In the parameter identification procedure, the compressor is first considered separately from the whole heat pump. On the basis of some necessary experimental results, the data needed for each working point are:

- The condensing and evaporating temperature,
- The possible subcooling and superheat, and
- The refrigerating capacity and the power consumed by the compressor.

Four parameters chosen to represent the geometry and dynamics of the compressor are estimated. These are:

$\dot{V}_s$ = piston displacement of the compressor, m^3/s or CFM

C_f = clearance factor

W_{lo} = constant part of the electromechanical losses, kW or Btu/hr

α = loss factor used to define another electromechanical loss that is supposed to be proportional to the compressor's internal power

The isentropic compression power is:

$$\dot{W}_s = \varepsilon_{vol} \dot{V}_s \frac{\gamma}{\gamma - 1} p_1 \left[\left(\frac{p_2}{p_1} \right)^{\frac{\gamma-1}{\gamma}} - 1 \right] \tag{2.25}$$

where $\dot{W}_s$ = isentropic compression power, kW or Btu/hr

$\dot{V}_s$ = piston displacement of the compressor, m^3/s or CFM

γ = isentropic coefficient

p_1 = pressure at the evaporator exhaust, kPa or psia

p_2 = pressure at the exhaust of the compressor cylinder, kPa or psia

$\varepsilon_{vol} = 1 + C_f - C_f\left(\frac{p_2}{p_1}\right)^{\frac{1}{\gamma}}$, volumetric effectiveness

C_f = clearance factor

The electric power consumed by the compressor is:

$$\dot{W} = \dot{W}_{lo} + (1+\alpha)\dot{W}_s \tag{2.26}$$

where $\dot{W}$ = electrical power consumed by the compressor, kW or Btu/hr

$\dot{W}_{lo}$ = constant part of the electromechanical losses, kW or Btu/hr

α = loss factor used to define another electromechanical loss that is supposed to be proportional to the compressor's internal power

$\dot{W}_s$ = isentropic compression power, kW or Btu/hr

When these parameters for the compressor are obtained, the whole chiller is considered. Here as mentioned above, only two parameters, the heat transfer coefficients (*UA*) for condenser and evaporator, shall be estimated. A set of coupled coefficients *UA*'s is extracted from a given domain of variation, and an objective function representing the relative error between experimental or catalog data and model calculation results for

power consumption and cooling capacity is set up. An exhaustive search method is employed to search for the optimal values of the heat transfer coefficients in this optimization problem.

2.1.2.5. Gordon and Ng Model

Gordon and Ng (1994) proposed a simple thermodynamic model for reciprocating chillers that they suggest might be valuable for diagnostic purposes. The model predicts the *COP* over a wide range of operation conditions from the inlet fluid temperatures and the cooling capacity, using three fitted parameters. The prediction of *COP* is remarkably good for a range of different chillers. However, the model doesn't predict the cooling capacity; it is required as an input.

The condenser and evaporator temperatures are approximated as constants, and expressed in terms of measured fluid temperatures and heat exchanger properties:

$$\begin{aligned} T_{cond} &= T_{cond}^{out} + \frac{Q_{evap}\left(1+\frac{1}{COP}\right)\left[\exp(NTU_{cond})-1\right]}{(mC)_{cond}} \\ &= T_{cond}^{in} + \frac{Q_{evap}\left(1+\frac{1}{COP}\right)\left[1-\exp(NTU_{cond})\right]}{(mC)_{cond}} \end{aligned} \tag{2.27}$$

$$\begin{aligned} T_{evap} &= T_{evap}^{in} - \frac{Q_{evap}\left[1-\exp(-NTU_{evap})\right]}{(mC)_{evap}} \\ &= T_{evap}^{out} - \frac{Q_{evap}\left[\exp(-NTU_{evap})-1\right]}{(mC)_{evap}} \end{aligned} \tag{2.28}$$

where 'in' and 'out' denote inlet and outlet fluid flows, 'cond' and 'evap' denote the condensing and evaporating temperatures, m is the mass flow rate, C is the coolant specific heat, and NTU is the number of transfer units.

Manufacturers' catalog data usually report COP and Q_{evap} values at assorted values of condenser inlet temperature or condenser outlet temperature, and evaporator outlet temperature.

Recognizing that entropy S is a state function, and that chiller operation is cyclic, we have:

$$\Delta S = 0 = \frac{Q_{cond} - q_{cond}^{loss}}{T_{cond}} - \frac{Q_{evap} + q_{evap}^{loss}}{T_{evap}} \tag{2.29}$$

where q^{loss} refers to the losses from heat leaks, fluid friction, throttling, and desuperheating, and where heat transfer processes have been approximated as isothermal. If heat leaks are dominated by a linear heat transfer law and if isentropic throttling and desuperheating losses are not large and are typical of those in actual commercial chillers, then the function form of q^{loss} should be:

$$q_{cond}^{loss} = -A_0 + A_3 T_{cond} \tag{2.30}$$

$$q_{evap}^{loss} = -A_2 + A_4 T_{evap} \tag{2.31}$$

The constants A_0, A_1 and A_2 characterize the irreversibilities of a particular chiller. The chiller can be characterized quantitatively by three parameters obtained by fitting the desired relation to sample measurements of the type reported in chiller catalogs. For particular realistic operating ranges of commercial chillers, not as a general cooling system description for all possible situations, a simplified expression for *COP* as a function of cooling rate, condenser inlet temperature, evaporator outlet temperature and other systems variables described above was obtained.

$$\frac{1}{COP} = -1 + \frac{T_{cond}^{in}}{T_{evap}^{out}} + \frac{-A_0 + A_1 T_{cond}^{in} - A_2 \left(T_{cond}^{in} / T_{evap}^{out}\right)}{Q_{evap}} \qquad (2.32)$$

It is demonstrated that the simple functional form predicted for the *COP* vs Q_{cool} curve agrees with actual performance data very well. The authors derived the equation for *COP* by actual experimental data with several constants to be determined and the accuracy of the predicted and measure *COP* was presented. However, the author did not provide any information about how to calculate the cooling capacity, power consumption and heat rejection by this model.

2.1.2.6. Parise Model

Parise (1986) developed a vapor compression heat pump simulation model to predict the overall performance of a system by employing a simple model for the

components of the heat pump cycle. Operating conditions, such as compressor speed, heat source and heat sink temperature, cooling and heating fluids flow rates, are entered as input data. Predetermined empirical parameters that characterize the components, such as the polytropic index of compression and heat exchangers' overall conductances, are also entered as input data. Predicted results were compared with experimental data. A typical application is presented at the end of the paper.

In the modeling of condenser and evaporator, these two heat exchangers are treated as having a constant overall heat transfer coefficient, based on the arithmetic overall temperature difference. For example, the heat transfer in the condenser is governed by the following equations,

$$\dot{Q}_{CD} = U_{CD} A_{CD} \left(\frac{T_2 + T_{CD}}{2} - \frac{T_{ci} + T_{co}}{2} \right) \tag{2.33}$$

$$\dot{Q}_{CD} = \dot{m}_F (h_2 - h_3) \tag{2.34}$$

$$\dot{Q}_{CD} = \dot{m}_c C_c (T_{co} - T_{ci}) \tag{2.35}$$

where $\dot{Q}_{CD}$ = condenser heat transfer rate, kW or Btu/hr

U_{CD} = overall heat conductance of condenser, kW/(m^2-°C)

A_{CD} = condenser heat transfer area, m^2 or ft^2

T_2 = compressor outlet temperature, °C or °F

T_{CD} = condensing temperature, °C or °F

T_{ci} = condenser cooling fluid inlet temperature, °C or °F

T_{co} = condenser cooling fluid outlet temperature, °C or °F

$\dot{m}_F$ = refrigerant mass flow rate, kg/s or lbm/hr

h_2 = refrigerant enthalpy at compressor outlet, kJ/kg or Btu/lbm

h_3 = refrigerant enthalpy at condenser outlet, kJ/kg or Btu/lbm

$\dot{m}_c$ = condenser cooling fluid mass flow rate, kg/s or lbm/hr

C_c = Specific heat at constant pressure for condenser cooling fluid,

kJ/(kg-°C) or Btu/(lbm-°F)

The evaporator follows the condenser model in the assumption of an overall heat transfer coefficient, U_{EV}, for both the two-phase and superheated regions. According to the author, the following parameters are required by the model:

- Compressor:

V_c = compressor displaced volume, m^3 or ft^3

r = clearance ratio

n = constant index of polytropic process

w = rotational speed, rad/s

C_v = volumetric coefficient

- Condenser:

T_{ci} = condenser cooling fluid inlet temperature, °C or °F

$\dot{m}_c$ = condenser cooling fluid mass flow rate, kg/s or lbm/hr

C_c = Specific heat at constant pressure for condenser cooling fluid,

J/(kg-°C) or Btu/(lbm-°F)

A_{CD} = heat transfer area of condenser, m^2 or ft^2

U_{CD} = overall heat conductance of condenser, kW/(m^2-°C) or Btu/(hr-ft^2-°F)

ΔT_{sc} = condenser subcooling, °C or °F

- Expansion valve:

ΔT_s = evaporator superheat, °C or °F

- Evaporator:

T_{hi} = evaporator heating fluid inlet temperature, °C or °F

$\dot{m}_h$ = evaporator heating fluid mass flow rate, kg/s or lbm/hr

C_h = Specific heat at constant pressure for evaporator heating fluid,

kJ/(kg-°C) or Btu/(lbm-°F)

A_{EV} = evaporator heat transfer area, m^2 or ft^2

U_{EV} = overall heat conductance of evaporator, kW/(m^2-°C) or Btu/(hr-ft^2-°F)

With so many parameters as input data, the author did not provide any information about how to identify these values.

2.1.2.7. Fischer and Rice Model

Fischer and Rice (1983) developed an air-to-air heat pump model to predict the steady-state performance of conventional, vapor compression, electrically-driven heat pumps in both heating and cooling modes. This model is also known as the ORNL Heat

Pump Design Model. The purpose for the development of this model is to provide an analytical design tool for use by heat pump manufacturers, consulting engineers, research institutions, and universities in studies directed toward the improvement of heat pump efficiency.

- *Compressor model*

Since the compressor is the heart of a heat pump system and the primary user of electrical power, accurate compressor modeling is important to good system performance prediction. This criterion, however, must be tempered by consideration of the type of information available to most potential users of the program and of the different types of heat pump studies in which the program may be used. For these reasons the ORNL Heat Pump Design Model does not incorporate a subroutine which rigorously models compressor performance using detailed hardware design parameters. Instead, users can choose between two simpler models depending upon their specific needs: (1) Map-based compressor model, and (2) Loss and efficiency-based compressor model.

The first compressor model is based on the use of compressor manufacturers' data (compressor maps) for a specific compressor or compressor type. The model has built-in corrections to adjust for levels of refrigerant superheat in reciprocating compressor which are different from those for which the maps were generated. Although this model was written for reciprocating compressor, it should be easy to modify for use with rotary,

screw, or centrifugal compressor. Accurate simulation of existing compressor is possible with this model.

The map-based compressor model uses empirical performance curves for reciprocating compressors obtained from compressor calorimeter measurements performed by the manufacturers. These performance curves provide compressor motor power input, refrigerant mass flow rate and/or refrigerating capacity as functions of "evaporator" saturation temperature (i.e., at compressor shell inlet) for four to six " condenser" saturation temperatures (i.e., at the compressor shell outlet). The map-based routine uses curve fits to the compressor motor power input (kW) and the refrigerant mass flow rate (lbm/h) as functions of compressor shell inlet and outlet saturation temperatures to model the published performance data. The user must provide sets of coefficients for bi-quadratic functions of the form given by Equation (2.36) for the power input and mass flow rate as functions of the inlet and outlet saturation temperature.

$$f(T_{outlet}, T_{inlet}) = C_1 T_{outlet}^2 + C_2 T_{outlet} + C_3 T_{inlet}^2 + C_4 T_{inlet} + C_5 T_{outlet} T_{inlet} + C_6 \qquad (2.36)$$

where T_{outlet} = inlet saturation temperature, °C or °F

T_{inlet} = outlet saturation temperature, °C or °F

$C_1 - - C_6$ = equation-fit coefficients

The user must also specify the total actual compressor displacement, the rated compressor motor speed, and the fixed refrigerant superheat or temperature at the

compressor shell inlet (upon which the map is based) for the compressor which is being modeled. The desired compressor displacement is also an input parameter. This value is used by the map-based model to scale the compressor performance curves linearly to represent a compressor with the same general performance characteristics as the original compressor but of a different capacity. For values of superheat or suction gas temperature other than those for which the maps were generated, Equations (2.37) and (2.38) are employed for correcting the compressor motor power input and the refrigerant mass flow rate.

$$\dot{m}_{r,actual} = \left[1 + F_V \left(\frac{v_{map}}{v_{actual}} - 1\right)\right] \dot{m}_{r,map} \tag{2.37}$$

where $\dot{m}_{r,actual}$ = actual refrigerant mass flow rate, kg/s or lbm/hr

F_V = volumetric efficiency correction factor

v_{map} = specific volume under map superheat conditions, m^3/kg or ft^3/lbm

v_{actual} = specific volume under actual superheat conditions,

m^3/kg or ft^3/lbm

$\dot{m}_{r,actual}$ = actual refrigerant mass flow rate, kg/s or lbm/hr

$$\dot{W}_{cm.actual} = \left(\frac{\dot{m}_{r,actual}}{\dot{m}_{r,map}}\right)\left(\frac{\Delta h_{isen,actual}}{\Delta h_{isen,map}}\right) \dot{W}_{cm,map} \tag{2.38}$$

where $\dot{W}_{cm,actual}$ = actual compressor motor power input, kW or Btu/hr

$\Delta h_{isen,actual}$ = actual isentropic process enthalpy change, kJ/kg or Btu/lbm

$\Delta h_{isen,map}$ = map isentropic process enthalpy change, kJ/kg or Btu/lbm

$\dot{W}_{cm,map}$ = map compressor motor power input, kW or Btu/hr

The enthalpy gain to the suction gas between compressor shell inlet and suction port due to motor and compressor cooling by the suction gas is assumed as follows.

$$\Delta h_{inlet,suction\ port} = F_{sh} \frac{\dot{W}_{cm,map}}{\dot{m}_{r,map}} \tag{2.39}$$

where F_{sh} = appropriate suction gas heating factor

Once the correction for actual superheat level have been applied to the values of $\dot{W}_{cm,map}$ and $\dot{W}_{r,map}$, the enthalpy at the compressor shell outlet, h_{outlet}, is computed from Equation (2.40).

$$h_{outlet} = \left(\dot{W}_{cm,actual} - \dot{Q}_{can}\right) / \dot{m}_{r,actual} + h_{inlet} \tag{2.40}$$

where $\dot{Q}_{can}$ = heat loss rate from the compressor shell, kW or Btu/hr

$\dot{Q}_{can}$ is specified by the user as either a fixed input value or as a specified fraction of actual compressor power.

The second model, a loss and efficiency-based compressor model, is intended for use in heat pump design studies, e.g., to predict how changes in compressor loss and efficiency terms affect system performance. It can also be used to model compressor performance with a new refrigerant. This more general routine models the internal energy balances in a reciprocating compressor using user-supplied heat loss and internal efficiency values. This model cannot predict compressor performance as accurately over the same range of operating conditions as the map-based model without local adjustment of some of the input efficiency and loss values. It is well suited, however, for studying internal compressor improvements and interactions and their effect on system performance about a particular design point.

The loss and efficiency-based compressor routine models the internal energy balance in a reciprocating compressor from user-supplied design, internal efficiency, and heat-loss values. The user is required to specify the following values:

D – total compressor displacement, m^3/s or CFM

C – actual clearance volume ratio

S_{input} – synchronous or actual compressor motor speed, RPM

$\dot{W}_{s,fl}$ – compressor motor full load shaft power, kW or Btu/hr

$\eta_{mot,\max}$ – maximum compressor motor efficiency

η_{mech} – compressor mechanical efficiency

η_{isen} – isentropic compression efficiency from suction to discharge port

This model can be treated as a supplement to the map-based model since it is not intended to be a rigorous tool to replicate the compressor performance.

- *Expansion device*

The ORNL Heat Pump Design model allows the user to specify a fixed level of condenser subcooling or design parameters for a particular expansion device in order to control the refrigerant flow between the high and low sides of the system. Three basic expansion device models have been developed: capillary tubes, thermostatic expansion valves (TXV), and short-tube orifices.

One of the options in the heat pump model is to simulate the operation of one or more capillary tubes in parallel. The capillary tube model requires the refrigerant pressure and degree of subcooling at the inlet of the capillary tube or tubes. The model consists of empirical fits to curves given in the ASHRAE equipment handbook for a standardized capillary tube flow rate as a function of inlet pressure and subcooling for R-12 or R-22.

The TXV model contains:

- a general model of a cross-charged thermostatic expansion valve
- specific empirical correlations for one size of distributor nozzle and tubes
- additional empirical equations to correct for nonstandard liquid line temperature, tube lengths and nozzle and tube loadings

The short-tube orifice model which is included in the ORNL Heat Pump Design Model uses correlations developed by Mei (1982). He obtained data for five 0.127 m (0.5 in.) long Carrier Accurators with diameters from 1.067 to 1.694 mm (0.0420 to 0.0667 inches) (L/D ratio from 7.5 to 11.9) using R-22. He observed pressure drops between 620 and 1515 kPa (90 and 220 psi) across the restrictor and levels of subcooling from 0 to 28 °C (0 to 50 °F) at the inlet. The observed refrigerant mass flow rates ranged from 68.0 to 213 kg/h (150 to 470 lbm/h).

- *condenser and evaporator model*

The ORNL Heat Pump Design Model calculates the performance of air-to-refrigerant condensers and evaporators by using:

- effectiveness vs. Ntu correlations for heat transfer for a dry coil
- a modified version of the effectiveness surface temperature approach when there is dehumidification
- the Thom correlation for two-phase refrigerant pressure drops and the Moody friction factor chart plus momentum terms for the single-phase refrigerant pressure drops
- friction factor equations for the air-side pressure drop for dry, partially wetted or fully wetted coils.

The calculation method which has been used assumes that the heat exchangers consist of equivalent, parallel refrigerant circuits with unmixed flow on both the air and refrigerant sides. The air-side mass flow rate and the estimated refrigerant mass flow rate

from the compressor model are divided by the number of circuits to obtain values for each circuit. The refrigerant-side calculations are separated into computations for the superheated and two-phase regions for the evaporator and for the superheated, two-phase and subcooled regions for the condenser.

The refrigerant heat transfer coefficient for the superheated region in the condenser is calculated by Equation (2.41) for gas flow from an abrupt contraction entrance.

$$h = C_1 G_r C_{p,v} N_{\mathrm{Pr}}^{-2/3} N_{\mathrm{Re}}^{C_2} \tag{2.41}$$

where h = heat transfer coefficient, kW/(m^2-K), or Btu/(hr-ft^2-°F)

C_1, C_2 = constants

G_r = refrigerant mass flux, kg/(m^2-s) or lbm/(ft^2-hr)

$C_{p,v}$ = refrigerant specific heat, kJ/(kg-K) or Btu/(lbm-°F)

N_{Pr} = Prandtl number

$N_{\mathrm{Re}} = G_r D / \mu$, Reynolds number

The refrigerant side or interior heat transfer coefficients for the subcooled region of the condenser and the superheated region in the evaporator are computed using the Dittus-Boelter correlation for fully developed flow.

$$h = 0.023 G_r C_p N_{\mathrm{Pr}}^{(C-1)} N_{\mathrm{Re}}^{-0.20} \tag{2.42}$$

where h = heat transfer coefficient, kW/(m^2-K), or Btu/(hr-ft^2-°F)

G_r = refrigerant mass flux, kg/(m^2-s) or lbm/(ft^2-hr)

C_p = refrigerant specific heat, kJ/(kg-K) or Btu/(lbm-°F)

N_{Pr} = Prandtl number

$N_{\mathrm{Re}} = G_r D/\mu$, Reynolds number

C is 0.3 when the refrigerant is being cooled and 0.4 when being heated.

The two-phase heat transfer coefficients for the condenser and the evaporator are average values obtained by effectively integrating local values over the length of the two-phase region. The actual integration is performed over the range of refrigerant quality where a length of tube *dz* is related to a change in quality of *dx* by,

$$dz \propto \frac{dx}{h(x)\Delta T} \tag{2.43}$$

and ΔT is the change in temperature between the refrigerant and the tube wall.

The air-side heat transfer coefficients are calculated by Equation (2.44).

$$h_a = C_o G_a C_{pa} N_{\mathrm{Pr}}^{-2/3} j\left[\frac{1-1280N_T N_{\mathrm{Re}}^{-1.2}}{1-5120N_{\mathrm{Re}}^{-1.2}}\right] \tag{2.44}$$

where h_a = heat transfer coefficient, kW/(m^2-K), or Btu/(hr-ft^2-°F)

G_a = air mass flux, kg/(m^2-s) or lbm/(ft2-hr)

$C_{p,a}$ = air specific heat, kJ/(kg-K) or Btu/(lbm-°F)

N_{Pr} = Prandtl number

$$j = 0.0014 + 0.2618\left(\frac{1}{1-F_a}\right)^{-0.15}\left(\frac{G_a D}{\mu}\right)^{-0.4}$$

N_T = number of tube rows in the heat exchanger in the direction of the air flow

$$N_{Re} = \frac{G_a W_T}{\mu}$$

and C_o =1.0, 1.45 or 1.75 depending on whether the fins are smooth, wavy, or louvered. The air-side heat transfer coefficient for the portion of the evaporator which is wetted due to dehumidification is calculated from the dry coefficient h_a by Equation (2.45).

$$h_{a,w} = 0.626\left(\frac{\dot{Q}}{A}\right)^{0.101} h_a \qquad (2.45)$$

where $h_{a,w}$ = heat transfer coefficient for wet coil, kW/(m^2-°K) or Btu/(ft^2-°F)

$\dot{Q}$ = heat transfer rate, kW or Btu/hr

A = frontal area of heat exchanger, m^2 or ft^2

To calculate the performance of the condenser and evaporator, the heat transfer for the liquid, vapor and two-phase refrigerant regions of the heat exchanger are computed using effectiveness vs. *Ntu* correlations, except for the two-phase refrigerant region of an evaporator with dehumidification. Except for this case, the number of heat transfer units for the two-phase region (condenser and evaporator) is given by Equation (2.46).

$$Ntu = \frac{UA}{C_{\min}} = \left(\frac{A_o}{C_{pm}\left[\frac{A_r}{\eta_a h_a A_a} + \frac{1}{h_{tp}} \right]} \right) \tag{2.46}$$

where Ntu = number of heat transfer units

UA = heat transfer coefficient product, kW/K or Btu/(hr-°F)

C_{min} = minimum of the heat capacity rates for the air and the refrigerant, kJ/K or Btu/°F

C_{pm} = specific heat of moist air, kJ/(kg-K) or Btu/(lbm-°F)

A_r = total refrigerant-side heat transfer area, m^2 or ft^2

η_a = heat exchanger overall surface effectiveness

h_a = air side heat transfer coefficient, kW/(m^2-K) or Btu/(hr-ft^2-°F)

A_a = air side fin and tube heat transfer area, m^2 or ft^2

h_{tp} = average condensing or evaporating heat transfer coefficient, kW/(m^2-K) or Btu/(hr-ft^2-°F)

C_{pm} is corrected for moist air conditions (i.e., $C_{pm} = C_{pa} + 0.444 \times W$ where W is the air humidity ratio), A_o is the refrigerant-side heat transfer area per unit of air mass flow rate. The effectiveness is given by Equation (2.47).

$$\varepsilon_{tp} = 1 - e^{-Ntu} \tag{2.47}$$

where ε_{tp} = heat exchanger effectiveness for two phase region

When there is moisture removal on the evaporator, it is assumed to occur only on the two-phase region of the coil.

2.1.2.8. The Comparison by Damasceno, et al.

Damasceno, et al. (1990) compared three steady-state air-to-air heat pump computer models. Two of them are available in the open literature, the third one was developed in-house. These are (1) the MARK III model, which is an updated version of an earlier program developed at Oak Ridge National Lab. by Fischer and Rice (1983) and Fischer et al. (1988) (2) HPSIM, developed at NBS by Domanski and Didion (1983) and (3) HN, developed by Nguyen and Goldschmidt (1986) and updated by Damasceno and Goldschmidt (1987). A summary of predicted capacity and *COP* discrepancies is presented in Table 2.1:

Table 2.1. Interpretation of Accuracy of Performance Predictions

MODEL	HEATING(47 °F)		COOLING(95 °F)	
	CAPACITY	COP	CAPACITY	COP
HPSIM	+15.5%	+7.1%	+3.0%	+7.5%
MARK III	+6.5%	-9.5%	+10.5%	+8.0%
HN	+19.5%	-2.5%	+13.0%	+8.0%

They concluded that the prediction of capacity and coefficient of performance (*COP*) are acceptable for all programs, but they failed to predict detailed refrigerant pressure and temperature distributions adequately.

2.1.2.9. Shelton and Weber Model

Shelton and Weber (1991) developed a chiller model based on manufacturers' performance data. The evaporator was characterized by an overall heat transfer coefficient (*UA*) function on the cooling load only. The condenser modeling led to a two-parameter correlation of the overall condenser *UA* with varying water tube velocity and condenser load. The compressor model was based on Carnot efficiency. Assuming an isentropic compressor, constant temperature heat rejection at T_C, and constant temperature heat input at T_E and using the Carnot principle leads to a Carnot-based kW/ton of cooling load calculated as follows:

$$[kW/ton]_{Carnot} = [T_c / T_E - 1] \cdot 3.517 \tag{2.48}$$

where T_C and T_E are in absolute temperature.

This model was corrected by means of compressor isentropic efficiency at design load, which included the motor efficiency, and an efficiency factor that decreased as load decreased due to off-design compressor operation.

$$kW/ton = \frac{[kw/ton]_{Carnot}}{\eta_{ISENT}\eta_{TON}} \tag{2.49}$$

The last two efficiencies (η_{ISENT}, η_{TON}) were determined from second-order polynomial equation equation-fits to the manufacturers' data points.

2.1.2.10. Greyvenstein Model

A computer model for the simulation of vapor-compression heat pumps and refrigeration systems with thermo-statically controlled expansion valve is presented. The model describes the performance of the system given its design, the fan curves, the compressor characteristics, the design of the heat exchangers and the condition of the external fluids flowing through the heat exchangers.

The compressor model consists of a performance data file and an interpolation routine which uses the data in the file to interpolate values of refrigerant mass flow and input power given the inlet and outlet pressures. The accuracy of the model therefore depends on the accuracy of the performance data. The evaporator is of fin and tube type in a stream of air. The heat absorbed by the refrigerant in the evaporator can be divided into two parts. The first parts is the heat necessary to evaporate all the liquid, while the second part is that necessary to heat the vapor to the superheated point. The heat absorbed by the refrigerant is transferred across the outside surface area of the evaporator. The total outside surface area can thus also be divided into two parts associated with the quantities of those two parts of the heat. The two air streams across the two parts are mixed after the evaporator. From the heat transfer relationships, we may have:

$$Q = UA\Delta T \tag{2.50}$$

where U = overall heat transfer coefficient, kW/(m^2-K) or Btu/(hr-ft^2-°F)

ΔT = log mean temperature difference, °C or °F

A = area, m^2 or ft^2

For two-phase region and superheated region, different correlations and equations are used for the U, ΔT and A respectively.

Similarly, the heat rejected by the refrigerant can be divided into three parts in the condenser. The first part is the heat necessary to cool the superheated refrigerant to saturated vapor. The second part is the heat associated with the condensation of the saturated vapor. The third part is the heat rejected in sub-cooling the saturated liquid. The heat transfer relationships are established from the same principle as evaporator.

The evaporator model was verified by comparing it with design data published by the Bohn Heat Transfer Division of the Gulf and Western Metals Forming Company. The Bohn data are based on laboratory findings and widely used in the refrigeration industry for the design of evaporator coils. No experimental data are available for the type of condenser. Some related data are adapted to this type, which is essentially the same as the water-cooled kind.

The author claimed that the model is a powerful and versatile tool for the design and optimization of refrigeration systems or heat pumps and has been used successfully to design a number of systems.

2.1.2.11. Dabiri Model

A steady state heat pump simulation model was developed by Dabiri (1982) that targeted at reducing the amount of testing required by DOE to obtain heat pump performance rating information. The Fisher and Rice (1981) air-to-air heat pump model that developed for design purposes was modified. Power inputs to indoor and outdoor fans, which were calculated as outputs in the original model, were inputs to this simulation model. Other modification such as a reversing valve model and refrigerant line losses was also discussed. The input variables to the heat pump simulation model for each component include redundant information that normally available for a research lab. For example, the required inputs for the condenser and evaporator are: outside diameter of tubes, inside diameter of tubes, fin thickness, fin pitch and configuration, thermal conductivity of the fins, heat exchanger frontal area, number of tubes in direction of airflow, number of parallel circuits in heat exchanger, spacing of tube passes perpendicular to airflow, spacing of tube rows in direction of airflow, total number of return bends in heat exchanger, and contact conductance between fins and tubes. The model's outputs include heating capacity, *COP*, mass flow rate through the compressor, refrigerant pressure and temperature at every point of the circuit, air pressure drops across the heat exchanger, and air temperature at the heat exchangers' exits. Compressor shell heat loss was considered in the model and no specific pattern exists in the relationship between the shell heat loss and evaporating temperature was observed. The compressor shell heat loss factor varied between 10% and 40%. The heat pump simulation model was applied to three different heat pumps and results were presented. The results presented

indicate that the simulation model predictions generally fall within the acceptable tolerance of the ARI standards and within the possible errors existing in the experimental measurements. A sensitivity analysis was made to assess the effect of possible variation of some of the inputs parameters on the system's thermal performance. The input parameters that could not be determined accurately were listed.

2.1.2.12. Ouazia and Snelson's Model

Ouazia and Snelson (1994) presented a simulation model suitable for the preliminary evaluation of refrigerants and refrigerant mixtures in a water-water heat pump test facility. The simulation is specific to the heat pump test facility and uses a semi-theoretical cycle analysis to predict steady-state operating conditions. The model is to calculate performance characteristics including evaporator capacity, compressor shaft power, refrigerant mass flow, cooling coefficient of performance, etc.

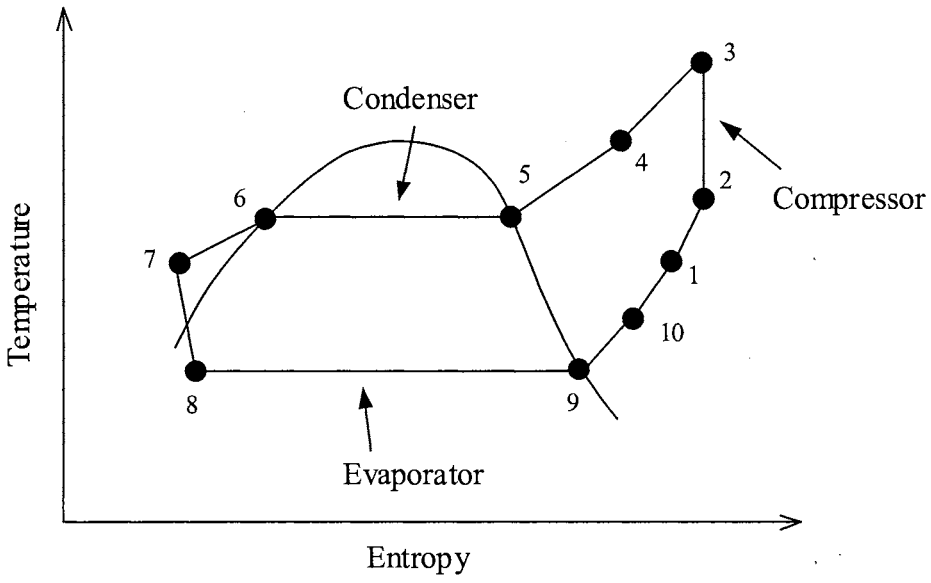

Figure 2.6. Temperature-entropy diagram for the simulated heat pump

The simulation uses a simplified model of an open-drive reciprocating compressor, and includes effects such as refrigerant subcooling at the condenser outlet, refrigerant superheating at the evaporator outlet, heat transfer and pressure drops in heat exchangers, and a representation of liquid line/suction line heat exchange. The temperature-entropy diagram shown in Figure 2.6 represents the basic vapor-compression cycle as modeled by the computer simulation. Assumptions made are: compression process 2-3 is isentropic; expansion process 7-8 is isenthalpic; condensation and evaporation processes are at constant pressure. To use the simulation program, it is necessary to specify the evaporator superheat, condenser exit subcooling, and secondary side temperatures for the condenser and evaporator. Initial estimates must also be provided of the refrigerant saturation temperatures at the condenser and evaporator and for the refrigerant mass flow rate.

2.1.2.13. Krakow and Lin's Model

A computer model of a multiple-source heat pump was presented by Krakow and Lin (1983). The model was used to simulate heat pump systems having solar insolation, ambient air, or storage water as energy source and space air or storage water as energy sink. The model determines steady-state performance characteristics of a heat pump interacting with the environment. The evaporators and condensers in the system are specified by values of heat exchanger effectiveness and heat capacities. The values of heat capacities of evaporators and condensers depend on the flow rate of air or water, not those of the refrigerant. For constant air or water flow rates, the values of heat capacities and heat exchanger effectiveness are assumed constant.

The compressor model permits the simulation of heat pump systems with reciprocating compressors. The performance of a reciprocating compressor is specified by,

$$e_{vi} = 1 + c - c \cdot \left(P_c / P_e\right)^{1/n} \tag{2.51}$$

$$e_v = e_r \cdot e_{vi} \tag{2.52}$$

$$m = e_v \cdot V / v \tag{2.53}$$

$$e_i = \left(h_{coi} - h_{ci}\right) / \left(h_{coa} - h_{ci}\right) \tag{2.54}$$

where c = clearance volume ratio

e_i = isentropic compression efficiency

e_r = volumetric efficiency ratio, actual/theoretical

e_v = actual volumetric efficiency of the compressor

e_{vi} = ideal volumetric efficiency of the compressor

h_{ci} = enthalpy at compressor inlet, kJ/kg or Btu/lbm

h_{coa} = actual enthalpy at compressor outlet, kJ/kg or Btu/lbm

h_{coi} = ideal enthalpy at compressor outlet, kJ/kg or Btu/lbm

m = refrigerant mass flow rate, kg/s or lbm/m

n = ratio of specific heats of the refrigerant vapor

P_c = condensation pressure, kPa or psi

P_e = evaporation pressure, kPa or psi

v = refrigerant specific volume at compressor inlet, m^3/kg or ft^3/lbm

V = rate of volumetric displacement, m^3/s or CFM

An air-cooled or a water-cooled condenser was simulated. The following equations were used to specify the performance of the condenser,

$$Q_c = e \cdot H \cdot (T_c - T_{snk}) \tag{2.55}$$

$$e = (T_{hot} - T_{snk})/(T_c - T_{snk}) \tag{2.56}$$

where e = heat exchanger effectiveness

H = heat capacity of space air or storage water, energy/time/degree temperature difference, kW/°C or Btu/(hr-°F)

Q_c = condenser heat transfer rate, energy/time, kW or Btu/hr

T_c = condensation temperature of the refrigerant, °C or °F

T_{snk} = inlet temperature of space air or storage water, °C or °F

T_{hot} = outlet temperature of space air or storage water, °C or °F

The heat pump under investigation used solar/air collectors, through which ambient air was circulated during the night and periods of low solar insolation. The collector's performance as an evaporator extraction heat from ambient air is specified by the heat capacity of the source and the heat exchanger effectiveness. A water-cooled storage evaporator may also be the same parameter. The performance of either of these evaporators is governed by,

$$Q = e \cdot H \cdot (T_{src} - T_e) \tag{2.57}$$

where e = heat exchanger effectiveness

H = heat capacity of the source, energy/time/degree temperature

2.2. Modeling of Heat Pump Components

Models for heat transfer process and primary components (i.e. heat exchangers, compressor, expansion devices) of heat pumps or chillers are focus of this section. Only models relevant to the basic heat pump components and fundamental techniques that might be useful in the future research work are discussed.

2.2.1. Analysis of Heat Transfer between Moist Air and Cold Surface by McElgin and Wiley

The transfer of heat from warm moist air to cold surface and thence through the fins and tubes to the cold water or refrigerant may best be analyzed by dividing the process into two distinct steps, (1) from the air to the wetted surface and (2) from the surface through the fins and tubes to the water. The total heat lost by the air in passing over an element of wetted area dAw is given by:

$$dH_T = \frac{f_g}{s}(h - h_s)dAw \tag{2.58}$$

where H_T= total heat lost by total weight of air flowing over wetted surface, kW or Btu/hr

f_g = sensible heat transfer coefficient, kW/(m^2-K) or Btu/(hr-ft^2-°F)

s = humid specific heat of air vapor mixture, kJ/(kg-K) or Btu/(lbm-°F)

h = total heat content of air vapor mixture per mass of dry air, kJ/kg or Btu/lbm

h_s = total heat content of air vapor mixture per mass of dry air at surface, kJ/kg or Btu/lbm

This equation which was originally derived by Merkel (1925), combines sensible heat transfer due to temperature difference and latent heat transfer due to vapor pressure difference into a single equation which states that the rate of simultaneous sensible and latent heat flow depends on the difference between the total heat of the air flowing over the surface and the total heat corresponding to saturation a the surface temperature. The total heat transferred from the element of area dAw through the fins and tubes to the water is given by:

$$dH_T = \frac{1}{R}(t_s - t_R)dAw \tag{2.59}$$

where t_s = surface temperature, °C or °F

t_R = refrigerant temperature, °C or °F

Where R is as defined above the composite resistance to heat flow imposed by the fins and tubes and the internal water film. Equations (2.58) and (2.59) are rearranged:

$$\frac{t_s - t_R}{h - h_s} = \frac{f_g R}{s} = C \tag{2.60}$$

The value of s, the humid specific heat of air, may be taken as constant for the range of comfort cooling. For a given coil, air velocity and refrigerant velocity, f_g and R are constant and thus C is a constant coil characteristic for given conditions.

2.2.2. Analysis of Air Side Heat Transfer in Finned Tube Heat Exchangers by Webb

When heat is transferred between air and sensible or two-phase fluids in tubes, finned tube heat exchangers are beneficial. In this case, the air-side heat transfer coefficient may be 10-50 times smaller than the tube-side coefficient. The use of a finned surface will increase the air-side conductance (hA) to more evenly proportion the thermal resistance on each side of the heat exchanger. In many applications, air-side extended surface can be added for much less unit cost than that if the base tube surface. The degree of heat transfer augmentation is dependent on the following factors:

1) Fin spacing
2) Fin efficiency
3) Use of special fin configuration to yield increased heat transfer coefficients

The significance of these factors on the resulting augmentation is given by Equation (2.61), which defines the overall heat transfer coefficient, based on the internal tube area:

$$\frac{1}{U} = \frac{A_i}{\eta h A} + \frac{1}{h_i} \tag{2.61}$$

where U = overall heat transfer coefficient, kW/(m^2-°K) or Btu/(hr-ft^2-°F)

A_i = inside surface area, m^2 or ft^2

η = total surface efficiency

Thus, the air-side conductance is:

$$K = \frac{\eta h A}{A_i} \tag{2.62}$$

An increased number of fins per centimeter will increase the conductance by increase the conductance by increase the ratio A/A_i. Also, the use of more closely spaced flat fin will increase the heat transfer coefficient h, because of a smaller hydraulic diameter. Or, the use of a special fin configuration, such as a "wavy" fin, will produce a higher heat transfer coefficient. The surface efficiency η is influenced by the fin thickness, thermal conductivity, and fin length. The fin efficiency may be calculated from appropriate graphs or equations given in most heat transfer textbook. The surface efficiency is calculated from Equation (2.63):

$$\eta = 1 - \frac{A_f}{A}\left(1 - \eta_f\right) \tag{2.63}$$

where A is the total external surface and A_f is the finned surface area.

2.2.3. Experimental Results of Chilled-Water Cooling Coils Operating at Low Water Velocities by Mirth et al.

Experimental results were presented that demonstrate that chilled-water cooling coils operating at low water-side Reynolds numbers do not perform as well as predicted by the manufacturer's software. The manufacturer's software overpredicts coil performance by as much as 8% at a water-side Reynolds number of 3100 (the lower Reynolds number limit certifiable under ARI standard 410-87). At a Reynolds number of

2300, the overpredictions range from 12% to 18%. An analysis revealed that this problem could be mitigated by using the Gnielinski correlation instead of the Dittus-Boelter correlation to predict the water-side heat transfer coefficient. When the coils were operating in the turbulent flow regime (Re_w>2300), a coil model using the Gnielinski correlation was able to predict coil performance to within 4% for wet fin surface conditions and to within 2% for dry surface conditions. A laminar, developing flow correlation that was tested for water-side Reynolds numbers less than 2300 underpredicted coil performance.

2.2.4. Comparison of Methods of Modeling the Air Side Heat and Mass Transfer in Chilled-Water Cooling Coils by Mirth and Ramadhyani

Three different methods of modeling the heat and mass transfer in chilled-water cooling coils are compared. A new model (model 3) is compared with discretized version of the models presented in ARI Standard 410-87 (model 1) and by McQuiston (model 2) and with the ARI log-mean enthalpy method. The models differ both in the method used to determined the heat transfer rate to primary surface and in the method used to determine the fin efficiency. It was summarized that the heat transfer rate predicted by model 1 agreed within 1% to 2% of the new model, while model 2 predicted heat-transfer rates 2% to 8% higher than did model 3. However, by modifying the assumptions used in model 2, it was possible to bring its predictions to within 2% of those of model 3. The ARI log-mean enthalpy method was also found to agree well within 2%.

2.2.5. Cooling Coil Model of Braun, et al.

Braun, et al. (1989) proposed an effectiveness model for cooling coils. The cooling coil model was developed from a basic analysis of cooling tower performance. The primary difference between the analysis of cooling coils and cooling towers is associated with the fact that the air and water streams are not in direct contact. A schematic of a counter-flow cooling tower showing the important states and dimensions is given in Figure 2.7.

From steady state energy and mass balances on an incremental volume, the following differential equations may be derived:

$$\frac{d\omega_a}{dV} = -\frac{Ntu}{V_T}\left(\omega_a - \omega_{s,w}\right) \tag{2.64}$$

$$\frac{dh_a}{dV} = -\frac{LeNTU}{V_T}\left[\left(h_a - h_{s,w}\right) + \left(\omega_a - \omega_{s,w}\right)\left(1/Le - 1\right)h_{g,w}\right] \tag{2.65}$$

$$\frac{dT_w}{dV} = \frac{\frac{dh_a}{dV} - C_{p,w}\left(T_w - T_{ref}\right)\frac{d\omega_a}{dV}}{\left[\frac{\dot{m}_{w,i}}{\dot{m}_a} - \left(\omega_{a,o} - \omega_a\right)\right]C_{p,w}} \tag{2.66}$$

where $Le = \dfrac{h_c}{h_D C_{p,a}}$

$$Ntu = \frac{h_D A_V V_T}{\dot{m}_a}$$

A = surface area, m^2 or ft^2

A_v = surface area of water droplets per volume of cooling tower, m^2 or ft^2

$C_{p,a}$ = constant pressure specific heat of moist air, kJ/(kg-K) or Btu/(lbm-°F)

$C_{p,w}$ = constant pressure specific heat of liquid water, kJ/(kg-K) or Btu/(lbm-°F)

C_s = derivative of saturation air enthalpy with respect to temperature, kJ/(kg-K) or Btu/(lbm-°F)

C^* = ratio of air to water capacitance rate for dry analysis

h_a = enthalpy of moist air per mass of dry air, kJ/kg or Btu/lbm

h_c = convection heat transfer coefficient, kW/(m^2-K) or Btu/(hr-ft^2-°F)

h_D = mass transfer coefficient, kg/(m^2-s) or lbm/(ft^2-hr)

h_g = enthalpy of water above reference state for liquid water at T_{ref}, kJ/kg or Btu/lbm

h_s = enthalpy of saturated air, kJ/kg or Btu/lbm

$\dot{m}_w$ = mass flow rate of water, kg/s or lbm/hr

$\dot{m}_a$ = mass flow rate of dry air, kg/s or lbm/hr

m^* = ratio of air to water effective capacitance rate for wet analysis

Le = Lewis number

Ntu = overall number of transfer units

$\dot{Q}$ = overall heat transfer rate, kW or Btu/hr

T_a = air temperature, °C or °F

T_{ref} = reference temperature for zero enthalpy of liquid water, °C or °F

T_s = surface temperature, °C or °F

T_w = water temperature, °C or °F

UA = overall heat transfer conductance, kW/K or Btu/(hr-°F)

V = volume, m^3 or ft^3

ε_a = air side heat transfer effectiveness

ω_a = air humidity ratio, kg/kg dry air

ω_s = humidity of saturated air, kg/kg dry air

Subscripts:

a = air stream conditions

dry = dry surface

e = effective

i = inlet or inside condition

o = outlet or outside conditions

s = surface conditions

T = total

w = water stream conditions

wet = wet surface

In order to simplify the analysis, Merkel made two assumptions:

- The water loss due to evaporation is neglected, such that the water flow rate at each point in the tower is constant and equal to the inlet flow.

• A Lewis number of unity is also assumed.

With these approximations, the equation for the cooling tower may be reduced to:

$$\frac{dh_a}{dV} = -\frac{Ntu}{V_T}\left(h_a - h_{s,w}\right) \tag{2.67}$$

$$\frac{dT_w}{dV} = \frac{\dot{m}_a\left(dh_a / dV\right)}{\dot{m}_w C_{p,w}} \tag{2.68}$$

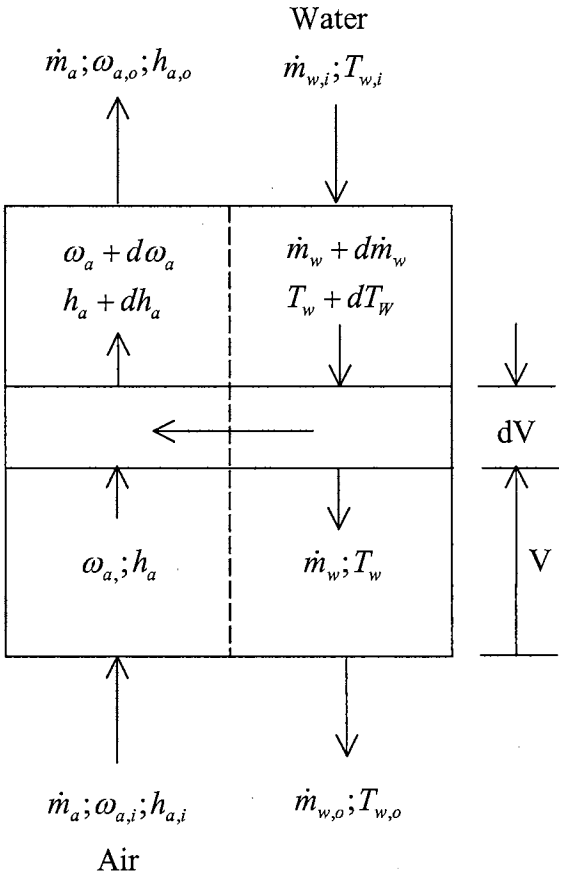

Figure 2.7. Schematic of a counter-flow cooling tower

Equation (2.68) may be rewritten in term of air enthalpies only by introducing the derivative of the saturated air enthalpy with respect to temperature evaluation at the water temperature.

$$\frac{dh_{s,w}}{dV} = \frac{\dot{m}_a C_s (dh_a / dV)}{\dot{m}_w C_{p,w}} \tag{2.69}$$

where $C_s = \left[\frac{dh_s}{dT}\right]_{T=T_w}$

C_s has the units of specific heat and will be termed the saturation specific heat. According to the authors, through the introduction of the air saturation specific heat and thus the effectiveness relationships, this approach has several advantages such as simplicity, accuracy and consistency with the methods for analyzing sensible heat exchangers. This paper presented the basic equations for effectiveness relationships for cooling coils analogous to those for sensible heat exchangers, and also provided a procedure to estimate the performance of a cooling coil having both wet and dry portions. The method was validated over wide range of conditions. The steps for determining the heat transfer and outlet conditions for a cooling coil are summarized as follows,

1) Assume that the coil is completely dry and apply the dry coil effectiveness method.
2) If the surface temperature at the air outlet determined with the dry analysis is less than the dew point of the entering air, then assume that the coil is completely wet and apply the wet coil effectiveness method.

3) If the surface temperature at the air inlet determined with the wet analysis is greater than the entering dew point temperature, then a portion of the coil is dry. At this point, the fractions of the coil that are wet and dry could be determined iteratively. More simply, choose the result of steps 1 or 2 that yields the largest heat transfer.

In order to simulate the performance of a cooling coil in a system, it is necessary to estimate the air side and water side transfer units as a function of the flows. In other words, the heat transfer coefficients *UA*'s are essential if the mass flow rate and specific heat are given according to the definition of NTU. Without specific details concerning the dimensions and configuration of the coil, the NTU is not readily available. The author provides an empirical solution as,

$$Ntu_i = k_1\left[\frac{\dot{m}_w}{\dot{m}_{w.des}}\right]^{k_2} \tag{2.70}$$

$$Ntu_o = k_3\left[\frac{\dot{m}_a}{\dot{m}_{a.des}}\right]^{k_4} \tag{2.71}$$

where $\dot{m}_w$ = water mass flow rate, kg/s or lbm/hr

$\dot{m}_a$ = mass flow rate of dry air, kg/s or lbm/hr

The author did not provide any information about how to get the values of so-called $\dot{m}_{w.des}$ and $\dot{m}_{a.des}$. But according to the form of Equations (2.70) and (2.71) which employs one of the commonly used regression techniques, they should have the values of some base case, say nominal flow rates for the heat exchanger. k_1, k_2, k_3 and k_4 are empirical

constants that may be determined with nonlinear regression applied to differences between measurements and cooling coil model predictions of the water and air outlet temperatures. This approach may not be feasible for modeling the chiller or heat pump because the detailed catalog data for the heat exchanger are usually not available from the chiller or heat pump manufacturers' catalog.

2.2.6. Parameter Estimation Technique of Rabehl, et al.

Rabehl, et al. (1999) presented a technique for developing models that can accurately reproduce cooling coil performance. This technique employed mechanistic relations with unspecified parameters as the basis for model relations. Catalog information is then used to estimate the optimal values of the parameters. Only a few geometric specifications are required. This technique is based on the fundamental heat and mass transfer correlations that are manipulated so that all geometric terms are lumped into characteristic parameters. Then the values of parameters are determined from curve fits to catalog data.

The author classified the models for heat exchangers by the degree of complexity and empiricism incorporated. Two extreme ends exist: at one end of the spectrum are simple models that highly empirical and require few geometry specifications; at the other end, detailed models for heat exchangers and coils have been developed. These detailed models are based on fundamental heat and mass transfer relations, but many require details on construction that are not often available from manufacturers' catalogs.

For chilled water cooling coil, the overall heat and mass transfer coefficient was assumed to be based on two heat transfer resistances in series: the convection heat transfer resistance between the tube fluid (e.g. chilled water) and the tube wall; and the convection heat transfer resistance between the tube/fin surface and the air. The resistance of the heat exchanger wall is neglected. The two convection resistances are assumed to have the same form of heat transfer coefficient:

$$Nu_D = C\,\mathrm{Re}_D^m\,\mathrm{Pr}^n \tag{2.72}$$

where C, m, and n are specific values for a given flow geometry. For the heat transfer coefficient between the tube/fin surface and the air, the Nusselt number relation of Zhukauskas was used as the basis for the model. Equation (2.72) was modified by introducing parameters that account for specific characteristics such as flow area, surface area, tube bank arrangement, fin efficiency, and fluid type. Generalizing Equation (2.72) yielded an equation for the heat transfer coefficient-area product in terms of the mass flow rate and fluid properties:

$$(hA)_o = C_f C_1 k_o \left(\frac{\dot{m}_o}{\mu_o}\right)^{C_2} \mathrm{Pr}_o^{0.36} \left(\frac{\mathrm{Pr}_o}{\mathrm{Pr}_{o,s}}\right)^{0.25} \tag{2.73}$$

where C_1 and C_2 are parameters that need to be determined. The effect of property variations across the flow were expressed as a Prandtl number ratio since the external

fluid is air. C_f is a convection coefficient correction factor that accounts for the totally wet operation.

The heat transfer coefficient between the inner fluid and the tube wall was based on the Sieder-Tate equation. In a manner similar to that for Equation (2.73), the relation for the heat transfer coefficient-area product inside the tubes was modified to be:

$$(hA)_i = C_3 k_i \left(\frac{\dot{m}_i}{\mu_i}\right)^{0.8} \mathrm{Pr}_i^{1/3} \left(\frac{\mu_i}{\mu_{i,s}}\right)^{0.14} \tag{2.74}$$

The values of the three characteristic heat transfer parameters C_1, C_2 and C_3 need to be fit using catalog data points.

2.2.7. Reciprocating Compressor Model of Popovic and Shapiro

Popovic and Shapiro (1995) proposed a semi-empirical model for modeling a reciprocating compressor in refrigeration systems simulations. The model is based on thermodynamics principles and a large database. The purpose of the model is to reduce the amount of data required to completely characterize compressor performance using alternative refrigerants. Two compressor performance parameters were defined. An effective pressure drop accounts for mass flow losses in the compressor, while numerically determined functional dependence of the heat transfer loss coefficient is related to compressor energy losses. The model depicted compressor operation with

reasonable accuracy. The model predicted mass flow rates and required compressor power for all data points within 10% of relative error.

As claimed by the authors, the McQuiston and Parker (1994) volumetric efficiency compressor model was the starting point in the model development. Several assumptions are incorporated into the modeling procedure. The final equation determining the refrigerant mass flow rate through the compressor is:

$$\dot{m} = \frac{RPD \cdot RPM}{v_{suc}} \left[1 + C - C \left(\frac{P_{dis}}{P_{suc}} \right)^{1/n} \right] \tag{2.75}$$

where $\dot{m}$ = refrigerant mass flow rate, kg/s or lbm/hr

RPD = rate of piston displacement, m^3/RPM or ft^3/RPM

RPM = compressor motor shaft speed (revolutions per minute)

v_{suc} = specific volume for suction state, m^3/kg or ft^3/lbm

C = clearance factor

P_{dis} = pressure at discharge state, kPa or psia

P_{suc} = pressure at suction state, kPa or psia

n = polytropic exponent

However, according to the literature survey, Threlkeld might be the first researcher who systematically presented the thermodynamic description of a mechanical vapor compression refrigeration cycle. In the book titled 'Thermal Environmental Engineering' published in 1962, he provided a few important definitions and equations that are still

widely used nowadays. The coefficient of performance expresses the effectiveness of a refrigeration system, it is a dimensionless ratio defined by the expression:

$$C.O.P. = \frac{Useful\ \ Refrigerating\ Effect}{Net\ Energy\ Supplied\ From\ External\ Source} \tag{2.76}$$

For a mechanical-compression system, work must be supplied by an external source, thus:

$$C.O.P = \frac{Q}{W} \tag{2.77}$$

where Q = refrigeration capacity, kW or Btu/hr

W = power consumption, kW or Btu/hr

In the model developed by Popovic and Shapiro (1995), the comparison was originally run assuming no pressure drops. Refrigerant mass flow rates calculated by Equation (2.75) significantly overestimated the measured mass flow rate. Thus, the presence of suction and discharge pressure drops was considered. Pressure drops were assumed to be processes with constant enthalpy in order to fix suction and discharge states for the compressor. To simplify the problem, the magnitudes of the suction and discharge pressure drops were set equal.

Accurate prediction of a refrigerant mass flow rate requires knowledge of the clearance factor, pressure drops, polytropic exponent, refrigerant inlet state, and

refrigerant outlet pressure. The clearance factor is a compressor design parameter that depends on compressor cylinder geometry. Unfortunately, compressor manufacturers were not willing to release this information. Hence, the clearance factor had to be taken as unknown parameter. The pressure drops were also taken as unknown, but were set equal to each other. In order to determine these three compressor parameters it was decided to vary each one looking for the minimum relative error between the calculated and measured mass flow rates.

2.2.8. ARI Standard 540-99

ARI standard 540-99 is to establish for positive displacement refrigerant compressors and compressor units for refrigeration application. This standard is intended for the guidance of the industry, including manufacturers, engineers, installers, contractors and users. In this standard, it is required that general performance data, covering the operational spectrum of the equipment be presented in tabular form within defined accuracies and ranges of operation. It is also required that a third order polynomial equation of 10 coefficients be used to represent the tabular data in the following form,

$$X = C_1 + C_2 \times (S) + C_3 \times D + C_4 \times (S^2) + C_5 \times (S \times D) + C_6 \times (D^2) + C_7 \times (S^3) + C_8 \times (D \times S^2) + C_9 \times (S \times D^2) + C_{10} \times (D^3) \quad (2.78)$$

Where C = equation coefficient, represents compressor performance

S = suction dew point temperature, °C or °F

D = discharge dew point temperature, °C or °F

X represents (as designated):

Power input, W or kW

Mass flow rate, lbs/hr or kg/hr

Current, A

Compressor or compressor unit efficiency

2.2.9. Ganesh et al. Coil Model

A new coil model (Ganesh 1987) for cooling and heating was employed by Ganesh et al. (1989) as a component in the overall system with either single phase (chilled or hot water coil) or two phase (DX or steam coil) fluid through the tubes. The effect of various coil parameters on the overall HVAC system performance was also studied.

Ganesh (1987) modeled steady state performance of heating and cooling coil with both one and two phase heating or chilled fluid flowing through the tubes. Once the inlet conditions of air and tube fluid is specified along with coil geometric configuration, the outlet conditions are predicted. The inlet air conditions include air flow rate, maximum air velocity, dry and wet bulb air temperatures. Coil configuration to be specified includes coil face area (length and height), tube outside diameter and thickness, tube, row and fin spacings and number of rows. If single phase fluid is used through tubes, inlet conditions are fluid velocity and temperature while for two phase fluid the inlet conditions is just the evaporating or condensing temperature.

In single phase flows, fluid inlet temperature and velocity are specified. In typical performance type calculation the length and height of the coil are specified and the temperature drop or rise is obtained form the program. In addition the program also calculates outlet air dry and wet bulb temperatures along with the total heat transfer. Coil circuitry is important since it influences the liquid mass flow and a standard coil with single row serpentine configuration and 'U' bends at opposite ends was assumed. In two phase flows, the inlet and exit conditions are fixed for the tube fluid and the mass flow rate is iterated such that both the thermodynamic and heat transfer relations are satisfied by suitable adjustments to the aspect ratio, if necessary. The output from the program is outlet air dry and wet bulb conditions and the total heat transfer. Sensible and latent components are also calculated. Coil circuitry is not critical for heat transfer calculation since the mass flow rate is iterated for convergence.

The following assumptions were made:

1) Heat transfer between heat exchanger and surroundings is negligible and that there are no thermal energy sources within the heat exchanger.
2) Only transverse heat flow across the tube wall is considered. First law of thermodynamics (ignored kinetic and potential energy changes) for an open system applied to both air side and tube fluid side. The heat exchanger equation (cross or counter-flow) is described by the log-mean temperature difference for the dry coil and by the log-mean enthalpy difference for the wet coil.

3) Thermophysical properties of moist air and tube fluid due to total pressure drop through the heat exchanger is negligible.

The main criteria used to determine whether a cooling coil is completely dry or completely wet or partially dry/wet is analogous to that used by Elmahdy and Mitalas:

1) If coil surface temperature at air inlet section is less than the dew point temperature of air at the inlet then the coil surface is all wet.
2) If the surface temperature at the air outlet section is greater than the dew point temperature of air at the inlet then the coil is completely dry.
3) If neither 1 or 2 is satisfied then the coil is partially dry/wet.

The derivation of the equations for the dry and wet portions of the coil is given in detail by Elmahdy and Mitalas (1977).

- *Cooling coil model for single phase tube fluid*

For cooling coils it is possible that dehumidification starts occurring at some point along the length of the coil when the coil surface temperature is less than the dew point temperature. This identification of the boundary is important since different equations and correlations apply to the dry and wet portion of the coil. Figure 2.8 gives a schematic of a cooling and dehumidifying coil along with the appropriate variables.

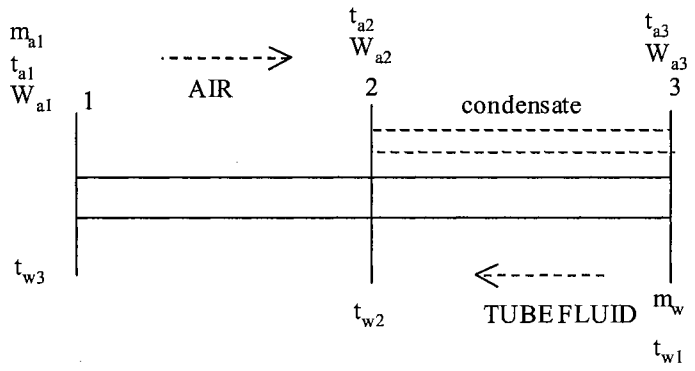

Figure 2.8. Schematic of cooling and dehumidifying coil

Dry surface:

$$Q = (t_{a1} - t_{a2})/X \tag{2.79}$$

$$Q = (t_{w2} - t_{w3})/Y \tag{2.80}$$

$$Q = U_{od} A_{od} \Delta t_{lm} \tag{2.81}$$

where $X = 1/(m_a C_{pa})$

$X = -1/(m_w C_{pw})$

$$\Delta t_{lm} = \frac{(t_{a1} - t_{w3}) - (t_{a2} - t_{w2})}{\ln(t_{a1} - t_{w3})/(t_{a2} - t_{w2})}$$

Q = heat transfer rate, kW or Btu/hr

t_{a1} = entering air temperature, °C or °F

t_{a2} = air temperature at interface, °C or °F

t_{w2} = tube fluid temperature at interface, °C or °F

t_{w3} = leaving tube fluid temperature, °C or °F

U_{od} = overall heat transfer coefficient, dry, kW/(m^2-°C) or Btu/(hr-ft^2-°F)

A_{od} = tube outside area, m^2 or ft^2

Δt_{lm} = log mean temperature difference, °C or °F

m_a = air mass flow rate, kg/s or lbm/hr

C_{pa} = air specific heat, kJ/(kg-°C) or Btu/(lbm-°F)

m_w = tube fluid mass flow rate, kg/s or lbm/hr

C_{pw} = tube fluid specific heat, kJ/(kg-°C) or Btu/(lbm-°F)

Solving the above system,

$$t_{a2} = t_{a1} - K_1(t_{a1} - t_{w2}) \tag{2.82}$$

$$t_{w3} = t_{a1} - K_2(t_{a1} - t_{w2}) \tag{2.83}$$

where $K_1 = X(Z-1)$

$K_2 = Z(X+Y)/W$

$Z = \exp\{U_{od} A_{od}(X+Y)\}$

$W = XZ + Y$

Coil surface temperature is computed from

$$(t_{s2} - t_{w2})/(t_{a2} - t_{w2}) = (\sum R - R_o)/\sum R \tag{2.84}$$

where $\sum R = R_i + R_f + R_p + R_c + R_o = 1/(U_{od} A_{od})$

$$R_i = 1/(h_i A_{pid})$$

$$R_f = F / A_{pid}$$

$$R_p = \delta_t / (k_t A_{pid})$$

$$R_c = 1/(A_{po} h_c)$$

$$R_o = 1/(h_{od} \eta_{od} A_{od})$$

t_{s2} = coil surface temperature, °C or °F

R_o = outside tube thermal resistance, m^2-°C/kW or hr-ft^2-°F/Btu

R_i = inside tube thermal resistance, m^2-°C/kW or hr-ft^2-°F/Btu

R_f = fin thermal resistance, m^2-°C/kW or hr-ft^{2}-°F/Btu

R_p = tube thermal resistance, m^2-°C/kW or hr-ft^2-°F/Btu

R_c = calculated thermal resistance, m^2-°C/kW or hr-ft2-°F/Btu

h_i = inside tube film heat transfer coefficient, kW/(m^2-°C) or

Btu/(hr-ft^2-°F)

A_{pid} = area, m^2 or ft^2

F = fouling factor

δ_t = tube thickness, m or ft

k_t = tube conductivity, kW/(m-°C) or Btu/(hr-ft-°F)

A_{po} = area, m^2 or ft^2

h_c = calculated film heat transfer coefficient, kW/(m^2-°C) or

Btu/(hr-ft^2-°F)

h_{od} = outside tube heat transfer coefficient, kW/(m^2-°C) or Btu/(hr-ft^2-°F)

η_{od} = fin effectiveness

wet surface:

$$Q = (h_{a2} - h_{a3}) / X' \tag{2.85}$$

$$Q = (h_{sw1} - h_{sw2}) / Y' \tag{2.86}$$

$$Q = U_{ow} A_{ow} \Delta h_{lm} \tag{2.87}$$

where $X' = 1 / m_a$

$$Y' = -b / (m_w C_{pw})$$

$$b = (h_{sw2} - h_{sw1}) / (t_{w2} - t_{w1})$$

In the analysis 'b' was assumed as constant since over a small range of tube fluid temperature variation this is valid.

$$\Delta h_{lm} = \frac{(h_{a2} - h_{sw2}) - (h_{a3} - h_{sw1})}{\ln(h_{a2} - h_{sw2}) / (h_{a3} - h_{sw1})} \tag{2.88}$$

Where h_{a2} = air enthalpy at interface, kJ/kg or Btu/lbm

h_{a3} = outlet air enthalpy, kJ/kg or Btu/lbm

h_{sw1} = tube surface enthalpy at tube fluid inlet, kJ/kg or Btu/lbm

h_{sw2} = tube surface enthalpy at tube fluid outlet, kJ/kg or Btu/lbm

U_{ow} = Pseudo overall heat transfer coefficient based on air enthalpy difference, kW-m^2-kJ/kg or Btu/hr-ft^2-Btu/lba

A_{ow} = area, m^2 or ft^2

Δh_{lm} = log mean enthalpy difference, kJ/kg or Btu/lbm

t_{wl} = inlet tube fluid temperature, °C or °F

Solving the above system,

$$h_{a3} = K_3 h_{a2} + K_4 h_{swl} \tag{2.89}$$

$$h_{sw2} = K_5 h_{swl} + K_6 h_{a2} \tag{2.90}$$

where $K_3 = (X'+Y')/W'$

$K_4 = X'(Z'-1)$

$K_5 = Z'(X'+Y')/W'$

$K_6 = Y'(1-Z')/W'$

$Z' = \exp\{U_{ow} A_{ow}(X'+Y')\}$

$W' = X'Z'+Y'$

Coil surface temperature is computed from:

$$h_{s2} = \Phi(t_{s2}) = R_o h_{sw2} / \sum R + (1 - R_o / \sum R) h_{a2} \tag{2.91}$$

where $\sum R = b_p (R_i + R_f + R_p + R_c) + b_w R_o = 1/(U_{ow} A_{ow})$

$R_i = 1/(h_i A_{piw})$

$$R_f = F / A_{piw}$$

$$R_p = \delta_t / (k_t A_{piw})$$

$$R_c = 1/(A_{po} h_c)$$

$$R_o = 1/(h_{ow} \eta_{ow} A_{ow})$$

b_p = value of slope 'b' evaluated at mean pipe temperature

b_w = value of slope 'b' evaluated at mean water film temperature

t_{s2} is obtained from h_{s2} by Newton-Raphson method, depending on the type of fit for $h_{s2}=\Phi(t_{s2})$. Care should be taken such that t_{s2} converges to the desired root. If h_{s2} is linear in t_{s2} in the temperature range within the coil, then t_{s2} may be solved exactly.

Outlet air temperature is calculated using the ARI Std 410-81 relation:

$$t_{a3} = t_{s3} + (t_{a2} - t_{s2}) \exp(-N) \tag{2.92}$$

$$N = A_{ow} h_{ow} \eta_{ow} / (C_{pa} m_a) \tag{2.93}$$

Partly dry and wet coil:

The appropriate equations for the dry and wet portion of the coil are applied, once the boundary between the dry and wet regions is computed.

Determination of boundary between dry/wet regions:

$$h_{a2} = h_{a1} + C_{pa} (t_{a2} - t_{a1}) \tag{2.94}$$

or

$$h_{a2} = h_{a1} - K_1 C_{pa}\left(t_{a1} - t_{w2}\right) \tag{2.95}$$

Equations (2.94) and (2.95) give:

$$h_{sw2} = \Phi(t_{w2}) = K_5 h_{sw1} + K_6\left\{h_{a1} - K_1 C_{pa}\left(t_{a1} - t_{w2}\right)\right\} \tag{2.96}$$

Since t_{w2} is the only unknown in Equation (2.96), it may be computed by Newton-Raphson technique or by solving for t_{w2} exactly if h_{sw} is linear in t_w. Once t_{w2} is computed all other quantities may be found. However, the boundary would be computed only when the coil surface temperature at the boundary is equal to the dew point temperature. An iterative algorithm was adopted. This simple algorithm always converged to the boundary, since if at any point, $t_{s2} \leq t_{dp2}$ we know that the boundary is definitely wet at that point, and that we should increase the wetted surface area. If $t_{s2} > t_{dp2}$ we know that the surface is dry at that point and that we should decrease the wetted surface area.

If the coil is partially or fully wet, one has to iterate for the mean pipe and water film temperature. In the present situation, fixed point iteration was employed and there was no problem of convergence. The equation used to check the assumed values of t_p and t_w are as follows:

$$t_{pm} = t_{w,av} + U_{ow} A_{ow}\left(h_{av} - h_{sw,av}\right)/\left(h_i A_{wi}\right) \tag{2.97}$$

$$h_{sw,m} = h_{av} - C_{pa} h_{ow} U_{ow}/\left(b_w h_{od}\right)\left\{1 - b_p U_{ow} A_{ow}/\left(h_i A_{wi}\right)\right\}\left(h_{av} - h_{sw,av}\right) \tag{2.98}$$

t_{wm} is then computed from Equation (2.96).

- *Heating coil model for single phase tube fluid*

In this case, the coil is always dry and the calculations are simplified considerably. The equations for cooling and dehumidifying coils for dry surface are true there.

- *Coil models for two phase tube fluid*

Evaporating refrigerant through tubes:

The temperature of evaporating refrigerant t_R is assumed constant through the tubes. The expressions for cooling coil model for single phase tube fluid are also valid here, but for two important changes:

1) set $Y=0=Y'$. This may be considered equivalent to sending liquid refrigerant with very high velocities through the tubes with tw1 being set equal to t_R.

2) inside film heat transfer coefficient hi for evaporating refrigerant is given by Bo Pierre's correlation for complete evaporation:

$Nu_{tp} = h_i d / k_1 = 0.0082\left(\mathrm{Re}^2\, K_f\right)^{0.5}$ for $10^9<\mathrm{Re}^2\mathrm{Kf}<0.7\times10^{12}$ and up to 11 °F superheat.

This correlation is within +10% and –20% with experiments.

Condensing steam through tubes:

This includes the following changes to the equations presented for heating coils with single phase tube fluid:

1) $tc=tw1$, $Y=0=Y'$

2) inside film heat transfer coefficient hi is given by the correlation due to Akers et al. (1959), which correlates experimental data to within 20%:

$$Nu_{tp} = h_i d / k_l = 5.0300\,\mathrm{Re}^{0.33}\,\mathrm{Pr}_l^{0.33} \quad \mathrm{Re}<5\times10^4$$

$$Nu_{tp} = h_i d / k_l = 0.0625\,\mathrm{Re}^{0.80}\,\mathrm{Pr}_l^{0.33} \quad \mathrm{Re}>5\times10^4$$

$$\mathrm{Re} = DG_{eq} / \mu_l,\ G_{eq} = G_1 + G_V\left(\rho_l / \rho_v\right)^{0.5}$$

The investigation extended the application of the new coil mode (Ganesh 1987) to other systems and showed how this model may be integrated with the performance of primary system components to estimate energy requirements during part-load operation.

The part load simulations using chilled or hot water coil was based on the performance curves for water chilling and heating equipment. Once the coil dimensions were specified, the chilling unit performance was described by two biquadratic-type equations relating the refrigerating capacity and compressor power to the suction (evaporating) temperature, and the outdoor air dry-bulb temperature as follows:

$$Q_{ref} = C_1 + C_2 t_e + C_3 t_o + C_4 t_e^2 + C_5 t_o^2 + C_6 t_e t_o + C_7 t_e^2 t_o + C_8 t_e t_o^2 + C_9 t_e^2 t_o^2 \quad (2.99)$$

$$P_c = C_1 + C_2 t_e + C_3 t_o + C_4 t_e^2 + C_5 t_o^2 + C_6 t_e t_o + C_7 t_e^2 t_o + C_8 t_e t_o^2 + C_9 t_e^2 t_o^2 \quad (2.100)$$

where C_1, C_2, ...C_9 are regression coefficients obtained by fitting regression equation to manufacturers' data. In the present situation, these equations were fitted to a commercially available condensing unit. and,

Q_{ref} = refrigerating capacity, kW or Btu/hr

P_c = compressor power, kW or Btu/hr

t_e = suction (evaporating) temperature, °C or °F

t_o = outdoor air dry bulb temperature, °C or °F

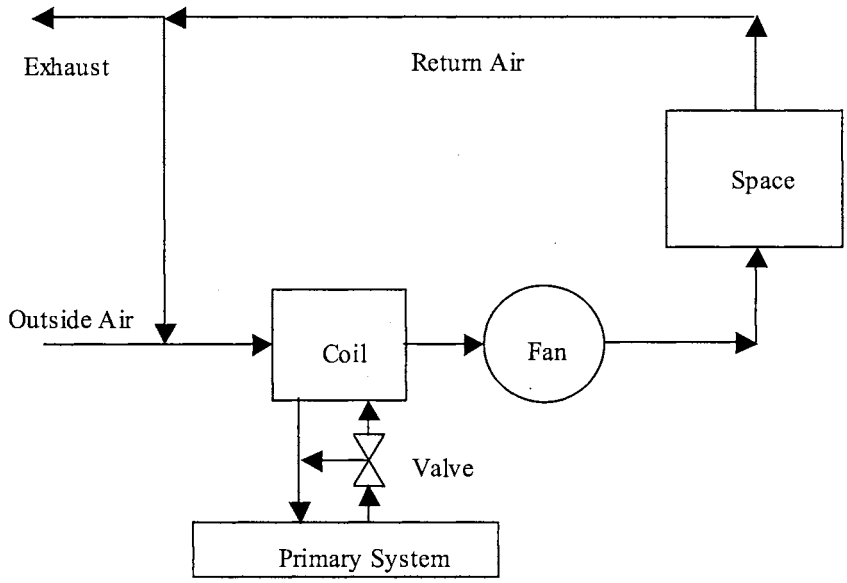

Figure 2.9. Schematic of simple HVAC system

A separate program was developed that performs multiple linear regression analysis to fit manufacturers' data in order to come up with the essential coefficient. The algorithm was obtained from Chapra and Canale (1985). Once the performance curves for the chilling and heating plant were input, the stage was set for part load simulations. Two iterative processes were involved: (1) for chilled or hot water flow rate convergence and (2) for humidity ratio convergence in space. In practice, chilled or hot water flow control may be attained by a three-way or modulating valve.

The part load simulations using DX coil that was a part of a vapor compression refrigeration system should be different. The expansion valve throttled the refrigerant such that a constant temperature was maintained at the evaporator during part-load operation. The mass flow rate of the refrigerant through the coil was adjusted such that thermodynamic and heat transfer relations were satisfied, and the convergence for air temperature off the coil and space humidity ratio were complete. This numerical control strategy has drawback, since a low evaporating temperatures (desirable due to the higher refrigeration capacity) and low loads, mass flow rates become very small and numerically it is possible for them to become negative. In such situations it would be appropriate to increase the evaporating temperature, which would result in a higher mass flow rate. The compressor performance was described by two biquadratic-type equations relating the refrigerating capacity and compressor power to the suction (evaporating) temperature and the condensing temperature as follows:

$$Q_{ref} = C_1 + C_2 t_e + C_3 t_c + C_4 t_e^2 + C_5 t_c^2 + C_6 t_e t_c + C_7 t_e^2 t_c + C_8 t_e t_c^2 + C_9 t_e^2 t_c^2 \quad (2.101)$$

$$P_c = C_1 + C_2 t_e + C_3 t_c + C_4 t_e^2 + C_5 t_c^2 + C_6 t_e t_c + C_7 t_e^2 t_c + C_8 t_e t_c^2 + C_9 t_e^2 t_c^2 \quad (2.102)$$

where C_1, C_2, ...C_9 are regression coefficients obtained by fitting regression equation to manufacturers' data. Data were fitted to a commercially available six-cylinder compressor. And,

Q_{ref}= refrigerating capacity, kW or Btu/hr

P_c = compressor power, kW or Btu/hr

t_e = suction (evaporating) temperature, °C or °F

t_o = outdoor air dry bulb temperature, °C or °F

2.2.10. Hassab and Kamal Coil Model

A model for the design of plain tube air coolers under wet, partially dry, or totally dry conditions was presented by Hassab and Kamal (1988). The authors give credit to Goodman (1938, 1939) for the fundamental work done half a century ago. Goodman assumed that the air-side heat transfer coefficient was the same for dry operating conditions as for condensing conditions. He suggested the correct driving potential for the energy transfer during forced flow condensation is the enthalpy potential. Departing from Goodman's classic approach (Goodman 1938, 1939), the new model employed new correlations for the heat and mass transfer coefficient within the heat exchanger to predict the variation of air states along the length, i.e., from one row to the next. The model was verified using a large number of test cases covering a wide range of flow rates and inlet conditions. It was then utilized to study the influence coil design parameters as well as air and water inlet conditions on its performance, characterized by the cooling load, air temperature drop, and the coil sensible heat factor. The comparison with experimental results proved the superiority of the model over procedures employing the Lewis relation.

When moist air is cooled in a cooling and dehumidifying coil, the moisture in the air is partially condensed into water in the part of coil whose temperature is lower than the local dew point of the air at this section of the coil. The simultaneous heat and mass transfer equations must be applied between air stream and the interface on one side in

conjunction with a heat transfer analysis between the cooling water and the interface on the other side. In the model the following assumption were made:

1. The basic equations are applied across each row of the coil.

2. The enthalpy of the condensate water is neglected.

3. The property of the air are evaluated at each row, based on the local mean temperature.

4. The mass transfer coefficient and heat transfer coefficient which are considered to vary from row to row are related through the correlation reported by Kamal and Hassab (1986) and given by:

$$\frac{K_{di}C_{pa}}{h_{ai}} = 1.34\left[\frac{T_{dpi}-T_{si}}{T_i-T_{si}}\right]^{-0.7}, \left(T_{dpi} > T_{si}\right) \qquad (2.103)$$

where the dew point temperature, T_{dpi} is related to the water vapor pressure, P_w (in kPa, by the following correlation:

$$T_{dp} = 6.972 + 14.427\ln\left(P_w\right) + 1.05\left[\ln\left(P_w\right)\right]^2 \qquad (2.104)$$

and,

K_{di} = local mass transfer coefficient for air, kg/m^2-s or lbm/ft^2-m

C_{pa} = air specific heat at constant pressure, kJ/(kg-°C) or Btu/(lbm-°F)

h_{ai} = local heat transfer coefficient for air, kW/(m^2-°C) or Btu/(hr-ft^2-°F)

T_{si} = tube surface temperature at the ith row, °C or °F

T_i = temperature of air outside boundary layer, °C or °F

conjunction with a heat transfer analysis between the cooling water and the interface on the other side. In the model the following assumption were made:

1. The basic equations are applied across each row of the coil.

2. The enthalpy of the condensate water is neglected.

3. The property of the air are evaluated at each row, based on the local mean temperature.

4. The mass transfer coefficient and heat transfer coefficient which are considered to vary from row to row are related through the correlation reported by Kamal and Hassab (1986) and given by:

$$\frac{K_{di}C_{pa}}{h_{ai}} = 1.34\left[\frac{T_{dpi}-T_{si}}{T_i - T_{si}}\right]^{-0.7}, \left(T_{dpi} > T_{si}\right) \qquad (2.103)$$

where the dew point temperature, T_{dpi} is related to the water vapor pressure, P_w (in kPa, by the following correlation:

$$T_{dp} = 6.972 + 14.427\ln(P_w) + 1.05[\ln(P_w)]^2 \qquad (2.104)$$

and,

K_{di} = local mass transfer coefficient for air, kg/m^2-s or lbm/ft^2-m

C_{pa} = air specific heat at constant pressure, kJ/(kg-°C) or Btu/(lbm-°F)

h_{ai} = local heat transfer coefficient for air, kW/(m^2-°C) or Btu/(hr-ft^2-°F)

T_{si} = tube surface temperature at the ith row, °C or °F

T_i = temperature of air outside boundary layer, °C or °F

Based on these assumptions, the governing equations for the process occurring in the differential area equal to the area of any row *i* may be written for cases of wet and dry surface conditions as follows.

Wet surface:

1. Mass transfer:

$$\delta m_{ci} = \dot{m}_a \delta w_i = K_{di} \delta A_i (w_i - w_{si}) \tag{2.105}$$

2. Sensible heat transfer from the air:

$$\delta Q_{ai} = \dot{m}_a C_{pa} \delta T_i = h_{ai} \delta A_i (T_i - T_{si}) \tag{2.106}$$

3. Total energy transfer form the moist air:

$$\delta Q_i = \dot{m}_a (C_{pa} \delta T_i + h_{fgi} \delta w_i) \tag{2.107}$$

4. Heat transfer to the chilled water:

$$\delta Q_i = U \delta A_i \frac{(T_{wo} - T_{wi})}{\ln\left(\frac{T_{si} - T_{wi}}{T_{si} - T_{wo}}\right)} = \dot{m}_w C_{pw} (T_{wo} - T_{wi}) \tag{2.108}$$

where m_{ci} = mass transfer rate, kg/s or lbm/hr

$\dot{m}_a$ = air mass flow rate, kg/s or lbm/hr

w_i = humidity ratio of the air outside boundary layer, kg/kg dry air or lbm/lbm dry air

A_i = coil surface area, m^2 or ft^2

w_{si} = air humidity ratio at tube surface, kg/kg dry air or lbm/lbm dry air

Q_{ai} = sensible heat transfer rate, kW or Btu/hr

Q_i = total heat transfer rate, kW or Btu/hr

h_{fgi} = latent heat of water vapor, kJ/kg or Btu/lbm

U = overall heat transfer coefficient on the water side, kW/(m^2-°C) or Btu/(hr-ft^2-°F)

T_{wo} = outlet temperature of cooling water, °C or °F

T_{wi} = inlet temperature of cooling water, °C or °F

$\dot{m}_w$ = mass flow rate of cooling water, kg/s or lbm/hr

C_{pw} = air specific heat at constant pressure, kJ/(kg-°C) or Btu/(lbm-°F)

Substitution of Equations (2.106) and (2.107) into Equation (2.108) gives:

$$\delta Q_i = h_{ai}\delta A_i(T_i - T_{si}) + K_{di}\delta A_i(W_i - W_{si})h_{fgi} \tag{2.109}$$

From Equation (2.109) one obtains:

$$\delta Q_i = U_e \delta A_i(T_{si} - T_{wi}) \tag{2.110}$$

Where $U_e = \dot{m}_w C_{pw}\left[1 - e^{-U\,\delta A_i / \dot{m}_w C_{pw}}\right] / \delta A_i$

Once the moist air becomes saturated at any section of the air cooler, it must remain saturated over the rest of the coil following that section. Under this restrictive condition, the mass transfer coefficient is to be determined at each row based on relative humidity equal to 100%. Accordingly, the process of cooling saturated air can be described by Equations (2.109) and (2.110) for the unknowns T_{i+1}, δQ_i, and T_{si}, respectively. Elimination of δQ_i and T_{si} between these equations leads to the following equation for T_{i+1}.

$$\left(1+\frac{U_e}{h_{ai}}\right)(T_i - T_{i+1}) + \frac{1}{C_{pa}}(w_i - w_{i+1})h_{fgi} - \frac{U_e \delta A_i}{\dot{m}_a C_{pa}}(T_i - T_{wi}) = 0 \qquad (2.111)$$

In above equation, the humidity ratio w_{i+1} is a known function of T_{i+1} only since air is saturated. After solving this equation for the temperature T_{i+1} (and w_{i+1}) using an iterative scheme, the variables T_{si}, δQ_i and δQ_{ai} can be determined from Equations (2.109) and (2.110), respectively. Knowning T_{si} (and w_{si}) the mass transfer coefficient, K_{di} can be determined at each row from Equation (2.108) as:

$$K_{di} = \frac{\dot{m}_a}{\delta A_i} - \left(\frac{w_i - w_{i+1}}{w_i - w_{si}}\right) \qquad (2.112)$$

Dry surface:

When the dew point temperature of the air T_{dpi} at row i becomes less than the temperature of the air at the interface T_{si}, the outer surfaces of the tubes of this row will be dry. In this case, the moisture in the air will not condensate, and the air is sensibly cooled. To determine the interface temperature T_{si}, Equation (2.111) and Equation (2.112) are combined yielding:

$$T_{si} = \left(h_{ai}T_i + U_e T_{wi}\right)/\left(h_{ai} + U_e\right) \tag{2.113}$$

The other variables, δQ_i (which equals δQ_{ai}) and $Ti+1$, can be determined from Equation (2.109).

Having evaluated the conditions of air at row i, the solution can advance up to the last row at which the conditions of the air and coolant leaving the coil are established. Furthermore, the total and sensible energy transfer from the air as well as the rate of the condensation on the coil are obtained by summing up their elemental quantities thus,

$$\begin{aligned} Q &= \sum_{i=1}^{n} \delta Q_i \\ Q_a &= \sum_{i=1}^{n} \delta Q_{ai} \\ m_c &= \sum_{i=1}^{n} \delta m_{ci} \end{aligned} \tag{2.114}$$

The coil sensible heat factor, a key design factor, is defined as:

$$SHF = Q_a / Q \tag{2.115}$$

2.2.11. Khan Coil Model

A heat and mass transfer performance analysis of a cooling and dehumidification coil at part load operating conditions was presented by Khan (1994). For this purpose, a set of coupled differential equations describing the heat and mass transfer from a water cooled coil is solved numerically. Several controlling parameters are identified to analyze the part load performance of a coil that is allowed to operate under dry, partially wet, and completely wet modes. Air side enthalpy and humidity effectiveness are defined and used to report the part load performance. Finally, the part load performance as predicted by the numerical model is compared with an easy-to-use procedure and with catalog data for commercially available cooling coils.

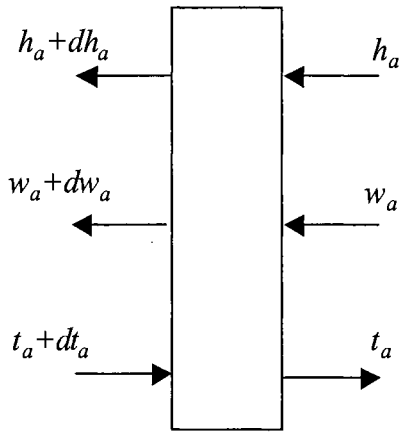

Figure 2.10. Schematic for counter flow cooling coil control volume

A differential control volume in a typical counter flow cooling and dehumidification coil is used to develop the governing equation. The following assumptions are made in the derivation of equations.

1. Dry air and water vapor in the air are treated as a non-reacting mixture of ideal gases.
2. Air and water flow directions are in an overall counter-flow configuration, as the local cross-flow effects in each control volume are neglected. This assumption is valid, as the performance of a cross-flow heat exchanger approaches that of a counter flow heat exchanger when the number of the tube passes is greater than four.
3. The air side heat transfer coefficient includes the additional thermal resistance due to the presence of dry, partially wet, or completely wet extended surfaces.
4. Both the air and the water are well mixed in the cross section normal to its flow; therefore, only gradients for each fluid exist in their respective flow directions.
5. In the case of dehumidification, the condensate is removed by gravity from the coil surface.

After the above assumptions are made, the change in the bulk air enthalpy and humidity ratio and the change in water temperature for the control volume considered in Figure 2.10 can be written as

$$\frac{dh_a}{dA_o} = -\frac{NTU_o}{A_o}\left[\left(h_a - h_{s,t_s}\right) + \left(w_a - w_{s,t_s}\right)\left(\frac{1}{Le_o} - 1\right)h_{v,t_s}\right] \qquad (2.116)$$

$$\frac{dw_a}{dA_o} = -\frac{NTU}{Le_o A_o}\left(w_a - w_{s,t_s}\right) \qquad (2.117)$$

and

$$\frac{dt_w}{dA_i} = \frac{NTU_i}{A_i}(t_w - t_s) \tag{2.118}$$

where

$$NTU_i = \frac{h_{c,i} A_i}{\dot{m}_w C_{p,w}} \tag{2.119}$$

$$NTU_o = \frac{h_{c,o} A_o}{\dot{m}_a C_{p,m}} \tag{2.120}$$

and

$$Le_o = \frac{h_{c,o}}{h_{d,o} C_{p,m}} \tag{2.121}$$

where h_a = specific enthalpy, moist air, kJ/kg or Btu/lbm

A_o = outside surface area, m^2 or ft^2

NTU_o = number of transfer unit for outside surface

$h_{s,ts}$ = specific enthalpy of saturated air at surface temperature, kJ/kg or Btu/lbm

w_a = air humidity ratio, kg/kg dry air

$w_{s,ts}$ = saturated air humidity ratio at surface temperature, kg/kg dry air

Le_o = outside surface Lewis number

$h_{v,ts}$ = specific enthalpy of water vapor at surface temperature, kJ/kg

t_w = water temperature, °C or °F

A_i = inside surface area, m^2 or ft^2

NTU_i = number of transfer unit for inside surface

t_s = surface temperature, °C or °F

$h_{c,i}$ = inside surface convective heat transfer coefficient, kW/(m^2-°C) or Btu/(hr-ft^2-°F)

$\dot{m}_w$ = water mass flow rate, kg/s or lbm/hr

$C_{p,w}$ = constant pressure specific heat of liquid water, kJ/(kg-°C) or Btu/(lbm-°F)

$h_{c,o}$ = outside surface convective heat transfer coefficient, kW/(m^2-°C) or Btu/(hr-ft^2-°F)

$\dot{m}_a$ = dry air mass flow rate, kg/s or lbm/hr

$C_{p,m}$ = constant pressure specific heat of moist air, kJ/(kg-°C) or Btu/(lbm-°F)

$h_{d,o}$ = outside surface mass transfer coefficient, m/s or ft/m

$h_{f,ts}$ = specific enthalpy of condensate water at surface temperature, kJ/kg

Also the equations for conservation of energy and mass for this control volume can be written as

$$\frac{dt_w}{dA_i} = \frac{-\dot{m}_a\left(\frac{dw_a}{dA_o}h_{f,ts} - \frac{dh_a}{dA_o}\right)}{\dot{m}_w C_{p,w}} \tag{2.122}$$

and

$$d\dot{m}_a = d\dot{m}_w = 0 \tag{2.123}$$

Thus, Equations (2.119) through (2.121) along with Equation (2.122), constitute the set of equations that can be solved for a given value of NTU_o, NTU_i, Le_o, the water-to-air

mass flow rate ratio, and the air and water inlet conditions to predict the air and water exit conditions for a cooling coil.

2.2.12. Expansion Device

The expansion device for controlling the refrigerant flow is normally a thermostatic expansion valve for heat pumps (ASHRAE 1996). A capillary tube is also used for some cases. But it may pass refrigerant at an excessive rate at low back pressures, causing liquid flood-back to the compressor. The thermostatic expansion valve controls the flow of liquid refrigerant entering the evaporator in response to the superheat of the gas leaving it. It functions to keep the evaporator active without permitting liquid to return through the suction line to the compressor. The thermostatic expansion valve is widely used for controlling refrigerant flow to all types of evaporators in air conditioning equipment (industrial, commercial, and residential applications). The capillary tube is especially popular for smaller unitary hermetic equipment. A wide range of conditions is often essential for heat pumps and a capillary tube won't be able to operate correctly over as wide a range of conditions as does a thermostatic expansion valve. Capillary tubes are not usually chosen as the expansion device for heat pumps. However, capillary tubes are less costly and may perform nearly as well for smaller units operating under a relatively narrow range of conditions. In the heat pump models previously developed, no matter what expansion device (capillary tube or thermostatic expansion valve) the authors claimed has been incorporated and simulated, usually an adiabatic throttling process was assumed. The heat pump models did not explicitly model the expansion device. The

refrigerant mass flow rate was determined by the compressor model. For example, this assumption can be found in the Greyvenstein (1988)'s heat pump model. It is a simplified approach to model the performance of the expansion device in heat pumps. However, since the target of those models is not trying to re-design the heat pump to improve its performance based on a more sophisticated evaluation of the expansion device, this simplification may be acceptable.

2.2.13. Modeling of Rotary Compressors

2.2.13.1. Analysis of Chu, et al.

The exact performance of a hermetic rolling-piston type rotary compressor used for domestic room air conditioner has been evaluated concerning with volumetric efficiency and power consumption (Chu, et al. 1978). To compute the power consumption, the authors considered gas compression work, mechanical loss, and driving motor loss.

The gas compression work is estimated based on the polytropic compression work, over-shooting loss in the discharge stage, under-shooting loss in suction stage, gas leakage loss, heating loss by oil leakage, and compression loss of the top clearance volume. The polytropic compression work is calculated as,

$$L_{pol} = v_2 \eta_v \frac{n}{n-1} P_s G_o \left[\left(\frac{P_d}{P_s} \right)^{\frac{n-1}{n}} - 1 \right] \tag{2.124}$$

where v_2 = specific volume at the suction state, m^3/kg or ft^3/lbm

η_v = volumetric efficiency

n = polytropic exponent

P_s = suction pressure, kPa or psia

G_o = theoretical refrigerant mass flow rate, kg/s or lbm/hr

P_d = discharge pressure, kPa or psia

Under-shooting in suction stage is reduced since no suction valve is present. Other losses are evaluated with integration of the parameters of detailed configuration and status data.

2.2.13.2. Analysis of Wakabayashi, et al.

Another analysis of the performance of a rolling piston type hermetic compressor for a room air conditioner has been presented by Wakabayashi et al. (1982). Influence of several factors on compressor performance were studied experimentally. Cylinder pressure as well as temperatures of refrigerant gas, oil, and cylinder wall were measured. A detailed distribution and rates of losses were calculated from the measurements. The heat exchange in the cylinder was simulated. The results from the simulation were found to agree with the experimental data favorably. The theoretical power was expressed by Equation (2.125),

$$L_{th} = \frac{k}{k-1} P_s v_s G_s \left[\left(P_d / P_s \right)^{\frac{k-1}{k}} - 1 \right] \qquad (2.125)$$

where k = adiabatic exponent

P_s = suction pressure, kPa or psia

v_s = specific volume of suction gas, m^3/kg or ft^3/lbm

G_s = measured gas flow rate, kg/s or lbm/hr

P_d = discharge pressure, kPa or psia

Simulation results such as leakage of hot refrigerant gas and oil through piston clearances, and heat transfer from cylinder wall to gas in cylinder have been compared with the experimental results. The authors concluded that decreasing heat transfer loss was very important for improving performance as well as decreasing leakage loss.

2.2.13.3. Simulation Model for Fixed Vane Rotary Compressor of Gyberg and Nissen

Gyberg and Nissen (1984) presented a model based on a control volume for suction and pressure volume. The first law of the thermodynamics and the law of continuity ub dynamic form are used on these control volumes. This means the thermodynamic properties, mass flow, heat effect and compression power are calculated as a function of the time or angle of rotation instead of a static average value.

2.2.13.4. Model of Rotary Compressor to Simulate its Transient Behavior by Yanagisawa et al.

A mathematical model of rotary compressor which can predict its transient behavior has been developed by Yanagisawa et al. (1990). The model takes compression work and heat transfer into consideration and consists of governing differential equations on specific enthalpy of refrigerant and temperature of a compressor body. To obtain a good agreement between model prediction and experimental results, some parameter values are used as follows,

(1) compression power – shaft power of motor
(2) representative temperature of heat transferring refrigerant in lower chamber – average of temperature after receiving compression power and temperature in lower chamber
(3) representative temperature of heat transferring refrigerant in upper chamber – average of lower chamber temperature and upper chamber temperature
(4) product of heat transfer coefficient and heat transfer surface area – empirical value estimated from compressor performance at standard operating condition.

2.2.13.5. An Analytical Model for Rotary Air Compressor by Huang

Huang (1999) developed an analytical model for a rotary compressor with diagonally symmetrical two inlet ports and two outlet ports, elliptical inner contour stator

and sliding blades. The displacement, velocity, acceleration of the blades were studied. The effects of the polytropic exponent and blades number on the air pressure and temperature were investigated using the continuity equations, ideal gas relation, compression polytropic process and conservation of energy. A value for the polytropic exponent is selected for prediction of the fluid properties, interactions of the blades with the rotor and the stator, and efficiency for the specified compressor. The blade segment volume, friction power loss and flow rate versus the rotor rotational speed are also analyzed.

2.2.13.6. Dynamic Analysis of a Rotary Compressor by Padhy

A theoretical treatment of the roller and vane dynamics of the rotary compressor has been presented by Padhy (1994). The total linear roller velocity at the vane and roller contact line is evaluated. The change in direction for the forces are incorporated. The vane slapping motion has been determined form the direction of the vane side reaction forces. Roller velocity was measured using high speed video technology and good agreement is found between the experimental data and the theoretical results.

2.2.13.7. A Simulation Model of an A/C Rotary Vane Compressor by Takeshita

A simulation model for rotary vane compressor has been developed by Takeshita (1997). The features of this model are the compression algorithm that makes extensive use of entropy tracking and the real R134a properties in the form of look-up table rather

than a polytropic equation. Compression process was modeled as an isentropic process with mass flow into and out of the compression chamber and flow through the valves. The simulation output included torque, torque variance, heat capacity, coefficient of performance. Two simulation examples have been presented to demonstrate how the model could provide useful insight for the design and part optimization.

2.2.13.8. A Computer Simulation of a Rotary Compressor by Ooi and Wong

Analytical studies of a fractional horse-power rotary refrigeration compressor has been presented by Ooi and Wong (1997). The model was used in assisting the design of new compressors. The study also paved a way for more comprehensive simulation studies and for possible overall computerized optimization design study in the future. The model incorporated basic working principles of the compressor, thermodynamic simulation of the working chamber, valve flow and valve dynamics, as well as the mechanical losses of the moving components.

2.2.13.9. Heat Transfer Analysis of a Rolling-Piston Rotary Compressor by Padhy and Dwivedi

Mathematical modeling of the heat transfer of a rolling-piston compressor has been described by Padhy and Dwivedi (1994). It is also called 'a lumped mass model' by the authors. The system equations were developed using the thermal conductance concept. Heat transfer coefficients were calculated from the empirical/theoretical equations

adapted from various sources. Mechanical and electrical losses were considered as heat additions to the system. The model is capable of predicting the temperature of the compressor at different locations, calculating the various heat transfers between components and evaluating the mechanical losses at various interfaces.

2.2.13.10. A review of Rotary Compressor Design Evolution for Heat Pump Application by Barratt and Murzinski

The paper of Barratt and Murzinski (1987) was to review the evolutionary changes that took place in developing a typical rotary compressor to meet the special challenge of heat pumps with long life and reliable performance. Emphasis was given to the introduction of improved materials used in the compressor design.

2.3. Literature Review Summary

The heat pump or chiller models presented in all the papers reviewed may be classified between the two extremes of the scheme introduced in section one. Traditional equation-fit model is one end of the spectrum and three models belong to this category: [Stoecker and Jones (1982), Allen and Hamilton, 1983; Hamilton and Miller, 1990]. This approach is widely used in a few building-HVAC simulation programs for its good accuracy within the allowed operation range and its simplicity of computation.

The rest of the models in the literature review actually fall between the two extremes, the detailed deterministic models often apply equation-fitting for some of the components. These models are aimed at modeling for chillers or heat pumps using the basic thermodynamics laws for the conservation of mass, energy and momentum and heat and mass transfer rate equations. Generally, such modeling approaches depend on the availability of internal measurements. However, the prediction accuracy is generally not as good as the equation-fit approach. It also requires more calculation effort than the equation-fit method. To improve on the "pure" deterministic models, some researchers (e.g. Bourdouxhe, et al. 1994) have developed models that introduce some equation-fitting into the deterministic approach. These modeling approaches have proved to be robust and they are capable of accurately replicating the catalog or experimental data over the entire operation range. They also provide comparatively detailed information for each component and the entire system.

3. Objectives and Scope

As mentioned in the introduction section, the specific objective of the research is to develop heat pump models based on the data published by manufacturers' catalogs where no detailed experimental internal measurements of each component are available. This model is expected to be an alternative for commonly used regression or equation-fitting approach in well-known computer programs such as TRNSYS, HVACSIM+ and Energyplus and is expected to be capable of reasonable accuracy over a wide operation range. The accomplishment of this dissertation may be divided into five stages. The focus of each stage is described as follows.

The first stage involves the review, analysis, evaluation and comparison of currently available chiller and heat pump simulation models. The goal at this stage is to acquire an extensive yet intensive understanding of the theoretical fundamentals of these models. The advantage and disadvantage of the currently available models are to be analyzed and evaluated in depth. The questions may include: how can a mathematical model of each component be established? how can each component model be combined together or what is the algorithm of the performance calculation for the whole heat pump? and what experimental data are required to estimate the performance of the heat pump? This literature survey shall become the basis of later research work and the model developed by the author. The literature survey has been described in Chapter 2 of this dissertation.

The next stage concerns the development of water-to-water heat pump and water-to-air heat pump simulation models that are capable of forecasting the performance with a reasonably good conformity to the catalog data. This model shall be different from other models developed so far from at least two viewpoints. First, it is similar to deterministic models that give each component of the heat pump a physically meaningful mathematical description. Secondly, since the experimental or catalog data available from the manufacturer are usually not in such detail as required by some models previously developed, this model will be capable of predicting the performance with only the limited information in the catalog data, such as load side and source side entering water temperature, mass flow rate, cooling capacity and power input. In other words, without detailed experimental data for each component, the model shall be able to identify the parameters that describe each component of the heat pump. Together with an appropriate algorithm, it will provide a relatively accurate prediction of the performance. A model for a water-to-water heat pump will be described in Chapter 4. Due to the complication of the load side heat exchangers in water-to-air heat pumps, a more sophisticated model for the load side heat exchanger shall be incorporated into the heat pump model with other components same as those of the water-to-water heat pump model developed. The water-to-air heat pump model will be the focus of Chapter 5.

The third stage involves the extensions of the heat pump models. Reciprocating compressors have been assumed in the water-to-water and water-to-air heat pump models. However, since scroll compressors and rotary compressors are two frequently used alternatives to reciprocating compressors, it is desirable to develop models of scroll

and rotary compressors that can replace the reciprocating compressor model in the heat pump models presented in Chapter 4 and Chapter 5. While necessary in many applications for providing freeze protection, antifreeze solutions adversely impact heat transfer performance. It is also desirable to be able to model water-source heat pumps when the secondary heat transfer fluid is a water-antifreeze mixture. Chapter 6 of this dissertation addresses this stage.

The fourth stage is to validate the water-to-water heat pump model. The parameter estimation based water-to-water heat pump model has been evaluated with selected experiments. The experiments were performed at the medium-scale bridge deck heating system set up for the experimental work of the Geothermal Smart Bridge project. Experimental data have been collected under various operation conditions. Three data sets that collected in December of 2000 and December of 2001 have been used to validate the parameter estimation model. The experimental validation of the water-to-water heat pump model is the topic of Chapter 7.

In the last stage, an experimental validation of the water-to-air heat pump model has been accomplished. Some monitored field data have been collected at the test cell building located to the north of Mechanical and Aerospace Engineering Research Labs. Comparisons between the model prediction and experimental data have been implemented. This topic will be addressed in Chapter 8.

4. A Parameter Estimation Based Model for Water-To-Water Heat Pumps

Reciprocating vapor compression heat pumps and chillers have been the target of a number of simulation models. Hamilton and Miller (1990) presented a classification scheme for air conditioning equipment with two extremes. At one end of the spectrum are equation-fit models, called "functional fit" models by Hamilton and Miller, which treat the system as a black box and fit the system performance to one or a few large equations. At the other end are deterministic models, called "first principle" models by Hamilton and Miller, which are detailed models based on applying thermodynamic laws and fundamental heat and mass transfer relations to individual components.

Many of the models found in the literature might actually fall between the two extremes, although the detailed deterministic models often apply equation-fitting for some of the components. For example, in the reciprocating chiller model proposed by Bourdouxhe, et al. (1994), the chiller was modeled as an assembly of several simplified components. Each component (e.g., compressor, evaporator, condenser, expansion device) is modeled with a detailed deterministic approach. The parameters describing the detailed physical geometry and operation of each component are then adjusted (i.e., in an equation-fitting procedure) to reproduce the behavior of the actual unit as accurately as possible. The model of Bourdouxhe, et al. requires more details for each component than are usually available from manufacturers' catalogs. This type of model is most suitable for users that have access to internally measured data (e.g., in Bourdouhxe's model,

condensing and evaporating temperatures and subcooling and superheating temperature differences) from the chiller or heat pump.

The alternative approach, equation-fitting, alleviates the need for internally measured data and usually maintains better fidelity to the catalog data. It also usually requires less computational time. These models are most suitable for users that only have access to catalog data. These models would not be useful for someone attempting to design a heat pump or chiller by modifying or replacing internal components. Especially troublesome for some applications, extrapolation of the model may lead to unrealistic results.

For use in energy calculation and/or building simulation programs, it is desirable to have a model that only requires catalog data, but allows extrapolation beyond the catalog data. In the authors' experience, this model has also been useful for modeling of ground source heat pumps in novel applications where the fluid temperatures occasionally go beyond the catalog data. It has also proven useful in simulations that are part of a ground loop sizing procedure. In this application, it often happens that the temperatures are well beyond the catalog data. Even though the ultimate outcome is that the ground loop heat exchanger size will be adjusted to bring the temperatures within reasonable limits, it is helpful to have a model that does not catastrophically fail when the temperatures are too high or too low.

The model presented in this paper uses deterministic models of each heat pump component. Each of the fundamental equations describing the system components may have one or more parameters, which are estimated simultaneously using catalog data only; no other experimental data are required. The parameter estimation is done with a multi-variable optimization method. Once the parameters have been estimated, the heat pump model may be used as part of a multi-component system simulation.

This modeling approach has the advantage of not requiring experimental data beyond what is published in the manufacturer's catalog. Yet, its predictions are of similar or better accuracy than previously published deterministic models that required additional experimental data. Unlike the equation-fit models, the model domain may be extended beyond the catalog data without catastrophic failure in the prediction.

Simulation models of vapor-compression refrigeration and air-conditioning systems such as heat pumps and chillers have been the topic of numerous papers. The models can generally be classified in terms of the degree of complexity and empiricism. A review of the literature reveals a few limitations on existing models. For the more deterministic models, there is a gap between what data are provided by manufacturers' catalogs and what data the simulation models require. For equation-fit models, the valid application is limited to the manufacturer-supplied data range and conditions.

Stoecker and Jones (1982), Allen and Hamilton (1983), and Hamilton and Miller (1990) have presented steady-state equation-fit models of vapor compression

refrigeration systems with reciprocating compressors. The Allen and Hamilton (1983) model utilizes overall system data, e.g. entering and leaving water temperatures and flow rates. The models of Stoecker and Jones (1982) and Hamilton and Miller (1990) require more detailed data, such as internal refrigerant pressures and temperatures. Consequently, the latter two models will be difficult to use for engineers who only have access to catalog data.

Gordon and Ng (1994) proposed a simple thermodynamic model for reciprocating chillers that they suggest might be valuable for diagnostic purposes. The model predicts the COP over a wide range of operation conditions from the inlet fluid temperatures and the cooling capacity, using three fitted parameters. The prediction of COP is remarkably good for a range of different chillers. However, the model doesn't predict the cooling capacity; it is required as an input. A chiller model presented by Shelton and Weber (1991), is similar in approach, and also has the same limitation of requiring the cooling capacity as an input.

The quasi-static reciprocating chiller model developed by Bourdouxhe, et al. (1994) are characterized by the authors as being part of a toolkit "oriented towards simple solutions with a minimum number of parameters" and being somewhere between "curve-fitting, the traditional way to describe the input-output relationships, and deterministic modeling, which is an exhaustive description of the physical phenomena". Their approach is to utilize a "conceptual schema" as a modeling technique to represent the unit as an assembly of classical and elementary components. The behavior of the each

component is then modeled by a deterministic approach. This approach requires fewer parameters and experimental data compared with the models developed previously. In the parameter identification procedure, the "available experimental data" such as the condensing and evaporating temperatures, the possible subcooling and superheating are required. Based on these experimental results, the parameters of the compressor are identified. Then the whole chiller is considered to identify the evaporator and condenser heat transfer coefficients. However, those experimental data are normally not available from manufacturers' catalogs.

Parise (1986) developed a vapor compression heat pump simulation model to predict the overall performance of a system. Simple models for the components of the heat pump cycle were employed. Input data include compressor speed, displacement volume, clearance ratio and other parameters for a comparatively detailed description of each component.

Cecchini and Marchal (1991) proposed a computer program for simulating refrigeration and air conditioning equipment of all types: air-to-air, air-to-water, water-to-water and water-to-air. Some parameters characterizing the components require experimental data from equipment testing, such as the heat exchanger mean surface temperatures, the saturation pressures in both evaporator and condenser, and superheating and subcooling. Again, these data are not typically provided in manufacturers' catalogs.

Fischer and Rice (1983) developed an air-to-air heat pump model to predict the steady-state performance of conventional, vapor compression heat pumps in both heating and cooling modes. The motivation for the development of this model is to provide an analytical design tool for use by heat pump manufacturers, consulting engineers, research institutions, and universities in studies directed toward the improvement of heat pump efficiency. The compressor was modeled using the data "curve-fits" and "compressor maps" provided by the manufacturers. Modeling of the other components employed many fundamental correlations and detailed design data are required. Hence, while this model may be useful in the heat pump design process, it is difficult or impossible for an engineer working from catalog data to use. Similarly, the water-to-air heat pump model developed by Greyvenstein (1988) is also based on detailed information component information, including the fan curve, compressor characteristics, heat exchanger geometry, etc.

The superheat–controlled water-to-water heat pump model developed by Stefanuk, et al. (1992) may be the most detailed model presented to date. The authors claim "The model is derived entirely from the basic conservative laws of mass, energy, momentum and equations of state as well as fundamental correlations of heat transfer." Values of the parameters that describe the behavior of the individual components are assumed to be available. For example, the parameters of the compressor are selected by "fitting the model to manufacturer-supplied performance curves that related mass flow rate and input electrical power to evaporation temperature and the compressor discharge pressure." However, they are not normally available in the heat pump manufacturers' catalogs.

Comparisons between the experimental measurements and model predictions for the evaporating and condensing pressures, the heat transfer rates in the evaporator and the condenser, and the COP of the heat pump are given. Except a few points with errors beyond ±10%, most of the results are generally acceptable. The predictions of the heat transfer rates in both heat exchangers are consistently too high. The authors explain that the cause for this phenomenon is the overestimated predictions of heat transfer coefficients since heat transfer coefficients used in the model are only known to within ±20%.

Damasceno, et al. (1990) compared three steady-state air-to-air heat pump computer models. Two of them are available in the open literature; the third one was developed in-house. These are: 1) the MARK III model, which is an updated version of an earlier program developed at Oak Ridge National Lab. by Fischer and Rice (1983) and Fischer et al. (1988), 2) HPSIM, developed at NBS by Domanski and Didion (1983) and 3) HN, developed by Nguyen and Goldschmidt (1986) and updated by Damasceno and Goldschmidt (1987). All three models require extensive test data for calibration. A more extensive comparison and summary of the heat pump and chiller models developed so far are shown in Table 4.1.

Domanski and McLinden (1992) presented a simulation model called 'Cycle-11'. 'Cycle-11' and its derived versions are models targeted at the preliminary evaluation of performance of refrigerant and refrigerant mixtures in the vapor compression cycle. Hence, to facilitate this function, the input to the program normally includes the outlet

temperature for the heat transfer fluids. In the UA version of 'Cycle-11' (Domanski 2000), the author simplified the heat exchanger model to use a constant heat transfer coefficient *UA*. However, the approach to obtain the value of this constant UA is not addressed explicitly. The input to the program also includes internal specifications for the components, such as the compressor swept volume, compressor speed, and electric-motor efficiency. The authors assumed that this information is already available. Some other internal pressure and temperature changes are calculated using simplified pressure-drop and heat transfer correlations. They are obtained from a separate program and specified as inputs for the model.

Clearly, while there are a number of models available for vapor compression refrigeration systems, all that provide the advantages of the deterministic approach require detailed data beyond what is typically provided in manufacturers' catalogs. However, many users of such models only have access to catalog data. Therefore, it would be useful to have a model that uses a deterministic approach, but only requires catalog data. Such a model has been developed and is the topic of this paper.

The objective of this research effort is to develop a water-to-water heat pump model suitable for use in energy calculation and/or HVAC system simulation programs. Furthermore, it is desired that the model accurately duplicate the water-to-water heat pump performance, utilize catalog data for parameter estimation, require a minimal number of data points, and allow extrapolation. The modeling method employs mechanistic relations of fundamental thermodynamic laws and heat transfer correlations

with parameters identified from catalog data. There are numerous options for the selection of parameters. A number of combinations of parameters have been investigated, and the scheme that provides the best results, i.e. least relative error, is presented in detail. The other schemes are discussed and their results are compared with the final one.

Table 4.1. Literature Review Summary for Heat Pump & Chiller Models

<table>
<tr><th rowspan="2">Author</th><th rowspan="2">Year</th><th colspan="4">Compressor</th><th colspan="3">Evaporator & Condenser</th><th>Expansion Device</th></tr>
<tr><th>Suction & Discharge Pressure Drop</th><th>Compression</th><th>Re-expansion of Clearance Vapor</th><th>Shell Loss or Efficiency</th><th>Refrigerant Pressure Drop</th><th>Superheating, & Subcooling</th><th>Heat Transfer Coefficient</th><th></th></tr>
<tr><td>Stoecker & Jones</td><td>1982</td><td colspan="8">Non-Deterministic/Component Level Equation-fit Model</td></tr>
<tr><td>Allen & Hamilton</td><td>1983</td><td colspan="8">Non-Deterministic/Overall System Level Equation-fit Model</td></tr>
<tr><td rowspan="3">Fischer & Rice (Mark I) Revisions of Fischer & Rice's Model, 1983 (Mark III to Mark V)</td><td rowspan="3">1983 to 1996</td><td colspan="4">Curve-fit/map-based model</td><td rowspan="3">Yes</td><td rowspan="3">Yes</td><td rowspan="3">Variable</td><td>1) Capillary tube: Equation-fit</td></tr>
<tr><td colspan="4">Deterministic/loss and efficiency-based model</td><td>2) TXV: General Model & Empirical Correlations</td></tr>
<tr><td>No</td><td>Isentropic</td><td>Yes</td><td>Yes</td><td>3) Short Tube Orifice: Empirical correlations</td></tr>
<tr><td rowspan="3">Domanski & Didion Revision of Domanski & Didion's Model</td><td rowspan="3">1984 to 2000</td><td rowspan="2">1) No</td><td>1) Isentropic</td><td>1) Zero clearance volume</td><td rowspan="3">Yes</td><td rowspan="3">Yes Specified as input</td><td rowspan="3">Yes Individual sections specified as input</td><td>1) Variable</td><td rowspan="3">Adiabatic

Detailed model for constant flow area expansion device</td></tr>
<tr><td>2) Polytropic</td><td rowspan="2">2) Typical clearance volume</td><td rowspan="2">2) Assumed Constant</td></tr>
<tr><td>2) Yes Specified as input</td><td>3) Either of above with volumetric efficiency</td></tr>
<tr><td>Parise</td><td>1986</td><td>No</td><td>Polytropic</td><td>Polytropic</td><td>No</td><td>No</td><td>Yes Account for the ΔT using arithmetic average with 2-phase temp</td><td>Assumed Constant specified as input</td><td>Isenthalpic</td></tr>
<tr><td>Greyvenstein</td><td>1988</td><td colspan="4">Interpolation of manufacturers' performance data</td><td>Yes</td><td>Yes</td><td>Variable</td><td>Adiabatic</td></tr>
<tr><td>Hamilton & Miller</td><td>1990</td><td colspan="8">Non-Deterministic/Component Level Equation-fit Model</td></tr>
<tr><td>Cecchini & Marchal</td><td>1991</td><td>No</td><td>Polytropic</td><td>Polytropic</td><td>No</td><td>No</td><td>Assumed Constant</td><td>Variable</td><td>Isenthalpic</td></tr>
<tr><td>Shelton & Weber</td><td>1991</td><td colspan="8">Only kW/ton is computed</td></tr>
<tr><td>Stefanuk et al</td><td>1992</td><td>Yes</td><td>Isentropic</td><td>Isentropic</td><td>Yes</td><td>No</td><td>Yes</td><td>Variable</td><td>Adiabatic Isenthalpic</td></tr>
<tr><td>Bourdouxhe et al.</td><td>1994</td><td>No</td><td>Isentropic</td><td>Isentropic</td><td>Yes</td><td>No</td><td>No</td><td>Assumed Constant</td><td>Adiabatic Isenthalpic</td></tr>
<tr><td>Gordon & Ng</td><td>1994</td><td colspan="8">Only COP is computed</td></tr>
</table>

4.1. System Description

The heat pump configuration used in this study is presented in Figure 4.1. The heat pump consists of four basic components: reciprocating compressor, evaporator, condenser and expansion device. Other components are neglected due to the comparatively small contribution to the thermodynamic analysis for the entire system. Assuming an isenthalpic process in the expansion device and no heat exchange between this system and its environment, in case of the cooling mode, we have:

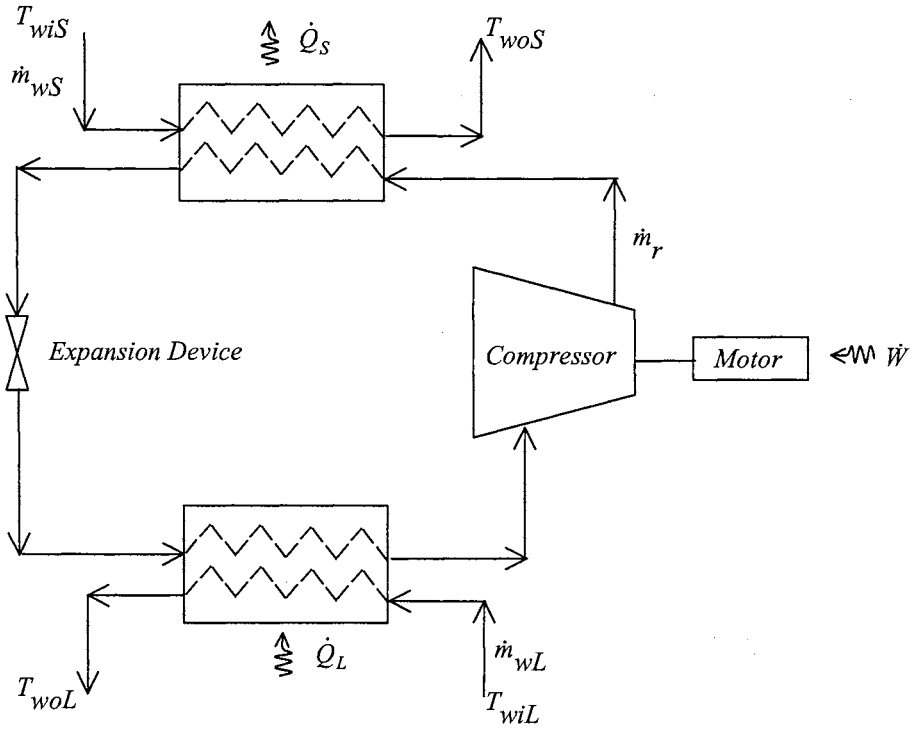

Figure 4.1. Basic heat pump configuration

$$\dot{Q}_S = \dot{W} + \dot{Q}_L \tag{4.1}$$

where $\dot{Q}_S$ = source side heat transfer rate, kW or Btu/hr

$\dot{W}$ = compressor power input, kW or Btu/hr

$\dot{Q}_L$ = load side heat transfer rate, kW or Btu/hr

Equation (4.1) assumes that no heat is lost from the compressor, when in actuality, there will be some heat transferred from the compressor shell. Generally, this loss will be fairly small, and heat pump manufacturers' catalog data neglects this heat loss. i.e., the catalog data is consistent with Equation (4.1).

4.2. Compressor Model

The thermodynamic cycle for an actual single-stage system may depart significantly from the theoretical cycle. The principal departure occurs in the compressor. Hence, it is worthwhile to pay more attention to the thermodynamic processes occurring within a reciprocating compressor. The representation of the compressor cycle, shown in Figure 4.2, follows that of Threlkeld (1962).

Several assumptions are incorporated into the modeling procedure:

- The modeled compressor cycle is only an approximation of the real compressor cycle
- The compression and expansion in the compressor cycle are isentropic processes with equal and constant isentropic exponents.
- The isentropic exponent is dependent on the refrigerant type; the values of the isentropic exponents are obtained from the Bourdouxhe et al. (1994) that are originally based on the study of Saavedra (1993).

- The oil has negligible effects on refrigerant properties and compressor operation.
- There are isenthalpic pressure drops at the suction and discharge valves.

For the compression process from 2 to 3 we will assume an isentropic process:

$$P_2 v_2^{\gamma} = P_3 v_3^{\gamma} \tag{4.2}$$

where P = the pressure, kPa or psia

v = the specific volume, m^3/kg or ft^3/lbm

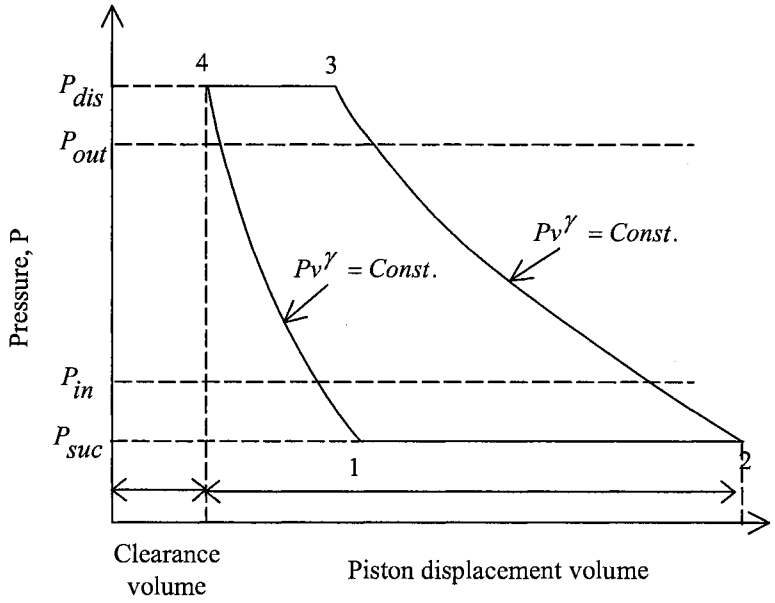

Figure 4.2. Schematic indicator diagram for a reciprocating compressor

We may further assume that the temperature change from point 3 to 4 is negligible. With this approximation, the specific volume at point 3 is equal to the specific volume at

point 4. If we denote the state of the re-expanded clearance vapor as 1, then for the re-expansion process, we have:

$$P_4 v_4^{\gamma} = P_1 v_1^{\gamma} \tag{4.3}$$

Due to the re-expansion of the refrigerant vapor in the clearance volume, the mass flow rate of the compressor refrigerant is a decreasing function of the pressure ratio,

$$\dot{m}_r = \frac{PD}{v_{suc}}\left[1 + C - C\left(\frac{P_{dis}}{P_{suc}}\right)^{1/\gamma}\right] \tag{4.4}$$

where $\dot{m}_r$ = refrigerant mass flow rate, kg/s or lbm/hr

PD = piston displacement, m^3/s or ft^3/hr

v_{suc} = specific volume at suction state, m^3/kg or ft^3/lbm

C = clearance factor

P_{dis} = discharge pressure, kPa or psia

P_{suc} = suction pressure, kPa or psia

γ = isentropic exponent

The suction and discharge pressures play important roles in varying the magnitude of the theoretical mass flow rate. These two pressures are different from the evaporating and condensing pressures due to the pressure drop across suction and discharge valves. According to the discussion of Popovic and Shapiro (1995), the inclusion of pressure drops across the suction and discharge valves led to a more accurate prediction for their

reciprocating compressor model. The pressure drop, ΔP, is also considered in the model. Results for versions of the model with and without pressure drops across the valves are presented below. Acceptable accuracy was not achieved in models that did not incorporate pressure drop.

An expression for the compressor work required may be derived subjected to the same approximations and limitations as used in the analysis above. The work is represented by the enclosed area of the diagram of Figure 4.2. Therefore,

$$\dot{W}_t = \int_2^3 VdP - \int_1^4 VdP \tag{4.5}$$

The compressor model has a power requirement based on the thermodynamic work rate of an isentropic process:

$$\dot{W}_t = \frac{\gamma}{\gamma - 1} \dot{m}_r P_{suc} v_{suc} \left[\left(\frac{P_{dis}}{P_{suc}} \right)^{\frac{\gamma - 1}{\gamma}} - 1 \right] \tag{4.6}$$

where $\dot{W}_t$ = theoretical power, kW or Btu/hr

γ = isentropic exponent

$\dot{m}_r$ = refrigerant mass flow rate, kg/s or lbm/hr

P_{suc} = suction pressure, kPa or psia

v_{suc} = specific volume at suction state, m^3/kg or ft^3/lbm

P_{dis} = discharge pressure, kPa or psia

A simple linear representation has been used to account for the electrical and mechanical efficiency of the compressor. The actual power input for the compressor is calculated by the following equation,

$$\dot{W} = \frac{\dot{W}_t}{\eta} + \dot{W}_{loss} \tag{4.7}$$

where $\dot{W}$ = compressor power input, kW or Btu/hr

$\dot{W}_{loss}$ = constant part of the electro-mechanical power losses, kW or Btu/hr

η = electro-mechanical efficiency

$\dot{W}_t$ = theoretical power, kW or Btu/hr

The refrigerant mass flow rate is not given in heat pump manufacturers' catalogs. In this parameter estimation model, the refrigerant mass flow rate is estimated first based on the estimated values of the selected parameters for the compressor using Equation (4.4). Then the compressor power is calculated accordingly using Equations (4.6) and (4.7). The enthalpy of the refrigerant at the suction state is determined from the evaporator model.

In addition, some superheat, ΔT_{sh}, is assumed to occur before entering the compressor, following Bourdouxhe, et al. (1994). To summarize, there are six parameters that have to be identified for the compressor. They are *PD, C,* ΔP, W_{loss}, ΔT_{sh}, and η.

It is not expected from this model that the values of the selected parameters derived with parameter estimation procedure will match the exact specifications of each component if they are readily available. The heat pump manufacturers' catalogs do not normally provide any compressor specifications, though they may be available from their compressor suppliers. However, proprietary information such as clearance factor is normally not available. If the exact values of a few of the selected parameters are available, those parameters could be eliminated from the list of the parameters to be estimated, and their actual values could be used. Due to the limitation of the available catalog data, it is virtually impossible that the estimated values of the parameters for each individual component will match the actual physical value

4.3. Condenser and Evaporator Models

The condenser and evaporator models are developed from fundamental analysis of the counter-flow heat exchangers. It is assumed that there is negligible pressure drop in the heat exchangers, and therefore the refrigerant is at a constant temperature while changing phase. Since the temperature of the refrigerant in the two-phase region is considered constant, it is not necessary to differentiate whether the heat exchanger is actually counter-flow or has some other configuration.

A more detailed approach, using the heat exchanger model of Rabehl, et al. (1999) was tried, but it did not significantly improve the prediction accuracy. Instead, the heat exchanger was treated as a simple heat exchanger with phase change on one side:

$$\varepsilon = 1 - e^{-NTU} \tag{4.8}$$

Where $NTU = \dfrac{UA}{\dot{m}_w C_{pw}}$

ε = thermal effectiveness of heat exchanger

NTU = number of transfer units

UA = heat transfer coefficient, kW/K or Btu/(hr-F)

$\dot{m}_w$ = mass flow rate of water, kg/s or lbm/hr

C_{pw} = specific heat of water, kJ/(kg-K) or Btu/(lbm-F)

Therefore, the heat transfer coefficients (UA) of the condenser and the evaporator are the last two parameters to be identified. The entire cycle is shown in Figure 4.3.

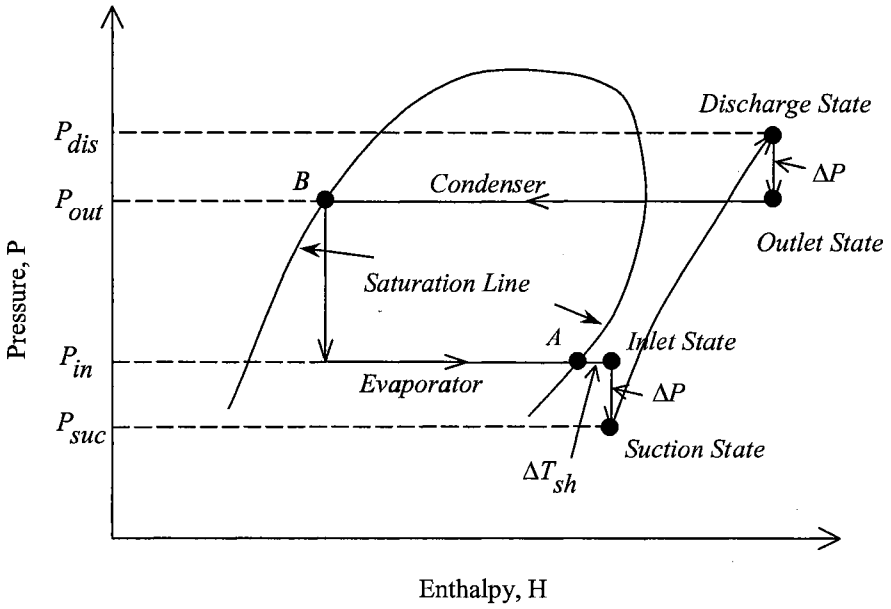

Figure 4.3. Pressure-enthalpy diagram for the refrigeration cycle

A constant value of (UA) for the condenser and evaporator is clearly not physically correct, yet it seems to be a reasonable approximation, given the overall goal of this model.

Furthermore, for the evaporator, the effect of refrigerant superheating is neglected in the evaporator model. If every other part of the heat exchanger model were "correct", this would result in under prediction of the evaporator heat transfer. However, this small systematic error is presumably compensated by a smaller estimated value of UA. Analogously, for the condenser, the neglect of the superheating and subcooling can also be compensated for by a smaller value of UA.

4.4. Expansion Device

The heat pump model does not explicitly model the expansion device. Rather, the amount of superheat is held constant, and the refrigerant mass flow rate is determined by the compressor model. This is a round-about way of modeling (or assuming the presence of) a thermostatic expansion valve. All of the heat pumps investigated with this model do utilize thermostatic expansion valves. To the best of the authors' knowledge, this is true for all water-to-water heat pumps manufactured in North America. Therefore, the model has not been tested with any other expansion devices, such as a capillary tube, and it may not be applicable for heat pumps with capillary tubes.

4.5. Parameter Estimation Procedure

The values of the parameters are estimated using the available catalog data. One set of parameters is estimated for the heating mode, and one set is estimated for the cooling mode. For each operating point, the data needed are:

- Source side entering water temperature, flow rate, and heat rejection (cooling mode) or heating extraction (heating mode)
- Load side entering water temperature, flow rate and cooling capacity (cooling mode) or heat capacity (heating mode)
- Compressor power consumption

The parameter estimation procedure minimizes the difference between the model results and the catalog data by systematically adjusting the values of the parameters. The difference between the model results and the catalog data is quantified in the form of an objective function. For any given set of parameters, PD, C, ΔP, W_{loss}, ΔT_{sh}, η, $(UA)_L$, and $(UA)_S$, in case of the cooling mode, the objective function is calculated as follows:

1. Calculate the evaporator and condenser effectiveness by Equations (4.9) and (4.10),

$$\varepsilon_L = 1 - \exp\left(-\frac{(UA)_L}{C_{pw}\dot{m}_{wL}}\right) \tag{4.9}$$

where ε_L = thermal effectiveness of evaporator

$(UA)_L$ = heat transfer coefficient for evaporator, kW/K or Btu/(hr-F)

$\dot{m}_{wL}$ = mass flow rate of water in evaporator, kg/s or lbm/hr

C_{pw} = specific heat of water, kJ/(kg-K) or Btu/(lbm-F)

$$\varepsilon_S = 1 - \exp\left(-\frac{(UA)_S}{C_{pw}\dot{m}_{wS}}\right) \tag{4.10}$$

where ε_S = thermal effectiveness of condenser

$(UA)_S$ = heat transfer coefficient for condenser, kW/K or Btu/(hr-F)

$\dot{m}_{wS}$ = mass flow rate of water in condenser, kg/s or lbm/hr

C_{pw} = specific heat of water, kJ/(kg-K) or Btu/(lbm-F)

2. Calculate the evaporating and condensing temperatures of the refrigerant:

$$T_e = T_{wiL} - \frac{\dot{Q}_L}{\varepsilon_L C_{pw}\dot{m}_{wL}} \tag{4.11}$$

where T_e = evaporating temperature, °C or °F

T_{wiL} = evaporator entering water temperature, °C or °F

$\dot{Q}_L$ = evaporator heat transfer rate, kW or Btu/hr

ε_L = thermal effectiveness of evaporator

$\dot{m}_{wL}$ = mass flow rate of water in evaporator, kg/s or lbm/hr

C_{pw} = specific heat of water, kJ/(kg-K) or Btu/(lbm-F)

$$T_c = T_{wiS} + \frac{\dot{Q}_S}{\varepsilon_S C_{pw} \dot{m}_{wS}} \tag{4.12}$$

where T_c = condensing temperature, °C or °F

T_{wiS} = condenser entering water temperature, °C or °F

$\dot{Q}_S$ = condenser heat transfer rate, kW or Btu/hr

ε_S = thermal effectiveness of condenser

$\dot{m}_{wS}$ =mass flow rate of water in condenser, kg/s or lbm/hr

C_{pw} = specific heat of water, kJ/(kg-K) or Btu/(lbm-F)

3. When the condensing and evaporating temperatures are obtained, the corresponding pressures and enthalpies can be derived using a refrigerant property subroutine. We used subroutines provided with an HVACSIM+ system simulation program (Clark and May 1985).

4. Identify the refrigerant state at the compressor suction port by adding the superheat to the evaporating temperature. The refrigerant enthalpy at this point is determined using the refrigerant property subroutines.

$$T_{icom} = T_e + \Delta T_{sh} \tag{4.13}$$

where T_{icom} = Compressor inlet temperature, °C or °F

T_e = evaporating temperature, °C or °F

ΔT_{sh} = superheat, °C or °F

5. Identify the compressor suction and discharge states by adding or subtracting the pressure drop. The specific volume at the suction state is determined by the refrigerant property subroutines.

$$P_{suc} = P_e - \Delta P \tag{4.14}$$

where P_{suc} = compressor suction pressure, kPa or psia

P_e = evaporating pressure, kPa or psia

ΔP = pressure drop across suction valve, kPa or psia

$$P_{dis} = P_c + \Delta P \tag{4.15}$$

where P_{dis} = compressor discharge pressure, kPa or psia

P_c = condensing pressure, kPa or psia

ΔP = pressure drop across discharge valve, kPa or psia

6. Calculate the refrigerant mass flow rate by Equation (4.4), the theoretical value of isentropic compression power by Equation (4.6) and the total power input by Equation (4.7).

7. Calculate the new value of the cooling capacity for cooling mode.

$$\dot{Q}_L = \dot{m}_r (h_A - h_B) \tag{4.16}$$

Or, for heating mode, the heating capacity is calculated using Equation (4.17).

$$\dot{Q}_L = \dot{W} + \dot{Q}_S \tag{4.17}$$

where h_A = enthalpy of the refrigerant leaving the evaporator, kJ/kg or Btu/lbm

h_B = enthalpy of the refrigerant entering the evaporator, kJ/kg or Btu/lbm

$\dot{Q}_L$ = heating capacity, kW or Btu/hr

$\dot{Q}_S$ = heat extraction that is determined through the same procedure as the cooling capacity in the cooling mode, kW or Btu/hr

Based on the given values of the parameters, the power consumption for the compressor and the cooling capacity (cooling mode) or heating capacity (heating mode) are calculated for each operation point. Then it is possible to compare the calculated results with the catalog performance data. The relative error between the catalog data and the calculated results for the power consumption and the cooling capacity or the heating capacity should be small. This is achieved by searching for the minimum value of the following objective function, which is the sum of the squares of the relative errors for both power consumption and load side heat transfer rate.

$$SSE = \sum_{i=1}^{N} \left[\left(\frac{(\dot{W}_{cat})_i - (\dot{W})_i}{(\dot{W}_{cat})_i} \right)^2 + \left(\frac{(\dot{Q}_{Lcat})_i - (\dot{Q}_L)_i}{(\dot{Q}_{Lcat})_i} \right)^2 \right] \tag{4.18}$$

where $\dot{W}_{cat}$ = catalog power consumption, kW or Btu/hr

$\dot{W}$ = calculated power consumption, kW or Btu/hr

$\dot{Q}_{Lcat}$ = catalog cooling capacity, kW or Btu/hr

$\dot{Q}_L$ = calculated cooling capacity, kW or Btu/hr

The optimal parameter values for a particular heat pump will be those associated with the minimum value of function SSE. Hence, the search for the optimal values of the selected parameters becomes a multi-variable optimization problem. To solve this problem, the widely used Nelder-Mead simplex (Kuester and Mize 1973) method is employed. A multi-start random sampling strategy was added to ensure the global minimum has been obtained. The flow chart for the computer program that implements the parameter estimation is shown in Figure 4.4.

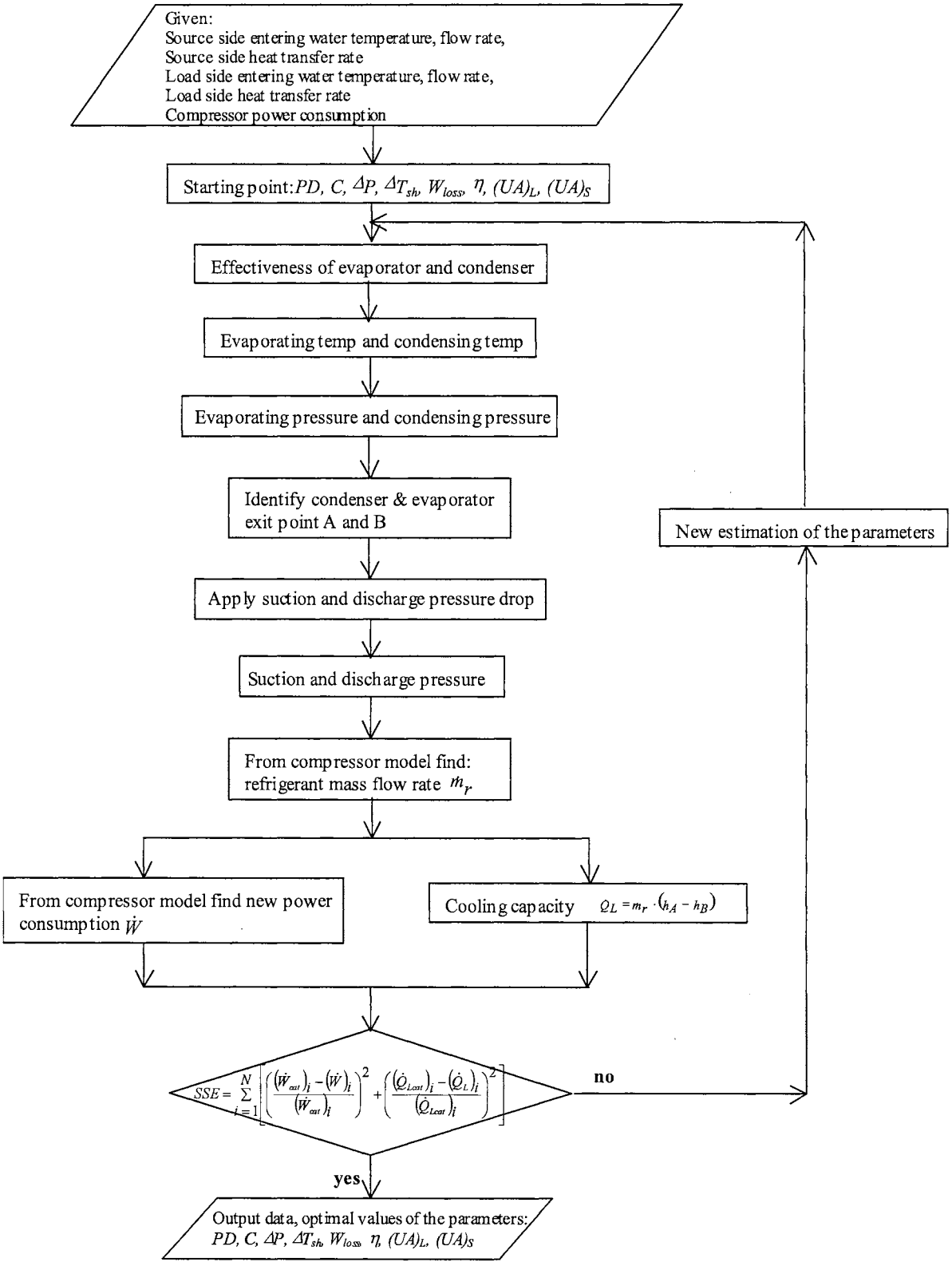

Figure 4.4. Flow diagram for parameter estimation computer program

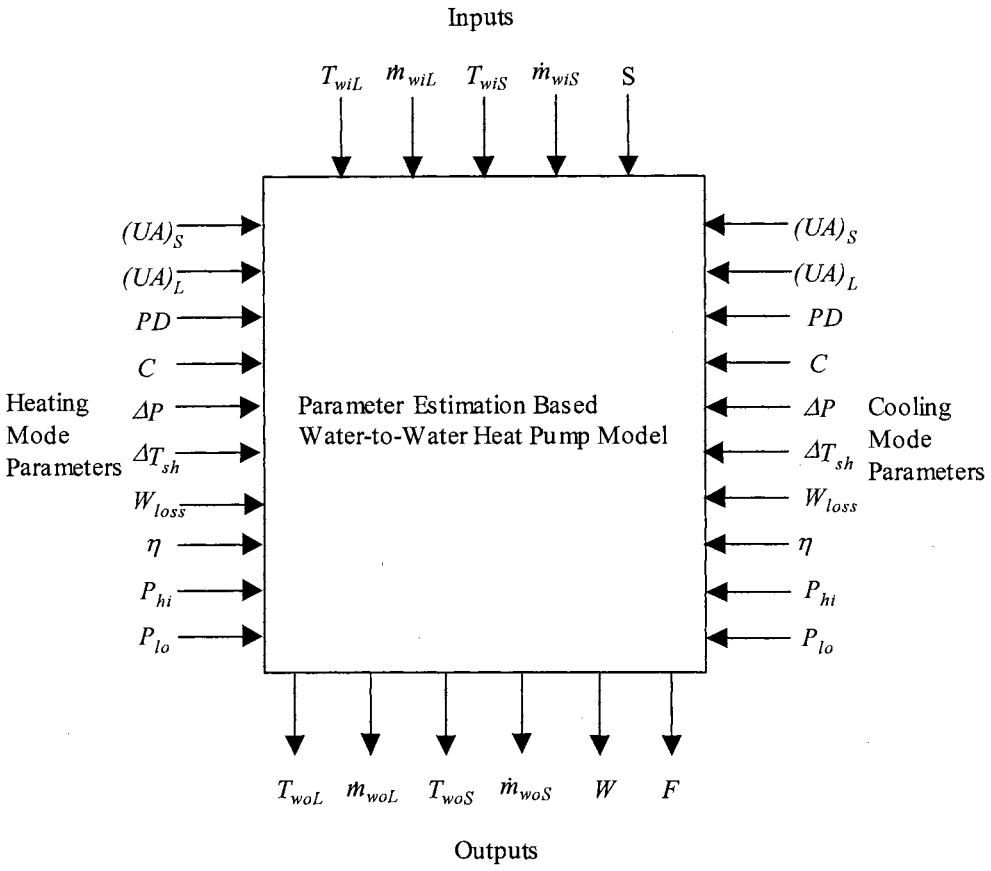

Figure 4.5. Information flow chart for model implementation

4.6. Model Implementation

The model is implemented in nearly the same way as the objective function evaluation described above. However, a thermostat signal is used as an input parameter to tell the model which set of parameters (heating mode or cooling mode) should be used. Also, the objective function evaluation takes advantage of the fact that the heat transfer rates are known, using the catalog data as an initial guess, then minimizing the difference between the predicted and measured heat transfer rates. However, for the model implementation, the heat transfer rates are solved simultaneously with successive

substitution, and this introduces an iterative loop not present in the objective function evaluation.

The model then determines the outlet temperatures for each of the fluid streams. Other information such as cooling and heating capacities, COP, etc., may be reported if desired. An information flow chart of the model implementation is presented in Figure 4.5. Figure 4.6 shows the cooling mode of the model implementation.

Table 4.2. Range of Water Flow Rates and Entering Water Temperatures

No.	Load Side		Source Side	
	EWT	Flow Rate	EWT	Flow Rate
1 (cooling)	25 °F (-3.89 °C) to 65 °F (18.33 °C)	4 GPM (0.25 kg/s) to 7 GPM (0.44 kg/s)	55 °F (12.78 °C) to 95°F (35 °C)	4 GPM (0.25 kg/s) to 7 GPM (0.44 kg/s)
2 (cooling)	25 °F (-3.89 °C) to 65 °F (18.33 °C)	20 GPM (1.26 kg/s) to 36 GPM (2.27kg/s)	55 °F (12.78 °C) to 95°F (35 °C)	20 GPM (1.26 kg/s) to 36 GPM (2.27kg/s)
3 (heating)	80 °F (26.67 °C) to 120 °F (48.89 °C)	4 GPM (0.25 kg/s) to 7 GPM (0.44 kg/s)	25 °F (-3.89 °C) to 65 °F (18.33 °C)	4 GPM (0.25 kg/s) to 7 GPM (0.44 kg/s)
4 (heating)	60 °F (15.56 °C) to 120 °F (48.89 °C)	45 GPM (2.84 kg/s) to 90 GPM (5.68 kg/s)	10 °F (-12.22 °C) to 70 °F (21.11 °C)	45 GPM (2.84 kg/s) to 90 GPM (5.68 kg/s)

This modeling approach has the advantage of not requiring experimental and component specification data beyond what are published in heat pump manufacturers' catalogs. Since the objective of this model is to eliminate the requirement for any internal measurements such as the refrigerant mass flow rate, temperature and pressure, all the comparisons are made based on the external measurements of water flow rates and temperatures for both source and load sides. These data are readily available in the heat pump manufacturers' catalogs. The ranges of flows and inlet temperatures in the catalog data for the heat pumps investigated are presented in Table 4.2.

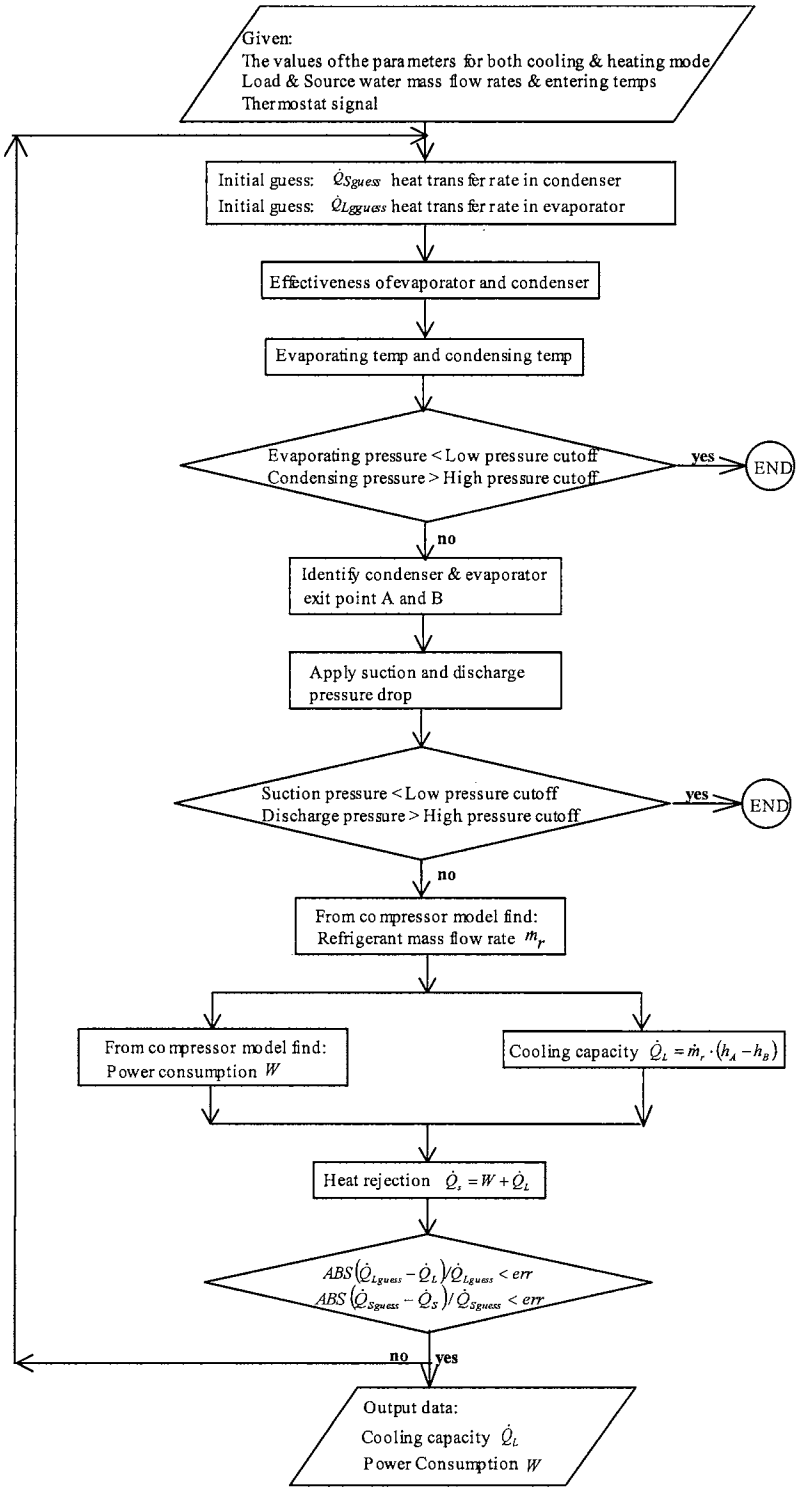

Figure 4.6. Flow diagram for model implementation computer program

4.7. Treatment of Extreme Operating Conditions

When this model is used inside of a transient system simulation program, it may encounter conditions not intended by the manufacturer, such as low water flow rates or extreme temperatures. This may happen even when the system simulation inputs are correct, as the equation solving process may occasionally try physically unrealistic values. Without any other checks, the model may then provide unrealistic results, or crash due to errors in the property routines.

In order to avoid this problem, a check is provided that is analogous to what happens in real heat pumps. Real heat pumps are usually equipped with protection against overly high pressures or overly low pressures that switch the compressor off when the limits are exceeded. These have been replicated in the model by incorporating a minimum evaporator pressure (P_{lo}) and maximum condenser pressure (P_{hi}) that may be set as parameters. If either of these is exceeded, the heat pump is turned off – outlet fluid temperatures are set equal to inlet fluid temperatures and power is set to zero.

4.8. Model Validation

The water-to-water heat pump model was validated using catalog data for three randomly-selected heat pumps made by two different manufacturers. In Table 4.3, a summary of the comparisons for units A and B, validated using the cooling mode data; and units A and C, validated using the heating mode data, is given. The heat pump

capacities, number of operating points given in the manufacturer's catalog, and the root-mean-square (RMS) error for capacity and power are shown in Table 4.3. The comparison showed a comparatively good agreement with generally acceptable accuracy. For the model of Stefanuk et al. (1992), Stefanuk (1990) reports errors between the model and the experimental data. Measured condenser heat transfer rates are, on average, 12% lower than the predicted rates. Measured evaporator heat transfer rates are, on average, 17% lower than the predicted rates. However, when the model is adjusted with a physically-measured refrigerant mass flow rate, the errors are significantly reduced, to between 3 and 5%, on average. As can be seen, the errors in Table 4.3 compare very favorably with the Stefanuk model, considering that making internal measurements is impractical for most engineers using simulation programs.

Table 4.3. RMS Errors of the Simulations for 4 Sets of Catalog Data

No.	Unit	Nominal Capacity		Number of Points	RMS	
		(W)	(Btu/hr)		Capacity	Power
1	A	7,034 (cooling)	24,000 (cooling)	81	4.57%	4.77%
2	B	43,965 (cooling)	150,000 (cooling)	81	4.71%	5.44%
3	A	7,620 (heating)	26,000 (heating)	81	2.66%	1.70%
4	C	99,654 (heating)	340,000 (heating)	234	3.08%	5.76%

A comparison of the results to the catalog data for the heat pump with the least satisfactory match is shown in Figures 4.7 and 4.8. A comparison of the results to the catalog data for the heat pump with the best match is shown in Figures 4.9 and 4.10. The

comparisons of the rest of the results to heat pumps are shown in Figures 4.11 through 4.14.

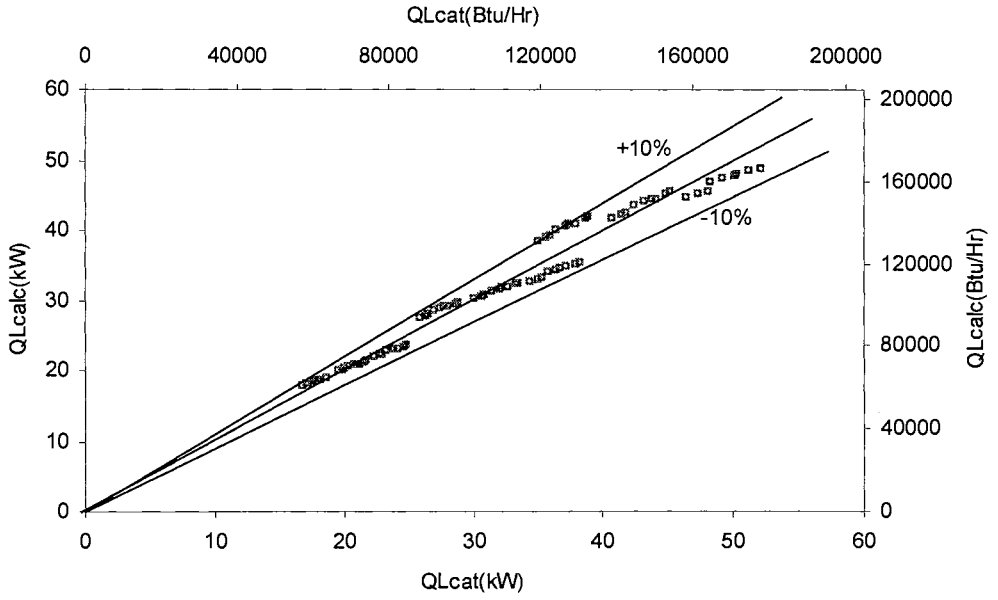

Figure 4.7. Calculated cooling capacity vs catalog cooling capacity (heat pump B)

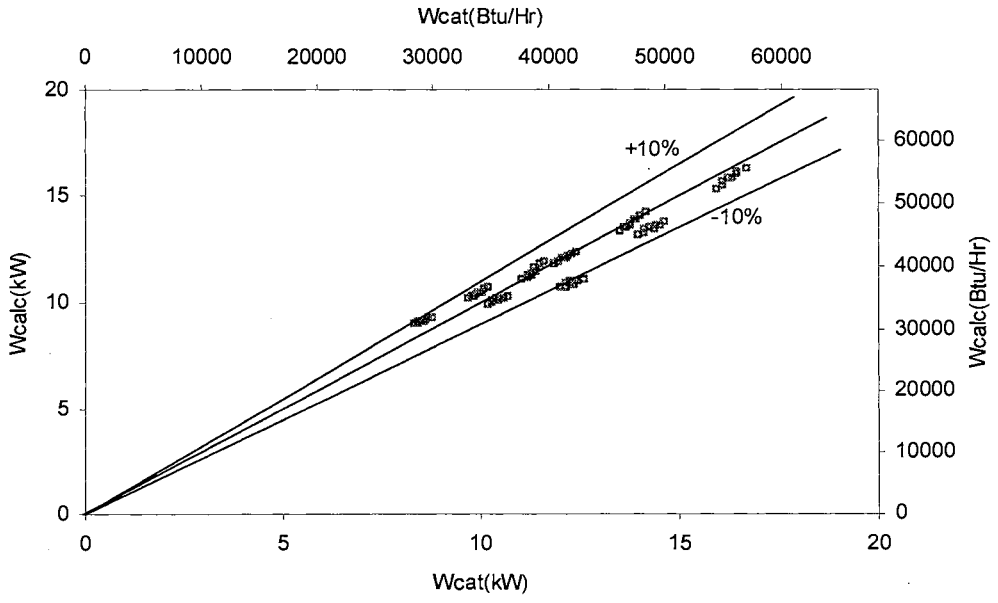

Figure 4.8. Calculated power vs catalog power (heat pump B)

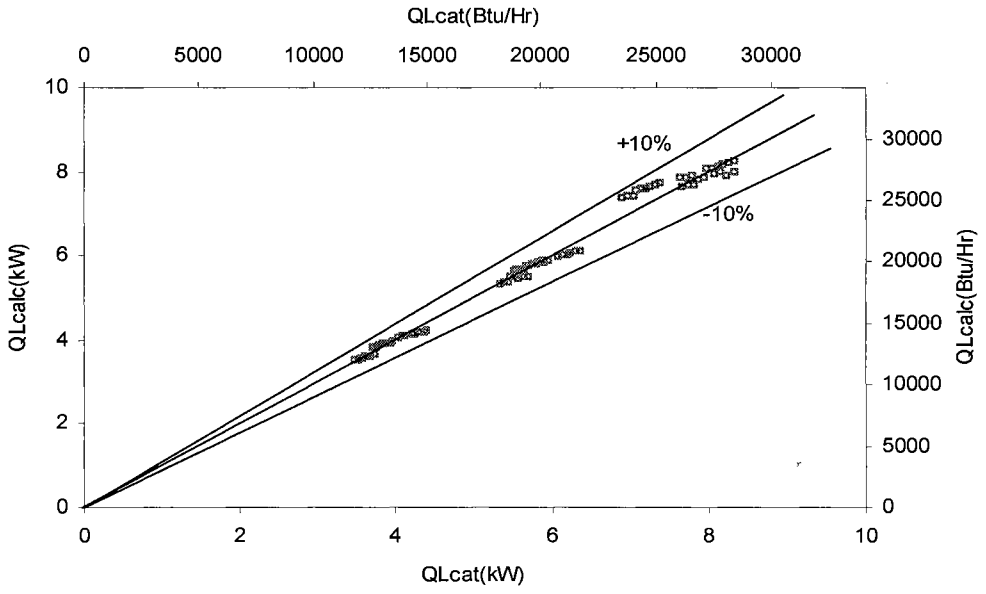

Figure 4.9. Calculated heating capacity vs catalog heating capacity (heat pump A)

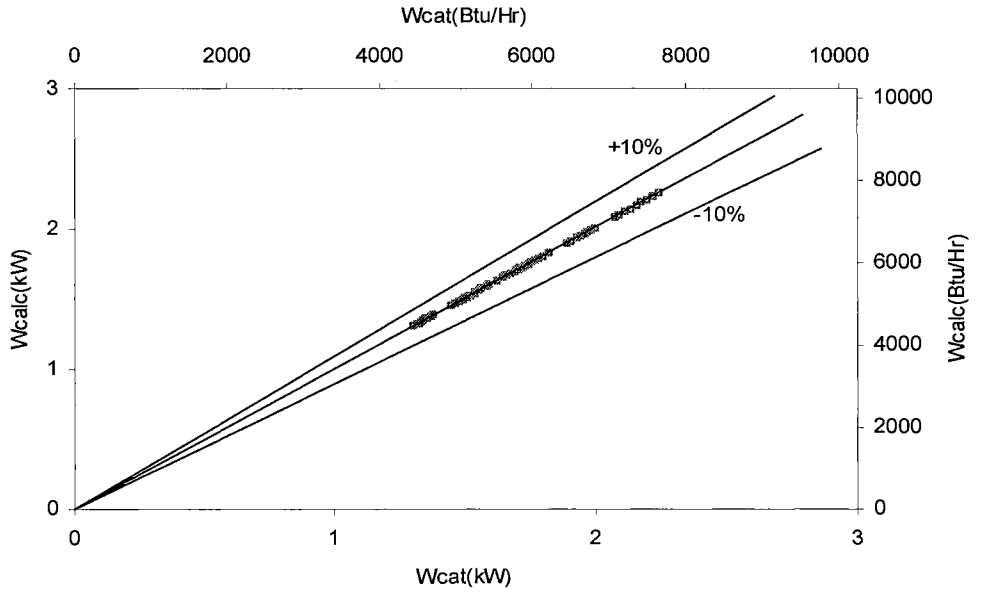

Figure 4.10. Calculated power vs catalog power (heat pump A)

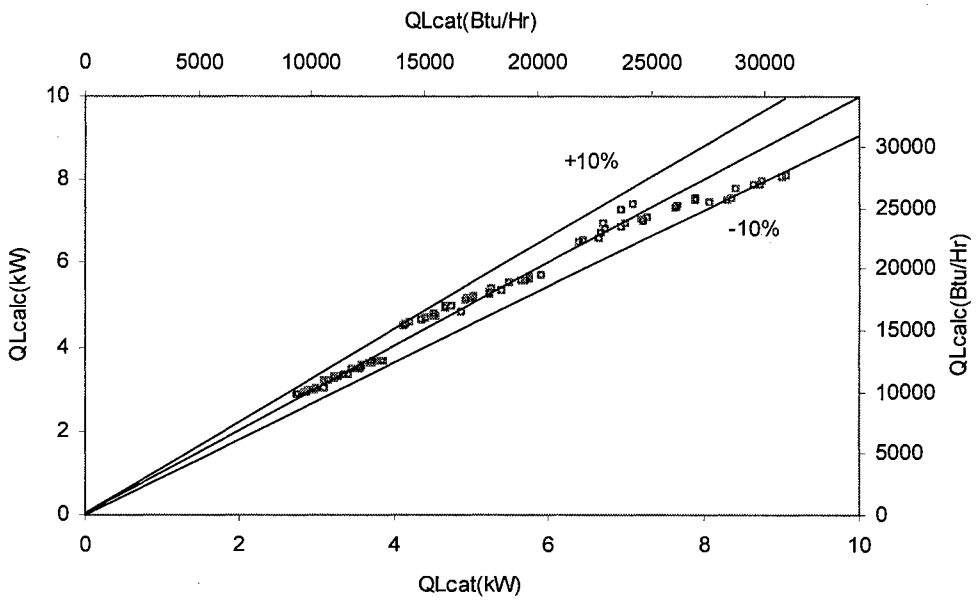

Figure 4.11. Calculated cooling capacity vs catalog cooling capacity (heat pump A)

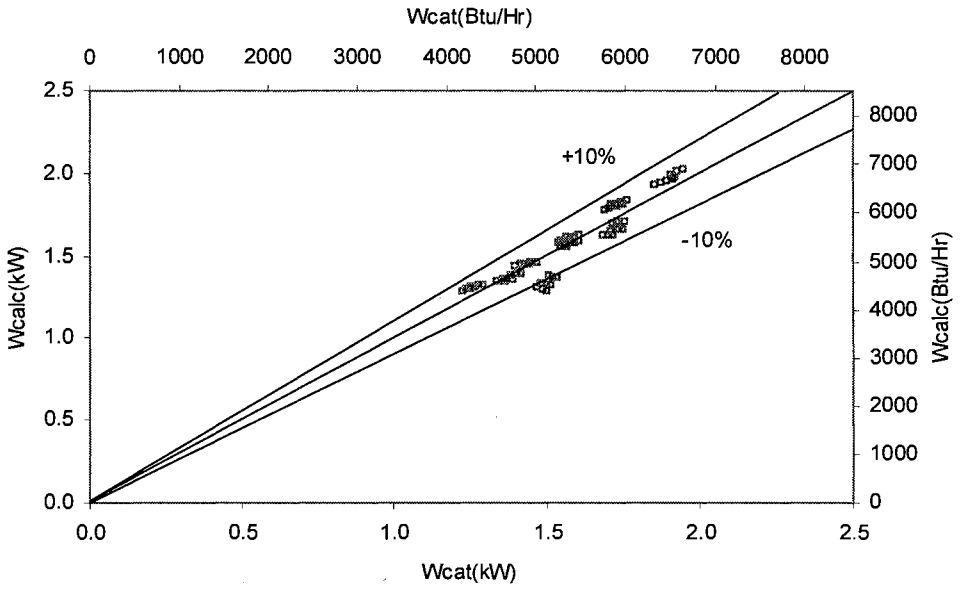

Figure 4.12. Calculated power vs catalog power (heat pump A)

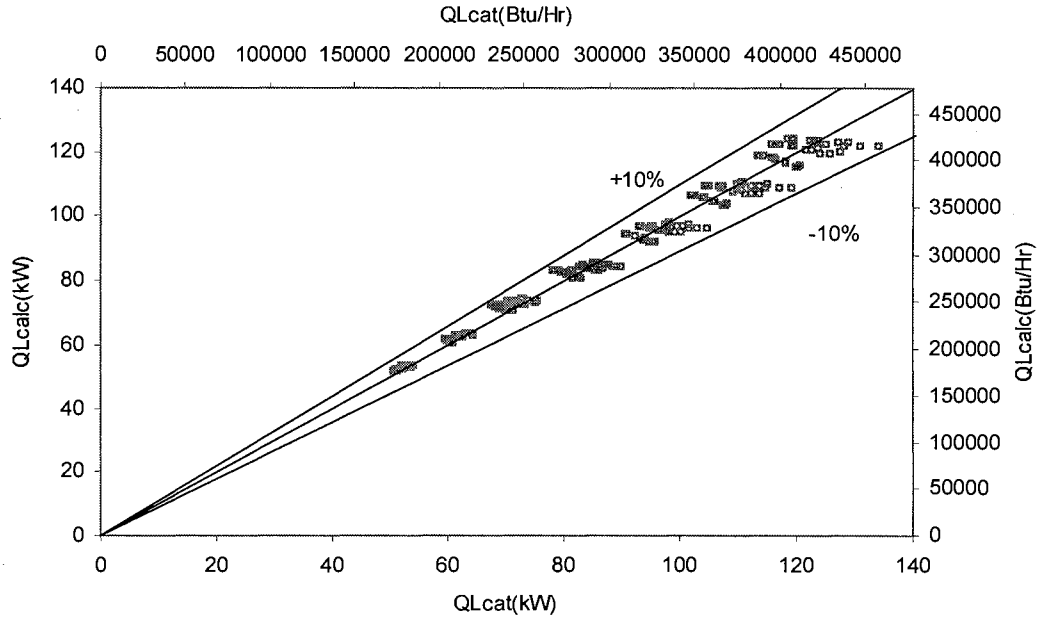

Figure 4.13. Calculated heating capacity vs catalog heating capacity (heat pump C)

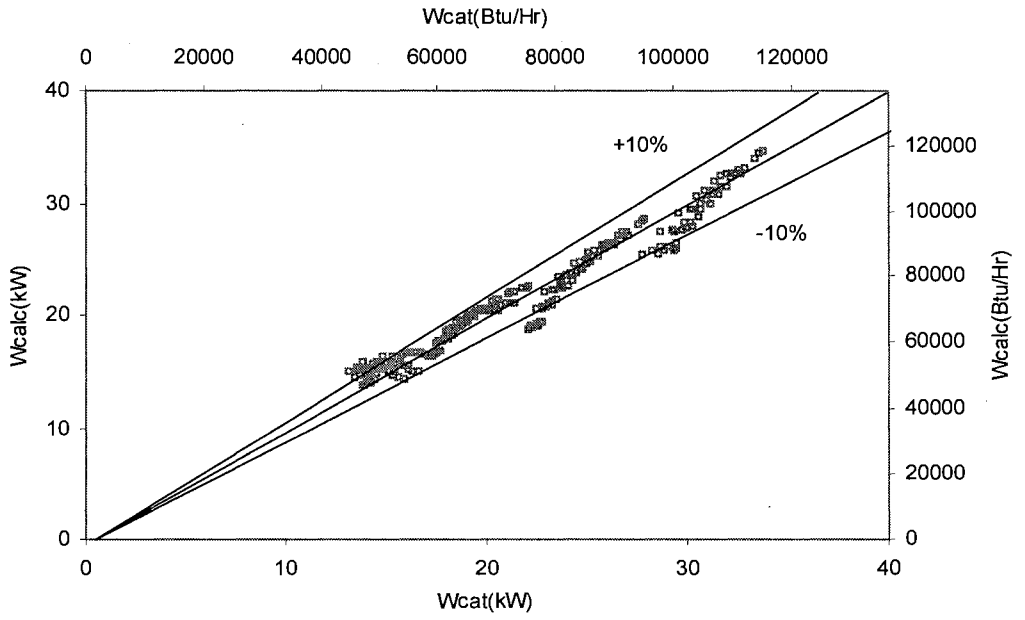

Figure 4.14. Calculated power vs catalog power (heat pump C)

4.9. Discussion of Parameter Selections

The model, as presented above, represents the final step in a series of incremental modifications. With each modification, new parameters were introduced, or in some cases, old parameters were removed. Some insight as to the relative importance of the different parameters may be gleaned from Table 4.4, which shows the estimated parameters and the SSE for seven different versions of the model, applied to a single heat pump in cooling mode. The catalog data used for the study is the heat pump A in cooling mode in Table 4.3.

It should be noted that the parameter estimation procedure can consume a significant amount of computer time. There is a trade-off between the number of parameters estimated and the required computational time. There are eight parameters selected for the final solution, scheme 7 in Table 4.4. For the case of heat pump C in Table 4.3, the parameter estimation process takes approximately 95 minutes computing time for a PC with Pentium II 333MHz CPU if all 234 operating points are used. If 16 points are used, the computing time is about 9 minutes. As will be demonstrated in the next section, 16 points should be sufficient. It might also be noted, that once all the parameters are known, the model can be executed on the same machine in about 0.0025 seconds for a single operating condition.

For the compressor model, the selection of $\dot{W}_{loss}$, the constant part of the electro-mechanical power losses and η, the loss factor that defines the electro-mechanical loss

proportional to the theoretical power contributes to the greatest improvement in the model from scheme 1 to scheme 2. An alternative improvement was the implementation of more detailed heat exchanger models (Rabehl, et al. 1999), as shown in scheme 3. Since the computer time required for estimation with more than eight parameters was deemed unacceptable, the detailed heat exchanger representation, which requires six parameters, was dropped.

Then, various combinations of suction and discharge pressure drops were added in schemes 4-6. It was noted that the separately estimated values of ΔP for both the suction side and discharge side were very nearly equal, so the final number of parameters was held to eight by estimating a single ΔP that is applied to both the suction side and discharge side.

Given the approximations in the parameter estimation procedure, and the fact that the approximations are compensated by artificially high or low values of parameters, it might be expected that estimated values of parameters for a given heat pump in heating mode and in cooling mode might be significantly different. Comparing the estimated parameters for data sets 1 and 3 may be instructive, since they represent the same heat pump operating in heating mode and cooling mode. However, the estimated parameters are surprisingly close... For the load side heat exchanger, the estimated value of UA for heating mode is 2.21 kW/°C (4,189 Btu/(hr-°F)) and for cooling mode is 2.10 kW/°C (3,981 Btu/(hr-°F)). For the source side heat exchanger, it is 1.54 kW/°C (2,919 Btu/(hr-

°F)) and 1.46 kW/°C (2,768 Btu/(hr-°F)) respectively. Table 4.5 presents a comparison of the parameter estimation results of cooling and heating mode for the same heat pump.

Table 4.4. Comparison of the Search Results of the Objective Function

Scheme			1	2	3	4	5	6	7
	P.D.	(m^3/s)	0.00205	0.00107	0.00459	0.00176	0.00137	0.00177	0.00175
		(ft^3/hr)	260.34	135.89	583.86	223.73	174.53	225.00	222.46
Parameter Estimation Model	C		0.0213	0.0499	0.0495	0.0498	0.0492	0.0482	0.0463
	η		-	0.381	-	0.541	0.470	0.575	0.824
	W_{loss}	(kW)	-	0.0000425	-	0.0129	0.00383	0.00919	0.586
		(Btu/hr)	-	0.145	-	43.94	13.06	31.36	1998.29
	$(UA)_{totev}$	(kW/K)	0.239	1.770	-	2.193	2.117	1.986	2.156
		Btu/(hr_F)	452.67	3353.26	-	4156.10	4013.36	3765.42	4087.10
	$(UA)_{totcon}$	(kW/K)	0.573	0.305	-	0.730	0.671	0.803	1.469
		Btu/(hr_F)	1085.23	578.14	-	1383.03	1272.37	1521.41	2784.64
	Suction ΔP	(kPa)	-	-	-	98.414	-	103.928	97.937
		(psi)	-	-	-	14.27	-	15.07	14.20
	Discharge ΔP	(kPa)	-	-	-	-	101.123	101.693	97.937
		(psi)	-	-	-	-	14.67	14.75	14.20
	ΔT_{sh}	(°C)	-	-	-	-	-	-	7.078
		(°F)	-	-	-	-	-	-	44.74
	Evap.	C_1	-	-	300.139	-	-	-	-
		C_2	-	-	-0.140	-	-	-	-
		C_3	-	-	0.250	-	-	-	-
	Cond.	C_4	-	-	700.301	-	-	-	-
		C_5	-	-	0.123	-	-	-	-
		C_6	-	-	0.275	-	-	-	-
SSE			23.907	2.331	6.769	1.111	1.594	0.943	0.419

Table 4.5. The Comparison of the Parameter Estiamtion Results for Heat Pump A in Cooling and Heating Modes

Parameter	Cooling	Heating
Piston Displacement	0.00175 m^3/s (222.46 ft^3/hr)	(0.00162 m^3/s) 205.93 ft^3/hr
Clearance Factor	0.0463	0.0690
Loss Factor	0.824	0.696
Constant Loss	0.586 kW (1,999.32 Btu/hr)	0.525 kW (1,791.20 Btu/hr)
Pressure Drop	97.937 kPa (14.20 psi)	99.29 kPa (14.40 psi)
Superheat	7.077 °C (12.74 °F)	9.82 °C (17.68 ° F)
Source Heat Transfer Coefficient	1.46 kW/°C (2,768 Btu/(hr-°F))	1.54 kW/°C (2,919 Btu/(hr-°F))
Load Heat Transfer Coefficient	2.10 kW/°C (3,981 Btu/(hr-°F))	2.21 kW/°C (4,189 Btu/(hr-°F))

It should be recognized that the development of the model is somewhat of an art. The selection of more sophisticated representation for a single component may not benefit the results in a manner proportional to the increase in computational cost. This seems to be the case for the heat exchangers.

4.10. Comparison to an Equation-fit Model

No generally accepted equation-fit model for water-to-water heat pumps is found in the literature. Due to the similarity between heat pump and chiller models, the steady state reciprocating chiller model recommended by Allen and Hamilton (1983) and the centrifugal and absorption water chiller model proposed by Stoecker et al. (1975), have been adapted to establish an equation-fit model for a water-to-water heat pump. Allen and Hamilton fit the cooling capacity and power consumption to a second order polynomial

in two variables: evaporator and condenser leaving water temperatures. In the chiller model proposed by Stoecker et al. (1975), the cooling capacity is also a function of two variables: the evaporator leaving water temperature and the condenser entering water temperature. In the equation-fit model used here, the condenser and evaporator entering water temperatures are chosen as the variables in the polynomial representation. This is more convenient for a component model when the inlet temperatures are known. This is also more convenient for equation fitting, since the heat pump catalog data are typically given in terms of four variables: load side entering water temperature, source side entering water temperature, load side water flow rate and source side water flow rate. Accordingly, the water flow rates for both sides are included as the other two variables in the equation-fit model.

As discussed by Stoecker et al. (1975), there is not a "best" equation for the simulation of heat pumps or chillers. A polynomial representation may be the best choice when no physical insight into the performance is available. Different combinations of variables and coefficients were tried to find the best equation form for a particular set of catalog data selected for comparison purposes. The final functional relationships for cooling capacity and compressor power are implemented with a second order polynomial in four variables, with eleven and thirteen coefficients, respectively:

$$P = C_1 + C_2 \cdot T_{Li} + C_3 \cdot T_{Li}^2 + C_4 \cdot T_{Si} + C_5 \cdot T_{Si}^2 + C_6 \cdot \dot{m}_L + C_7 \cdot \dot{m}_L^2 + C_8 \cdot \dot{m}_S + C_9 \cdot \dot{m}_S^2 + C_{10} \cdot T_{Li} \cdot \dot{m}_L + C_{11} \cdot T_{Si} \cdot \dot{m}_S \quad (4.19)$$

$$Q = C_{12} + C_{13} \cdot T_{Li} + C_{14} \cdot T_{Li}^2 + C_{15} \cdot T_{Si} + C_{16} \cdot T_{Si}^2 + C_{17} \cdot \dot{m}_L + C_{18} \cdot \dot{m}_L^2 + C_{19} \cdot \dot{m}_S + C_{20} \cdot \dot{m}_S^2 + C_{21} \cdot T_{Li} \cdot \dot{m}_L + C_{22} \cdot T_{Si} \cdot \dot{m}_S + C_{23} \cdot T_{Li} \cdot T_{Si} + C_{24} \cdot \dot{m}_L \cdot \dot{m}_S \quad (4.20)$$

where P = power consumption, kW or Btu/hr

Q = heating or cooling capacity, kW or Btu/hr

T_{Li} = load side entering water temperature, °C or °F

T_{Si} = source side entering water temperature, °C or °F

$\dot{m}_L$ = load side water mass flow rate, kg/s or lbm/hr

$\dot{m}_S$ = source side water mass flow rate, kg/s or lbm/hr

$C_1 - - C_{24}$ = quadratic equation-fit constants.

The parameter estimation procedure has two significant advantages over the equation-fit model: improved fidelity to the catalog data and improved extrapolation beyond the catalog data. Heat pump C in Table 4.3 is selected for comparison purpose. There are 234 operating points in the heating mode given in the catalog for the selected heat pump. The 234 points cover a range of entering water temperatures (EWT) and mass flow rates on both sides of the heat pump. In order to compare the parameter estimation model to the equation-fit model, parameters or coefficients were determined for each model using all 234 points, all of the points except the 45 with the highest load side EWT, all of the points except the 63 with the lowest load side EWT, all of the points except the 45 hightest and 63 lowest load side EWT, and 16 points representing combinations of the highest and lowest values of the EWT and mass flow rates on each side. Once the parameters or coefficients were determined, each model was applied to all 234 operating points. The maximum relative error, average absolute error, and RMS error were calculated for all 234 operating points.

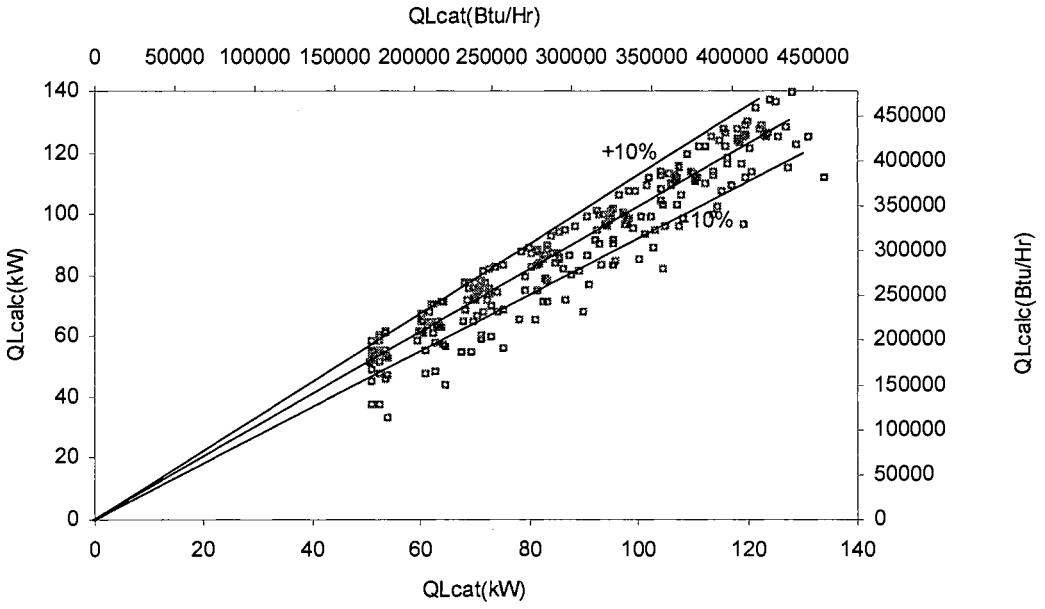

Figure 4.15. Calculated heating capacity vs catalog heating capacity using equation-fit (heat pump C)

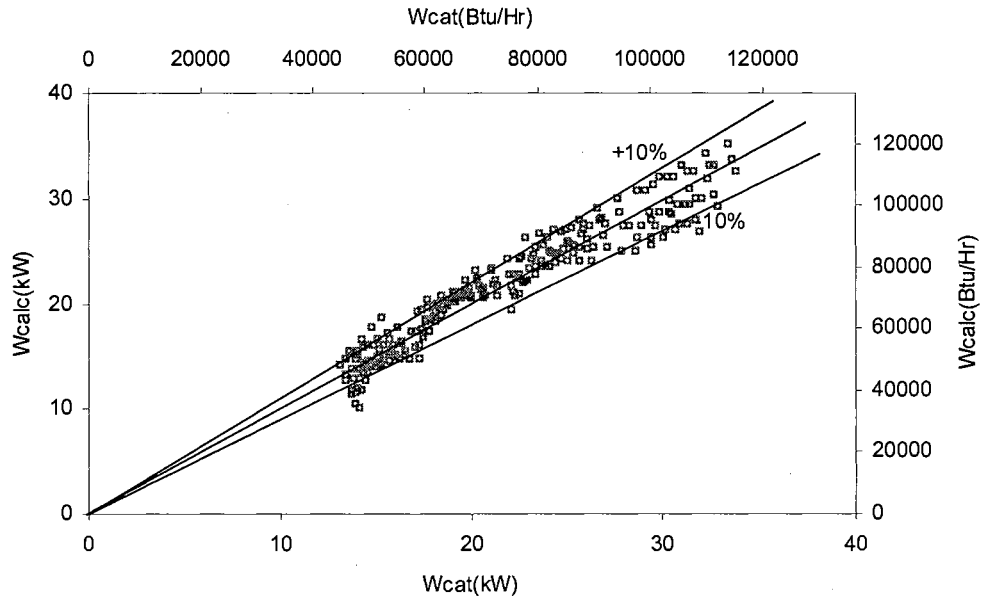

Figure 4.16. Calculated power vs catalog power using equation-fit (heat pump C)

The comparisons of the results are summarized in Tables 4.6 and 4.7. For both heating capacity and power consumption, for every combination of operating points used to estimate parameters or coefficients, for every characterization of the error, the parameter estimation model performs better than the equation-fit model. For both results, but particularly for the heating capacity, the parameter estimation extrapolates much better (shown in the 2nd, 3rd, and 4th rows) and performs much better with a very limited data set (shown in the 5th row). In fact, the parameter estimation model performs almost as well with 16 data points as with 234 data points. This represents a significant advantage if the model user has to manually transcribe the data from the catalog! The idea to use 16 data points representing the combination of the lowest and highest values of the input variables came from Rabehl, et al. (1999), who applied it in their heat exchanger model.

Table 4.6. The Comparison of the Relative Error of Power Consumption Simulated by Parameter Estimation and Equation-fit Models

Catalog Data Used	Relative Error					
	Max. (abs. value)		Average (abs. value)		RMS	
	Parameter Estimation	Equation-Fit	Parameter Estimation	Equation-Fit	Parameter Estimation	Equation-Fit
Entire 234 Points	16.06%	29.12%	4.21%	6.33%	5.76%	7.84%
w/o 45 Highest Points	17.49%	25.54%	4.40%	6.73%	6.13%	8.56%
w/o 63 Lowest Points	30.82%	36.94%	4.60%	6.49%	6.93%	8.54%
w/o 45 Highest & 63 Lowest Points	30.41%	37.64%	4.56%	6.07%	6.86%	8.53%
16 Points	21.96%	33.46%	4.19%	6.85%	5.77%	8.54%

Table 4.7. The Comparison of the Relative Error of Heating Capacity Simulated by Parameter Estimation and Equation-fit Models

Catalog Data Used	Relative Error					
	Max. (abs. value)		Average (abs. value)		RMS	
	Parameter Estimation	Equation -Fit	Parameter Estimation	Equation -Fit	Parameter Estimation	Equation-Fit
Entire 234 Points	8.17%	38.50%	2.46%	7.41%	3.08%	9.65%
w/o 45 Highest Points	8.31%	35.72%	2.44%	7.96%	3.00%	10.81%
w/o 63 Lowest Points	8.00%	32.36%	2.71%	11.36%	3.26%	13.64%
w/o 45 Highest & 63 Lowest Points	8.00%	40.93%	2.49%	7.56%	3.03%	10.57%
16 Points	8.77%	49.24%	2.80%	12.55%	3.39%	16.45%

4.11. Conclusion for Water-to-Water Heat Pump Model

This paper has presented a water-to-water heat pump model suitable for use in building energy analysis and HVAC system simulation programs. The model has been developed so as to require only commonly available data from manufacturers' catalogs in order to estimate the model coefficients. As compared to more detailed deterministic models, it does not require internally measured data usually unavailable to building system designers and simulationists. It also works well with only 16 data points for each mode, making it reasonably convenient when the data must be manually transcribed from a catalog.

Furthermore, the model's performance compares favorably against the most detailed deterministic model previously published, having a similar RMS error to the model described by Stefanuk, et al. (1992). As compared to equation-fit models, this model retains the physically-based representation of the heat pump, which allows some

extrapolation beyond the catalog data. It also performs significantly better when a limited number of operating points are utilized for estimation of parameters or coefficients.

5. A Parameter Estimation Based Model for Water-to-Air Heat Pumps

Following the parameter estimation based model for water-to-water heat pumps, a water-to-air heat pump model has been developed and is described in detail in this chapter. The schematic of a water-to-air heat pump is shown in Figure 5.1. The objective of this research effort is to develop a water-to-air heat pump model suitable for use in energy calculation and/or HVAC system simulation programs. It is desired that the model is able to accurately predict the water-to-air heat pump performance, such as cooling capacity, heating capacity, power consumption, heat rejection and heat extraction. With a similar parameter estimation technique to that discussed in the water-to-water heat pump model, the water-to-air heat pump model requires a minimal number of data points, which are normally available from the specification data published in manufacturers' catalogs.

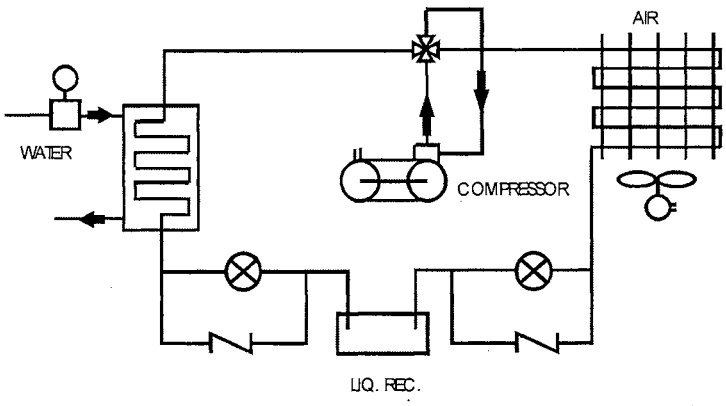

Figure 5.1. Schematic of a water-to-air heat pump

The modeling approach employs accepted mechanistic relations of fundamental thermodynamic and heat transfer principles with parameters identified and estimated

using manufacturers' catalog data. Some extrapolation of the catalog data is allowed. The selection of parameters for water-to-air heat pump model evolved from the final parameter selection scheme of water-to-water heat pump model. The main difference between the water-to-water and water-to-air heat pump models involves the load side heat exchanger. For the water-to-air heat pump model, condensation of water vapor may occur in cooling operation. Simultaneous sensible and latent heat transfer further complicates the model development. Since for heating operation, the water-to-air heat pump model is identical to the water-to-water heat pump model, this chapter will focus on the cooling mode of the water-to-air heat pump model.

5.1. System Description

The heat pump consists of four basic components: reciprocating compressor, evaporator, condenser and expansion device. The only difference between the water-to-air heat pump configuration shown in Figure 5.2 and that of the water-to-water heat pump is the load side heat exchanger. Other less important components are neglected due to their comparatively small contribution to the thermodynamic analysis for the entire system. Assuming an isenthalpic process in the expansion device and no heat exchange between this system and its environment, in case of the cooling mode, we have:

$$\dot{Q}_S = \dot{W} + \dot{Q}_L \tag{5.1}$$

where $\dot{Q}_S$ = source side heat transfer rate, kW or Btu/hr

$\dot{W}$ = compressor power input, kW or Btu/hr

$\dot{Q}_L$ = load side total heat transfer rate, kW or Btu/hr

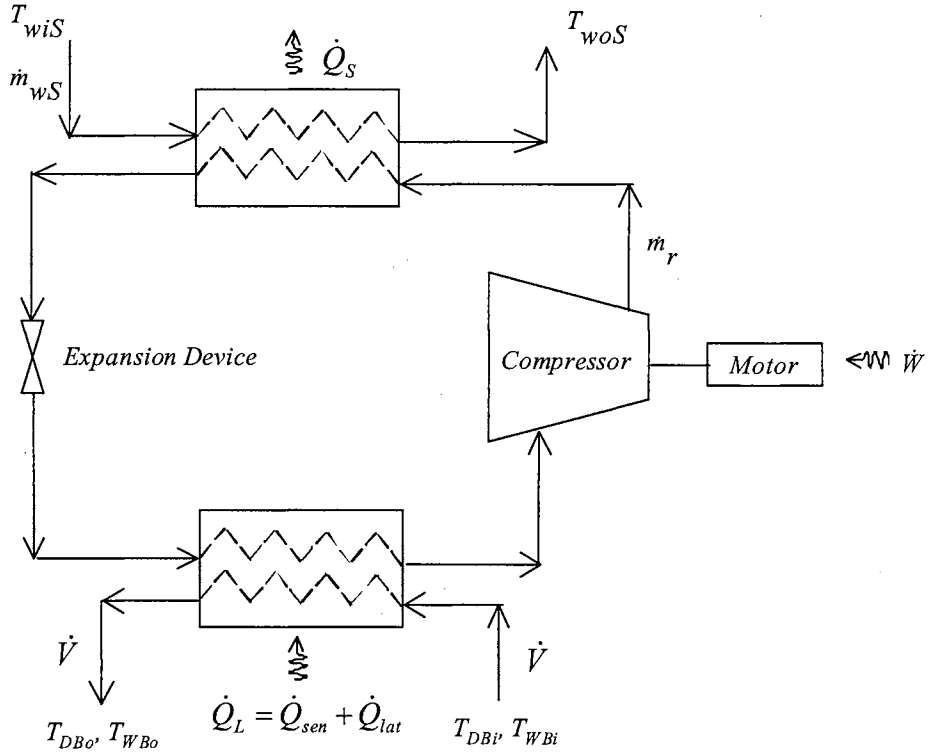

Figure 5.2. Basic water-to-air heat pump configuration (cooling operation)

Equation (5.1) assumes that no heat is lost from the compressor, when in actuality, there will be some heat transferred from the compressor shell. Generally, this loss will be fairly small, and heat pump manufacturers' catalog data neglect this heat loss. i.e., the catalog data is consistent with Equation (5.1).

5.2. Compressor Model

Since reciprocating compressor is assumed in the heat pump configuration, the modeling of compressor in the water-to-air heat pump model is the same as that of the

water-to-water heat pump model described in Chapter 4. If alternative compressor type such as scroll compressor or rotary compressor is used, the parameters selected for the reciprocating compressor need to be replaced by some other parameters selected for that type of compressor. The modeling of compressors other than reciprocating type will be discussed in Chapter 6.

5.3. Sensible Heat Exchanger Model

As discussed in Chapter 4, the condenser and evaporator models developed for water-to-air heat pump model are also based on the fundamental analysis of the counter-flow heat exchangers. The assumptions and simplifications are same as those of the heat exchanger models described in Chapter 4.

For a water-to-air heat pump, the source side heat exchanger in both heating and cooling mode, as well as the load side heat exchanger in heating mode are identified as sensible heat exchangers. The sensible heat exchanger is simply treated as heat exchanger with phase change on one side. Hence, its thermal effectiveness can be calculated as,

$$\varepsilon = 1 - e^{-NTU} \tag{5.2}$$

Where $NTU = \dfrac{UA}{\dot{m}_F C_{pF}}$

ε = heat transfer effectiveness

NTU = number of transfer units

UA = heat transfer coefficient, kW/K or Btu/(hr-°F)

$\dot{m}_F$ = water mass flow rate or air mass flow rate in case of heating operation, kg/s or lbm/hr

C_{pF} = water or air specific heat, kJ/(kg-K) or Btu/(lbm-°F)

Therefore, the heat transfer coefficients (UA) of the source side heat exchanger and the load side heat exchanger in case of heating mode are the parameters to be estimated. A constant value of (UA) is clearly not physically correct, yet it seems to be a reasonable approximation, given the overall goal of this model. Identical to the heat exchanger model in water-to-water heat pump model, superheat in the evaporator and subcooling in the condenser are neglected. However, superheating is selected as a parameter for the compressor model.

To summarize, the heat transfer coefficients are presumed to be independent of the physical condition for the heat exchanger under different operation conditions, such as water flow rates or entering water temperatures. The heat transfer coefficients $(UA)_L$ of the load side heat exchanger and the heat transfer coefficients $(UA)_S$ of the source side heat exchanger are the parameters selected.

5.4. Direct Expansion Cooling Coil Model

A schematic of a direct expansion cooling coil is shown in Figure 5.3. In reality, the outside surface of the cooling coil may be completely dry, complete wet or partly wet and

partly dry. This significantly complicates the heat exchanger model, compared to the sensible only model described above. The first step that should be accomplished before the performance prediction is to identify the dry or wet condition for a specific input state. A sophisticated analysis would involve finding the point on the coil surface where the surface temperature of the coil is equal or below the dew point temperature of the entering air. Unfortunately, this complicated calculation requires more information than what is available from manufacturers' catalogs. In addition, an iterative process introduced accordingly by the partly dry and partly wet modeling approach will require a significant increase in the computational time for an annual building energy consumption analysis.

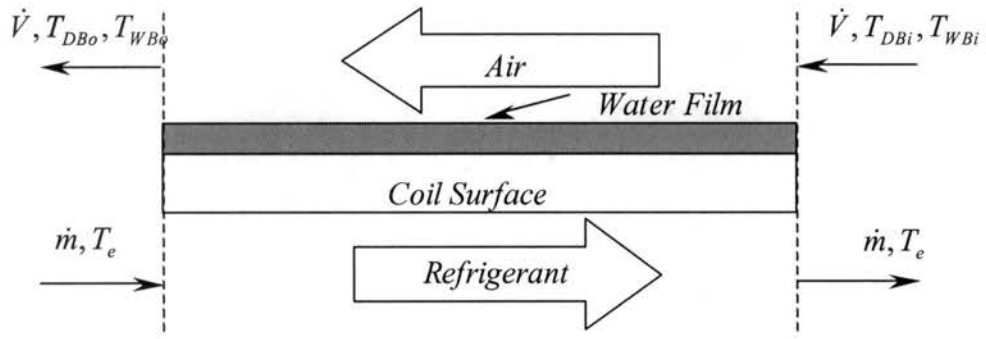

Figure 5.3. Schematic of a counter-flow direct expansion coil

Braun et al. (1989) presented a simplified method to overcome this complication by assuming that the coil is either completely dry or completely wet. Since both of the assumptions tend to under-predict the heat transfer rate, the larger one between the solutions is chosen as the final result. It is understood that only sensible heat transfer rate (equal to total heat transfer rate) is considered with the complete dry coil assumption. A

review of water-to-air heat pump catalog shows that almost no data are available for this condition. Therefore, the direct expansion cooling coil is always assumed to be wet. As will be shown later, it is still possible that with dry entering air conditions the model will show sensible heat transfer. Other than always assuming wet coil conditions, the model follows Braun's (1989) model closely. Another simplified model for the chilled water cooling coils has been presented by Morisot et al. (2002). It also assumes that the coil is either completely dry or completely wet even if it is partially wet. The errors associated with this assumption have been investigated and fall into an acceptable range for the building energy calculation.

The completely wet or completely dry assumption discussed above was originally developed for models of chilled water cooling coils. The difference between direct expansion cooling coils and chilled water cooling coils makes this approximation even more appropriate for the direct expansion coils. According to the ASHRAE Handbook of HVAC Systems and Equipment (ASHRAE 2000), the typical air side thermal resistance is around 0.07-0.12 °F·ft^2·h/Btu (0.012-0.021 m^2·°C/W) and the convective heat transfer coefficient is 8.3-14.3 Btu/(h·ft^2·°F) (47.1-81.2 W/m^2·°C). The typical total metal thermal resistance is around 0.0125-0.014 °F·ft^2·h/Btu (0.0022-0.0024 m^2·°C/W) and the metal conductance is around 71.4-80 Btu/(h·ft^2·°F) (405-454 W/m^2·°C). In comparison, the typical refrigerant side thermal resistance is around 0.001-0.0033 °F·ft^2·h/Btu (0.000176-0.000587 m^2·°C/W) and the convective heat transfer coefficient (R22) is around 300-1,000 Btu/(h·ft^2·°F) (1,704-5,679 W/m^2·°C) (ASHRAE 2001). The greatest thermal resistance is associated with air side heat transfer. Thus, the temperature difference

between the coil surface and refrigerant is relatively small compared to that of the air side and coil surface. Considering the refrigerant as having constant evaporating temperature, the coil surface temperature could be approximated as uniform, if the resistance between coil surface and refrigerant is negligible. If the coil surface temperature is assumed to be uniform throughout the air flow, the cooling coil will definitely either completely wet or completely dry.

A coil that effects moisture removal in addition to sensible heat cooling is termed a dehumidifying coil. When cooling coils act as dehumidifying coils, water vapor is transported from the main air stream and condensed on the coil surface. At the same time, the air is being cooled because of the transfer of sensible heat. This simultaneous transfer of both sensible and latent heat can be solved by a method developed by McElgin and Wiley (1940), which is called 'enthalpy potential' method by later authors. The total heat transfer from the air stream to coil surface is a combination of sensible heat transfer due to temperature difference and latent heat transfer due to the vapor pressure difference.

5.4.1. Total Heat Transfer Rate

Using the enthalpy potential method, the total heat lost by the air in passing over an element of wetted area dA_w is given by:

$$dH_T = \frac{h}{C_p}(i - i_s)dA_W \tag{5.3}$$

$$i = 1.006T' + w \cdot (2501 + 1.805T') \tag{5.4}$$

where H_T = total heat transfer rate (sensible + latent) of air flowing over wetted surface, kW or Btu/hr

h = sensible heat transfer coefficient through air film, kW/(m^2-K) or Btu/(hr-°F-ft^2)

C_p = specific heat of air vapor mixture, kJ/(kg dry air-°C) or Btu/(lbm dry air-°F)

i = enthalpy of air vapor mixture per pound of dry air evaluated at the main stream temperature, kJ/kg or Btu/lbm

i_s = enthalpy of saturated air vapor mixture per pound of dry air evaluated at the surface temperature, kJ/kg or Btu/lbm

A_w = wetted airside surface area on which moisture is condensing, m^2 or ft^2

This equation, originally derived by Merkel (1925), combines sensible heat transfer due to the temperature difference and latent heat transfer due to the pressure difference of vapor into a single equation. It was recognized that simultaneous sensible and latent heat flow or total heat flow depends on the enthalpy difference between the main air flow over the surface and the saturated air at the surface temperature.

Based on the enthalpy potential method, the wet coil heat transfer effectiveness is defined as,

$$\varepsilon_{wet} = \frac{i_{a,i} - i_{a,o}}{i_{a,i} - i_{s,e}} \tag{5.5}$$

where $\varepsilon_{wet} = 1 - e^{(-NTU_{wet})}$ (5.6)

$i_{a,i}$ = enthalpy of moist air at inlet state, kJ/kg or Btu/lbm

$i_{a,o}$ = enthalpy of moist air at outlet state, kJ/kg or Btu/lbm

$i_{s,e}$ = enthalpy of moist air at evaporating temperature, kJ/kg or Btu/lbm

The overall number of transfer units is slightly different from that of a sensible heat exchanger, in that the total heat transfer driving force is split into two parts.

$$NTU_{wet} = \frac{1}{\left(\dot{m}_a C_{pa}\right)\left(\frac{1}{h_{c,o}A_o} + \frac{C_{ps}}{C_{pa}(UA)_i}\right)} \quad (5.7)$$

Where C_{ps} is the specific heat of saturated air defined by: $C_{ps} = \left(\frac{dh_s}{dT}\right)_{T=T_e}$

$h_{c,o}A_o$ = outside surface heat transfer coefficient, W/K or Btu/(hr-°F)

$(UA)_i$ = inside surface heat transfer coefficient, W/K or Btu/(hr-°F)

$\dot{m}_a$ = air mass flow rate, kg/s or lbm/hr

C_{pa} = air specific heat, kJ/(kg-C) or Btu/(lbm-F)

Analogous to sensible heat exchanger, a total heat transfer coefficient may be defined as follows,

$$(UA)_{tot} = \frac{1}{\frac{1}{h_{c,o}A_o} + \frac{C_{ps}}{C_{p,a}(UA)_i}} \quad (5.8)$$

And the number of transfer units can be simplified as,

$$NTU_{wet} = \frac{(UA)_{tot}}{(\dot{m}_a C_{pa})} \tag{5.9}$$

Hence, the total heat transfer rate for a completely wet coil is,

$$\dot{Q}_{wet} = \varepsilon_{wet} \dot{m}_a (i_{a,i} - i_{s,e}) \tag{5.10}$$

5.4.2. Split of Total Heat Transfer Rate

Based on the analysis of the performance of dehumidifying coils in ASHRAE Handbook of HVAC Systems and Equipment (ASHRAE 2000), the effective surface temperature $T_{s,e}$ is used to determine the sensible heat transfer rate of the cooling coil. The effective surface temperature can be derived from the corresponding enthalpy $i_{s,s,e}$ of saturated air. The enthalpy of saturated air is,

$$i_{s,s,e} = i_{a,i} - \frac{i_{a,i} - i_{a,o}}{1 - e^{\left(-\frac{h_{c,o} A_o}{m_a C_{pa}}\right)}} \tag{5.11}$$

Inlet and outlet air enthalpy difference can be computed from the total heat transfer rate,

$$\dot{Q}_{wet} = \dot{m}(i_{a,i} - i_{a,o}) \tag{5.12}$$

Let $\varepsilon' = 1 - e^{\left(-\frac{h_{c,o}A_o}{m_a C_{pa}}\right)}$, which is called 'air side effectiveness' in ASHRAE Handbook, Equation (5.11) can be reduced to,

$$i_{s,s,e} = i_{a,i} - \frac{i_{a,i} - i_{a,o}}{\varepsilon'} \tag{5.13}$$

Analogous to the sensible heat exchanger, 'number of air-side transfer of units' could be defined as,

$$NTU_a = \frac{h_{c,o}A_o}{\dot{m}_a C_{pa}} \tag{5.14}$$

Thus, the air side effectiveness is simplified to,

$$\varepsilon' = 1 - e^{(-NTU_a)} \tag{5.15}$$

The effective surface temperature may be found iteratively from its corresponding enthalpy. The approach is discussed briefly as follows, which is based on the ASHRAE Handbook of Fundamentals (ASHRAE 2001).

The pressure of the saturated water vapor is computed from,

$$\ln(P_{w,s}) = \frac{-5.8002206\times10^3}{T} + 1.3914993 - 4.8640239\times10^{-2}T +$$

$$4.1764768\times10^{-5}T^2-1.4452093\times10^{-8}T^3+6.5459673\ln(T) \qquad (5.16)$$

where, $P_{w,s}$ = saturated pressure, kPa

T = absolute dry bulb temperature, °K=°C+273.15

When the partial pressure of the water vapor is obtained, the humidity ratio of the saturated air can be found as,

$$w=0.62198\frac{P_{w,s}}{P-P_{w,s}} \qquad (5.17)$$

where, w = humidity ratio, kg/kg dry air

P = total mixture pressure, kPa

$P_{w,s}$ = saturated pressure, kPa

Finally, the enthalpy of the saturated air is determined by,

$$i=1.006T'+w\cdot(2501+1.805T') \qquad (5.18)$$

where, i= enthalpy of moist air, kJ/kg

w = humidity ratio, kg/kg dry air

T' = moist air dry bulb temperature, °C

By comparing the calculated enthalpy and the targeted enthalpy, the initial guess of the effective surface temperature will be adjusted, and then substituted into Equations (5.16), (5.17) and (5.18) until it converges within a specified error.

Once the effective surface temperature is obtained, the sensible heat transfer rate is,

$$\dot{Q}_{sen} = \varepsilon' \dot{m}_a C_{pa} \left(T_{a,i} - T_{s,e} \right) \tag{5.19}$$

where $T_{a,i}$ = inlet air dry bulb temperature, °C or °F

The latent heat transfer rate is obtained when the sensible heat transfer rate $\dot{Q}_{sen}$ is subtracted from the total heat transfer rate $\dot{Q}_{wet}$.

$$\dot{Q}_{lat} = \dot{Q}_{wet} - \dot{Q}_{sen} \tag{5.20}$$

The outlet air dry bulb temperature, is determined by the following equation,

$$T_{a,o} = T_{s,e} + \left(T_{a,i} - T_{s,e} \right) e^{(-NTU_a)} \tag{5.21}$$

To summarize, the parameters identified and shall be estimated are total heat transfer coefficient $(UA)_{tot}$, and external heat transfer coefficient $h_{c,o}A_o$.

5.5. Expansion Device

To the author's knowledge, the expansion devices used in the water-to-air heat pumps manufactured in North America are all thermostatic expansion valves. A relatively constant superheat temperature shall be achieved with the thermostatic expansion valve

in the refrigeration cycle. Hence, the modeling of expansion device in the water-to-air heat pump model is the same as that of the water-to-water heat pump model described in Chapter 4.

5.6. Parameter Estimation Procedure

The values of the parameters are estimated using the available catalog data. One set of parameters is estimated for the heating mode, and one set is estimated for the cooling mode. For each operating point, the data needed are:

- Source side entering water temperature, flow rate, and heat rejection (cooling mode) or heating extraction (heating mode)
- Load side entering air dry bulb/wet bulb temperature, flow rate, total cooling capacity, sensible cooling capacity and latent cooling capacity (cooling mode) or load side entering air dry bulb temperature, flow rate and heating capacity (heating mode)
- Compressor power consumption

The parameter estimation procedure minimizes the difference between the model results and the catalog data by systematically adjusting the values of the parameters. The difference between the model results and the catalog data is quantified in the form of objective functions.

The splitting of total heat transfer rate into sensible and latent parts is one of greatest challenges in the modeling of cooling coils. The parameter estimation procedure for this model takes advantage of the fact that the external heat transfer coefficient $h_{c,o}A_o$ is the only parameter involved in the splitting of total heat transfer rate into sensible and latent parts. Since the sensible heat transfer is determined based on the effective coil surface temperature, which is calculated from its corresponding saturation enthalpy, the estimation of the parameter associated with the splitting of total heat transfer rate can be isolated from the estimation of the parameters associated with the overall heat pump performance. Therefore, it is possible to estimate the external heat transfer coefficient $h_{c,o}A_o$ separately. Another objective function is established to estimate the remaining parameters associated with the overall heat pump performance including the total heat transfer rate of the coil. One single objective function that combines the two separate parameter estimation routines has also been attempted. However, for a sophisticated multi-variable optimization problem, better search results may be expected with fewer variables. Since the separation helps to improve the model accuracy on the split of total heat transfer rate considerably, it is recommended that the external heat transfer coefficient $h_{c,o}A_o$ be estimated using a separate routine.

Two objective functions are established: one is used to estimate the external heat transfer coefficient $h_{c,o}A_o$ based on the catalog data, in which total heat transfer, sensible heat transfer rate and latent heat transfer rate are all given for a range of operating conditions. The other is used to estimate the remaining parameters involved in the

determination of the total heat transfer rate, heat rejection and power consumption: *PD*, *C*, ΔP, W_{loss}, ΔT_{sh}, η, $(UA)_S$, $(UA)_{tot}$.

5.6.1. Objective function #1 for external heat transfer coefficient $h_{c,o}A_o$

1. Calculate the inlet and outlet air enthalpy difference using Equation (5.12).
2. Calculate the air side effectiveness using Equation (5.15). Note that this relies only on the air mass flow rate from catalog data, air specific heat C_{pr} and $h_{c,o}A_o$.
3. Calculate the saturated surface enthalpy using Equation (5.13).
4. Calculate the corresponding effective surface temperature using Equations (5.16), (5.17) and (5.18). Since no explicit solution has been found, the temperature needs to be calculated from its corresponding enthalpy iteratively.
5. Calculate the sensible heat transfer rate using Equation (5.19).
6. Calculate the latent heat transfer rate using Equation (5.20).

Based on the given value of $h_{c,o}A_o$, the sensible and latent heat transfer rates are calculated for each operation point. A best estimate of $h_{c,o}A_o$ is found by searching for the minimum value of the following objective function, which is the sum of the squares of the relative errors for both sensible and latent heat transfer rates.

$$SSE_1 = \sum_{i=1}^{N}\left[\left(\frac{(\dot{Q}_{sencat})_i - (\dot{Q}_{sen})_i}{(\dot{Q}_{sencat})_i}\right)^2 + \left(\frac{(\dot{Q}_{latcat})_i - (\dot{Q}_{lat})_i}{(\dot{Q}_{latcat})_i}\right)^2\right] \qquad (5.22)$$

where $\dot{Q}_{sencat}$ = catalog sensible cooling capacity, kW or Btu/hr

$\dot{Q}_{sen}$ = calculated sensible cooling capacity, kW or Btu/hr

$\dot{Q}_{latcat}$ = catalog latent cooling capacity, kW or Btu/hr

$\dot{Q}_{lat}$ = calculated latent cooling capacity, kW or Btu/hr

The optimal parameter values of the external heat transfer coefficient $h_{c,o}A_o$ will be the one associated with the minimum value of function SSE_1. Any appropriate single independent variable optimization approach can be used. A flow chart for the computer program that implements the parameter estimation is shown in Figure 5.4.

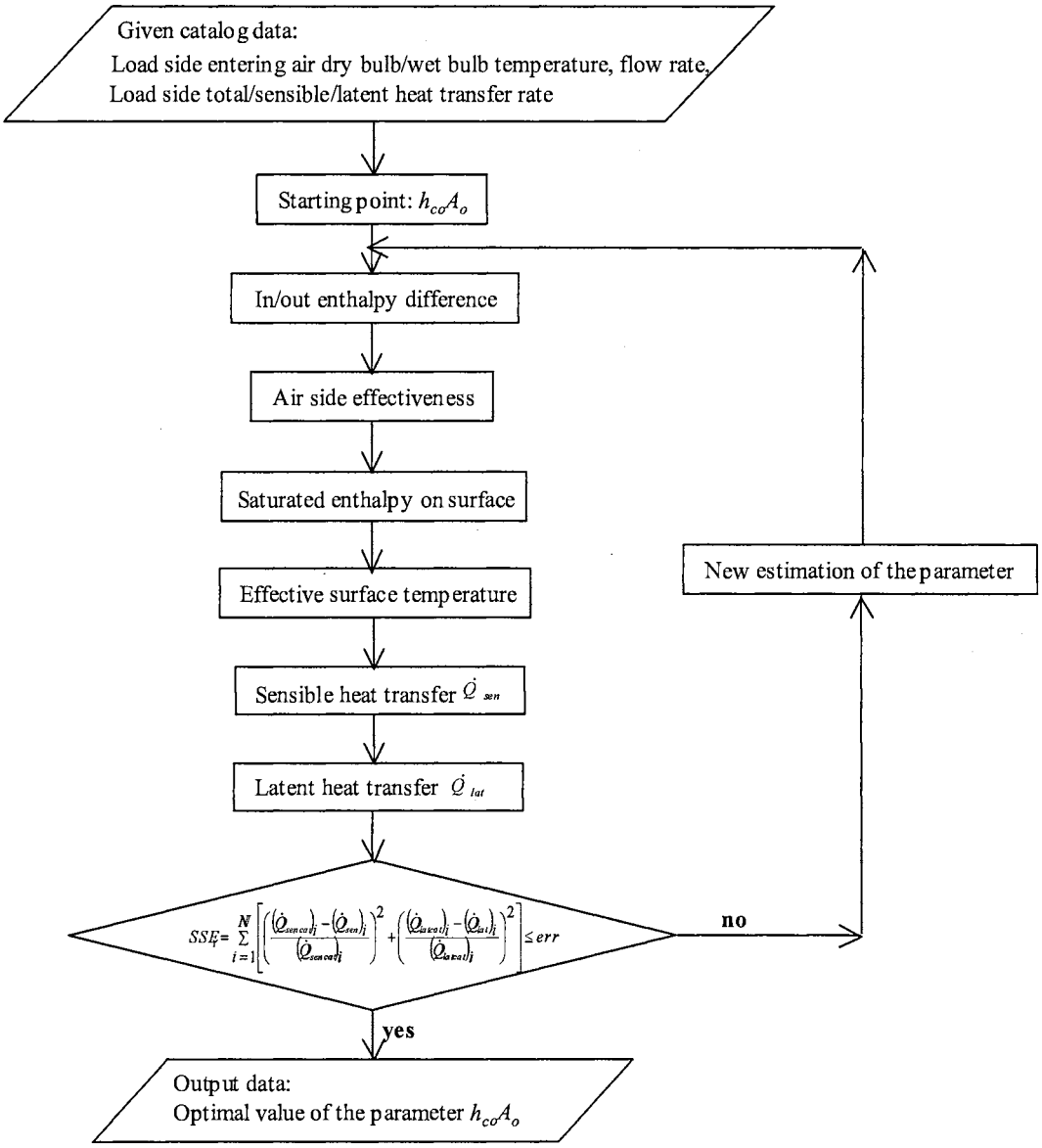

Figure 5.4. Flow diagram for parameter estimation computer program (#1)

When the optimal value of external heat transfer coefficient $h_{c,o}A_o$ is found, the next step is to search for the optimal values of the rest of the parameters, keeping the $h_{c,o}A_o$ fixed. The rest of the parameters are *PD, C, ΔP,* W_{loss}, ΔT_{sh}, η, $(UA)_S$, $(UA)_{tot}$.

5.6.2. Objective function #2 for the remaining parameters

1. Calculate the condenser effectiveness using Equation (5.2).
2. Calculate the evaprator effectiveness using Equation (5.6),
3. Calculate the evaporating and condensing temperatures of the refrigerant. The condensing temperature is determined using effectiveness model of sensible heat exchanger. However, since the driving potential for the heat transfer of the wet coil is enthalpy instead of temperature, the enthalpy is calculated first and the corresponding evaporating temperature is determined accordingly. The evaporating temperature is calculated using Equations (5.16), (5.17) and (5.18).
4. When the condensing and evaporating temperatures are obtained, the corresponding pressures and enthalpies can be derived using a refrigerant property subroutine. We used subroutines provided with an HVAC system simulation program (Clark and May 1985).
5. Identify the refrigerant state at the compressor suction port by adding the superheat to the evaporating temperature. The refrigerant enthalpy at this point is determined using the refrigerant property subroutines.
6. Identify the compressor suction and discharge states by adding or subtracting the pressure drop. The specific volume at the suction state is determined by the refrigerant property subroutines.
7. Calculate the refrigerant mass flow rate by Equation (4.4), the theoretical value of isentropic compression power by Equation (4.6) and the total power input by Equation (4.7).

8. Calculate the new value of the total cooling capacity for cooling mode using Equation (4.16).
9. The new value of heat rejection is calculated by adding up the power consumption and total cooling capacity.

Based on the given values of the parameters, the power consumption for the compressor, the total cooling capacity and the heat rejection are calculated for each operation point. The relative error between the catalog data and the calculated results for the power consumption, the total cooling capacity and the heat rejection should be small. This is achieved by searching for the minimum value of the following objective function, which is the sum of the squares of the relative errors.

$$SSE_2 = \sum_{i=1}^{N}\left[\left(\frac{(\dot{W}_{cat})_i - (\dot{W})_i}{(\dot{W}_{cat})_i}\right)^2 + \left(\frac{(\dot{Q}_{wetcat})_i - (\dot{Q}_{wet})_i}{(\dot{Q}_{wetcat})_i}\right)^2 + \left(\frac{(\dot{Q}_{scat})_i - (\dot{Q}_s)_i}{(\dot{Q}_{scat})_i}\right)^2\right] \quad (5.23)$$

where $\dot{W}_{cat}$ = catalog power consumption, kW or Btu/hr

$\dot{W}$ = calculated power consumption, kW or Btu/hr

$\dot{Q}_{wetcat}$ = catalog total cooling capacity, kW or Btu/hr

$\dot{Q}_{wet}$ = calculated total cooling capacity, kW or Btu/hr

$\dot{Q}_{scat}$ = catalog heat rejection, kW or Btu/hr

$\dot{Q}_s$ = calculated heat rejection, kW or Btu/hr

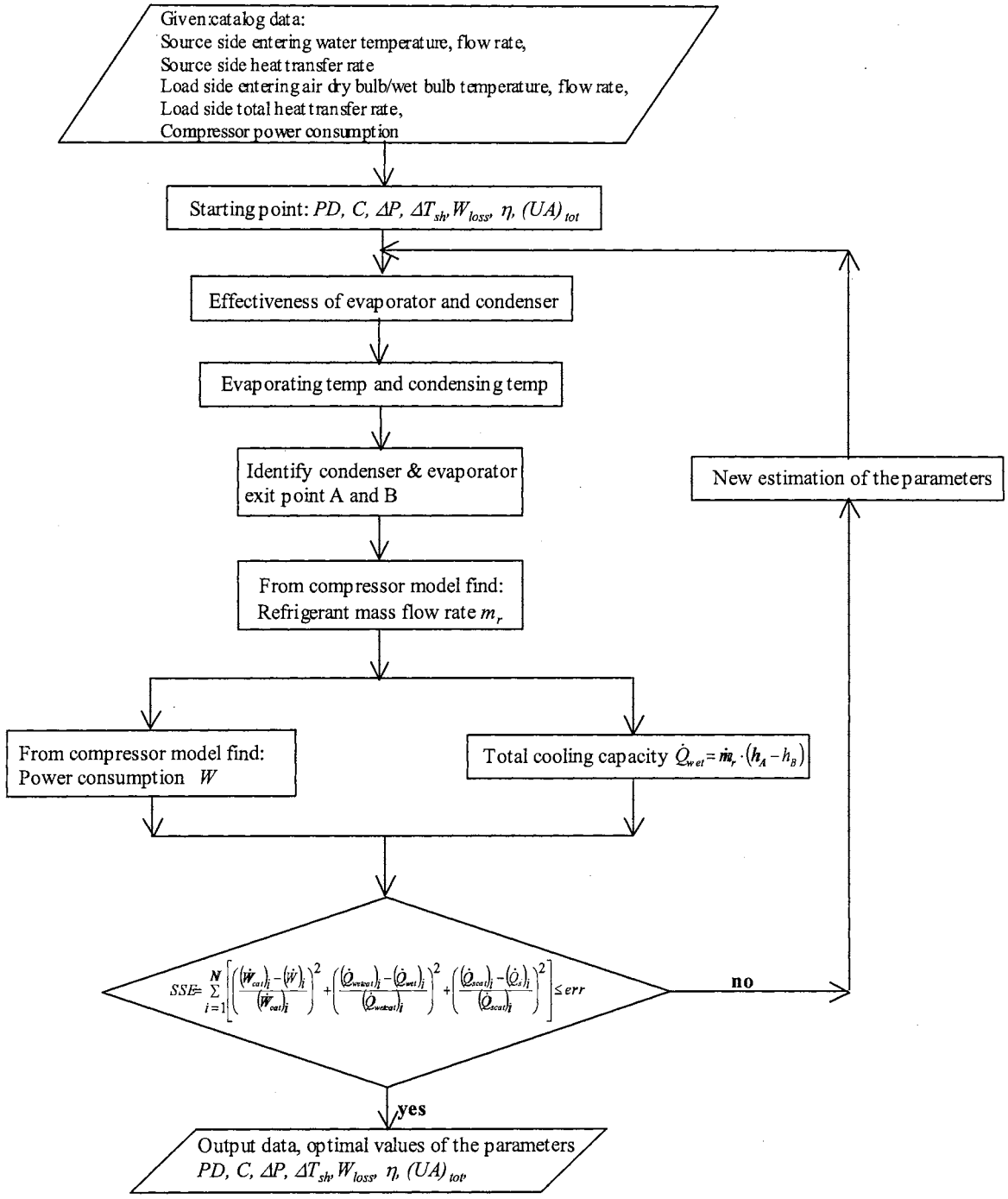

Figure 5.5. Flow diagram for parameter estimation computer program (#2)

The optimal parameter values for a particular heat pump will be those associated with the minimum value of function SSE_2. Again, the Nelder-Mead simplex (Kuester and

Mize 1973) method is employed. The flow chart for the computer program that implements the parameter estimation is shown in Figure 5.5.

5.7. Model Implementation

The model is implemented in a similar way as the objective functions evaluation described above. However, the model implementation program combines the two separate parameter estimation subroutines into one single procedure. A thermostat signal is used as an input parameter to tell the model which set of parameters (heating mode or cooling mode) should be used. Also, the objective function evaluation takes advantage of the fact that the heat transfer rates are known, using the catalog data as an initial guess, then minimizing the difference between the calculated and catalog heat transfer rates. However, for the model implementation, the heat transfer rates are solved simultaneously with successive substitution, and this introduces an iterative loop not present in the objective function evaluation.

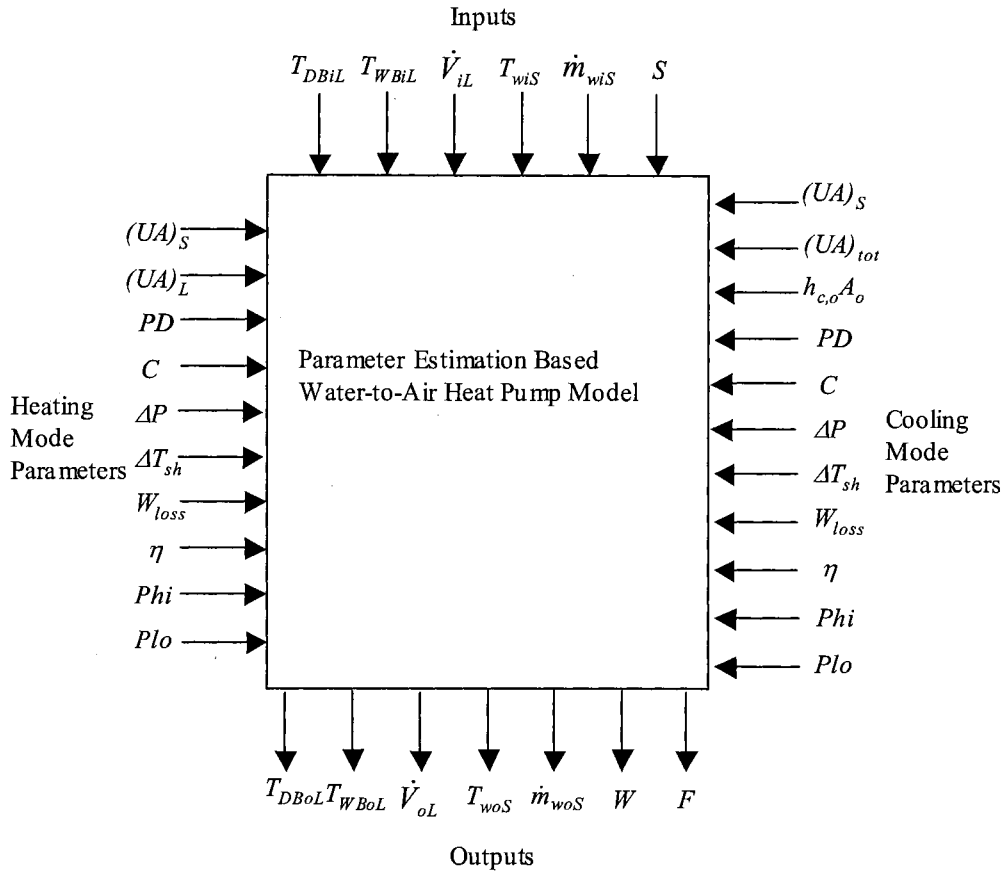

Figure 5.6. Information flow chart for model implementation

The model then determines the total/sensible cooling capacity, heating capacity, heat rejection, heat extraction, etc. The outlet temperatures can also be reported if desired. An information flow chart of the model implementation is presented in Figure 5.6. Similar to that of parameter estimation computer program, a logic diagram for model implementation is presented in Figure 5.7.

It is noted that in the model implementation, the total cooling capacity calculated using Equation (5.10) may be less than the sensible cooling capacity calculated using Equation (5.19) when the humidity ratio of the inlet air drops below the point of

completely dry coil. This departure from reality results from the approximation of using an analysis based on wet coil condition to predict dry coil condition. The enthalpy of saturated air at the coil surface is calculated by Equation (5.11). The humidity ratio of the saturated air at the coil surface is determined accordingly. In all cases, the humidity ratio of the air at the coil surface should be less than or equal to that of the main air flow. For a wet coil, the humidity ratio of the air at the coil surface is lower than that of the main air flow. For a dry coil, the humidity ratios are equal. However, the humidity ratio of the air at the coil surface determined from Equation (5.11) may be greater than that of the main air flow when the inlet air humidity ratio is very low. As a result, the sensible heat transfer rate calculated by Equation (5.19) may be greater than the total heat transfer rate calculated by Equation (5.10). Since this problem only occurs when the inlet air humidity ratio drops below the threshold of completely dry coil conditions, the solution is as simple as setting the sensible heat transfer rate equal to the total heat transfer rate. In fact, this condition may be looked upon as a signal for completely dry coil conditions, when the previous approach for splitting total heat transfer rate cannot be expected to work properly.

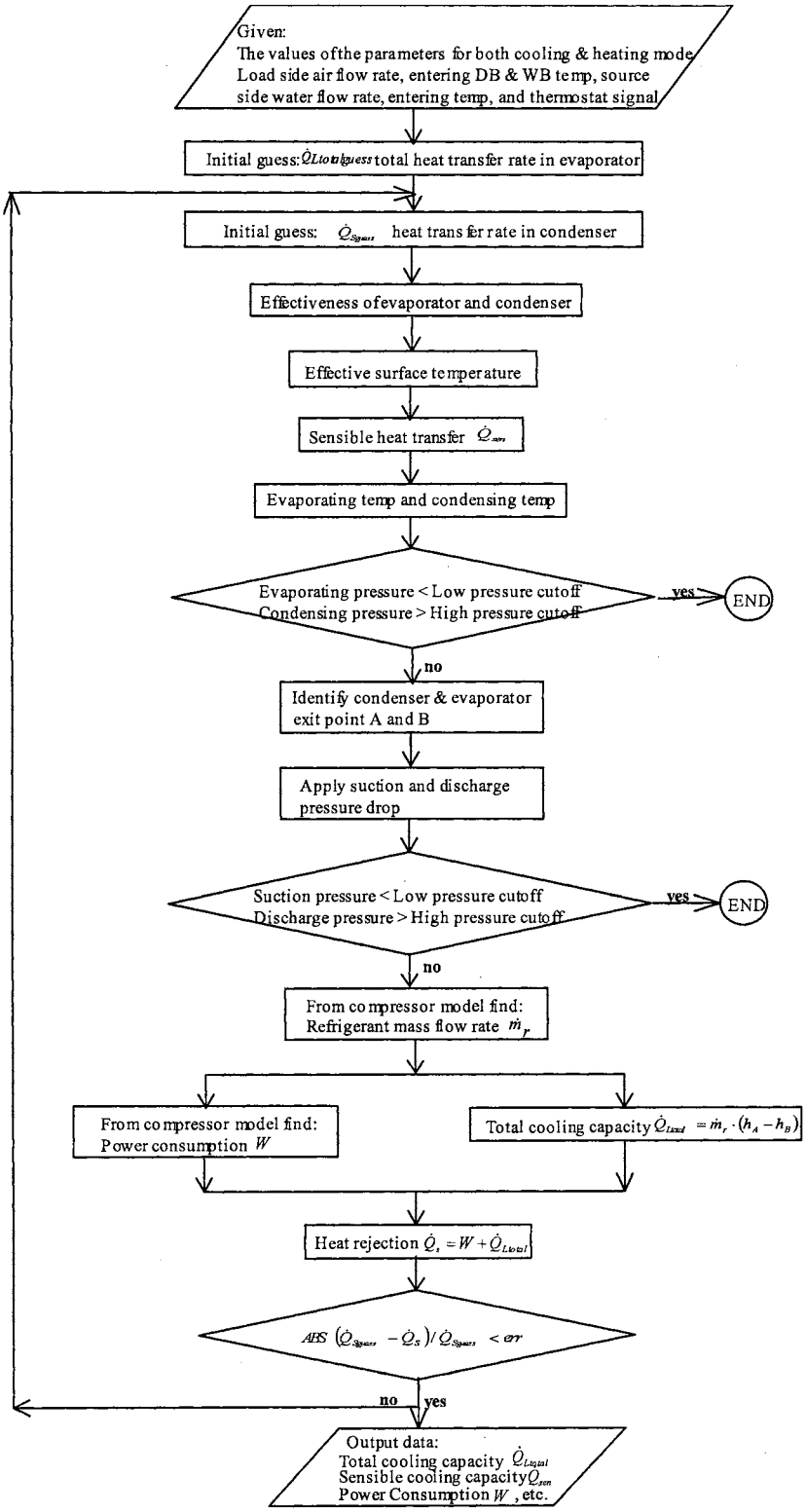

Figure 5.7. Flow diagram for model implementation computer program

5.8. Treatment of Extreme Operating Conditions

As discussed in Chapter 4, the model may encounter conditions not intended by the manufacturer, such as low water flow rates or extreme temperatures. This may happen even when the system simulation inputs are correct, as the equation solving process may occasionally try physically unrealistic values. Without any other checks, the model may then provide unrealistic results, or crash due to errors in the property routines. The treatment of extreme operating conditions in the water-to-air heat pump model is the same as that of the water-to-water heat pump model described in section 4.7, i.e. checks for the suction and discharge pressures are performed.

5.9. Model Validation

The water-to-air heat pump model was validated using catalog data for five heat pumps made by three different manufacturers. Since the cooling mode which involves dehumidification is the major concern, heat pump #1 to #5 are all validated using the cooling mode catalog data. Validation of the heating mode of the water-to-air heat pump model is fundamentally same as that of water-to-water heat pumps. For sake of brevity, it is not discussed in this chapter. A brief description of the heating mode validation for a water-to-air heat pump can be found in Chapter 8. It is noted that the manufacturers' tabulated performance data are originally given for one single combination of entering air dry bulb and wet bulb temperatures and air flow rate specified by ARI standard 320. Correction factors for variation in entering air temperature and air flow rate are also provided by the manufacuturers. In the model validation, the correction factors have been

used to expand the original data over a range of air temperatures and flow rates. Necessarily, these data are only as accurate as the manufacturers' correction factors. Since each correction factor is applied to multiple operating points (i.e. different entering water temperature, water flow rate and air flow rate), these data are presumed to have lower accuracy than the other tabulate data.

The root-mean-square (RMS) error for the total cooling capacity, sensible cooling capacity, latent cooling capacity and power are shown in Table 5.1. RMS errors for latent capacity are given in Watts and Btu/Hr instead of percentage, because the latent cooling capacity is sometimes zero, and the percentage error then become meaningless. The RMS errors between model prediction and catalog data for the total cooling capacity range from 2.4% to 6.2%. Those of power consumption range from 3.5% to 7.4%. However, some relatively larger errors occur for the splitting of the total cooling capacity into sensible and latent parts. The greatest error is 6.4% for the sensible and 0.82 kW (2,798 Btu/Hr) for the latent respectively. The least error is 4.3% for the sensible and 0.14 kW (478 Btu/Hr) for the latent respectively. Given the complication and limitation involved in the modeling of the direct expansion cooling coil, the comparison shows a comparatively good agreement between model prediction and catalog data.

As with the water-to-water heat pump model, this modeling approach also has the advantage of not requiring experimental and component specifications data beyond what is published in the heat pump manufacturer's catalogs. All the comparisons are made based on the external measurements of water flow rates and temperatures for both source

and load sides. The ranges of flows and inlet temperatures in the catalog data for the heat pumps investigated are presented in the Table 5.2 and Table 5.3.

Table 5.1. A List of the HP's used for Model Verification

No			1	2	3	4	5
Make			Addison	Climate Master	Trane	Addison	Trane
Model			WPG017-1A	HS006	WPHF021	WPG036-1A	WPHF040
Nominal Cooling Capacity		Btu/Hr	16,000	7,400	21,000	35,000	40,000
		Watts	4,690	2,170	6,155	10,260	11,700
Total Points			2,544	2,981	1,339	2,536	1,435
RMS	Total Capacity	All Points	2.92%	4.72%	5.46%	2.39%	6.22%
		32 Points	4.32%	5.68%	5.57%	2.99%	7.01%
	Sensible Capacity	All Points	6.43%	6.33%	4.26%	5.26%	4.97%
		32 Points	6.64%	15.4%	4.78%	6.47%	10.52%
	Latent Capacity	All Points	0.16 kW (546 Btu/Hr)	0.14 kW (478 Btu/Hr)	0.39 kW (1,331 Btu/Hr)	0.25 kW (853 Btu/Hr)	0.82 kW (2,798 Btu/Hr)
		32 Points	0.25 kW (853 Btu/Hr)	0.27 kW (921 Btu/Hr)	0.43 kW (1,467 Btu/Hr)	0.27 kW (921 Btu/Hr)	1.23 kW (4,196 Btu/Hr)
	Heat Rejection	All Points	2.67%	3.71%	4.73%	2.43%	5.50%
		32 Points	4.47%	3.78%	6.29%	2.95%	6.37%
	Power	All Points	3.47%	6.38%	6.25%	6.51%	7.41%
		32 Points	6.13%	8.58%	10.3%	7.49%	13.7%

Table 5.2. Range of Flow Rates and Temperatures (IP units)

No	Source Side		Load Side		
	EWT (°F)	Flow Rate (GPM)	Dry Bulb (°F)	Wet Bulb (°F)	Flow Rate (CFM)
1	40 to 110	2 to 4	70 to 90	61 to 73	400 to 550
2	40 to 110	1 to 2.4	70 to 90	61 to 73	165 to 320
3	45 to 120	2.5 to 6	70 to 85	45 to 78	480 to 720
4	40 to 110	5 to 9	70 to 90	61 to 73	800 to 1100
5	45 to 120	4.5 to 13	70 to 85	45 to 78	960 to 1440

Table 5.3. Range of Flow Rates and Temperatures (SI units)

No	Source Side		Load Side		
	EWT (°C)	Flow Rate (L/S)	Dry Bulb (°C)	Wet Bulb (°C)	Flow Rate (L/S)
1	4.4 to 43.3	0.13 to 0.25	21.1 to 32.2	16.1 to 22.8	189 to 260
2	4.4 to 43.3	0.06 to 0.15	21.1 to 32.2	16.1 to 22.8	77.9 to 151
3	7.2 to 48.9	0.16 to 0.38	21.1 to 29.4	7.2 to 25.6	227 to 340
4	4.4 to 43.3	0.32 to 0.57	21.1 to 32.2	16.1 to 22.8	378 to 519
5	7.2 to 48.9	0.28 to 0.82	21.1 to 29.4	7.2 to 25.6	453 to 680

Once the air inlet condition correction factors have been utilized, there are thousands of operating points given in the catalog for all five heat pumps. The points cover a range of entering water temperatures and water flow rates on source side, and a range of entering air dry bulbtemperatures, wet bulb temperatures and air flow rate on the load side of the heat pump. The idea to use data points representing the combination of the lowest and highest values of the input variables described in chapter 4 for the water-to-water heat pump model can also be applied to the water-to-air heat pump model. Since air temperature should be described by both dry bulb temperature and wet bulb temperature, 32 data points have been used to represent the combination of the lowest and highest values of the input variable. Parameters were determined for each heat pump using all points and then 32 points representing combinations of the highest and lowest values of the temperatures and mass flow rates on each side, Once the parameters were determined, both sets of parameters were applied to all operating points. The comparisons of the results are summarized in Table 5.1. In fact, the parameter estimation model performs almost as well with 32 data points as with all the data points. This represents a significant advantage if the model user has to manually transcribe the data from the catalog. The model accuracy for using all the data points and 32 data points are plotted in Figures 5.8. through 5.17. for heat pump #1.

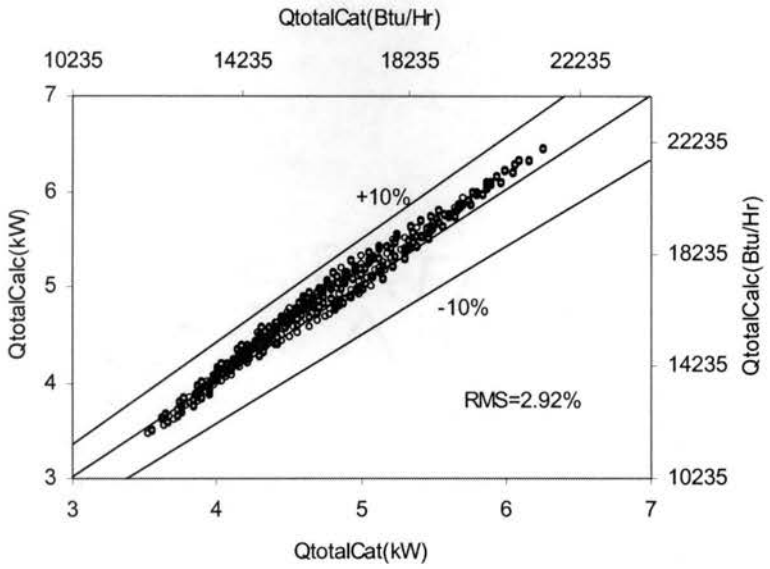

Figure 5.8. Calculated total cooling capacity vs. catalog total cooling capacity (heat pump #1 all points)

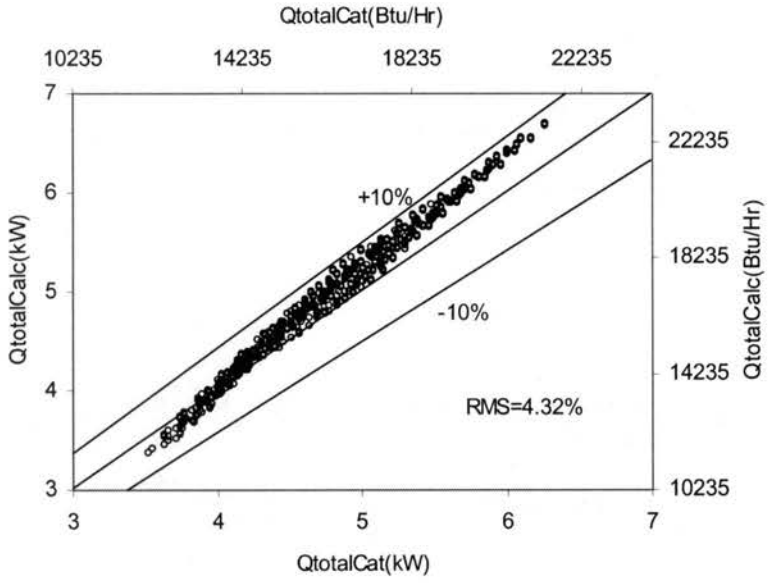

Figure 5.9. Calculated total cooling capacity vs. catalog total cooling capacity (heat pump #1 32 points)

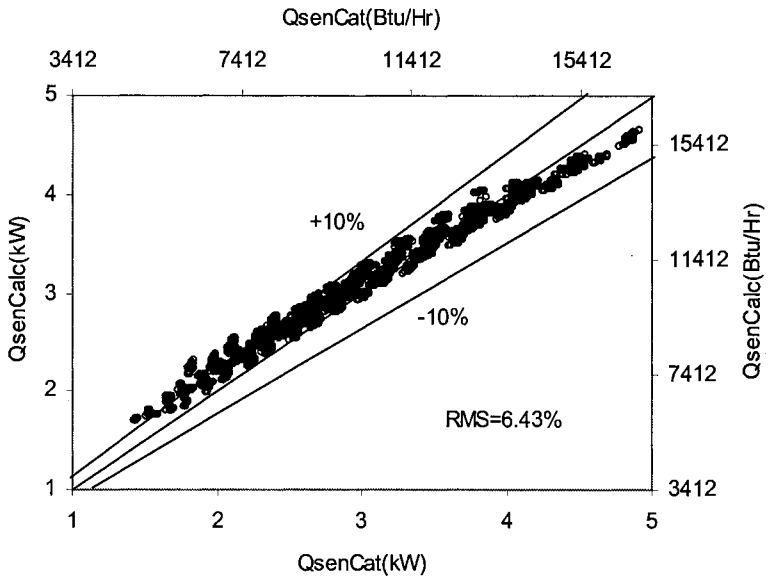

Figure 5.10. Calculated sensible cooling capacity vs. catalog sensible cooling capacity (heat pump #1 all points)

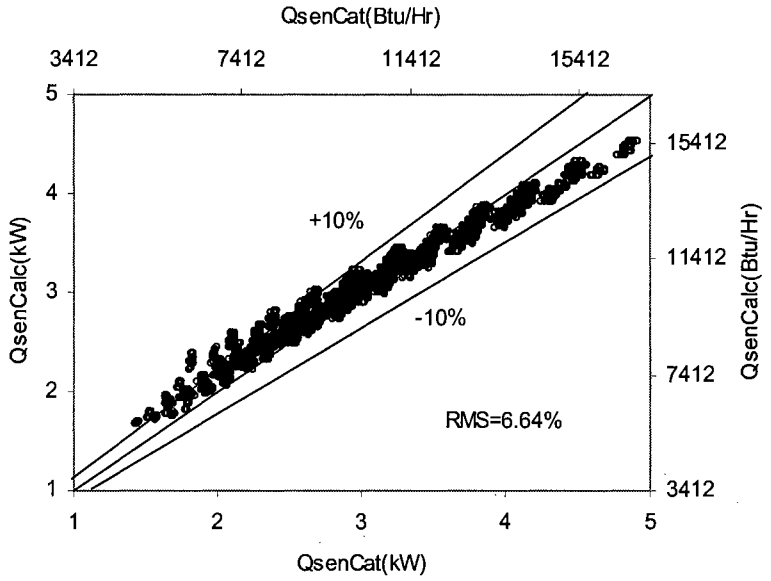

Figure 5.11. Calculated sensible cooling capacity vs. catalog sensible cooling capacity (heat pump #1 32 points)

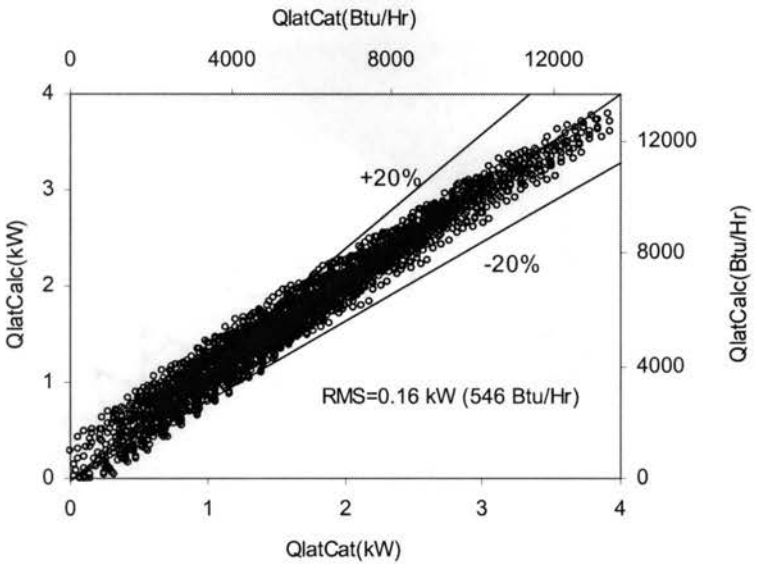

Figure 5.12. Calculated latent cooling capacity vs. catalog latent cooling capacity (heat pump #1 all points)

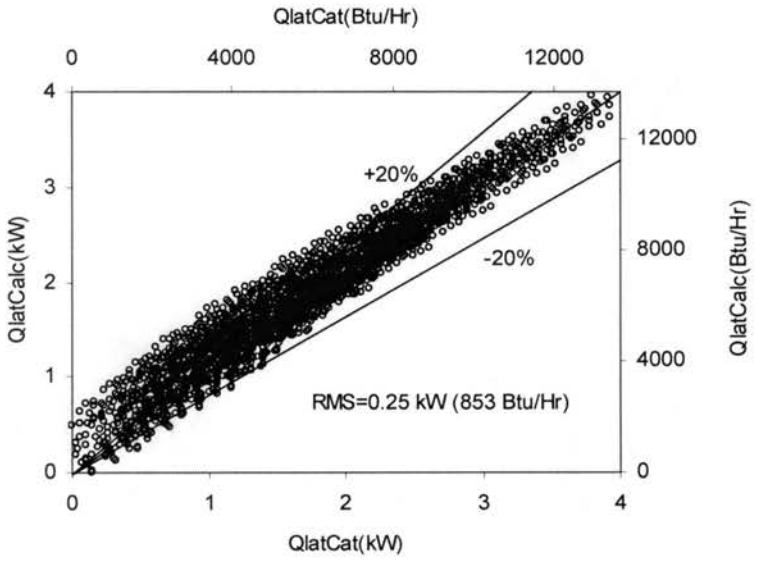

Figure 5.13. Calculated latent cooling capacity vs. catalog latent cooling capacity (heat pump #1 32 points)

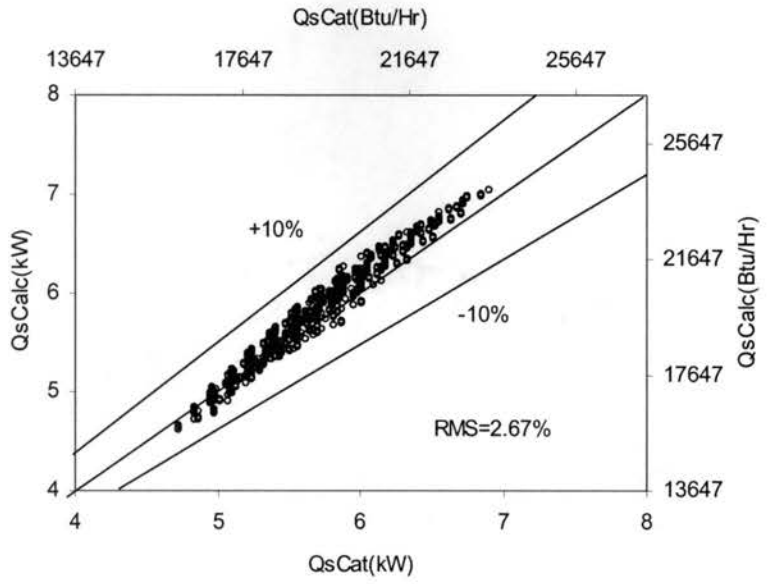

Figure 5.14. Calculated heat rejection vs. catalog heat rejection (heat pump #1 all points)

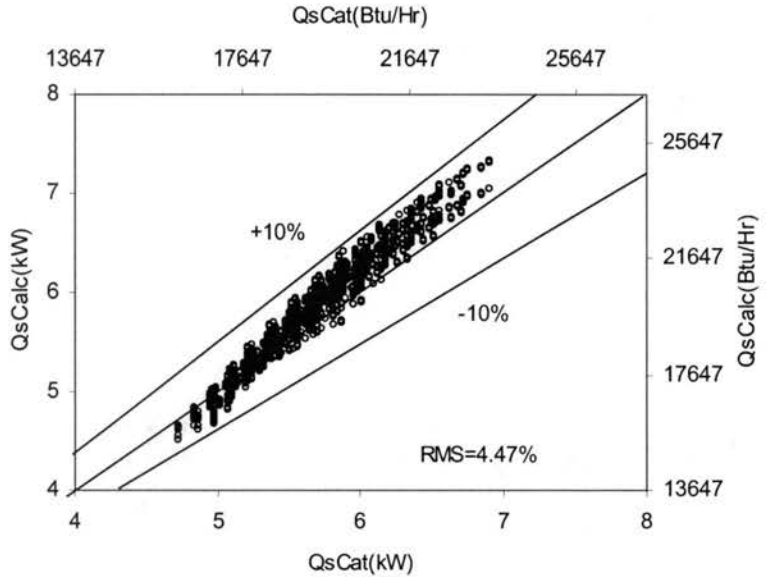

Figure 5.15. Calculated heat rejection vs. catalog heat rejection (heat pump #1 32 points)

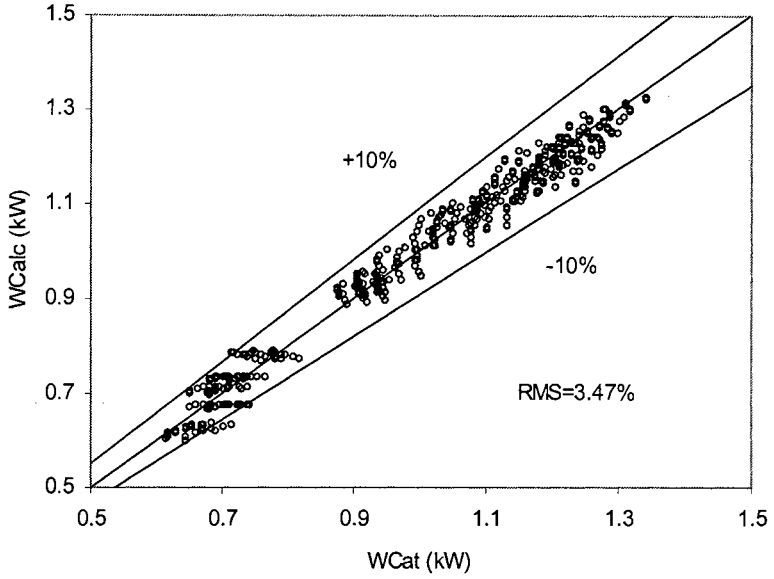

Figure 5.16. Calculated power consumption vs. catalog power consumption (heat pump #1 all points)

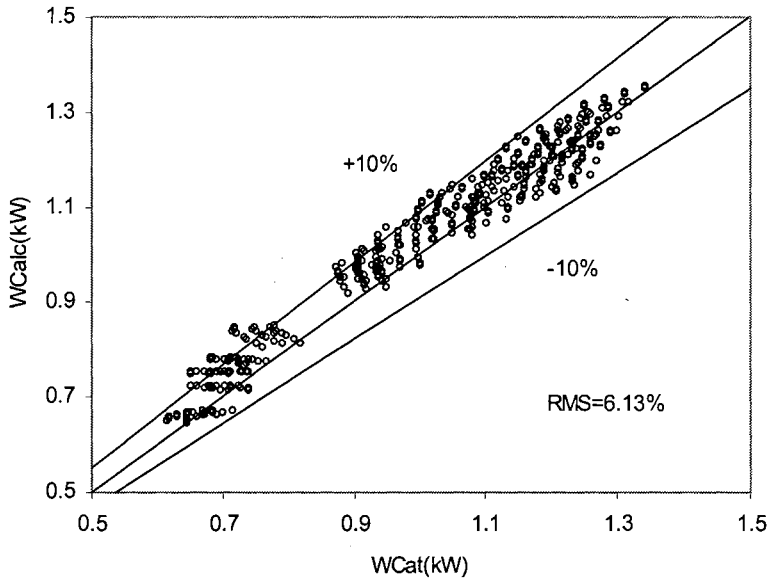

Figure 5.17. Calculated power Consumption vs. catalog power consumption (heat pump #1 32 points)

5.10. Prediction of Dry Coil Condition using Wet Coil Parameters

The total and sensible heat transfer calculation discussed above is based on the completely wet coil assumption. However, this analysis can also be used for completely dry calculation as an approximation. Morisot et al. (2002) discussed the error induced by the wet or dry determination method and the use of wet coil external heat transfer coefficient for both wet and dry conditions. In the model implementation discussed previously, it could be assumed that if the predicted total heat transfer rate and sensible heat transfer rate are very close to each other, the coil is likely to be under completely dry condition. However, it is not expected that the model is able to predict the dry coil or partly dry coil condition with 100% confidence based on completely wet coil assumption. The analysis for completely wet coil is useful to some extent to predict the performance with dry coil. This section will examine this prediction.

Heat pump #1 in the model validation has been used to test the model behavior in response to the inlet air humidity ratio. Data points with the lowest dry bulb temperature of 21.1 °C (70 °F), medium dry bulb temperature of 26.7 °C (80 °F) and highest dry bulb temperature of 32.2 °C (90 °F) are selected from the manufacturer's catalog. The wet bulb temperature is reduced by an appropriate step starting from the value equal to dry bulb temperature. The model predicted latent heat factor, which is the ratio of latent cooling capacity and total cooling capacity is plotted in Figure 5.18 through Figure 5.20 against wet bulb temperature. The catalog latent heat factors are also plotted. It is reasonable to assume that the points with wet bulb temperature close to that of the

maximum latent heat factor can be regarded as in completely wet coil condition. There exists a wet bulb temperature, above which the latent cooling or condensation occurs. The points with wet bulb temperature close to or below that temperature can be regarded as in the completely dry coil condition. As can be seen from the figures, the model performance is physically realistic as the air becomes dryer.

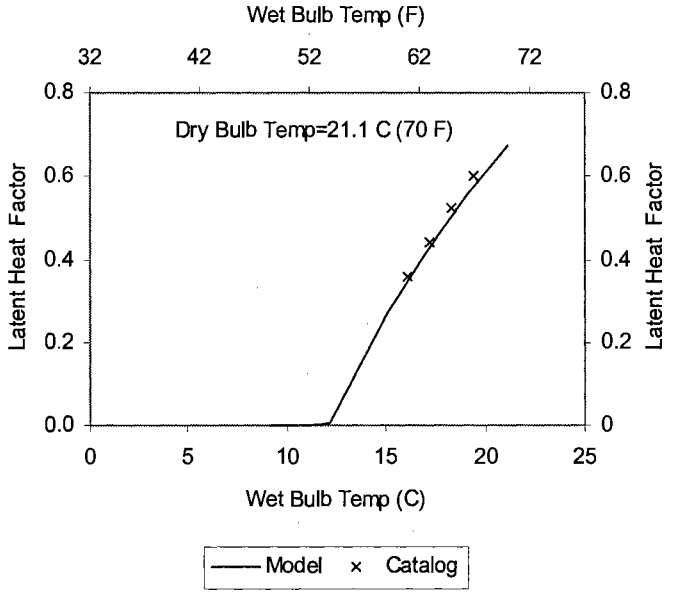

Figure 5.18. Latent heat factor vs. wet bulb temperature (low dry bulb temp)

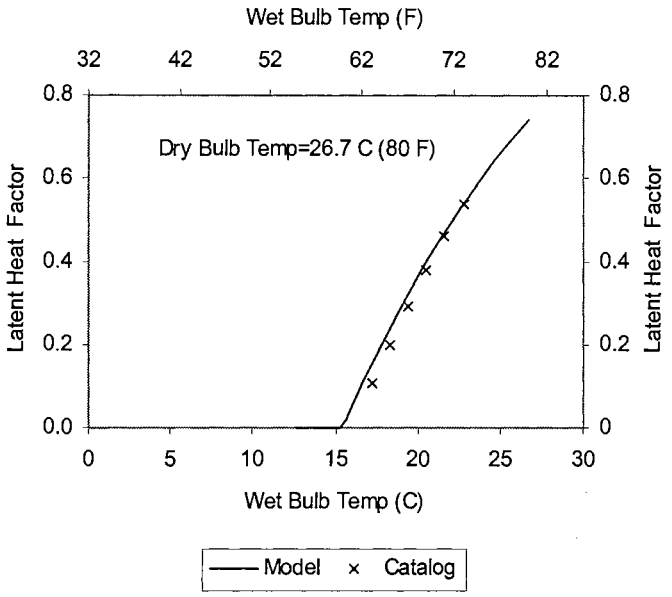

Figure 5.19. Latent heat factor vs. wet bulb temperature (medium dry bulb temp)

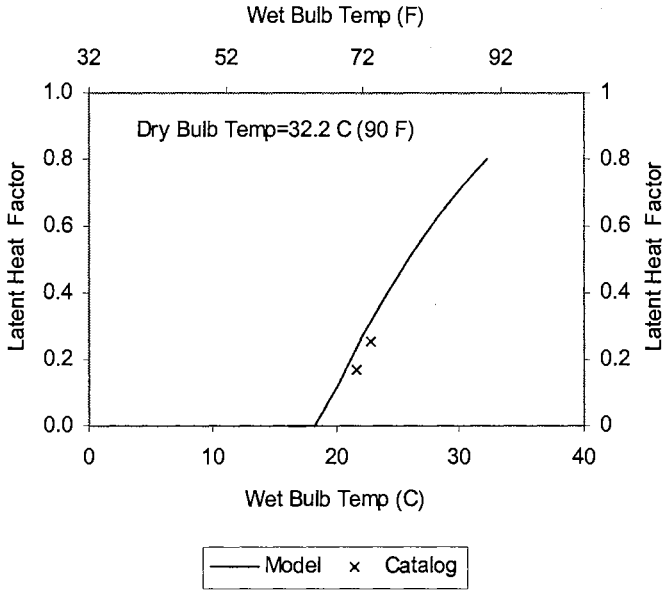

Figure 5.20. Latent heat factor vs. wet bulb temperature (high dry bulb temp)

5.11. Conclusion for Water-to-Air Heat Pump Model and Recommendations for Future Work

This chapter has presented a water-to-air heat pump model suitable for use in building energy analysis and HVAC system simulation programs. The model has been developed so as to require only commonly available data from manufacturers' catalogs in order to estimate the model coefficients. As compared to more detailed deterministic models, it does not require internally measured data usually unavailable to building system designers and simulationists.

The previously developed evaporator and condenser models are based on availability of the detailed information of the dimensions and configuration of the heat exchangers, such as tube and fin sizes, row numbers, fin spacing and type, and circuit types, etc. The complication associated with the co-existence of dry and wet regions with variable (UA) then can be solved. However, the information required for such detailed models is not typically given in the heat pump manufacturers' catalogs, and it may also requires some internal measurements to refine the model to such a detailed level. Hence, it is not set up as the target of this research effort.

In addition, the values of the other parameters need to have physical meanings. In other words, they should fall into some physically reasonable range that may be realistic for the actual heat pump performance and its component specifications. However, it is not expected that the estimated parameter values shall match the exact specifications of the heat pump and its components if they are available. Instead, this research effort is trying to establish a model that can replicate the heat pump performance published in the

manufacturers' catalogs, and some desirable prediction beyond the catalog data using a parameter estimation technique.

The parameter estimation based water-to-air heat pump model has been developed so as to require only commonly available data from manufacturers' catalogs in order to estimate the model coefficients. As compared to more detailed deterministic models, it does not require internally measured data usually unavailable to building system designers and simulationists. It also works well with only 32 data points, making it reasonably convenient when the data must be manually transcribed from a catalog. As compared to equation-fit models, this model retains the physically-based representation of the heat pump, which allows some extrapolation beyond the catalog data. The complication associated with the water-to-air heat pump exists in the modeling of load side heat exchanger, or direct expansion cooling coil specifically. Difficulty was encountered in the distinguishing of dry and wet conditions with limited information available from the catalog data. This has been solved by the approximation of using wet coil external convection heat transfer coefficient to predict dry coil condition. The model predicts sensible and latent capacities acceptably well when the coil approaches completely dry conditions.

The potential exists for significantly increasing the performance of water-to-air heat pump model. Further research is suggested in the following areas:

- Modeling of the direct expansion coil operating in cooling mode is the greatest challenge in the water-to-air heat pump model. A small change of

inlet air condition may result in a significant change in cooling capacity and outlet air condition. The transition from completely dry coil to partly dry and partly wet coil, and the transition from partly dry and partly wet coil to completely wet coil are not the focus of this model. However, if a more full description of the DX coil and air condition is required, additional research using more detailed information of the coil and entire heat pump may be needed.

- Additional validation of the model, using data from an experimental system, would be highly useful. The manufacturers' catalog data have unknown accuracy at conditions other than the ARI operating point. Particularly, the correction factors for variation in entering air temperature and air flow rate may be a fairly rough approximation since one single factor is used for multiple operating points with different water temperature and flow rate. As a result, the performance data calculated using the correction factors for conditions other than standard may not be as accurate as the data for standard conditions.

Another possibility is that manufacturers could use this parameter estimation based model to generate catalog data for non-measured conditions. This could give significantly improved catalog data as compared to the equation-fit procedures that are apparently used now.

- As it is noticed in the model validation results, the split of total cooling capacity into sensible and latent parts are not very satisfactory for a few cases. One of the reasons may be due to the completely wet coil assumption. The author believes that a better understanding of the co-existence of the dry and wet regions and the transition point on the cooling coil may be necessary to refine the model.
- Only two-phase region is considered for the heat exchanger model. Refrigerant superheat and subcooling may also have influence on the heat exchanger performance to some extent. Thus, if more detailed insight into the heat exchangers is expected, a more sophisticated model, which accounts for subcooling and superheat may be necessary.

6. Extensions for the Parameter Estimation Based Heat Pump Models

This chapter covers three important extensions to the water-to-water and water-to-air heat pump models – scroll compressors, rotary compressors and antifreeze. Scroll compressors and rotary compressors are two frequently used alternatives to reciprocating compressors. Therefore, it is desirable to develop models of scroll and rotary compressors that can replace the reciprocating compressor model in the heat pump models presented in Chapter 4 and Chapter 5. In this chapter, a five parameter (including intake volumetric flow rate, built-in compression ratio, leakage coefficient and two efficiency-related parameters) scroll compressor model and a four-parameter (displacement, discharge pressure drop, two efficiency-related parameters) rotary compressor model will be presented.

While necessary in many applications for providing freeze protection, antifreeze solutions adversely impact heat transfer performance. It is also desirable to be able to model water-source heat pumps when the secondary heat transfer fluid is a water-antifreeze mixture. An approach to adjust the heat exchanger model by modifying the heat transfer coefficient, as a result of the change in the physical properties of the secondary heat transfer fluid will also be presented.

6.1. Modeling of Scroll Compressor

6.1.1. Model

The scroll compressor is a member of the big family of positive displacement compression machines. For the scroll compressor, compression is accomplished by the

rotary motion of two interfacing, spiral-shaped scrolls. At the suction state, refrigerant vapor is trapped in a pocket at the outer periphery of the scrolls. As the scrolls move, this pocket is continuously made smaller, compressing the vapor as it proceeds toward the discharge port. The scroll compressor's fixed volume ratio is set by the geometry of the scrolls and the location of the discharge port. This feature provides the scroll compressor with different performance characteristics from those of reciprocating compressors. Pressure losses are minimized with large suction and discharge ports. High volumetric efficiency over a wide range of operation conditions is achieved as a result of the absence of valves and re-expansion volumes, and the continuous flow process. Figure 6.1 shows the compression process schematically.

A few scroll compressor models have been described in the literature (Morishita 1984, Qu et al. 1998, Bush and Elson 1988, Ikegawa et al. 1984, Etemad and Mieter 1988). However, these models are targeted at the re-design of the scroll compressor for improved performance. The models require an exhaustive description of all the components in the compressor such as the configuration of the scrolls, the location of the ports, and the rotation speed, etc. The high number of parameters in these models make them infeasible to use with the parameter estimation based modeling approach, at least in cases where the overall heat pump performance is modeled.

Winandy, et al. (2002) presented a hermetic scroll refrigeration compressor model, which shares some significant features with the screw compressor model presented by Lebrun, et al. (1999). Both types of compressors trap a volume of refrigerant and

continuously reduce the size of the volume up to the discharge port. The characteristics shared by the twin-screw compressor and scroll compressor make it possible to duplicate most of the thermodynamic analysis for twin-screw compressors for use in the scroll compressor model.

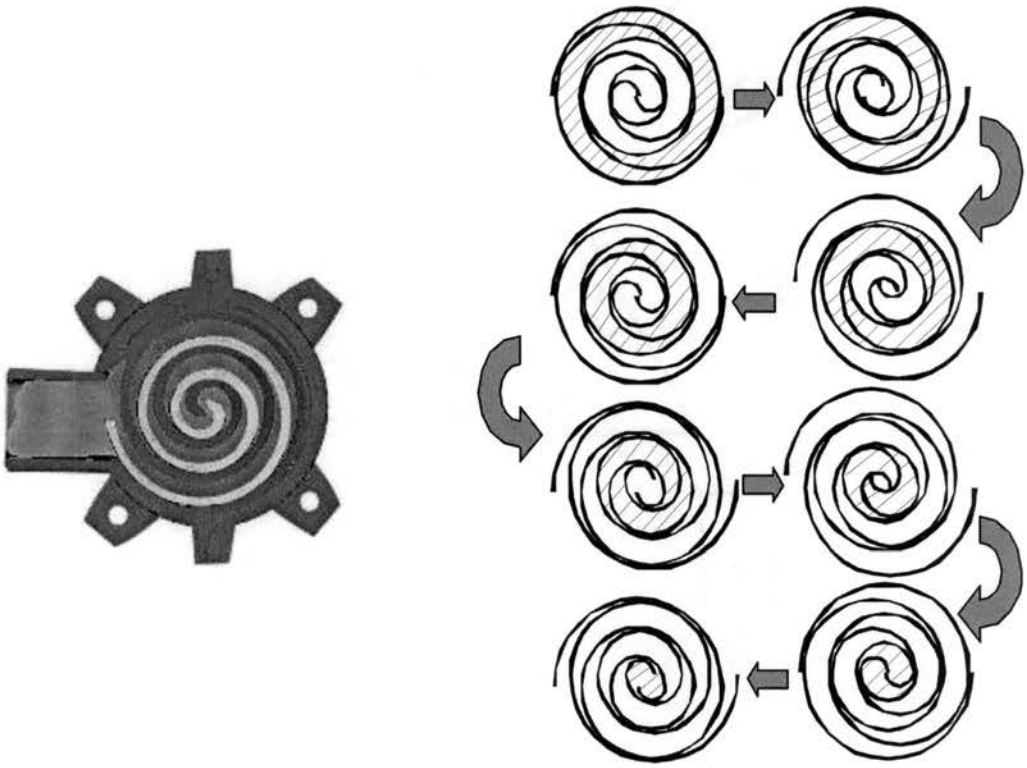

Figure 6.1. Scroll compression process

(ASHRAE handbook of HVAC systems and equipment)

First, both of them have a feature called 'built-in' pressure ratio or internal pressure ratio. This feature, the 'built-in' compression ratio may be defined by the following equation,

$$\pi_i = \frac{P_i}{P_e} \tag{6.1}$$

where π_i = the 'built-in' pressure ratio

P_i = the internal discharge pressure, kPa or psia

P_e = the evaporating pressure, kPa or psia

Another related characteristic to the 'built-in' pressure ratio is the 'built-in' volume ratio v_i, which is the ratio of the volume of the trapped gas pocket immediately after closing, to the volume of trapped gas pocket immediately before opening to discharge. The relationship between 'built-in' pressure ratio and 'built-in' volume ratio may be derived as follows if the compression is assumed to be isentropic,

$$\pi_i = v_i^{\gamma} \tag{6.2}$$

Analogously, scroll compression also involves another important term as 'external pressure ratio', which is the ratio of the condensing pressure, denoted as P_c to the evaporating pressure, denoted as P_e. This ratio was defined by LeBrun et al. (1999) as follows,

$$\pi = \frac{P_c}{P_e} \tag{6.3}$$

The difference between external pressure ratio and 'built-in' pressure ratio results in three modes of operation of the scroll compression process – design operation, over compression and under compression. Under design conditions, the 'built-in' pressure ratio is equal to the external pressure ratio. This should be the optimal operating point. However, the scroll compressor operates over a range of conditions where the external pressure ratio varies and it does not match the internal pressure ratio.

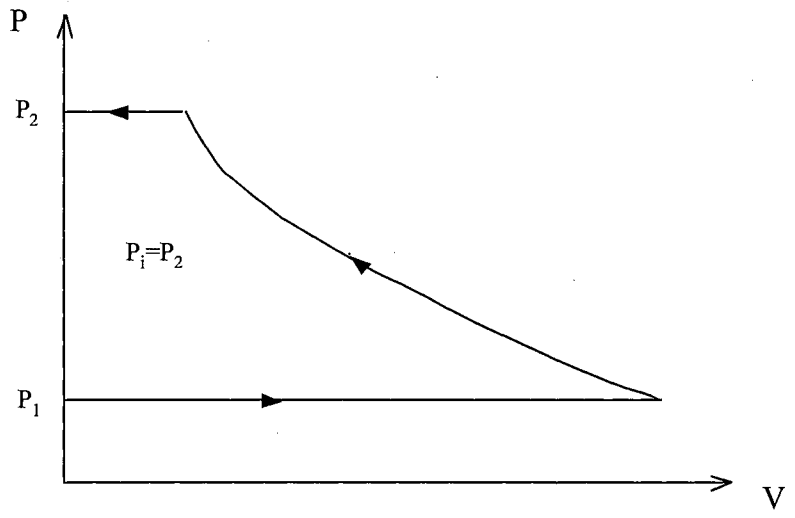

Figure 6.2. Thermodynamic cycle of a scroll compressor under design condition

When the condensing pressure is lower than internal discharge pressure, over-compression occurs. In this case, the trapped gas pocket is compressed above the condensing pressure and expand into the discharge as the port is uncovered, with resultant lost work.

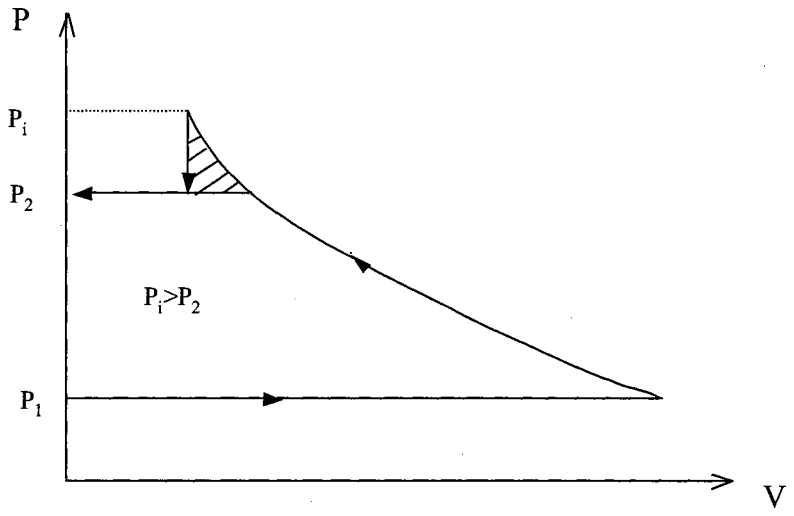

Figure 6.3. Thermodynamic cycle of a scroll compressor with over-compression loss

When the condensing pressure is higher than the internal discharge pressure, under-compression occurs. In this case, trapped pocket opens early to a higher pressure in the discharge line and then must pump against this higher pressure for the remaining rotary motion of the scrolls, requiring higher torque than would have been required if the pressure had built up gradually to the condensing pressure.

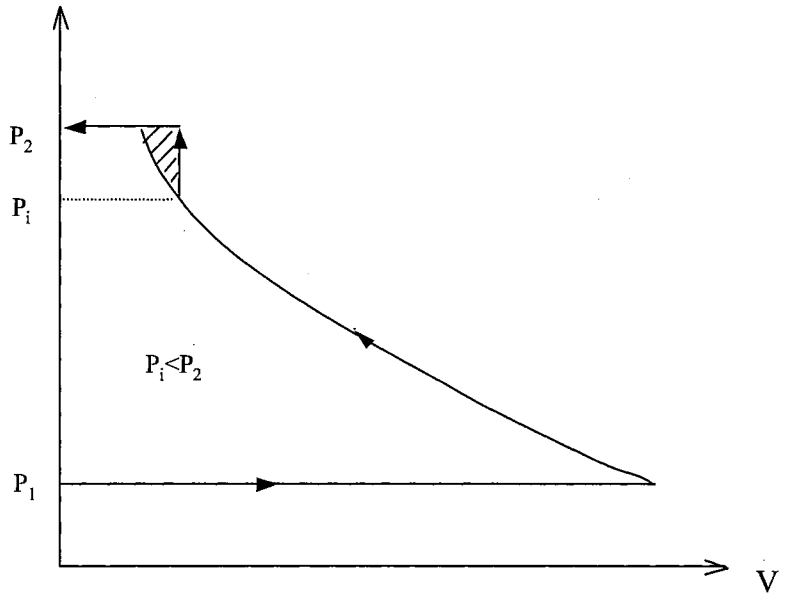

Figure 6.4. Thermodynamic cycle of a scroll compressor with under-compression loss

Both over compression and under compression may lead to energy losses in the compressor. The theoretical power consumption of the compressor will be a little higher than the power required to perform a pure isentropic compression. Figures 6.2-6.4 show the actual compression processes schematically. The shaded areas constitute the energy losses when the 'built-in' pressure ratio and external pressure ratio are not equal to each other.

If external pressure ratio matches the 'built-in' pressure ratio, isentropic power consumption is,

$$W_t = \frac{\gamma}{\gamma - 1} P_e \dot{V}_r \left[\pi^{\frac{\gamma-1}{\gamma}} - 1 \right] \tag{6.4}$$

where P_e = the evaporating pressure, kPa or psia

$\dot{V}_r$ = the refrigerant volume flow rate at the beginning of the compression, m^3/s or ft^3/min

γ = isentropic exponent

If external pressure ratio does not match the 'built-in' pressure ratio, the power consumption will be higher than that of the isentropic process.

$$W_t = \frac{\gamma}{\gamma - 1} P_e \dot{V}_r \left[\frac{\gamma - 1}{\gamma} \frac{\pi}{v_i} + \frac{1}{\gamma} \pi_i^{\frac{\gamma-1}{\gamma}} - 1 \right] \tag{6.5}$$

A simple linear representation, which follows the same modeling approach as reciprocating compressor discussed previously, has been used to account for the electrical and mechanical efficiency of the compressor. The actual power input for the compressor is calculated by the following equation,

$$\dot{W} = \frac{\dot{W}_t}{\eta} + \dot{W}_{loss} \tag{6.6}$$

where $\dot{W}$ is the compressor power input, $\dot{W}_t$ is the theoretical power, η is the electro-mechanical efficiency , $\dot{W}_{loss}$ is the constant part of the electro-mechanical power losses.

Due to the absence of suction and discharge valves and theoretically negligible re-expansion volumes, the refrigerant volume flow rate at the beginning of the compression $\dot{V}_r$ is equal to the product of the volume of the pockets that seal the suction gas at the

beginning the compression and the rotational speed. This volume should be a value defined by its configuration and dimension for a given compressor. Thus, the refrigerant mass flow can be determined as,

$$\dot{m}_r = \frac{\dot{V}_r}{v_{suc}} \tag{6.7}$$

Where v_{suc} = specific volume at the suction state, m^3/kg or ft^3/lbm

In practice, leakage will reduce the refrigerant mass flow rate in the scroll compressor calculated by Equation (6.7). In the scroll compressor model presented by Chen et al. (2000), the leakage due to the gap between the bottom/top plate and the scrolls and the gap between the flanks of the two scrolls has been discussed quantitatively. Based on the analysis of Chen et al. (2000), the leakage was found to be a function of the ratio of discharge pressure and suction pressure. To simplify the calculation, the discharge pressure is assumed to be equal to condensing pressure and the suction pressure is equal to the evaporating pressure. Hence, the leakage rate is defined as follows:

$$\dot{m}_{leak} = C \cdot \frac{P_c}{P_e} \tag{6.8}$$

Where P_c is condensing pressure, P_e is evaporating pressure and C is coefficient to define the relationship between pressure ratio and leakage rate.

The refrigerant mass flow rate calculated in Equation (6.7) is then corrected by subtracting the leakage mass flow rate calculated in Equation (6.8). To summarize, the parameters chosen to represent the scroll compressor model will be $\dot{V}_r$, v_i, C, W_{loss} and η. These parameters, along with the UA values for both heat exchangers and the superheat, are estimated from catalog heat pump data. (As described below, use of antifreeze further increases the parameters.)

6.1.2. Algorithm

As an example, the algorithm for the water-to-water heat pump model, with the scroll compressor, is summarized below. For the sake of brevity, only the heating mode of the model is described.

For any given set of parameters, $\dot{V}_r$, v_i, C, W_{loss}, η and ΔT_{sh}, $(UA)_L$, $(UA)_S$, which are defined previously in Chapter 4, and initial guesses of load side heat transfer rate $\dot{Q}_L$ and source side heat transfer rate $\dot{Q}_S$, the model is implemented as follows.

1. Calculate the evaporator and condenser effectiveness by Equations (6.9) and (6.10),

$$\varepsilon_S = 1 - \exp\left(-\frac{(UA)_S}{C_{pw}\dot{m}_{wS}}\right) \tag{6.9}$$

where ε_S = thermal effectiveness of evaporator

$(UA)_S$ = heat transfer coefficient for evaporator, kW/K or Btu/(hr-F)

$\dot{m}_{wS}$ = mass flow rate of water in evaporator, kg/s or lbm/hr

C_{pw} = specific heat of water, kJ/(kg-K) or Btu/(lbm-F)

$$\varepsilon_L = 1 - \exp\left(-\frac{(UA)_L}{C_{pw}\dot{m}_{wL}}\right) \tag{6.10}$$

where ε_L = thermal effectiveness of condenser

$(UA)_L$ = heat transfer coefficient for condenser, kW/K or Btu/(hr-F)

$\dot{m}_{wL}$ = mass flow rate of water in condenser, kg/s or lbm/hr

C_{pw} = specific heat of water, kJ/(kg-K) or Btu/(lbm-F)

2. Calculate the evaporating and condensing temperatures of the refrigerant:

$$T_e = T_{wiS} - \frac{\dot{Q}_S}{\varepsilon_S C_{pw}\dot{m}_{wS}} \tag{6.11}$$

where T_e = evaporating temperature, °C or °F

T_{wiS} = evaporator entering water temperature, °C or °F

$\dot{Q}_S$ = source side heat transfer rate, kW or Btu/hr

ε_S = thermal effectiveness of evaporator

$\dot{m}_{wL}$ = mass flow rate of water in evaporator, kg/s or lbm/hr

C_{pw} = specific heat of water, kJ/(kg-K) or Btu/(lbm-F)

$$T_c = T_{wiL} + \frac{\dot{Q}_L}{\varepsilon_L C_{pw} \dot{m}_{wL}} \tag{6.12}$$

where T_c = condensing temperature, °C or °F

T_{wiL} = condenser entering water temperature, °C or °F

$\dot{Q}_L$ = load side heat transfer rate, kW or Btu/hr

ε_L = thermal effectiveness of condenser

$\dot{m}_{wL}$ =mass flow rate of water in condenser, kg/s or lbm/hr

C_{pw} = specific heat of water, kJ/(kg-K) or Btu/(lbm-F)

3. When the condensing and evaporating temperatures are obtained, the corresponding pressures and enthalpies can be derived using a refrigerant property subroutine. We used subroutines provided with an HVACSIM+ system simulation program (Clark and May 1985).

4. Identify the refrigerant state at the compressor suction port by adding the superheat to the evaporating temperature. The refrigerant enthalpy at this point is determined using the refrigerant property subroutines.

$$T_{icom} = T_e + \Delta T_{sh} \tag{6.13}$$

where T_{icom} = Compressor inlet temperature, °C or °F

T_e = evaporating temperature, °C or °F

ΔT_{sh} = superheat, °C or °F

5. Identify the compressor suction and discharge states. Assuming no pressure loss at the suction and discharge ports, the suction pressure is equal to the evaporating pressure and the discharge pressure is equal to the condensing pressure. The specific volume at the suction state is determined by the refrigerant property subroutines.

$$P_{suc} = P_e \tag{6.14}$$

where P_{suc} = compressor suction pressure, kPa or psia

P_e = evaporating pressure, kPa or psia

$$P_{dis} = P_c \tag{6.15}$$

where P_{dis} = compressor discharge pressure, kPa or psia

P_c = condensing pressure, kPa or psia

6. Calculate the refrigerant mass flow rate $\dot{m}_r$ by Equation (6.7) and Equation (6.8), the theoretical value of isentropic compression power by Equation (6,5) and the total power input by Equation (6.6).

7. Calculate the new value of the source side heat transfer rate.

$$\dot{Q}_S = \dot{m}_r (h_A - h_B) \tag{6.16}$$

where h_A = enthalpy of the refrigerant leaving the evaporator, kJ/kg or Btu/lbm

h_B = enthalpy of the refrigerant entering the evaporator, kJ/kg or Btu/lbm

8. The new value of the load side heat transfer rate is calculated using Equation (6.17).

$$\dot{Q}_L = \dot{W} + \dot{Q}_S \tag{6.17}$$

where h_A = enthalpy of the refrigerant leaving the evaporator, kJ/kg or Btu/lbm

h_B = enthalpy of the refrigerant entering the evaporator, kJ/kg or Btu/lbm

$\dot{Q}_L$ = load side heat transfer rate, kW or Btu/hr

$\dot{Q}_S$ = source side heat transfer rate, kW or Btu/hr

For the model implementation, the heat transfer rates are solved simultaneously with successive substitution, thus an iterative loop is introduced. When the heat transfer rates converge to a specified error, the model then determines the outlet temperatures for each of the fluid streams. Other information such as cooling and heating capacities, COP, etc., may be reported if desired.

6.1.3. Validation

Since, in our application, the scroll compressor model is only used within a heat pump model, it is difficult to directly validate its operation. One indirect validation is to apply two variations of a water-to-water heat pump model – one with reciprocating compressor, the other with scroll compressor, to a water-to-water heat pump model that actually has a scroll compressor. The scroll compressor model may be judged successful if it improves the overall performance of the heat pump model. A Florida Heat Pump model WP 120, which utilizes a Copeland scroll compressor, has been modeled with both variations of the water-to-water heat pump model. Figures 6.5 and 6.6 show the heating capacity and power consumption when the heat pump is modeled with a hypothetical reciprocating compressor. Figures 6.7 and 6.8 show the heating capacity and power consumption when the heat pump is modeled with a scroll compressor. The RMS errors are summarized in Table 6.1. In addition, Table 6.1 shows the RMS errors of the heat pump model prior to adding the leakage parameter "C" to the model. It noticeably improves the model performance.

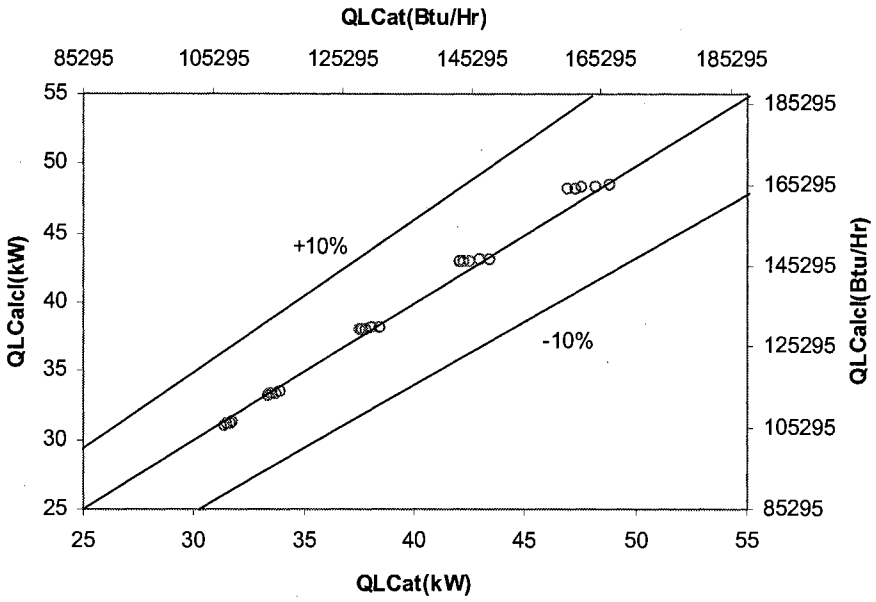

Figure 6.5. Calculated heating capacity vs catalog heating capacity (Hypothetical reciprocating compressor)

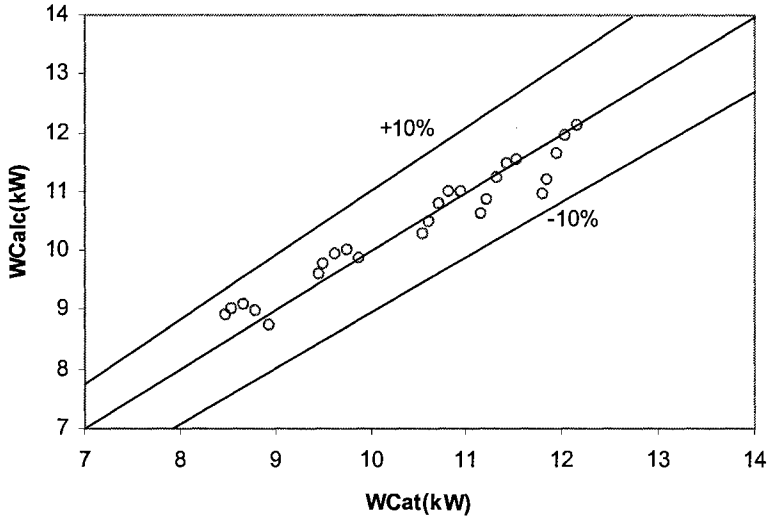

Figure 6.6. Calculated power vs catalog power (Hypothetical reciprocating compressor)

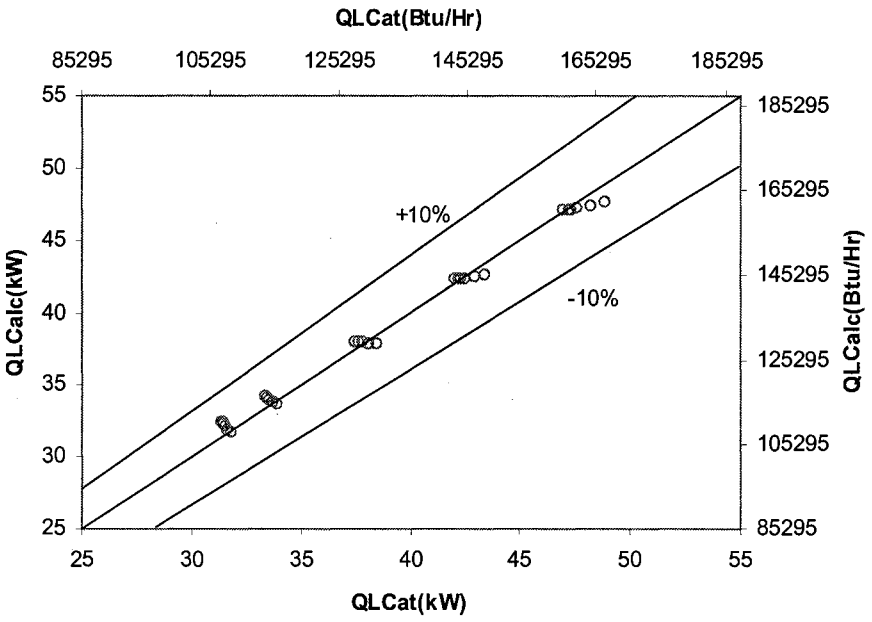

Figure 6.7. Calculated heating capacity vs catalog heating capacity (Scroll compressor)

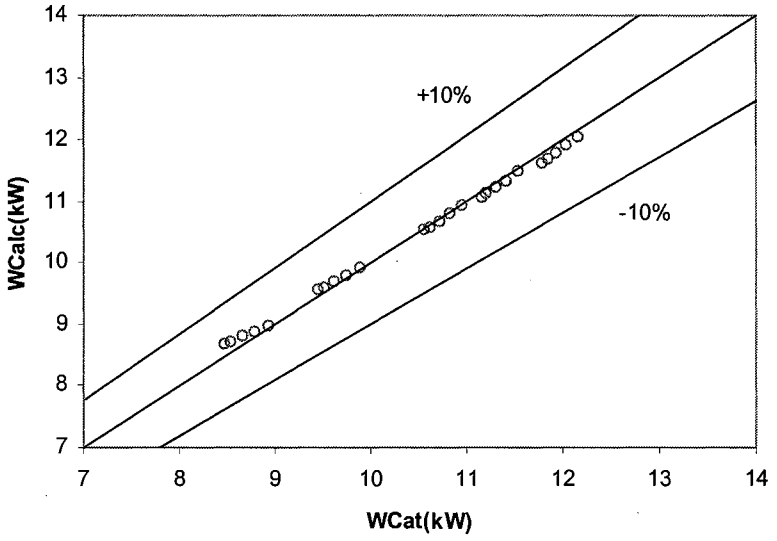

Figure 6.8. Calculated power vs catalog power (Scroll compressor)

Table 6.1. A Comparison of the Model Prediction RMS Errors

	Heating Capacity	Power	Heat of Extraction
Reciprocating Compressor	1.27%	3.15%	2.19%
Scroll Comp. w/o Leakage	1.32%	1.03%	2.15%
Scroll Comp. w/ Leakage	0.30%	0.67%	0.62%

As can be seen from Figures 6.5-6.8, the performance of the heat pump model is significantly improved, both for predicting heating capacity and power, when the scroll compressor equipped heat pump is modeled with the scroll compressor version of the heat pump model. Therefore, use of the scroll compressor model is recommended for heat pump with scroll compressors.

6.2. Modeling of Rotary Compressor

Another type of compressor used in the heat pump technology is rotary compressor. Rotary compressors actually comprise two sub-types, rolling piston compressor and rotary vane compressor. This section will focus on the modeling of rolling piston compressors. In a rolling piston rotary compressor, a rolling piston or roller is mounted on an eccentric shaft. A fixed vane sliding in a slot machined in the non-rotating cylinder block remains in contact with the roller. The eccentrically moving roller causes the reciprocating motion of the blade in the slot. Vapor refrigerant enters the compression chamber through the suction inlet and is compressed by the eccentric motion of the roller. When the rolling piston is in contact with the top of the cylindrical housing, the hot gas is squeezed out through the discharge valve. A schematic diagram of the rolling piston compressor is shown in Figure 6.9. The inherent design features include high volumetric

efficiency due to the small clearance volume and low re-expansion losses accordingly. Only a discharge valve is necessary for rolling piston rotary compressors; no suction valve is required. Displacement for the rolling piston compressor can be calculated from

$$\dot{V}_d = \pi H\left(A^2 - B^2\right)/4 \tag{6.18}$$

Where, $\dot{V}_d$ = displacement, m^3/s or CFM

H = cylinder block height, m or inch

A = cylinder diameter, m or inch

B = roller diameter, m or inch

Obviously, the displacement $\dot{V}_d$ is a value defined by its configuration and dimension for a given rotary compressor, which means it may be chosen as a parameter for the rotary compressor.

Like the scroll compressor, previously published models for rotary compressors (Chu et al. 1978, Wakabayashi, et al. 1982, Gyberg and Nissen 1984, Huang 1999, Takeshita 1997, Ooi and Wong 1997) have been targeted at the re-design of the rotary compressor for improved performance. Again, the high number of parameters in these models make them infeasible to use with the parameter estimation based modeling approach.

However, a review of the performance characteristics of rotary compressors shows it may be feasible to adapt the reciprocating compressor model discussed previously to

rotary compressors. Due to the re-expansion of the refrigerant vapor in the clearance volume of the reciprocating compressors, the mass flow rate of the refrigerant is a decreasing function of the pressure ratio,

$$\dot{m}_r = \frac{PD}{v_{suc}}\left[1 + C - C\left(\frac{P_{dis}}{P_{suc}}\right)^{1/\gamma}\right] \tag{6.19}$$

where $\dot{m}_r$ = refrigerant mass flow rate, kg/s or lbm/hr

PD = piston displacement, m^3/s or CFM

v_{suc} = specific volume at suction state, m^3/kg or ft^3/lbm

C = clearance factor

P_{dis} = discharge pressure, kPa or psia

P_{suc} = suction pressure, kPa or psia

γ = isentropic exponent

For a rotary compressor, the PD term or piston displacement in Equation (6.19) may be replaced by displacement $\dot{V}_d$ discussed above. The C term or clearance factor in Equation (6.19) is negligible due to the small clearance volume and corresponding low re-expansion losses of rotary compressors. If $C \cong 0$, Equation (6.19) can be simplified as,

$$\dot{m}_r = \frac{\dot{V}_d}{v_{suc}} \tag{6.20}$$

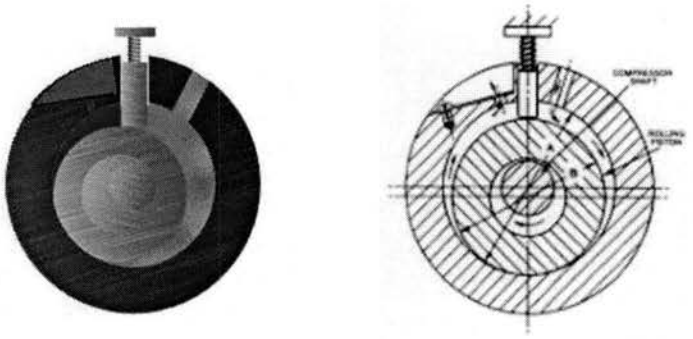

Figure 6.9. Rotary compressor -- rolling piston type
(ASHRAE handbook of HVAC systems and equipment)

Analogously, the theoretical compressor power for the isentropic process is,

$$\dot{W}_t = \frac{\gamma}{\gamma - 1} \dot{m}_r P_{suc} v_{suc} \left[\left(\frac{P_{dis}}{P_{suc}} \right)^{\frac{\gamma - 1}{\gamma}} - 1 \right] \tag{6.21}$$

where $\dot{W}_t$ = theoretical power, kW or Btu/hr

γ = isentropic exponent

$\dot{m}_r$ = refrigerant mass flow rate, kg/s or lbm/hr

P_{suc} = suction pressure, kPa or psia

v_{suc} = specific volume at suction state, m^3/kg or ft^3/lbm

P_{dis} = discharge pressure, kPa or psia

Since discharge valve is required by rolling piston rotary compressors, pressure drop ΔP across the discharge valve will be considered. However, the suction pressure is

assumed to be equal to the evaporating pressure since there is no suction valve. Figure 6.10 shows the compression cycle schematically.

$$P_{suc} = P_e \tag{6.22}$$

where P_{suc} = compressor suction pressure, kPa or psia

P_e = evaporating pressure, kPa or psia

$$P_{dis} = P_c + \Delta P \tag{6.23}$$

where P_{dis} = compressor discharge pressure, kPa or psia

P_c = condensing pressure, kPa or psia

ΔP = pressure drop across discharge valve, kPa or psia

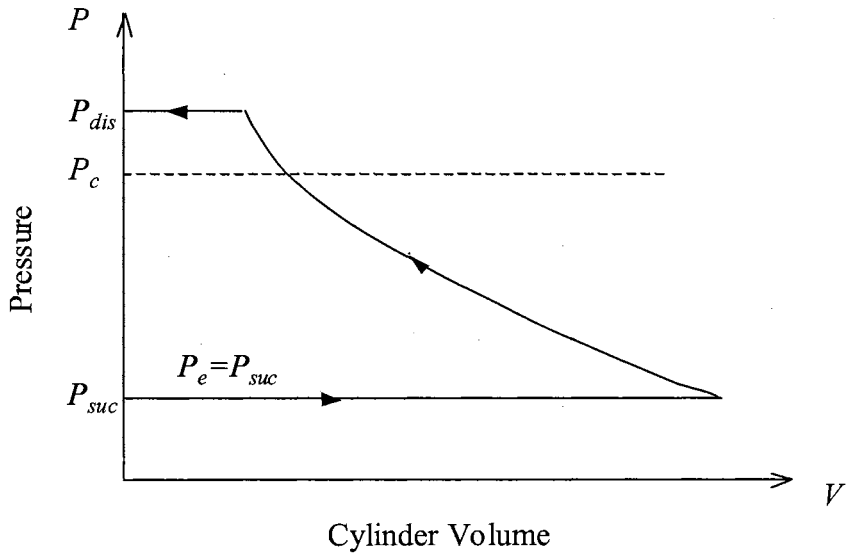

Figure 6.10. Thermodynamic cycle of a rotary compressor

A simple linear representation has been used to account for the electrical and mechanical efficiency of the compressor. The actual power input for the compressor is calculated by the following equation,

$$\dot{W} = \frac{\dot{W}_t}{\eta} + \dot{W}_{loss} \tag{6.24}$$

where $\dot{W}$ = compressor power input, kW or Btu/hr

$\dot{W}_{loss}$ = constant part of the electromechanical power losses, kW or Btu/hr

η = electro-mechanical efficiency

$\dot{W}_t$ = theoretical power, kW or Btu/hr

To summarize, the parameters chosen to represent a typical rotary compressor will be $\dot{V}_d$, ΔP, W_{loss} and η.

Since the rotary compressor model is, in the end, a simplified version of the reciprocating compressor model, it is not expected to give better results than the reciprocating compressor model. Presumably, the extra parameters in the reciprocating compressor model will allow it to fit any data set better. However, it makes more physical sense than the reciprocating compressor model and should give similar results, while taking less time for parameter estimation. Experience with a limited number of rotary compressor heat pumps has shown that the performance is roughly the same, regardless of whether a reciprocating compressor or rotary compressor model is used.

6.3. Modeling of Heat Pump Performance with Anti-Freeze

It is common in ground source heat pump systems to utilize an antifreeze mixture, also called 'coolant' alternatively, as secondary heat transfer fluid. As compared to system using pure water, this degrades the heat pump performance. It would be useful to be able to model the impact of antifreeze on the performance of the heat pump. Unfortunately, very little information is available from manufacturers with regards to the change in system performance when antifreeze mixtures are used. The Trane Company has provided the most detailed procedures to adjust the catalog data for pure water to the performance with antifreeze mixtures (Newton 2001). The correction factors for heating capacity, cooling capacity and power consumption are presented versus the concentration of the antifreeze mixture in manner of tables and charts. Given the very limited amount of data available only a preliminary effort has been made to develop a procedure for adjusting the model. This procedure is described below along with a check of how it performs compared to the Trane correction factors.

Heat transfer taking place in the condenser or evaporator will be affected by the degraded heat transfer coefficient, density and specific heat of the fluid. In the parameter estimation model, the previously assumed constant heat transfer coefficient will be replaced by a variable heat transfer coefficient that depends upon the fluid side volumetric flow rate. This allows the separate estimation of the refrigerant side resistance and coolant side resistance. Assuming the forms of the correlation for the fluid to heat exchanger wall convection allows an estimate of a degradation factor by substituting in correct values of density, specific heat, viscosity and conductivity. The degradation factor

multiplies the fluid-side heat transfer coefficient estimated for pure water, so that the heat pump performance with antifreeze can be predicted.

According to the smart bridge development strategy, the ground source heat pump system will be switched on to heat up the fluid that will be circulated through the bridge deck when icing is going to accumulate on it. However, the temperature of the bridge deck and the hydronic piping system may potentially drop below the freezing point of straight water when the system is shut off. Antifreeze is necessary in this case for providing freeze protection. In this experimental set up, a 42% by weight aqueous propylene glycol solution has been used. For the experiment in winter of 2000/2001, the 42% by weight propylene glycol solution was only used on the load (bridge deck) side of the heat pump. Pure water was used for the source side or ground loop side. Starting in the winter of 2001/2002, propylene glycol solution has been used in both sides.

6.3.1. Derivation of Antifreeze Degradation Factor

The overall heat transfer resistance may consist of coolant side convection heat transfer resistance, refrigerant side convection heat transfer resistance, tube wall resistance and fouling resistance. According to classical heat transfer theory, the coolant side convection heat transfer resistance is a function of fluid velocity and physical properties. Thus, it may vary considerably as a result of changes in fluid properties when antifreeze is added to water. The geometry of the heat exchanger may not be known, but is likely to be a co-axial heat exchanger. Some manufacturers may also use compact heat

exchangers. For purpose of calculating a degradation factor, it is reasonable to assume a co-axial heat exchanger geometry, with the coolant flowing through the inner tube. In this case, the Sieder-Tate correlation (Kern 1950) may be taken a reasonable approximation:

$$\mathrm{Nu} = 0.027\,\mathrm{Re}^{0.8}\,\mathrm{Pr}^{0.33}\left(\mu/\mu_w\right)^{0.14} \tag{6.25}$$

where $\mathrm{Re} = ud/\nu$, Reynolds number

$\mathrm{Pr} = C_p\mu/k$, Prandtl number

$\mathrm{Nu} = hd/k$, Nusselt number

u = fluid velocity, m/s or ft/min

d = diameter of tubes or pipes, m or ft

ν = kinematic viscosity, m^2/s or ft^2/sec

C_p = specific heat, J/(kg-°C) or Btu/(lbm-°F)

μ = dynamic viscosity, N-s/m^2 or centipoise

k = thermal conductivity, W/(m-°C) or Btu/(hr-ft-°F)

h = convection heat transfer coefficient, W/(m^2-°C) or Btu/(hr-ft^2-°F)

However, since we are only interested in the relative performance, we are only assuming that the exponents are correct.

Substituting the definitions of the dimensionless group into Equation (6.25) yields,

$$h = 0.027u^{0.8}d^{-0.2}\mu^{-0.47}\rho^{0.8}C_p{}^{0.33}k^{0.67} \tag{6.26}$$

The relationship of the convection heat transfer coefficients between fluids with different physical properties can be found as follows, providing same volumetric flow rate or velocity.

$$\frac{h_1}{h_2} = \left(\frac{\mu_1}{\mu_2}\right)^{-0.47} \left(\frac{\rho_1}{\rho_2}\right)^{0.8} \left(\frac{C_{p1}}{C_{p2}}\right)^{0.33} \left(\frac{k_1}{k_2}\right)^{0.67} \tag{6.27}$$

If a degradation factor of the convection heat transfer coefficients between antifreeze and pure water is defined as,

$$DF = \frac{(hA)_{antifreeze}}{(hA)_{water}} \tag{6.28}$$

Where

$(hA)_{antifreeze}$ = product of coolant side convection heat transfer coefficient and heat transfer area for anti-freeze, W/°C or Btu/(hr-°F)

$(hA)_{water}$ = product of coolant side convection heat transfer coefficient and heat transfer area for straight water, W/°C or Btu/(hr-°F)

Since the dimensions such as heat transfer area of the heat exchanger should always be constant, the degradation factor can be reduced to,

$$DF = \frac{h_{antifreeze}}{h_{water}} = \left(\frac{\mu_{antifreeze}}{\mu_{water}}\right)^{-0.47} \left(\frac{\rho_{antifreeze}}{\rho_{water}}\right)^{0.8} \left(\frac{C_{p\,antifreeze}}{C_{p\,water}}\right)^{0.33} \left(\frac{k_{antifreeze}}{k_{water}}\right)^{0.67} \tag{6.29}$$

The degradation factor for propylene glycol solution is plotted in Figure 6.11 against the concentration by percent volume with different temperatures. The propylene glycol properties were calculated with the functions developed by Rees (2002).

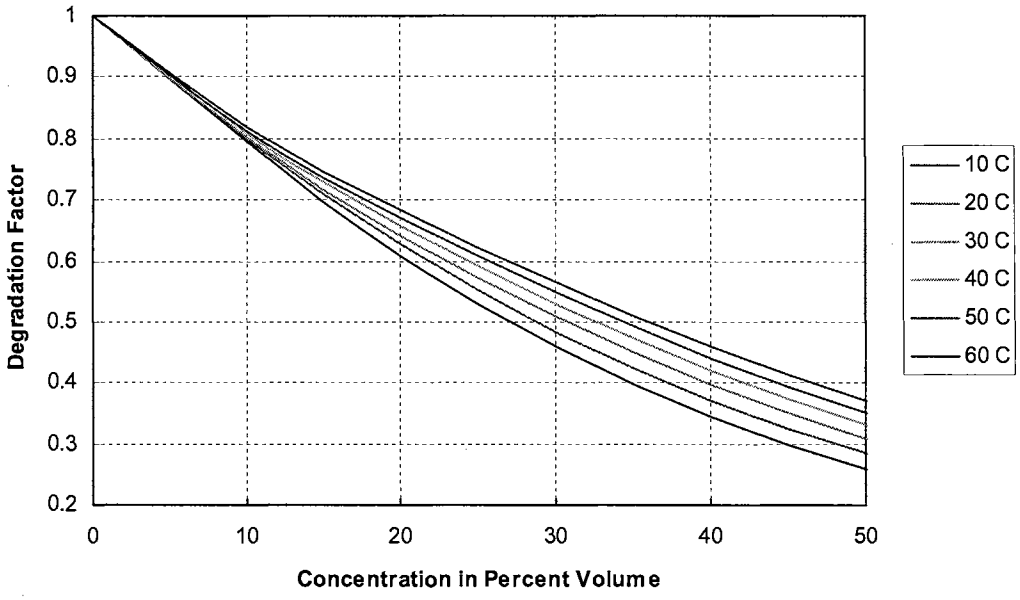

Figure 6.11. Degradation factor for propylene glycol/water mixture by percent volume

6.3.2. Volumetric Flow-Dependent Heat Exchanger Model

In order to apply the degradation factor developed in the last section, it is necessary to split the heat transfer resistance between the coolant side convection and the other parts (refrigerant side convection, tube wall resistance and fouling). The heat pump models described in Chapter 4 and 5 only estimate a single *UA* value for each heat exchanger. This did not lend itself to differentiating between the two resistance components.

Several different approaches were considered before setting on the approach described in this section. In short, the procedure takes advantage of the fact that water source heat pump catalogs give performance data for a range of water flow rates. Using an analogy to the Wilson Plot (Wilson 1915) will allow the two resistances to be estimated separately when pure water is used. Then, the degradation factor described in the last section may be applied when antifreeze is used.

The overall heat transfer coefficient is a function of coolant side heat transfer coefficient, refrigerant side heat transfer coefficient, tube wall resistance and fouling resistance.

$$\frac{1}{(UA)_{total}} = \frac{1}{(hA)_{refrigerant}} + \frac{1}{(hA)_{coolant}} + R_{wall} + R_{fouling} \tag{6.30}$$

where

$(UA)_{total}$ = overall heat transfer coefficient, W/°C, or Btu/(hr-°F)

$(hA)_{refrigerant}$ = product of refrigerant side convection heat transfer coefficient and heat transfer area, W/°C or Btu/(hr-°F)

$(hA)_{coolant}$ = product of coolant side convection heat transfer coefficient and heat transfer area, W/°C or Btu/(hr-°F)

R_{wall} = heat transfer resistance of tube wall, °C/W or (hr-°F)/ Btu

$R_{fouling}$ = heat transfer resistance of fouling, °C/W or (hr-°F)/ Btu

If the sum of the resistances of refrigerant side, tube wall and fouling is assumed constant and defined as,

$$R' = \frac{1}{(hA)_{refrigerant}} + R_{wall} + R_{fouling} \tag{6.31}$$

Then Equation (6.30) can be reduced to,

$$\frac{1}{(UA)_{total}} = \frac{1}{(hA)_{coolant}} + R' \tag{6.32}$$

From Sieder-Tate Correlation, coolant side convection heat transfer coefficient is,

$$h = 0.027u^{0.8}d^{-0.2}\mu^{-0.47}\rho^{0.8}C_p{}^{0.33}k^{0.67} \tag{6.33}$$

Since the temperature range in which the coolant operates is relatively small, the variation of the physical property of pure water is negligible. Thus, for pure water, the convection heat transfer coefficient may be assumed to be a function of fluid velocity only.

Let $(hA)_{water} = \frac{u^{0.8}}{C_1}$, $R' = C_2$, Equation (6.32) becomes,

$$\frac{1}{(UA)_{total\_water}} = \frac{C_1}{u^{0.8}} + C_2 \tag{6.34}$$

Or

$$(UA)_{total\_water} = \frac{1}{C_1 u^{-0.8} + C_2} \tag{6.35}$$

Since fluid velocity is related to the volumetric flow rate by the cross-sectional area of the pipe as,

$$u = \frac{\dot{V}}{A} \tag{6.36}$$

Then

$$(UA)_{total\_water} = \frac{1}{C_1\left(\frac{\dot{V}}{A}\right)^{-0.8} + C_2} \tag{6.37}$$

Let $C_3 = C_1 A^{0.8}$, then the overall heat transfer coefficient takes the form as,

$$(UA)_{total\_water} = \frac{1}{C_3 \dot{V}^{-0.8} + C_2} \tag{6.38}$$

This part of the procedure is analogous to a technique introduced by Wilson (1915). The technique, which is often called 'Wilson Plot' by later authors, is used to infer heat transfer coefficients on both sides of a heat exchanger when the total resistance is

measured for series of tests where the flow rate is varied on one side of the heat exchanger. As discussed previously, for a water-cooled condenser, total heat transfer resistance, denoted $1/U_o$, is the sum of the individual resistances including water side heat transfer resistance, tube wall resistance, refrigerant side resistance and fouling resistance if applicable. The water side convection heat transfer coefficient, denoted as h_i, can be assumed to follow the relationship given by Equation (6.39), provided the temperature range is not large.

$$h_i = (\text{constant})(V^{0.8}) \tag{6.39}$$

The 'Wilson Plot' for the condenser then will be a graph of $1/U_o$ vs $1/V^{0.8}$. If the refrigerant side heat transfer coefficient remains constant, the overall heat transfer resistance should be a straight line in the plot. The intercept of the straight line on the $1/U_o$ axis is equal to the sum of refrigerant side resistance and tube wall resistance.

In other words, $C_3\dot{V}^{-0.8}$ is the estimated coolant side resistance and C_2 is the estimated resistance due to refrigerant to tube wall convection, tube wall conduction and fouling if any. C_2 and C_3 can be estimated from catalog data given for use with pure water.

Then, the degradation factor can be applied when the model is used with antifreeze:

$$(UA)_{total\_antifreeze} = \frac{1}{C_3 \dot{V}^{-0.8} / DF + C_2} \tag{6.40}$$

6.3.3. Antifreeze Model Performance

Regrettably, there is little data available from manufacturers of water-source heat pumps regarding performance with antifreeze. What is available only covers water-to-air heat pumps. As a preliminary check on the effect of antifreeze on the water-to-water heat pump model, we have used it to model a water-to-air heat pump for which the manufacturer has provided correction factors for use with antifreeze (a Trane GSUJ 018, which utilizes a scroll compressor), operating in heating mode only. In heating mode, the water-to-water heat pump performs much like the water-to-air heat pump, since there is no condensation of water vapor on the refrigerant-to-air heat exchanger.

The manufacturer has tabulated performance data for operation with pure water. In addition, three groups of correction factors for cooling capacity, heating capacity and pressure drop across the heat pump are also provided by the manufacturer in case an antifreeze mixture (propylene glycol, ethylene glycol, or methanol) is used as the source side secondary heat transfer fluid. The parameters estimated for the heat pump model (with scroll compressor and two-parameter evaporator model) are given in Table 6.2. The parameter values estimated with data of pure water have been used in model implementation to assess the accuracy of the model prediction. A comparison of model prediction to catalog data for pure water is shown in Figure 6.12 and Figure 6.13. A summary of the RMS errors is presented in Table 6.3.

Table 6.2. Parameter Estimation Results for the Trane Water-to-Air Heat Pump Model GSUJ 018 (Heating)

Parameter	Estimated Value
product of the volume of the pockets that seal the suction gas at the beginning the compression and the rotational speed $\dot{V}_r$	1.28×10^{-3} m^3/s (162.7 ft^3/hr)
Built-in volume ratio v_i	2.21
Load side heat exchanger heat transfer coefficient	0.425 kW/°C
Source side heat exchanger heat transfer resistance coefficient *3*	0.125
Source side heat exchanger heat transfer resistance coefficient *2*	1.11 °C/kW (5.86×10^{-4} (hr-°F)/Btu)
Loss factor used to define the electro-mechanical loss that is supposed to be proportional to the theoretical power η	0.897
Constant part of the electro-mechanical power losses W_{loss}	0.55 kW (1,877 Btu/hr)
Superheat ΔT_{sh}	16.79 °C (30.22 °F)

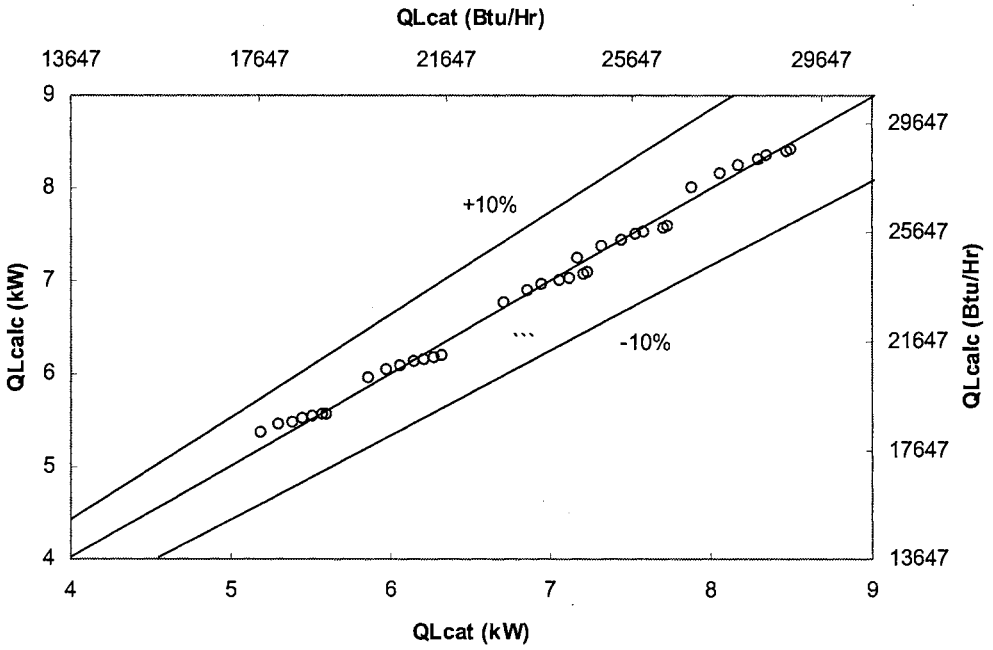

Figure 6.12. Calculated heating capacity vs catalog heating capacity

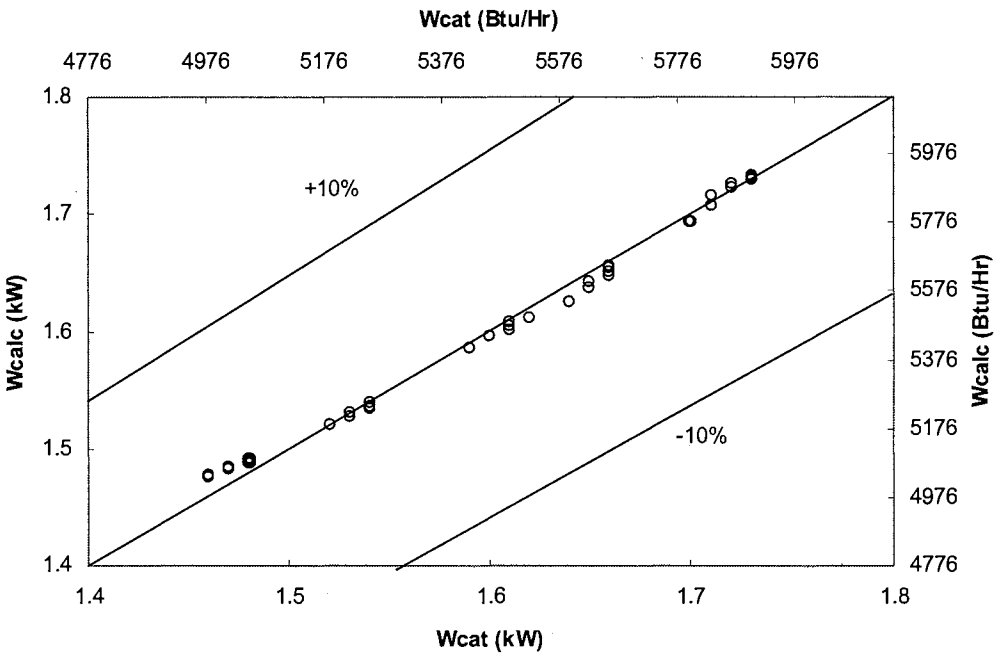

Figure 6.13. Calculated power vs catalog power

Table 6.3. RMS Errors of Model Prediction Compared with Catalog Data (Trane GSUJ & WPVJ 018 Water-to-Air Heat Pump)

Nominal Capacity		Number of Points	RMS		
(W)	(Btu/hr)		Heating Capacity	Heat Extracted	Power
4,100 (Heating)	18,000 (Heating)	35	1.35%	1.68%	.052%

As can be seen in Figure 6.11, the degradation factor varies with both antifreeze concentration and temperature. Since temperature varies throughout the simulation, the degradation factor is recalculated at every model iteration as a function of temperature and concentration. The temperature is taken as the average of the inlet and outlet coolant temperatures. Once calculated, the degradation factor is applied as shown in Equation (6.40). In addition, the properties such as density and specific heat used in the model

implementation have to be changed to match the temperature and concentration of the antifreeze solution.

The model then has been run with the same inlet temperatures and volumetric flow rates given in the catalog, along with a range of concentrations of propylene glycol. Figure 6.14 shows the resulting resistances for three different flow rates, averaged for all entering fluid temperatures, as a function of propylene glycol concentration. The water-side resistance varies significantly as the propylene glycol concentration increases. The effect is most significant at low flow rates.

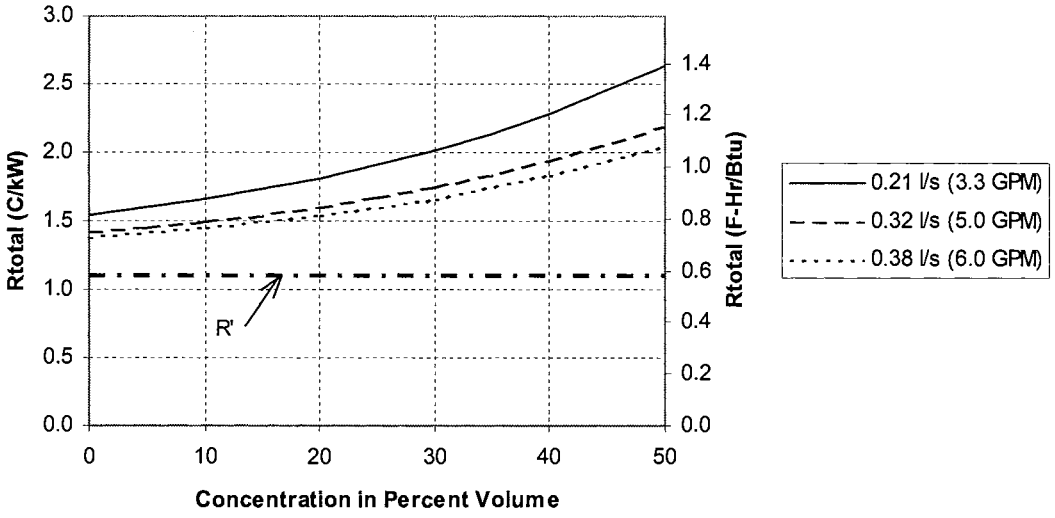

Figure 6.14. Evaporator overall heat transfer resistance
(Trane GSUJ 018 water-to-air heat pump)

The increased heat transfer resistance that occurs with increasing concentration of propylene glycol results in a decreasing heating capacity. The manufacturer has provided a correction factor that multiplies the heating capacity with pure water to give the heating

capacity with an antifreeze mixture. This is given only as a function of the concentration of propylene glycol. Presumably, the reduction in heating capacity varies also with the flow rate and entering fluid temperature. We have calculated the reduction in heating capacity for a range of propylene glycol concentrations, fluid flow rates, and entering fluid temperatures. The calculated correction factor is taken as the ratio of the heating capacity calculated with antifreeze to the heating capacity calculated (with the model) for pure water.

Correction factors provided by the heat pump manufacturer may be compared to correction factors calculated with the water-to-water heat pump model in Figure 6.15. The model-calculated correction factors are averaged for all catalog-specified entering fluid temperatures at each flow rate. As can be seen, the correction factors for the three different flow rates show some divergence from the manufacturer's single curve. Assuming for a moment that the curves calculated with the model are correct, the manufacturer's single curve probably provides a reasonable approximation for designers. However, it is desirable for modeling purposes to be able to more accurately represent the effects of antifreeze. Further experimental work is needed to establish the accuracy of the model.

Since propylene glycol properties vary significantly with temperature, the sensitivity to heat pump entering fluid temperature was also examined. For a single, intermediate flow rate, the correction factors were calculated for three different entering fluid temperatures. The results are shown in Figure 6.16. While some variation in

correction factor may be observed, the differences over the expected range of temperature are not as significant as the differences over the allowable range of fluid flow rates.

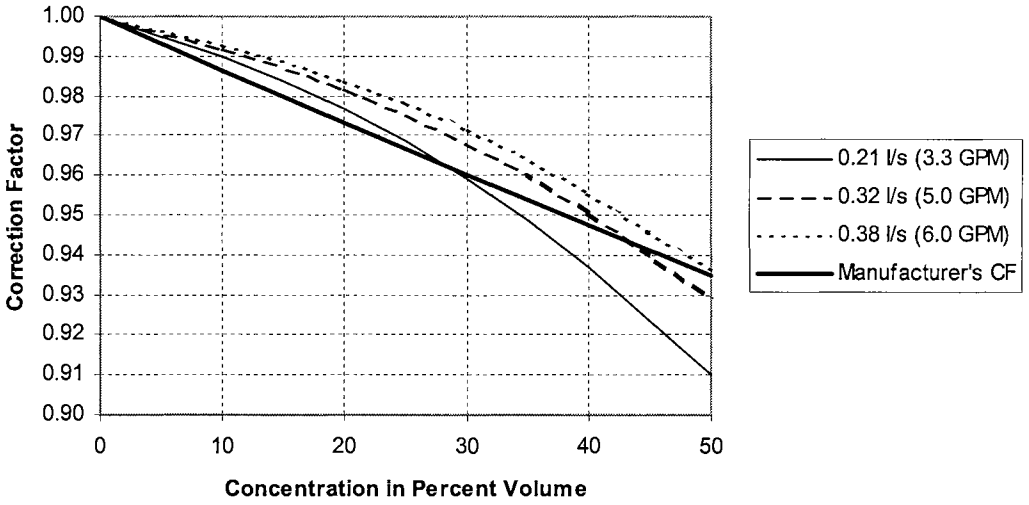

Figure 6.15. Heating capacity correction factor with varying flow rates (Trane GSUJ 018 water-to-air heat pump)

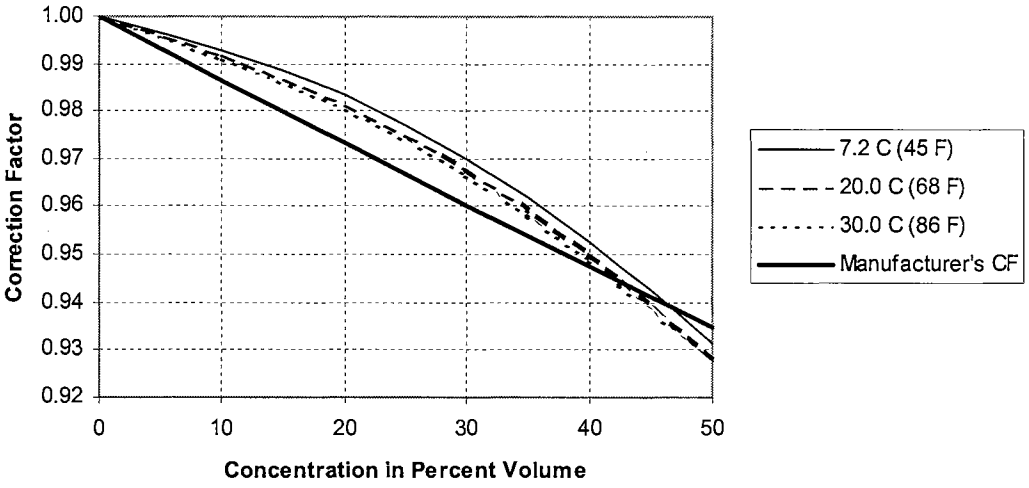

Figure 6.16. Heating capacity correction factor with varying entering fluid temperatures (Trane GSUJ water-to-air heat pump)

6.4. Conclusions and Recommendations

A parameter estimation based model of water-to-water heat pumps has been revised to include scroll compressors and allow an accounting for the effects of antifreeze. A five-parameter scroll compressor model has been incorporated into the heat pump model. As the goal of the heat pump model is to produce a physically-realistic model for which all parameters can be estimated from catalog data, the scroll compressor sub-model was validated by comparing the results of both the scroll-compressor-equipped and reciprocating-compressor-equipped heat pump models applied to catalog data for a scroll-compressor-equipped heat pump. The scroll compressor version of the heat pump model gives noticeably improved results over the reciprocating compressor version. It was noted that the overall accuracy of the heat pump model was improved by including the fifth parameter into the scroll compressor model: a differential pressure-dependent leakage.

A rotary compressor model, which is a simplified version of the reciprocating compressor model, has also been presented. It has been developed to make more physical sense if a rotary compressor is used in the heat pump. It is not expected to give better results than the reciprocating compressor model, since the extra parameters in the reciprocating compressor model will allow it to fit any data set better. Experience with a limited number of rotary compressor heat pumps has shown that the performance is roughly the same, regardless of whether a reciprocating compressor or rotary compressor model is used.

A preliminary investigation of a methodology for modeling the use of antifreeze solutions with water-to-water heat pumps has been described. The methodology retains the physically-realistic approach of the heat pump model, and should, in theory, allow the prediction of heat pump performance to be extended to a range of antifreeze solutions, even when only pure-water-based catalog data are available. To date, we can only say that the results appear to be approximately consistent with the correction factors offered by one manufacturer. The model does show sensitivity to flow rates and fluid temperatures that are not reflected in the manufacturer's recommendations. It would be desirable to perform an experimental investigation of the antifreeze effects on water-to-water heat pumps under laboratory conditions, where entering fluid temperature, flow rate and antifreeze concentration can be more easily changed and controlled.

7. Water-to-Water Heat Pump Model Validation

This chapter describes a 'field' validation of the water-to-water heat pump model using an existing experimental apparatus. The experiment has been implemented to support the 'Geothermal Smart Bridge' project. In the experiment, a water-to-water heat pump was selected and installed to supply heating for the bridge deck. However, some instrumentation has been added which provides measurements of the essential external performance data to validate the heat pump model.

7.1. Background and a Brief Description of Experimental Apparatus

Research is ongoing at OSU to develop and implement a bridge deck heating system that will eliminate preferential icing on the nation's bridges. This new technology makes use of a ground source heat pump system that recovers energy stored in the earth and uses it to heat fluid that is circulated through the bridge deck.

A simple heating system might be composed of an electric-powered pump that circulates earth-heated fluid through piping to the deck. Should additional heat be necessary or desirable, a heat pump could be incorporated into the system. Fluid could also be circulated on some hot days in the summer. The sun's radiant heat would be transported from the deck to "recharge" the ground. Heat removed during the previous cold season would be replaced.

An experiment has been implemented to support this project. It will be used for model validation and testing of control strategies. This work has involved the construction, instrumentation, operation, and analysis of a medium-scale (60'x20') bridge deck and of which one half is heated with a ground source heat pump-based bridge deck heating system. The construction and data collection for this experiment have been conducted by researchers affiliated with the Division of Engineering Technology at Oklahoma State University, supervised by Dr. Marvin Smith.

A schematic diagram of the experimental facility is shown in Figure 7.1. Since the objective of the research effort discussed in this part of the project is to validate the parameter estimation based model of water-to-water heat pumps, only those test facilities related to the model validation are described here. The necessary components are: a water-to-water heat pump, two circulating pumps for load and source loop respectively, a heat source (ground loop heat exchanger), a heat sink (medium-scale bridge deck), valves, fitting and pipes, etc. For the load side, the fluid is circulated between bridge deck and the condenser (load side heat exchanger). For the source side, the fluid is circulated between the ground loop heat exchanger and the evaporator (source side heat exchanger). The instrumentation and data acquisition equipment include four thermistor probes, two fluid flow meters and three watthour meters.

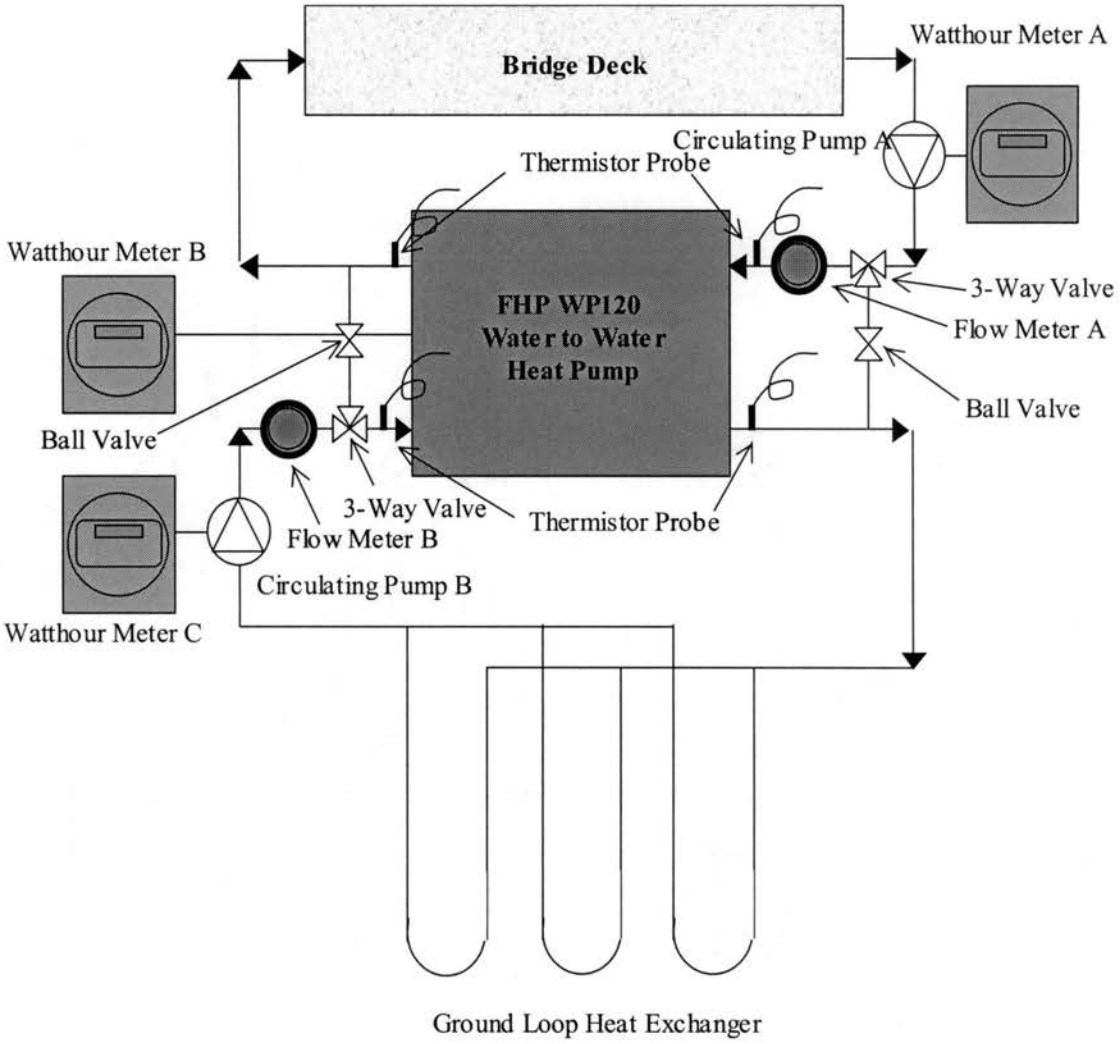

Figure 7.1. System schematic of the water-to-water heat pump experiment

The experimental apparatus is described in two parts: the hydronic heating system, and the instrumentation. The hydronic heating system is comprised of a water-to-water heat pump, circulating pumps, some valves and pipes. The instrumentation includes sensors, transducers, and transmitters for the fluid flow rate, the inlet and outlet fluid temperatures, the power consumption and finally data acquisition.

7.2. The Hydronic Heating System

7.2.1. Water-to-Water Heat Pump

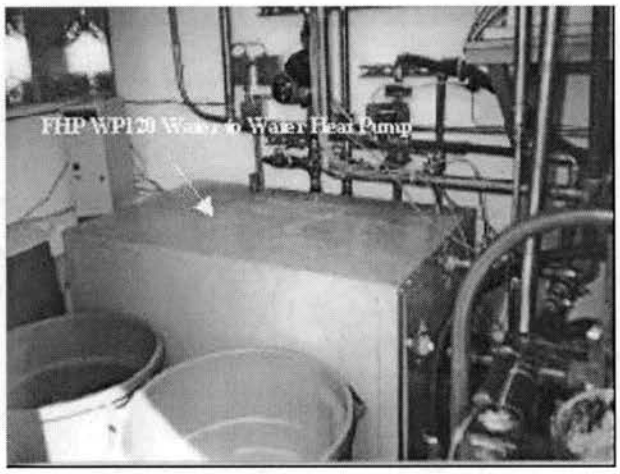

Figure 7.2. Water-to-water heat pump in the instrumentation building

The test was performed on an FHP model WP120 water-to-water heat pump with nominal cooling capacity of 10 tons (35.2 kW). The unit is design to operate with entering fluid temperatures between 20 °F (-7 °C) and 120 °F (49 °C). Table 7.1 shows the heating performance data extracted from the FHP WP series catalog. The heating performance is based on 24 GPM (1.51 l/s) and 10 °F (5.56 °C) rise on load side. The unit contains a sealed refrigerant circuit including a hermetic scroll compressor, bi-directional thermal expansion valve metering device, coaxial style fluid-to-refrigerant heat exchangers, refrigerant reversing valve and service ports. A view of the heat pump in the instrumentation building is shown in Figure 7.2.

Table 7.1. Heating Capacity Data for Model WP120

Source	Source EFT	LOAD LEAVING FLUID TEMPERATURE					
		100 °F (37.78 °C)		110 °F (43.33 °C)		120 °F (48.89 °C)	
		BTUH	kW	BTUH	kW	BTUH	kW
24 GPM (1.51 L/S)	40 °F (4.44 °C)	115,727	33.92	115,067	33.73	114,442	33.54
	70 °F (21.11 °C)	166,727	48.87	164,507	48.22	162,348	47.58
Source	Source EFT	LOAD LEAVING FLUID TEMPERATURE					
		125 °F (51.67 °C)		130 °F (54.44 °C)			
		BTUH	kW	BTUH	kW		
24 GPM (1.51 L/S)	40 °F (4.44 °C)	114,142	33.46	113,847	33.37		
	70 °F (21.11 °C)	161,290	47.27	160,245	46.97		

7.2.2. Water Circulation Pumps

Another important component in the heating system is the circulating pump. The two pumps, located in the equipment room, on the load side and source side are both Grundfos Type UPS 32 series. The UPS 32 pump has a flow range of 9-78 GPM and head range of 1 to 46 feet.

7.2.3. Ground Loop Heat Exchanger

The borehole field of the ground source heat pump system consists of six vertical boreholes arranged in a 2×3 rectangular configuration. The borehole depths range from 209 ft (63.7 m) to 225 ft (68.58 m) and each borehole has a diameter of 5.25 inches (133.35 mm). The ground loop heat exchangers are 1 inch (25.4 mm) nominal high-density polyethylene U tube pipes. The boreholes are spaced 25 ft (7.62 m) apart from each other, center-to-center. Fluid flow to and from the borehole field through the

horizontally buried piping connected to the water-to-water heat pump and circulation pump in the instrumentation building. The heat transfer fluid circulated in the pipes was pure water originally, but it was changed to 42% aqueous solution of propylene glycol in 2001.

7.2.4. Medium-Scale Bridge Deck

The medium-scale bridge deck is 60 ft long and 30 ft wide. Only the south half is heated. The concrete slab has a thickness of 5 inches (127 mm) at edge and 7 inches (177.8 mm) in the center. The heating elements in the bridge deck are ¾ inch (19.05 mm) nominal E-PexB pipes, buried 2.5 inches (63.5 mm) below the surface at the edge of the bridge deck and 3.5 inches (88.9 mm) in the center. There are ten flow circuits and the pipe for each circuit is 65 ft (19.812 m) long. The circuits are connected to the supply header and the reverse return header pipes at the center of the bridge. At the north end of the bridge, the supply and return headers go vertically to the ground and pipes are buried in a trench leading to the heat pump in the instrumentation building. The heat transfer fluid circulating in the pipes is 42% aqueous propylene glycol solution all the time.

7.3. Instrumentation

The measurement of the temperatures, flow rates and power consumption is made in the instrumentation building.

7.3.1. Fluid Flow Rates

The fluid flow rates are measured by two Gems Sensors RFA type volumetric measuring flow meters, which utilize a paddlewheel design. The model used in this experiment is a Gems Sensors Type RFA RF-2500 rotor flow sensor with a brass body. It needs an input power of 24VDC ±10%. The standard output signal is 0-10 VDC analog signal. The standard range and accuracy according to the published catalog is 6.0 to 30.0 GPM (±15.0%) for port size of 0.75". The flow meters have been calibrated by the researchers in the Division of Engineering Technology. Calibration data and regression equations are given in Appendix A. The estimated uncertainty is ±3 % (Holloway 2000).

7.3.2. Inlet and Outlet Fluid Temperatures

The fluid temperatures are measured at the inlet and outlet of the heat pump. The sensors for all the temperature measurements are YSI 55031 10K H mix glass encapsulated thermistors potted into an 1/8" OD, 3" long tubular probe with 12" of round PVC cable. The interchangeability tolerance level is ±1°C. The probes are embedded in a Pete's port and immersed into the circulating fluid. Each probe is attached to a voltage divider in which the other resistor of the voltage divider is a precise 10 K resistor. The analog voltage output signals are picked up by the data logging system and converted into corresponding temperature readings. The thermistors have been calibrated by the researchers in the Division of Engineering Technology. Calibration data and regression

equations are given in Appendix A. The estimated uncertainty is ±0.18 °F (±0.1 °C) (Holloway 2000).

7.3.3. Power Consumption

Three watthour meters are put in place to measure power input to the heat pump, load loop circulating pump and source loop circulating pump. The watthour meters are manufactured by Sangamo Electric and Westinghouse. One is a Sangamo Electric Type J4S and the other two are Westinghouse Type D4S-8M. Each watthour meter has a sensor that detects one revolution of the meter and sends a pulse to a circuit that toggles the output high and low. In other words, when a pulse is detected, the output of the circuit goes high, when another pulse is detected, the output of the circuit goes low. The software detects a change in state of the output to count the revolutions. The revolutions are counted over a five-minute interval (same as the data-saving interval) and power consumption is calculated. The watthour meters were calibrated and sealed before shipment. The estimated uncertainty including the uncertainty of the rotational sensor is ±1% ±0.22 kW (Holloway 2000).

7.3.4. Data Acquisition and Logging

The analog output signals from all of the sensors are measured by a data logging system. The signals are actually DC voltages and pulses configured on the different

output scales for each measurement. The signals sent to the data logger from each sensor are:

1–4) Entering/leaving fluid temperatures on both sides (analog voltage)

5–6) Fluid flow rates on both sides (analog voltage)

7–9) Power consumptions of the heat pump and each circulation pump (pulse)

Each signal is retrieved at specified time interval and saved as an ASCII data file.

7.4. Physical Properties of the Propylene Glycol Solution

Equation (7.1) has been used to find the load side and the source side heat transfer rates for the experimental data.

$$\dot{Q} = \dot{V}\rho C_p \Delta T \tag{7.1}$$

Where $\dot{Q}$ = heat transfer rate, W or Btu/hr

$\dot{V}$ = volumetric flow rate, m^3/s or GPM

ρ = density, kg/m^3 or lbm/ft^3

C_p = specific heat, J/(kg-°C) or Btu/(lbm-°F)

ΔT = temperature difference, °C or °F

A propylene glycol solution is used instead of pure water in the bridge deck heating system in order to provide freeze protection. Since propylene glycol properties vary widely over the range of the temperature occurring in the experiment, the assumption of

constant properties may result in a considerable error in the calculation. Therefore, the propylene glycol properties were calculated with the functions developed by Rees (2002).

Thermal properties of interest for a 42% by weight propylene glycol solution are shown in Figure 7.3 through Figure 7.6.

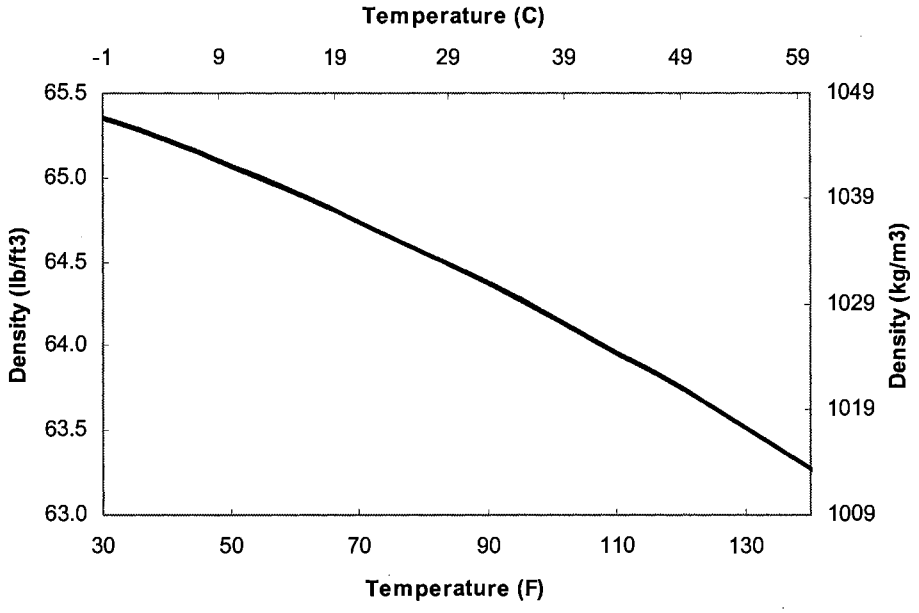

Figure 7.3. Density of aqueous solution of propylene glycol (42% by weight)

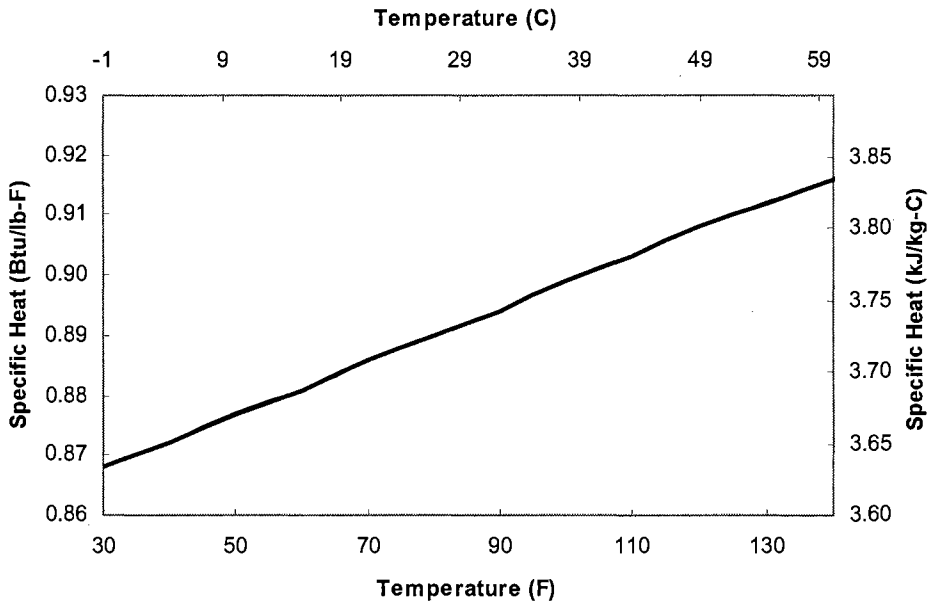

Figure 7.4. Specific heat of aqueous solution of propylene glycol (42% by weight)

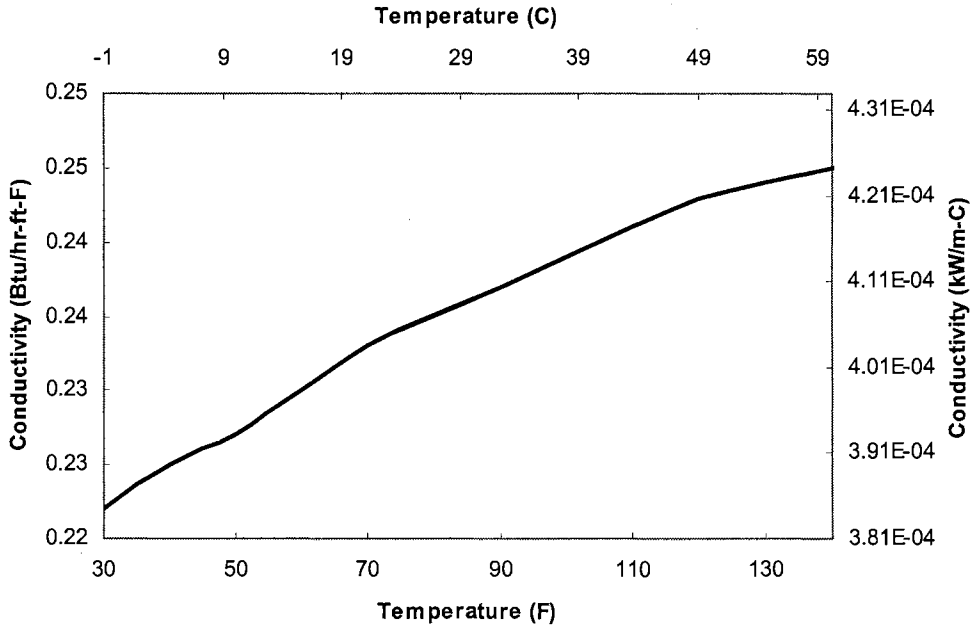

Figure 7.5. Thermal conductivity of aqueous solution of propylene glycol (42% by weight)

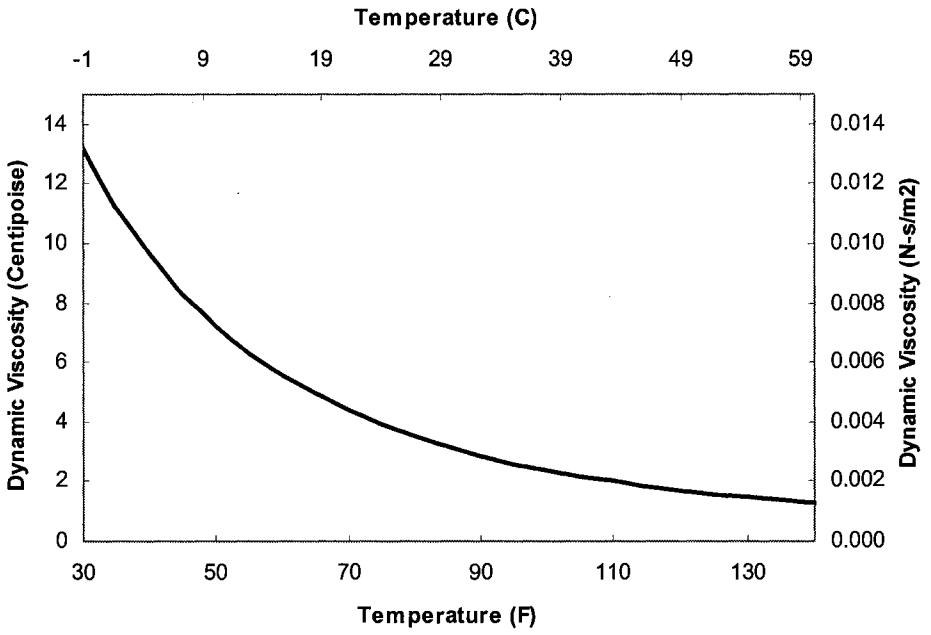

Figure 7.6. Dynamic viscosity of aqueous solution of propylene glycol (42% by weight)

The physical properties involved in the calculation of heat transfer rate based on the experimental data are density and specific heat. To investigate the impact of the errors associated with the properties on the accuracy of heat transfer rate, some typical inlet and outlet temperatures for load side as 95.1 °F (35.0 °C) and 125.6 ° F (52.0 °C) in the experimental data have been chosen. The temperature difference across the heat pump leads to a difference of 10.5 kg/m^3 (0.66 lbm/ft^3) or 1.0% in density and a difference of 0.06 kJ/(kg-C) (0.014 Btu/(lbm-F)) or 1.5 % in specific heat. Thus the total error in the heat transfer rate due to the uncertainties in the density and specific heat is calculated as,

$$E_h = \sqrt{(E_\rho)^2 + (E_{Cp})^2} = \sqrt{(\pm 0.01)^2 + (\pm 0.015)^2} = \pm 1.8\% \qquad (7.2)$$

where E_ρ = density error

E_{Cp} = specific heat error

Also, for the antifreeze-adapted model described in Chapter 6, a detailed description of the physical properties of the antifreeze for different concentrations and temperatures is also required to determine the degradation factor of the coolant side heat transfer coefficient. The subroutines given in Appendix X are utilized for this purpose.

7.5. A Preliminary Analysis of Experimental Uncertainty

The main source of error in the measurement of heat transfer rates and power consumption are identified as: (1) Calibration error in the thermistor probes used for entering and leaving fluid temperature measurements on both sides; (2) Calibration error in the flow meters used for fluid flow rate measurements and (3) Calibration error in the watthour meter used for power measurement.

The uncertainties for individual measurements have been presented previously. The heat transfer rate can be calculated using Equation (7.1). From Equation (7.1), the total error of the heat transfer rate consists of two individual errors, the flow rate error and the temperature difference error. The flow rate measurement error, E_v, is ±3% as described previously. The error associated with the temperature difference ΔT across the heat pump is calculated based on the error of each temperature measurement. Since inlet and outlet temperature measurements are assumed to be independent from each other, their errors

may be added in quadrature. Then the error for temperature difference can be computed as,

$$E_{\Delta T} = \sqrt{(E_{EFT})^2 + (E_{LFT})^2} \tag{7.3}$$

where E_{EFT} = entering fluid temperature error

E_{LFT} = leaving fluid temperature error

The temperature difference error may be converted into the percentage error,

$$E'_{\Delta T} = E_{\Delta T} / \Delta T \tag{7.4}$$

Where $E'_{\Delta T}$ = temperature difference error in percentage

ΔT = temperature difference

The total uncertainty in heat transfer rate is calculated as,

$$E_h = \sqrt{(E_V)^2 + (E'_{\Delta T})^2} \tag{7.5}$$

The error of power consumption consists of two individual errors also. They are the internal error of watthour meter and the error of the rotational sensor as described previously. Analogously, the error of rotational sensor can be converted into percentage error as,

$$E_s' = E_s / P \tag{7.6}$$

Where E_s' = rotational sensor error in percentage

E_s = rotational sensor error

P = power consumption

Then the total uncertainty in power consumption is determined as,

$$E_p = \sqrt{(E_m)^2 + (E_s')^2} \tag{7.7}$$

Where E_p = power consumption error

E_m = watthour meter error

E_s' = rotational sensor error in percentage

As a preliminary example, some typical temperature differences across the heat pump and power consumption have been chosen. They are 31.3 °F (17.4 °C) for load side temperature difference, 7.5 °F (4.3 °C) for source side temperature difference and 10.9 kW for power consumption. The propagated uncertainties are, load side heat transfer: ±3.0%, source side heat transfer rate: ±4.5% and power consumption: ±2.3%, respectively.

7.6. The Manufacturer's Catalog Data for the Heat Pump

The heat pump in this experiment is a model WP 120 made by FHP Manufacturing (http://www.fhp-mfg.com/). The catalog data are available in FHP published catalog set

and the FHP web site as well. The catalog data for the heating mode are re-organized and presented in both IP and SI units in Table 7.2 and Table 7.3. Unfortunately, only data for the performance with pure water is available from the heat pump manufacturer. Therefore, the antifreeze-adapted heat pump model can only be compared to experimental data and not to the catalog data.

Table 7.2. FHP WP 120 Catalog Data (IP Units)

No	Load Liquid			Source Liquid			Power (kW)
	EWT (F)	Volumetric Flow Rate (GPM)	Heating Capacity (MBTUH)	EWT (F)	Volumetric Flow Rate (GPM)	Heat of Extraction (MBTUH)	
1	90.0	23.0	115.7	40.0	24.0	86.6	8.5
2	90.0	26.1	131.2	50.0	24.0	101.7	8.7
3	90.0	29.5	148.2	60.0	24.0	118.2	8.8
4	90.0	33.2	166.7	70.0	24.0	136.2	8.9
5	100.0	22.9	115.1	40.0	24.0	82.6	9.5
6	100.0	25.9	130.1	50.0	24.0	97.3	9.6
7	100.0	29.2	146.6	60.0	24.0	113.3	9.8
8	100.0	32.7	164.5	70.0	24.0	130.8	9.9
9	110.0	22.8	114.4	40.0	24.0	78.2	10.6
10	110.0	25.7	129.0	50.0	24.0	92.5	10.7
11	110.0	28.9	145.0	60.0	24.0	108.1	10.8
12	110.0	32.3	162.3	70.0	24.0	124.9	10.9
13	115.0	22.7	114.1	40.0	24.0	75.9	11.2
14	115.0	25.6	128.5	50.0	24.0	89.9	11.3
15	115.0	28.7	144.2	60.0	24.0	105.3	11.4
16	115.0	32.1	161.3	70.0	24.0	121.9	11.5
17	120.0	22.7	113.8	40.0	24.0	73.4	11.9
18	120.0	25.5	128.0	50.0	24.0	87.3	11.9
19	120.0	28.6	143.5	60.0	24.0	102.4	12.0
20	120.0	31.9	160.2	70.0	24.0	118.8	12.2

Table 7.3. FHP WP 120 Catalog Data (SI Units)

No	Load Liquid			Source Liquid			Power (kW)
	EWT (C)	Volumetric Flow Rate (L/S)	Heating Capacity (kW)	EWT (C)	Volumetric Flow Rate (L/S)	Heat of Extraction (kW)	
1	32.2	1.5	33.9	4.4	1.5	25.4	8.5
2	32.2	1.6	38.5	10.0	1.5	29.8	8.7
3	32.2	1.9	43.4	15.6	1.5	34.6	8.8
4	32.2	2.1	48.9	21.1	1.5	39.9	8.9
5	37.8	1.4	33.7	4.4	1.5	24.2	9.5
6	37.8	1.6	38.1	10.0	1.5	28.5	9.6
7	37.8	1.8	42.9	15.6	1.5	33.2	9.8
8	37.8	2.1	48.2	21.1	1.5	38.3	9.9
9	43.3	1.4	33.5	4.4	1.5	22.9	10.6
10	43.3	1.6	37.8	10.0	1.5	27.1	10.7
11	43.3	1.8	42.5	15.6	1.5	31.7	10.8
12	43.3	2.0	47.6	21.1	1.5	36.6	10.9
13	46.1	1.4	33.5	4.4	1.5	22.2	11.2
14	46.1	1.6	37.7	10.0	1.5	26.4	11.3
15	46.1	1.8	42.3	15.6	1.5	30.9	11.4
16	46.1	2.0	47.3	21.1	1.5	35.7	11.5
17	48.9	1.4	33.4	4.4	1.5	21.5	11.9
18	48.9	1.6	37.5	10.0	1.5	25.6	11.9
19	48.9	1.8	42.1	15.6	1.5	30.0	12.0
20	48.9	2.0	46.9	21.1	1.5	34.8	12.2

7.7. Parameter Estimation and a Comparison Between Model Prediction and Catalog Data

The catalog data were used to fit coefficients for the water-to-water heat pump model described in Chapter 4, with the modifications described in sections 6.1 and 6.3. As discussed in section 6.3, it is desirable to use the flow-rate-dependent form of the heat exchanger model when antifreeze will be used. Since this heat pump utilizes a scroll compressor, the scroll compressor model described in section 6.1 is used. The parameters selected for the modified heat exchanger model have been estimated simultaneously with the parameters for the compressor model and the results are shown in Table 7.4.

Table 7.4. Parameter Estimation Results for the HP Water-to-Water Heat Pump Model WP120

Parameter	Estimated Value
product of the volume of the pockets that seal the suction gas at the beginning the compression and the rotational speed $\dot{V}_r$	8.09×10^{-3} m^3/s (1,028 ft^3/hr)
Built-in volume ratio v_i	2.43
Load side heat exchanger heat transfer resistance coefficient *3*	6.095×10^{-2}
Load side heat exchanger heat transfer resistance coefficient *2*	0.186 °C/kW (9.82×10^{-5} (hr-°F)/Btu)
Source side heat exchanger heat transfer resistance coefficient *3*	5.747×10^{-2}
Source side heat exchanger heat transfer resistance coefficient *2*	6.086×10^{-2} °C/kW (3.21×10^{-5} (hr-°F)/Btu)
Loss factor used to define the electro-mechanical loss that is supposed to be proportional to the theoretical power η	0.95
Constant part of the electro-mechanical power losses W_{loss}	3.35 kW (11,430 Btu/hr)
Superheat ΔT_{sh}	16.70 °C (30.06 °F)

The model output for pure water is compared to the catalog data in Figure 7.7 through Figure 7.9. A summary of the RMS error for heating capacity, heat of extraction and power consumption is presented in Table 7.5. A review of Figure 7.7 through Figure 7.9 and Table 7.5 shows that the model prediction compares favorably to the catalog data. The RMS errors are all within 2%.

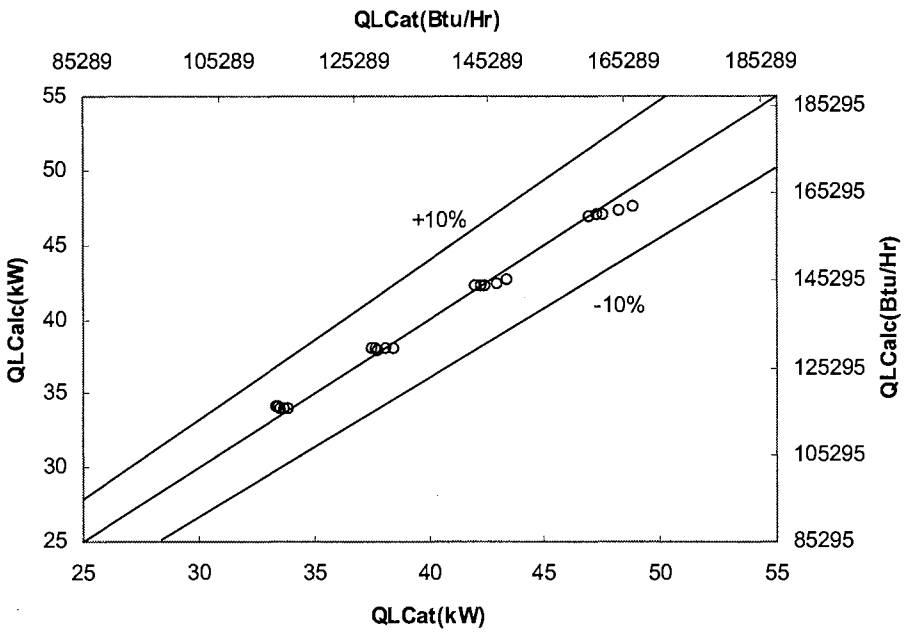

Figure 7.7. Calculated heating capacity vs catalog heating capacity

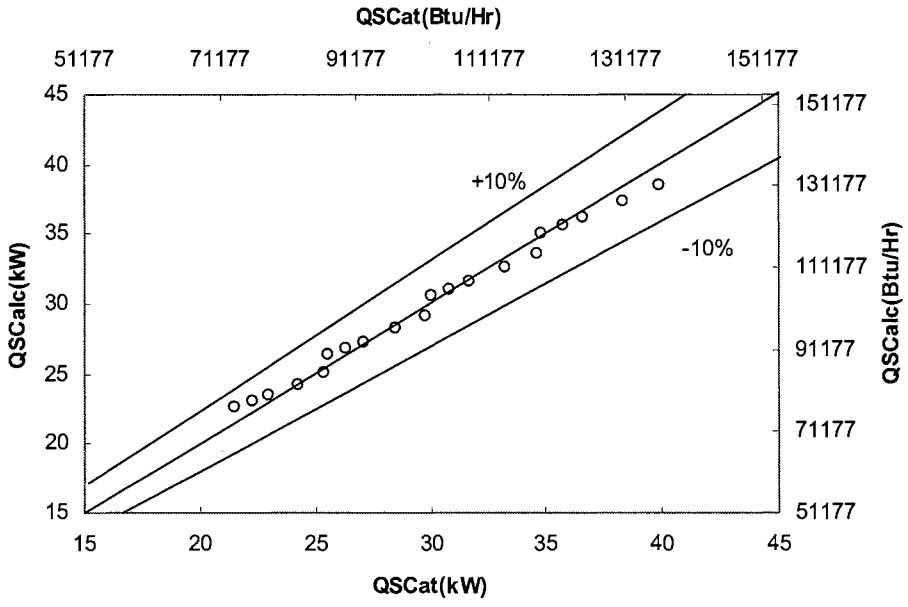

Figure 7.8. Calculated extracted heat vs catalog extracted heat

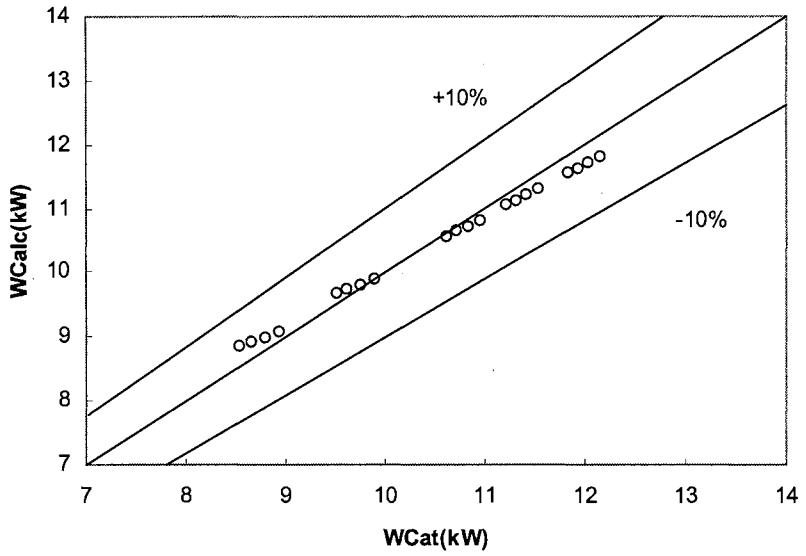

Figure 7.9. Calculated power vs catalog power

Table 7.5. RMS Errors of the Simulations for the Catalog Data

Nominal Capacity		Number of Points	RMS		
(W)	(Btu/hr)		Heating Capacity	Heat Extracted	Power
48,655 (Heating)	166,000 (Heating)	20	1.28%	1.99%	1.78%

7.8. Model Uncertainty

Uncertainty in the model results is due to two factors: 1) uncertainty in the catalog data and 2) uncertainties in the model that are reflected in the fact that the model doesn't exactly match the catalog data.

Water-source heat pumps are subjected to testing and rating requirements of ARI standard 320. The units are tested at ARI specified condition and certified as to

performance. ARI standard allowable tolerance is ±5% from the catalog data. The ARI rated condition is only one of the numerous data points in the catalog. For those operation points different from the ARI rated condition, the deviation may be greater than 5%. As a result, the heat pump model, using parameters estimated from the manufacturer's catalog data, has an inherent uncertainty between model prediction and observation of no less than ±5%.

As an example, one source of error is that both manufacturer's catalog data and the model assume zero energy imbalance among source side heat transfer, load side heat transfer and power consumption. However, the energy imbalance will not be perfectly zero because of the compressor shell loss, which may constitute a few percent of the power consumption. Hence, there are some errors associated with model predictions caused by this assumption.

Secondly, as shown previously, the model may not be expected to furnish perfect fidelity (i.e. 0% RMS error) to the catalog data. There is no general theory known to the author for estimating the uncertainty in this type of parameter estimation. However, as might be noticed in Figures 7.7 to 7.9, there is an analogy to linear regression if the final result (estimated value) is compared to the catalog data. Therefore, the uncertainty has been calculated as if a linear regression was being performed on the data set consisting of model estimated values and catalog values. As in a linear regression, the probability distribution of the random error is assumed to be normal and the variance of the random error is equal to a constant. For any linear regression using least squares approach, the

mean of the errors of all the fitted points is zero, but it is not necessarily true for the parameter estimation modeling approach. Nevertheless, the normal distribution of the errors of the parameter estimation can be calculated based on the mean of the errors and their variance. For the twenty catalog data points in this case, the mean of errors, denoted by μ, and the standard deviation, denoted by σ, as an estimation of the variance are given in Table 7.6. The profile of the assumed normal distribution of the errors is plotted in Figure 7.10.

Table 7.6. Mean of Errors and Standard Deviation

	Load Side Heating Capacity	Source Side Heat Extraction	Power
μ	-0.112	-0.0415	-0.0695
σ	0.564	0.677	0.223

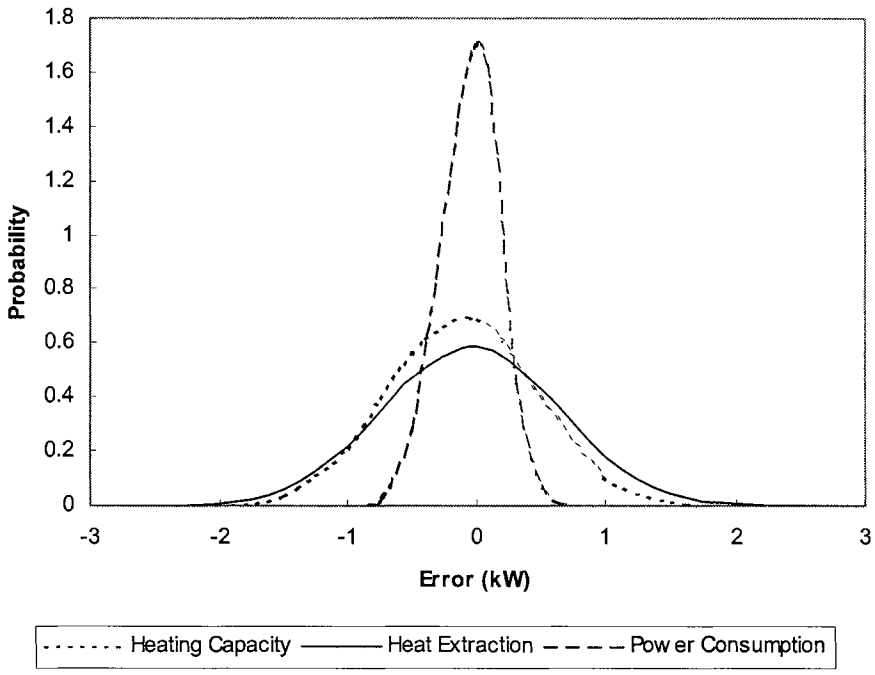

Figure 7.10. Error Distribution

The confidence of any possible error is obtained by calculating the area under the normal distribution curve for the interval of the specified error. This calculation can be readily accomplished by looking up the table in any classical statistics books, in which the tabulated probability values are organized as a function of standard normal random variable. The standard normal random variable z is defined by the following equation,

$$z = \frac{x - \mu}{\sigma} \tag{7.8}$$

where x = the normal random variable (the uncertainty)

In Equation (7.8), the variable x represents the uncertainties of heating capacity, heat extraction and power consumption in our case. Experimental uncertainties are typically given for 95% confidence, and we will follow that convention here. That means the area over the interval we are seeking is 0.95. Since normal distribution is symmetric, the area is 0.475 if half the profile is considered. From McClave and Dietrich (1994), we find the standard normal random variable z is 1.96 for an area of 0.475. Hence, the uncertainties of heating capacity, heat extraction and power consumption can be computed using Equation (7.8). They are ±1.1 kW (±3,753 Btu/Hr), ±1.3 kW (±4,435 Btu/Hr) and ±0.44 kW (±1,501 Btu/Hr) respectively. In other words, they are ±2.7% of a typical heating capacity, ±4.3% of a typical heat of extraction and ±4.2% of a typical power consumption.

Another factor involved in the propagation of overall uncertainty is the adjusted total heat transfer resistance as a result of the estimated degradation of the fluid side heat

transfer coefficient when antifreeze is used. This uncertainty may be estimated as ±1% based on the description of model extension on antifreeze applications in Chapter 6. All the errors are then compounded by adding in quadrature to find the overall uncertainty of the model prediction.

To summarize, the estimated uncertainties for model prediction are ≥5.8% with heating capacity, ≥6.7% with heat extraction, and ≥6.6% with power consumption.

It is noted that the model uncertainty discussed above is limited to the operation ranges of inlet temperatures and flow rates in the catalog. If the inlet temperatures and flow rates are considerably away from the catalog specified range, the model uncertainty is expected to be higher than what we have estimated.

7.9. Experiments

On December 11, 2000 and December 12, 2000, two sets of data were collected when the heat pump system was running with 42% by weight propylene glycol solution on the load side, and pure water on the source side to investigate the validity of the adapted heat pump model. The data of December 11, 2000 represent continuous heat pump operation, so that quasi steady state operation is achieved. The data of December 12, 2000 represent another typical example of the system operation with frequent on-off cycles. On December 30, 2001, data were collected with 42% by weight propylene glycol solution on both sides. Again, the heat pump was operating with frequent on-off cycles.

This set of data will be used to assess the adapted heat pump model for antifreeze on both sides. The following three sections describe the three experiments and the associated model validation.

7.10. Dec. 11 2000 Experiment

The load/source side fluid flow rates in the experimental data of Dec. 11, 2000 are presented in Figure 7.11. The load/source side entering and leaving fluid temperatures and power consumption can be found below in Figure 7.13 through Figure 7.15 in section 7.10.3. The plots show that the heat pump was operating in a comparatively stable manner for bout nine hours, although the last five hours represent the most stable operation period.

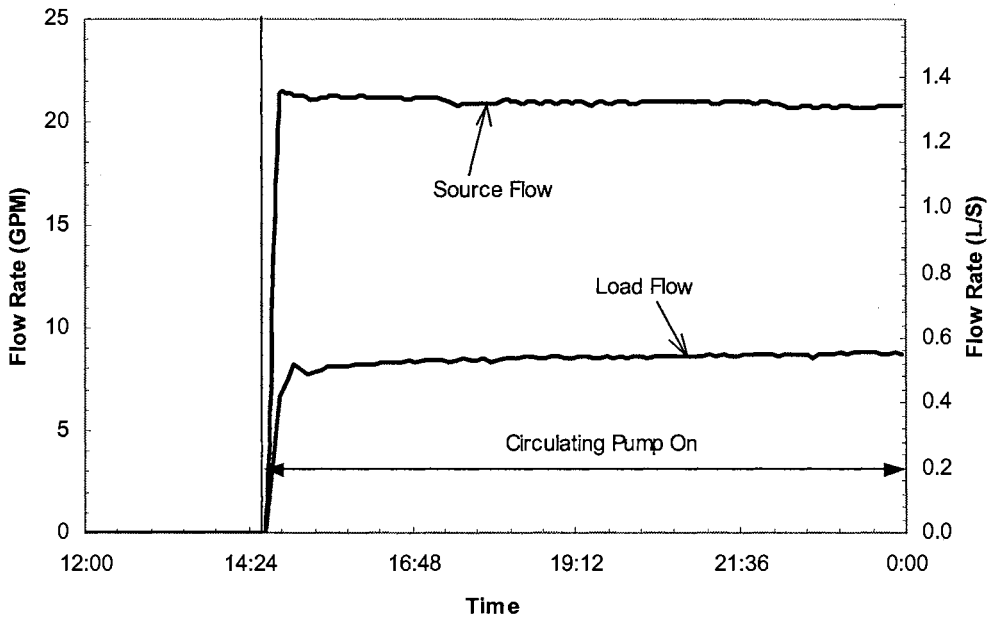

Figure 7.11. Heat pump load/source side flow rates

7.10.1. Experimental Uncertainty

The time period between 19.00 and 24.00 on Dec. 11, 2000 is selected for comparison, as the heat pump was running under fairly stable conditions. The average temperatures and power consumption are given in Table 7.7. The uncertainties of load side heat transfer, source side heat transfer and power consumption are calculated accordingly as discussed in the section 7.5. The results are shown in Table 7.8.

Table 7.7. Average Temperature Differences and Power Consumption used to Compute the Relative Uncertainties

Date	Load Side Avg ΔT	Source Side Avg ΔT	Avg Power
12/11/2000	31.3 °F (17.4 °C)	7.4 °F (4.3 °C)	11.7 kW

Table 7.8. Derived Uncertainties of Heat Transfer Rate and Power Consumption

Date	Load Side Heat Transfer Rate	Source Side Heat Transfer Rate	Power
12/11/2000	±3.0%	±4.5%	±2.1%

7.10.2. Energy Imbalance

In order to verify the reasonableness of the experimental measurements, an energy balance is made. As discussed in Chapter 4, the manufacturers usually assume that there is no heat loss from the compressor shell or other locations in the heat pump. Thus, a perfect energy balance may be obtained theoretically. For example, load side heating capacity is equal to the sum of source side heat of extraction and compressor power when the heat pump operates in heating mode. In practice, the difference between load side

heat and source side heat plus compressor power will not approach 'zero' due to shell loss and error of the measurements. However, shell loss should constitute a fairly small portion of total energy provided by the heat pump. Therefore, it is still desirable to check the energy balance to ensure it falls into a reasonably small range, say ±10%. In case of heating mode, the percentage imbalance is calculated as,

$$\text{Imbalance}(\%) = \frac{\text{ABS}(\text{Load Side H. T.} - \text{Source Side H. T.} - \text{Compressor Power})}{\text{Load Side H. T.}} \times 100\% \tag{7.9}$$

The energy imbalance as a percentage of the load side heat transfer rate of the data for Dec. 11, 2000 is plotted in Figure 7.12. It is noticeable that there is a significant imbalance at the first few points. Presumably this is due to the heat accumulation or dissipation inside the heat pump and fluid transient delay during the starting period. When the operation approaches a quasi steady state, this high imbalance diminishes rapidly. Since high energy imbalance only takes place in one or two data points at the beginning period, the remaining experimental data are still useful for the model validation purpose. Furthermore, given the uncertainties in experimental measurement and compressor shell loss, the imbalance shown in Figure 7.12 is quite reasonable.

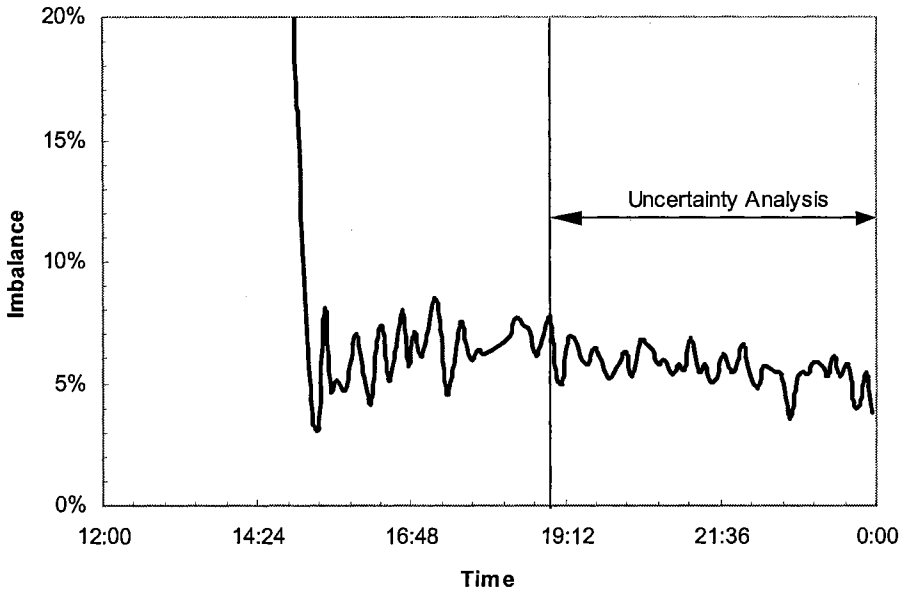

Figure 7.12. Heat pump energy imbalance (12/11/00)

For the selected analysis period (19.00 -- 24.00), the average load side heat transfer rate, average source side heat transfer rate and average power consumption with their uncertainties are presented in Table 7.9. Table 7.9 shows that the energy imbalance as the residual by subtracting source heat transfer and power consumption from load heat transfer is between -0.3 kW -1,024 Btu/Hr) and 4.3 kW (14,671 Btu/Hr) when the uncertainty of the instrumentation is included. It could range from 0% to 12.2% of the load side heat transfer rate. The energy imbalance plotted in Figure 7.12 for the selected time block falls into the band of estimated uncertainty, even without accounting for the compressor shell loss.

Table 7.9. Energy Imbalance with Estimated Uncertainties (12/11/2000)

Load Heating Capacity	Source Heat of Extraction	Power Consumption
35.3 ± 1.1 kW (120,437 ± 3,646 Btu/Hr)	22.0 ± 0.9 kW (75,060 ± 3,088 Btu/Hr)	11.3 ± 0.3 kW
Imbalance = Load Heating Capacity - Source Heat of Extraction - Power		
2.0 ± 2.3 kW or -0.3 kW ≤ imbalance ≤ 4.3 kW (6,824 ± 7,847 Btu/Hr or -1,024 Btu/Hr ≤ imbalance ≤ 14,671 Btu/Hr)		

7.10.3. A Comparison of Model Prediction to the Experimental Data

A comparison of model prediction to the measured field data is desirable in order to assess the validity of the adapted heat pump model for antifreeze application. The model has been evaluated using the measured entering fluid temperatures. Then the predicted leaving fluid temperatures are compared with the measured temperatures and predicted power consumption is compared with the measured power consumption. The comparisons are presented in Figure 7.13 through Figure 7.15 for the data collected on December 11, 2000. A review of Figure 7.13 through Figure 7.15 shows favorable agreement. The maximum deviation (around 4 °C or 7 °F) is observed at the beginning two points due to the transient behavior of the heat pump discussed previously in the section 7.10.3.

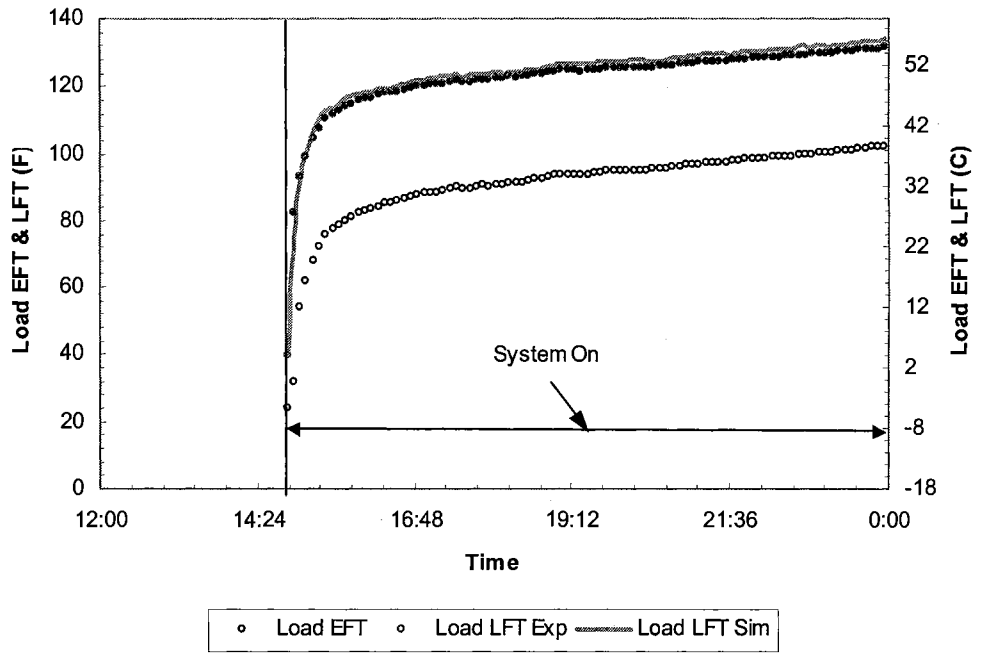

Figure 7.13. Heat pump model validation in heating mode: load side entering/leaving fluid temp

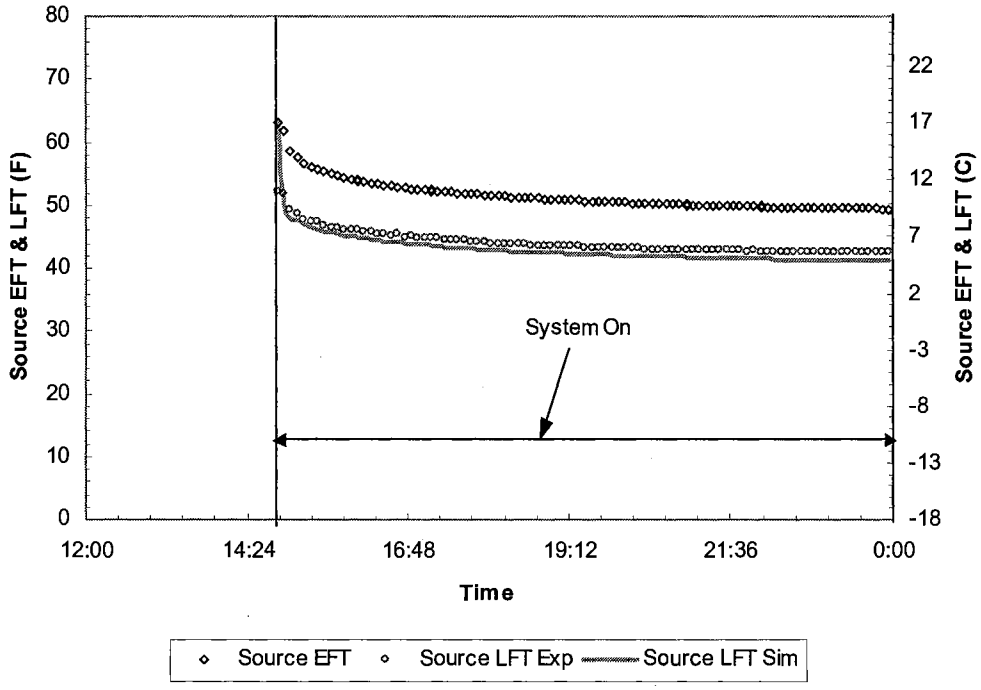

Figure 7.14. Heat pump model validation in heating mode: source side entering/leaving fluid temp

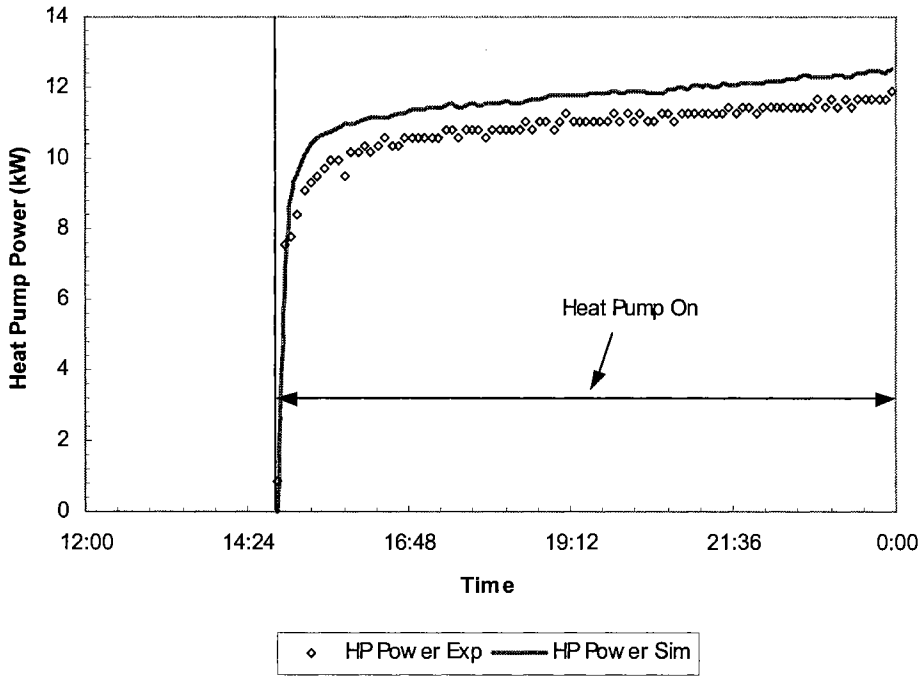

Figure 7.15. Heat pump model validation in heating mode: power input

As discussed in section 7.8, the estimated uncertainties of model prediction are ±5.8% for heating capacity, ±6.7% for heat extraction, and ±6.6% for power consumption. The average estimated uncertainties of experimental data collected in Dec. 11, 2000 are ±3.1% for heating capacity, ±4.5% for heat of extraction and ±2.1% for power consumption. Thus, deviations between model predictions and experimental data of ±8.9% for heating capacity, ±11.2% for heat of extraction and ±8.7% for power consumption, respectively may be accounted for by the uncertainty analysis.

Figures 7.16 through Figure 7.18 show the percentage error between model predictions and experimental measurements for the data collected on December 11, 2000. Each plot also shows the amount of error that can be explained by the uncertainty

analysis, if the catalog data are assumed to have an uncertainty of ±5%. For the most part, except during the initial transients, the model predictions match the experimental results within the bands of estimated uncertainty. The average load side heat transfer rate, average source side heat transfer rate and average power consumption of the model simulation and experimental data for the selected time period are given in Table 7.10.

Table 7.10. Average Heat Transfer Rates and Power Consumption (19:00 –24:00)

	Experiment	Model	Deviation
Load side heat transfer rate	35.3 kW (120,437 Btu/Hr)	37.8 kW (128,966 Btu/Hr)	2.5 kW (8,530 Btu/Hr)
Source side heat transfer rate	22.0 kW (75,060 Btu/Hr)	24.9 kW (84,954 Btu/Hr)	2.9 kW (9,894 Btu/Hr)
Power	11.3 kW	12.1 kW	0.8 kW

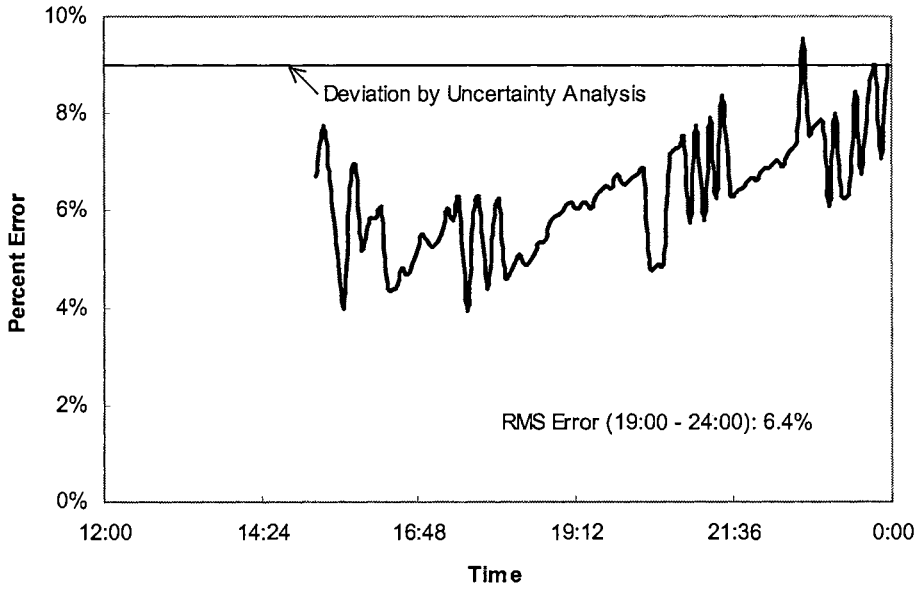

Figure 7.16. Heat pump model validation in heating mode: heating capacity percentage error between model and experiment

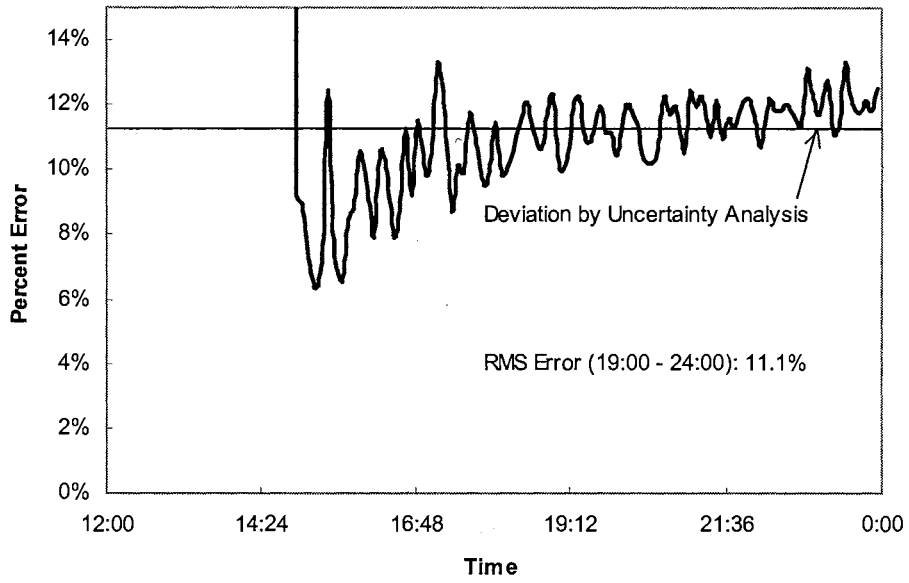

Figure 7.17. Heat pump model validation in heating mode: heating of extraction percentage error between model and experiment

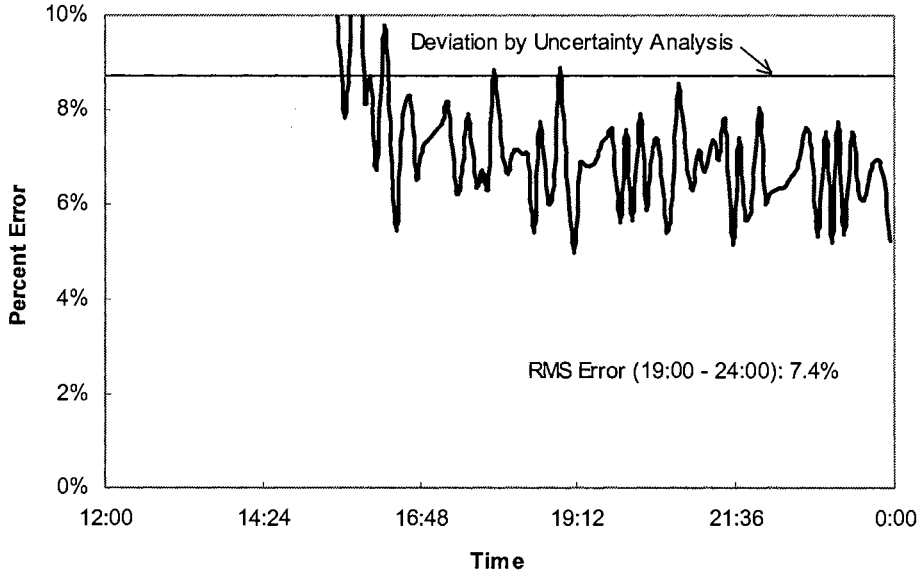

Figure 7.18. Heat pump model validation in heating mode: power consumption percentage error between model and experiment

7.11. Dec. 12, 2000 Experiment

The load/source side fluid flow rates in the experimental data of Dec. 12 2000 is presented in Figure 7.19. This experiment follows immediately from the data described in the previous section. Due to the heating requirements of the bridge deck, the heat pump has now begun to cycle. The load/source side entering and leaving fluid temperatures and power consumption can be found below in Figure 7.20 through Figure 7.22. The time blocks when the heat pump and circulation pump were on are marked by black dots in the plots. The plots show that the heat pump was operating with frequently on-off cycle during a period of 12 hours.

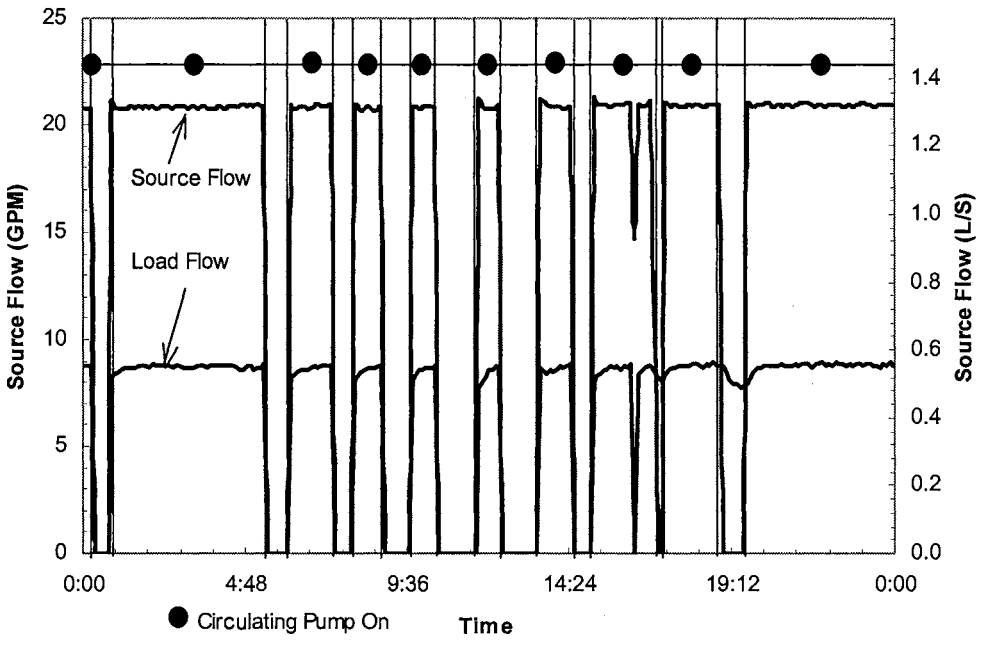

Figure 7.19. Heat pump load/source side flow rates

As described in section 7.10.3, the model prediction for leaving fluid temperatures and power consumption are compared to the experimental measurements in Figure 7.20 to 7.22. The comparison shows that the behavior of the model prediction is very similar to the behavior shown in section 7.10 except for the first two measurement points (12 min.) of each on-cycle. The deviation between the model and the experimental are within the bands of the uncertainty analysis. After the first 12 minutes, the model prediction of the load side heat transfer rate is typically within the 7.6 % of the experimental measurement; the model prediction of the source side heat transfer rate is typically within the 11.7 % of the experimental measurement; the model prediction of the power consumption is typically within the 6.0 % of the experimental measurement.

The first two data points that show significant transients represent the behavior of 12 minutes at the beginning of each on-cycle. It is noticed that the shortest on-cycle in this data set last about one hour and the longest last about 5 hours. Thus, the model is not able to simulate the heat pump performance for about 1/5 of the shortest on-cycle and about 1/25 of the longest on-cycle with an acceptable accuracy. If the time period of the on-cycle drops to close to the time for the heat pump to finish its transient behavior, this steady state model could fail the simulation completely. A transient heat pump model is necessary in this case, which is not the objective of this dissertation.

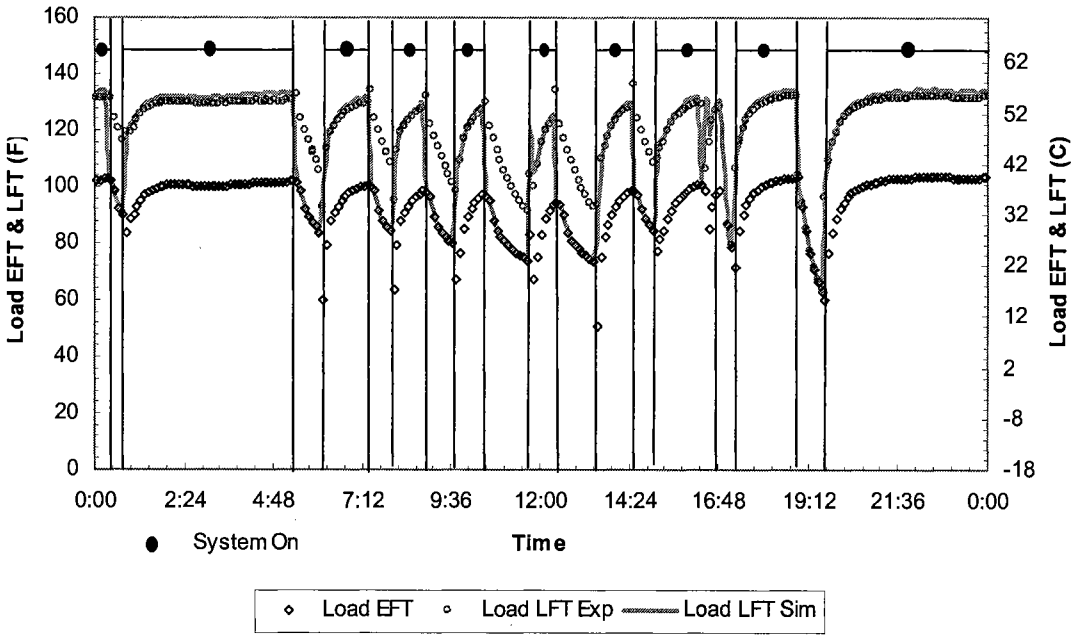

Figure 7.20. Heat pump model validation in heating mode: load side entering/leaving fluid temp

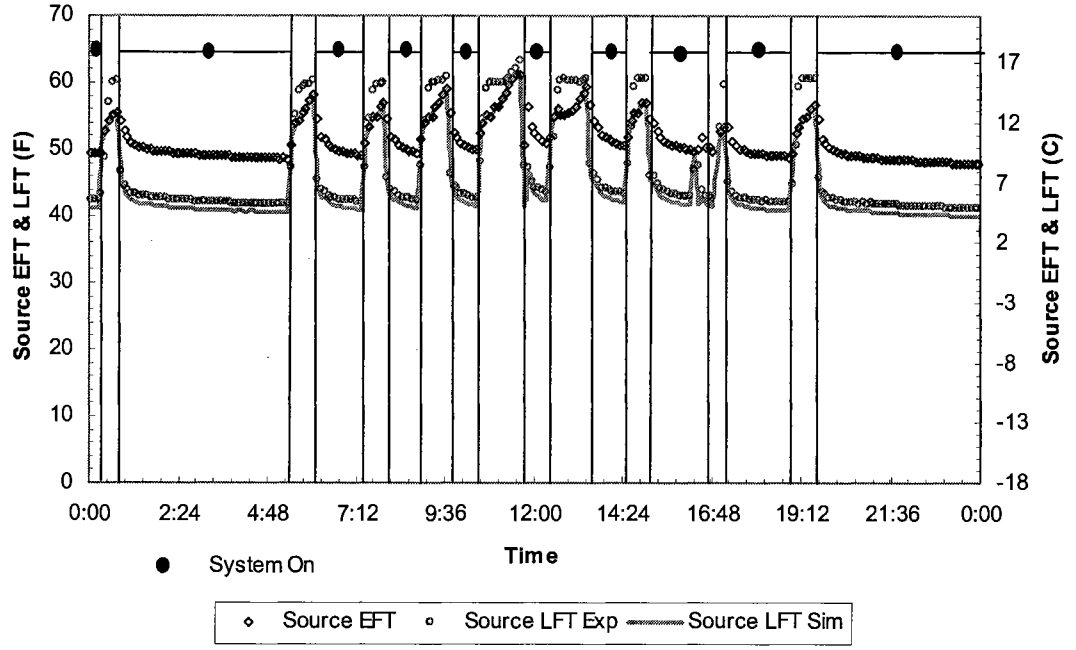

Figure 7.21. Heat pump model validation in heating mode: source side entering/leaving fluid temp

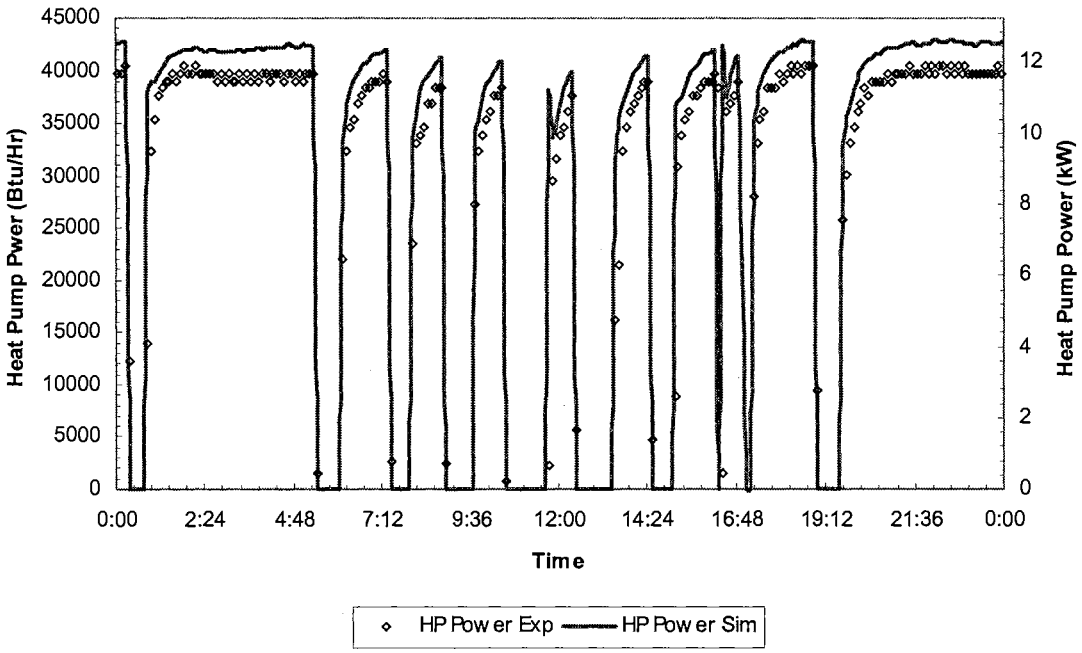

Figure 7.22. Heat pump model validation in heating mode: power input

7.12. Dec. 30, 2001 Experiment

This experiment took place in December of 2001, which is one year after the experiments described in section 7.10 and 7.11. The load/source side fluid flow rates in the experimental data are presented in Figure 7.23. The load/source side entering and leaving fluid temperatures and power consumption can be found below in Figure 7.25 through Figure 7.27 in section 7.12.4.

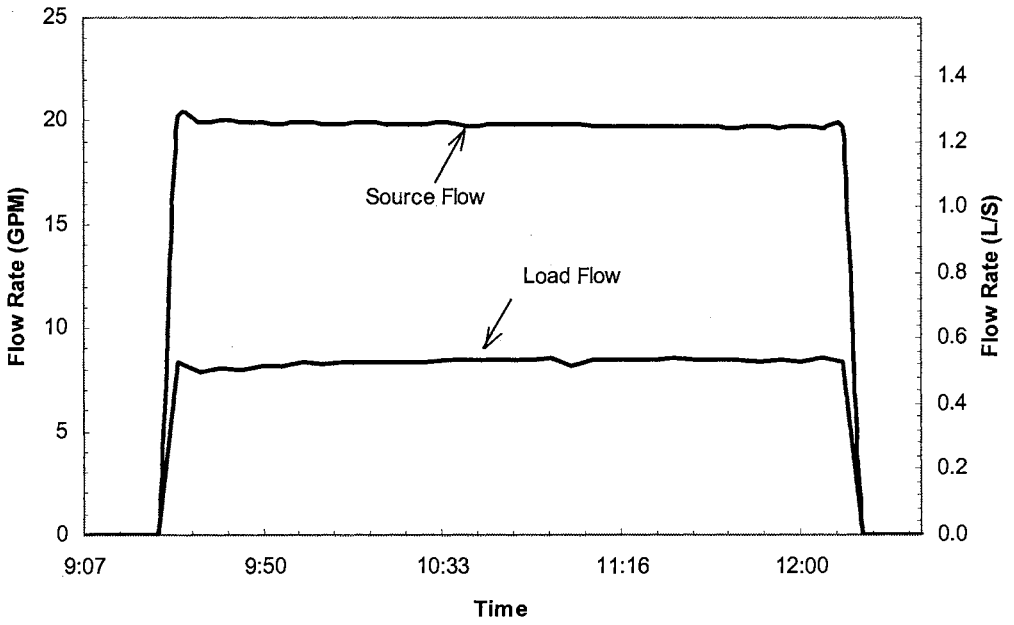

Figure 7.23. Heat pump load/source side flow rates

7.12.1. Experimental Uncertainty

Since this experiment was implemented one year after the previous two experiments and antifreeze was applied to the source side, it is desirable to investigate the experimental uncertainty again. The time period between 10.00 AM and 11.30 AM on Dec. 30, 2001 is selected for comparison, as the heat pump was running under fairly stable conditions. The average temperatures and power consumption are given in Table 7.11. The uncertainties of load side heat transfer, source side heat transfer and power consumption are calculated accordingly as discussed in the section 7.5. The results are shown in Table 7.12.

Table 7.11. Average Temperature Differences and Power Consumption used to Compute the Relative Uncertainties

Date	Load Side Avg ΔT	Source Side Avg ΔT	Avg Power
12/30/2001	29.7 °F (16.5 °C)	7.6 °F (4.2 °C)	9.9 kW

Table 7.12. Derived Uncertainties of Heat Transfer Rate and Power Consumption

Date	Load Side Heat Transfer Rate	Source Side Heat Transfer Rate	Power
12/30/2001	±3.1%	±4.5%	±3.7%

7.12.2. Energy Imbalance

Due to the same reason described in the section above, it is also desirable to assess the energy imbalance of the data for Dec. 30, 2001. The imbalance is plotted in Figure 7.24.

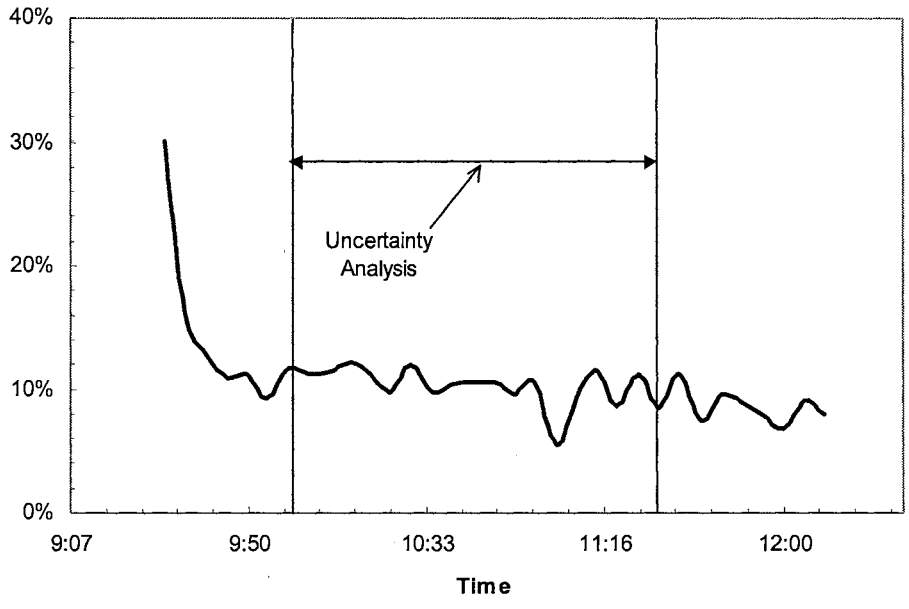

Figure 7.24. Heat pump energy imbalance

For the selected analysis period (10.00AM and 11.30AM), the average load side heat transfer rate, average source side heat transfer rate and average power consumption with their uncertainties are presented in Table 7.13. Table 7.13 shows that the energy imbalance as the residual by subtracting source heat transfer and power consumption from load heat transfer is between 1.3 kW (4,435 Btu/Hr) and 6.1 kW (20,812 Btu/Hr) when the uncertainty of the instrumentation is included. It could range from 3.8 % to as high as 18.0% of the load side heat transfer rate. The energy imbalance plotted in Figure 7.24 for the selected time block falls into the band of estimated uncertainty.

Table 7.13. Energy Imbalance with Estimated Uncertainties (12/30/2001)

Load Heating Capacity	Source Heat of Extraction	Power Consumption
33.8 ± 1.1 kW (115,319 ± 3,753 Btu/Hr)	20.2 ± 0.9 kW (68,918 ± 3,071 Btu/Hr)	9.9 ± 0.4 kW
Imbalance = Load Heating Capacity - Source Heat of Extraction - Power		
3.7 ± 2.4 kW or 1.3 ≤ imbalance ≤ 6.1 kW (12,624 ± 8,188Btu/Hr or 4,435 ≤ imbalance ≤ 20,812 Btu/Hr)		

7.12.3. A Comparison of Model Prediction to the Experimental Data

Again, the model predictions for leaving fluid temperatures and power consumption are compared with the experimental data in Figures 7.25 to 7.27.

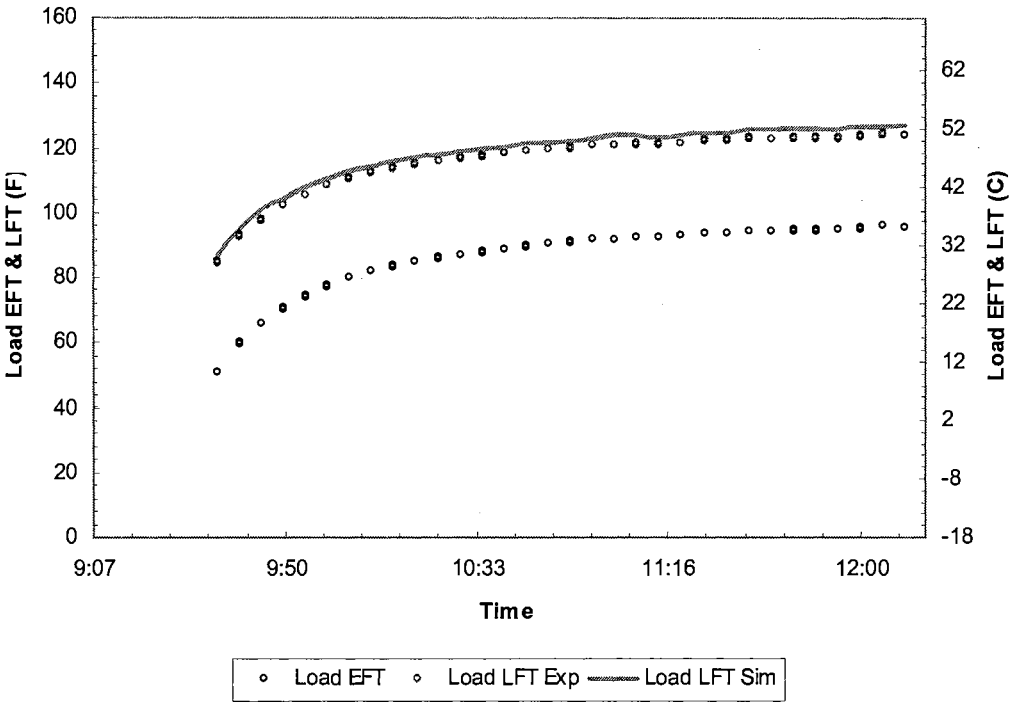

Figure 7.25. Heat pump model validation in heating mode: load side entering/leaving fluid temp

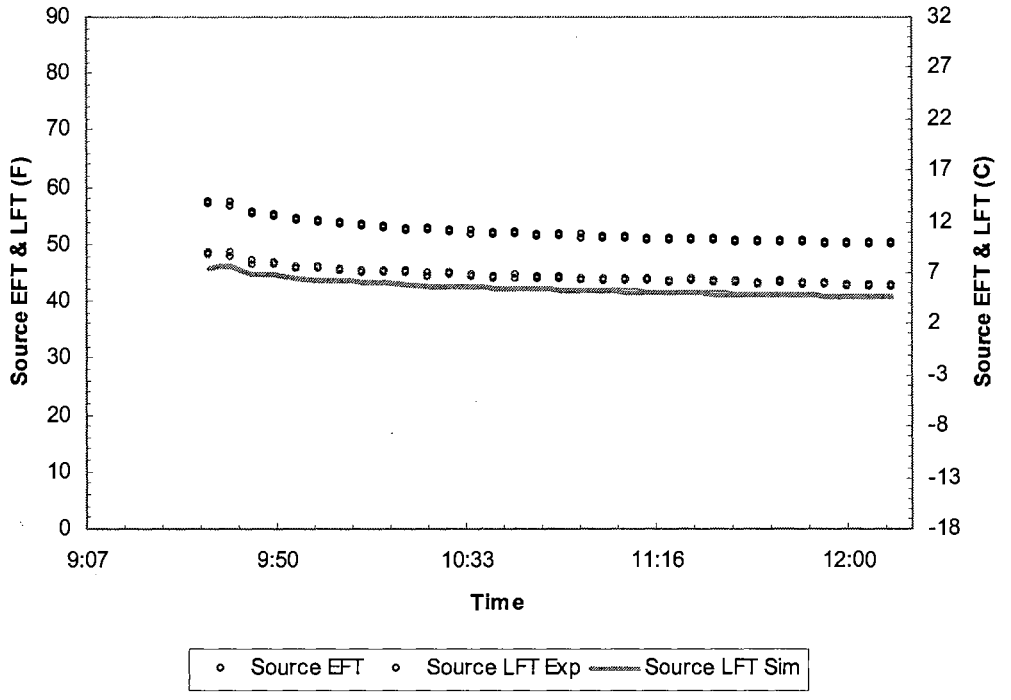

Figure 7.26. Heat pump model validation in heating mode: source side entering/leaving fluid temp

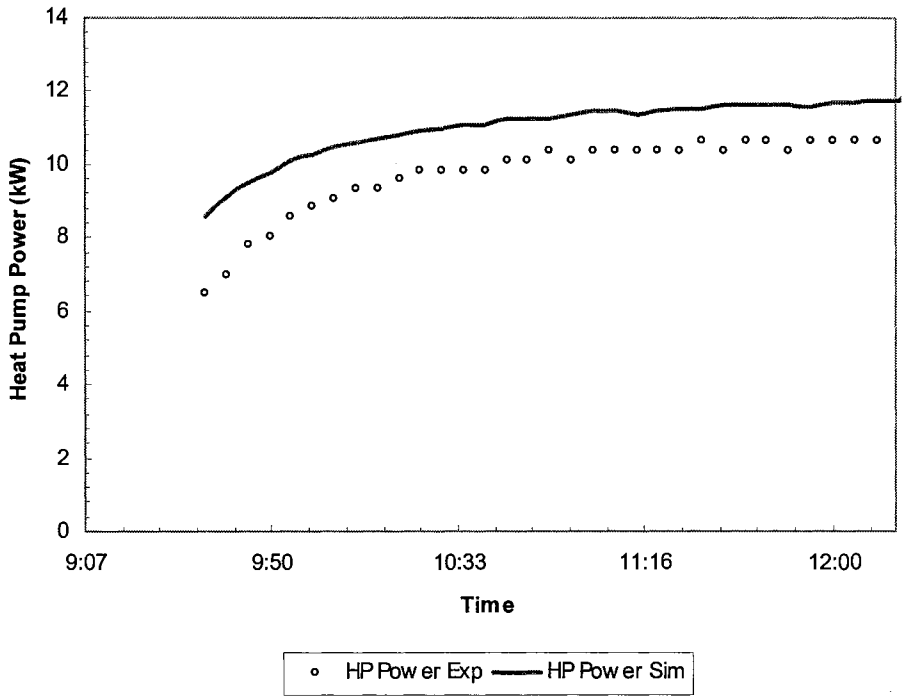

Figure 7.27. Heat pump model validation in heating mode: power input

As discussed in section 7.8, the estimated uncertainties of model prediction are ±5.8% for heating capacity, ±6.7% for heat extraction, and ±6.6% for power consumption. The estimated uncertainties of experimental data collected in Dec. 30, 2001 are ±3.1% for heating capacity, ±4.5% for heat of extraction and ±3.7% for power consumption. Thus, deviations between model predictions and experimental data of ±8.9% for heating capacity, ±11.2% for heat of extraction and ±10.3% for power consumption, respectively may be account for by the uncertainty analysis.

Figure 7.28 through Figure 7.30 show the percentage error between model predictions and experimental measurements for the data collected on December 30, 2001.

The RMS errors between model prediction and experimental data for the selected time block are given in Table 7.14. For the heating capacity and power consumption, the amount of difference can be explained by the uncertainty analysis as they are shown in each plot. For the most part, except during the initial transients, the model predictions match the experimental results within the bands of estimated uncertainty. However, for the heat extraction, the difference between model prediction and experimental data goes out of the band of uncertainty. There may be several explanations for this relatively large error. First, the heat pump was set up about three years ago. After this considerably long period of time, it is reasonable to assume that fouling may cause the degradation of the heat pump performance to some extent. Secondly, as discussed in section of model uncertainty, the estimated model uncertainty is limited to the operation ranges of inlet temperatures and flow rates provided in the catalog. If the inlet temperatures and flow rates are considerably away from the catalog specified range, the model uncertainty is expected to be higher. Thirdly, it is noticed in Table 7.13 that the imbalance among load side heating capacity, source side heat extraction and power is positive. It goes oppositely to the way that could be explained by the compressor shell loss. Also, the error is still on order of the model uncertainty. Fourthly, the flow meters are calibrated for pure water. Its accuracy is questionable when the fluid is changed to antifreeze solution whose viscosity is significantly different from pure water.

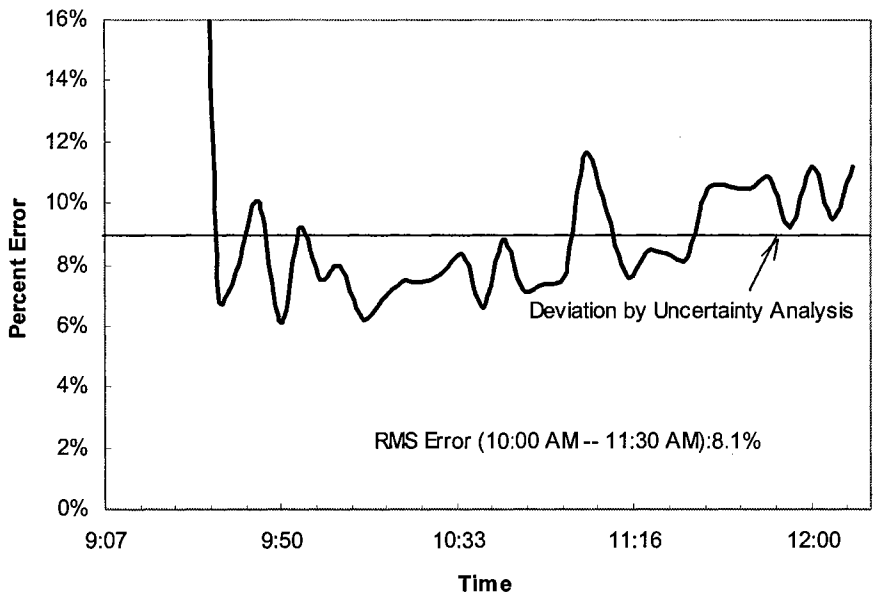

Figure 7.28. Heat pump model validation in heating mode: heating capacity percentage error between model and experiment

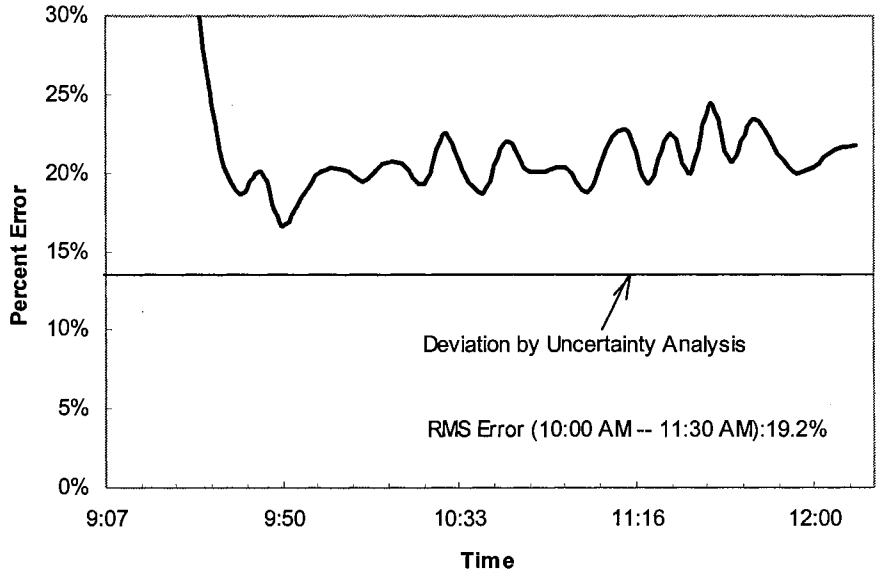

Figure 7.29. Heat pump model validation in heating mode: heating of extraction percentage error between model and experiment

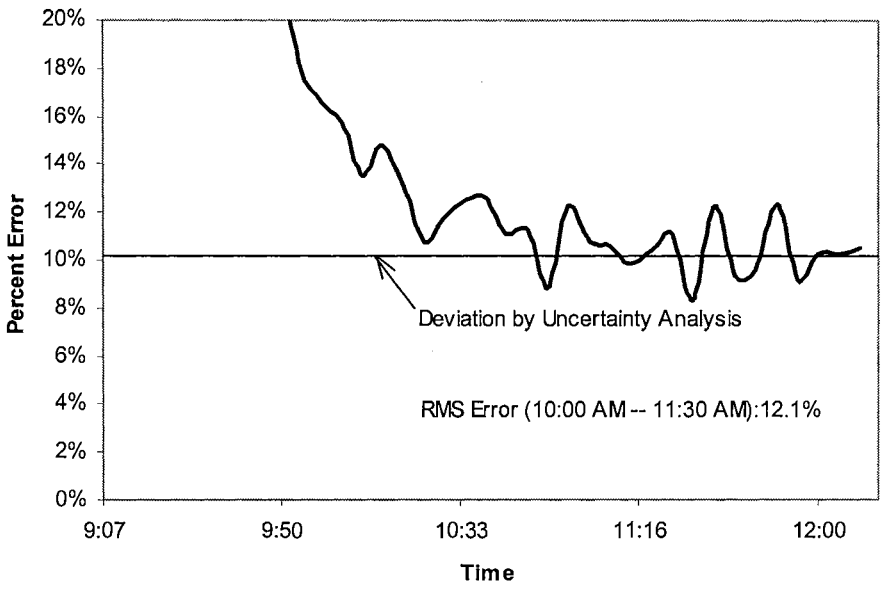

Figure 7.30. Heat pump model validation in heating mode: power consumption percentage error between model and experiment

Table 7.14. RMS Errors between Model Prediction and Experimental Data

Date	Heating Capacity	Heat Extracted	Power
10.00 AM – 11.30 AM 12/30/01	8.1%	19.2%	12.1%

7.13. Summary

Good agreement between the predicted and the measured leaving water temperatures and power consumption is obtained. The maximum deviations are observed at the beginning of on-cycle. Presumably this is due to the heat accumulation or dissipation inside the heat pump and fluid transient delay during the starting period. The points with relatively high deviation only constitute very small portion of the entire data set. Its influence on the accuracy of the overall energy calculation is negligible.

Conclusively, the comparison between the predicted and measured temperatures and power input shows the parameter estimation heat pump model works effectively for the simulation of ground source heat pump bridge deck heating system.

8. Water-to-Air Heat Pump Model Validation

This chapter describes a 'field' validation of the water-to-air heat pump model using an existing experiment apparatus. The experiment apparatus has been established for an ASHRAE research project. In the experiment, a water-to-air heat pump was installed to supply cooling for the test cell, which was built to validate the heat balance and radiant time series cooling load calculation procedures. However, some instrumentation has been added which provides measurements of the essential external performance data to validate the heat pump model.

8.1. Background and a Brief Description of Experimental Apparatus

The experimental apparatus is in a test cell building located to the north of Mechanical and Aerospace Engineering Research Lab. This test cell building was constructed for experimental validation of cooling load calculation method as a research project from American Society of Heating, Refrigerating and Air-conditioning Engineers. A schematic diagram of the experimental facility is shown in Figure 8.1. The first floor of the building is the instrumentation room. The second floor of the building is a space that can be cooled or heated by the water-to-air heat pump housed in the instrumentation room. Air is circulated in a loop including the space of simulated load, the load side of the heat pump, a booster fan and some necessary ductwork. Meanwhile, water is circulated in a loop including a ground loop heat exchanger and the source side of the heat pump. The instrumentation and data acquisition devices are also contained

within the instrumentation room. The instrumentation and data acquisition devices include two groups of exposed junction thermocouples, a chilled mirror dew point transmitter, a nozzle, a pressure transducer, two thermocouple probes, a water flow meter, a watt transducer, a scale and two Fluke datgaloggers.

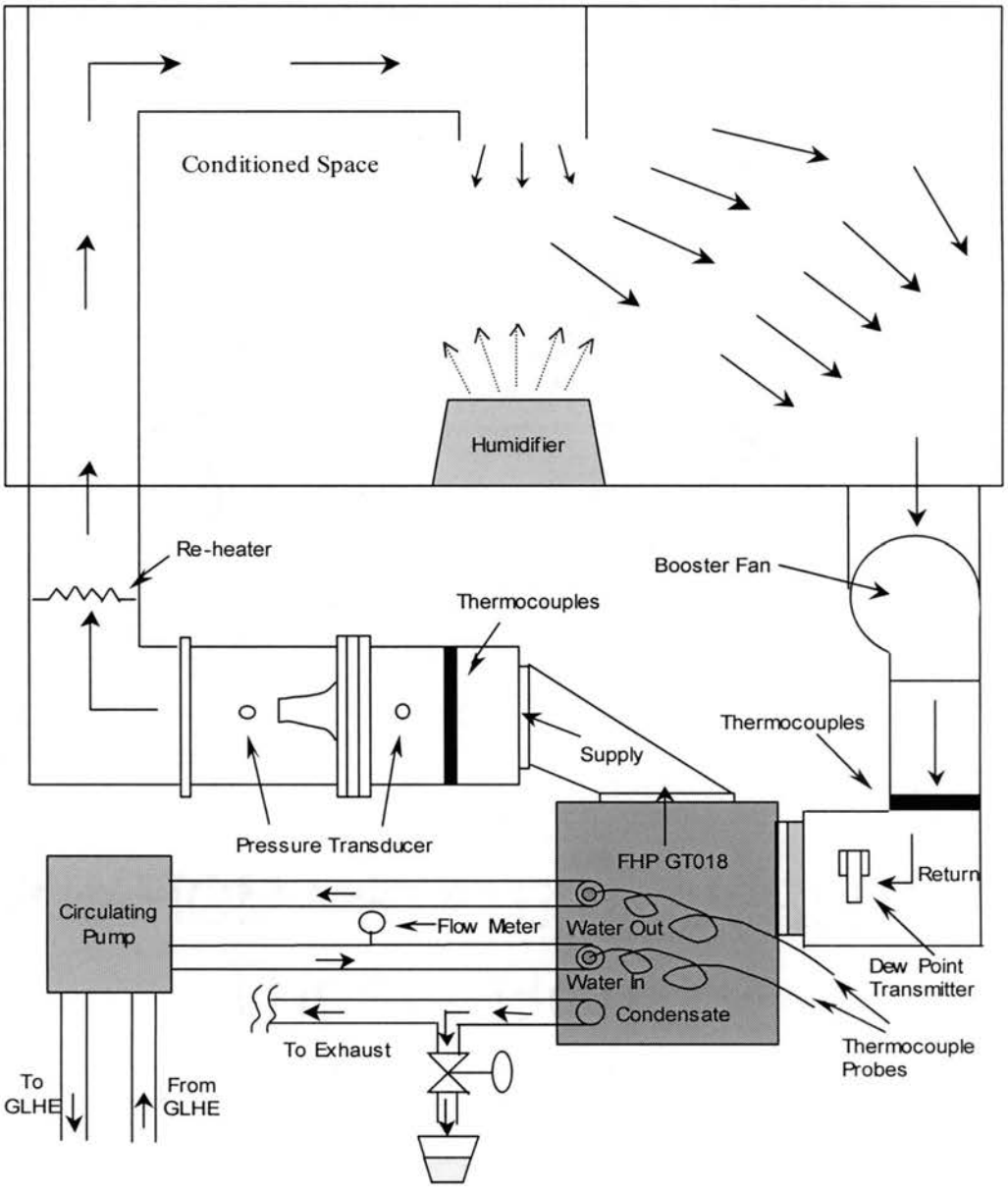

Figure 8.1. System schematic of the water-to-air heat pump experiment

The experimental apparatus is described in two parts: the heating and air conditioning system and the instrumentation. The heating and air conditioning system is comprised of the air conditioned space, a water-to-air heat pump, an electric re-heater, a booster fan, two humidifiers, a water circulation pump, the ground loop heat exchanger, some valves, pipes and ductwork. The instrumentation includes sensors, transducers, and transmitters for the air flow rate, the return and supply air dry bulb temperatures, the return air dew point temperature, the condensate, the water flow rate, the inlet and outlet water temperatures, the power consumption and finally data acquisition.

8.2. The Heating and Air Conditioning System

8.2.1. Water-to-Air Heat Pump

The test was performed on an FHP model GT018 water-to-air heat pump. The performance of the heat pump is certified to ARI/ISO standard 13256-1 for water loop heat pumps, ground water heat pumps and ground loop heat pump applications. The heat pump is designed to operate with entering water temperatures between 25 °F (-3.9 °C) and 110 °F (43.3 °C). Nominal cooling capacity is 1-1/4 ton (4.4 kW) at ARI/ISO 13256-1 rated air flow rate (550 CFM).

Figure 8.2. Front side of the tested water-to-air heat pump

The heat pump contains a sealed refrigerant circuit including a hermetic rotary compressor, bi-directional thermal expansion valve metering device, finned tube air-to-refrigerant heat exchanger, refrigerant reversing valve and service ports. A view of the heat pump in the instrumentation room is presented in Figure 8.2. A few of the instruments placed on the heat pump, return and supply ductwork near the heat pump are also in the sight.

8.2.2. Humidifier

Two humidifiers have been placed to maintain a considerable amount of latent cooling load in the air-conditioned space. The humidifier is of cool mist type with a capacity up to 10 gallons per day. It draws relatively dry air through its rear air intake grill area. This air is then passed through a moisture-laden wick filter, which retains the minerals and deposits in the water. The resulting moist air is directed back into the room from the top air grill.

8.2.3. Booster Fan

The internal fan of the heat pump is designed for normal pressure drop in the ductwork. A booster fan is installed at the return duct to compensate for the significant pressure loss across the nozzle that used to measure the air flow rate.

8.3. Instrumentation

8.3.1. Air Flow Rate

The air flow rate is determined from the pressure difference measured across a nozzle installed in a chamber in line with the supply air ductwork. The dimensions of the nozzle are shown in Figure 8.3. The volume flow rate can be calculated from (IP units),

$$\dot{V} = 1096\left(\sum CA\right)Y\left(\Delta P/\rho_5\right)^{0.5} \tag{8.1}$$

Where C = nozzle discharge coefficient

A = cross section area of the nozzle at designated plane, ft^2

Y = expansion factor

ΔP = pressure drop, in. H_2O

ρ = density of air, lbm/ft^3

There are four plastic tubes connected to the four sides of the chambers at both up-stream and down-stream of the nozzle. And then these four tubes are connected altogether to a manifold. Another tube goes from the manifold to the pressure transducer.

Thus, the pressure delivered from the manifold represents the average of four pressures at the four sides of the chamber. The pressure transducer is SETRA model 264. Its standard accuracy is of ±1.0% Full Scale and the standard pressure range is 0-2.5" WC, with 10 PSI overpressure. The pressure transducer has an analog output signal of 0-5 VDC of full-scale reading. The signal from the pressure transducer is received by the Fluke Data Logger and can be displayed and saved on a personal computer. The estimated uncertainty for the air flow rate measurement is ± 3.8% (Ferguson 1997).

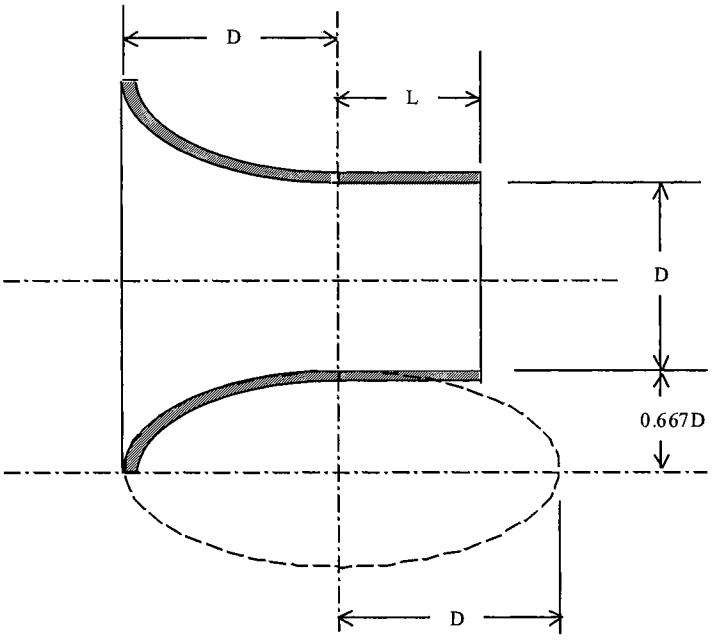

Figure 8.3. Nozzle without throat taps (L = D = 5)

8.3.2. Return and Supply Air Dry Bulb Temperatures

The return and supply air dry bulb temperatures are measured by two groups of widely used type T exposed junction thermocouples. To obtain a comparatively complete picture of the temperature through the cross-sectional area of the duct, two wired screens with nine thermocouples evenly distributed on it have been placed at the inlet and outlet of the heat pump respectively. The layout of the thermocouples on the screen is shown in Figure 8.4. Besides, the screen is installed to straighten the air flow.

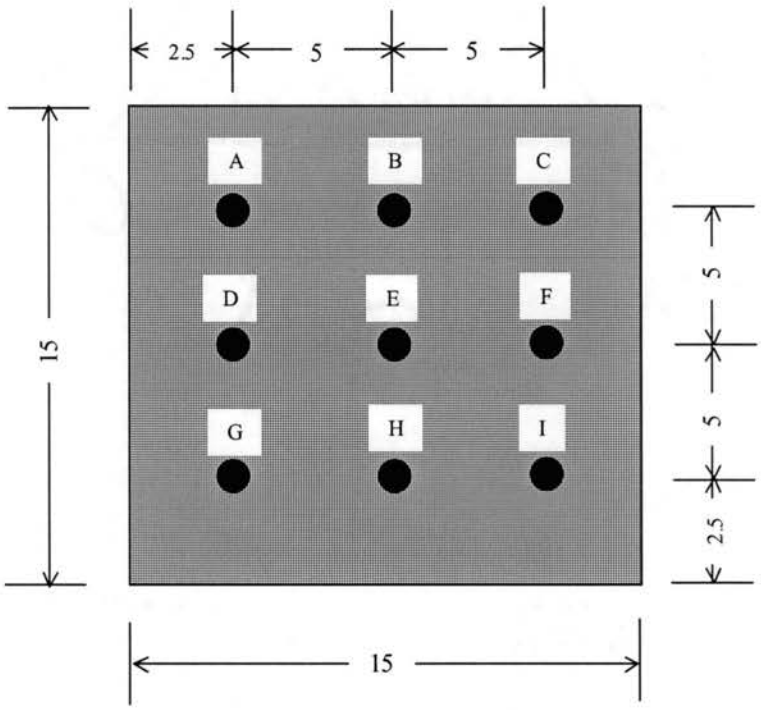

Figure 8.4. Lay-out of the thermocouples on the screen used to measure the inlet and outlet air temperatures

The nine thermocouples are connected to the data logger by individual channels. The signals received by the data logger are converted into the corresponding temperatures

respectively. Average of the temperatures measured at the nine thermocouples can be calculated automatically by the data logger, then displayed and saved on expanded channels. If the temperatures are relatively uniform throughout the cross-sectional area, the average temperature should be very close to all of the individual measurement. All the thermocouples have been calibrated and the calibration results are presented in Appendix B. The estimated uncertainty of type T thermocouple is ±0.3 °C (±0.54 °F) based on the calibration data.

8.3.3. Return Air Dew Point Temperature

It is necessary to know the humidity ratio or any related property of the moist air at the inlet of the heat pump to determine its latent cooling capacity with each inlet condition. This is accomplished in this experiment by measuring the dew point temperature of the return air. A dew point sensor is installed near the air return of the heat pump. The dew point sensor is OMEGA model RHCM-20-3-100F duct mounted type. It uses the chilled mirror technology to generate 4–20 mA (0° to 100°F or –17.78° to 37.78°C) output in accordance with the dew point temperature. According to the operator's manual, no routine calibration is needed. The output of the dew point sensor is received by the Fluke Data Logger with a 200Ω resistor connected across load terminals to obtain 0.8–4 VDC signal. The transmitter has a ±1°F (±0.56 °C) dew point accuracy as stated by the manufacturer.

8.3.4. Condensate

If the heat pump operates in cooling mode, the removal of moisture occurs when the air is cooled down below its dew point temperature. Vapor condenses on the surface of the evaporator, or direct expansion cooling coil in this case. In other words, the humidity ratio of the air leaving the heat pump will be lower than that of the air entering the heat pump. The difference between the inlet and outlet multiplied by the air flow rate is equal to the condensate. The latent heat associated with the phase change from vapor into liquid or vice versa is approximately equal to the latent cooling capacity of the heat pump. Therefore, the condensate, which usually flows in a drain pan and then is discarded, will be measured to determine the latent cooling capacity of the heat pump. This is accomplished by a portable digital scale. The scale has a capacity up to 1200 grams with precision of 0.1 gram. A ball valve has been installed close to the condensate connection of the heat pump. When the ball valve is open, the condensate will flow into a small cup sitting underneath instead of to the draining pipe. The inaccuracy of the condensate measurement would be caused mainly by the water trapped in the system, rather than the error of the scale. Thus, the uncertainty associated with the condensation measurement is estimated as the difference between two measurements during two consecutive time periods when the heat pump was operating in a steady state. The greatest difference observed is 18.2 g (0.04 lbm) for a period of fifteen minutes, which leads to an uncertainty of about 0.05 kW for the latent cooling capacity.

8.3.5. Water Flow Rate

The source side water flow rate is measured by an OMEGA FTB-105 turbine meter. The flow meter provides a 0-5 V output that runs off user supplied 10-40 V dc power. Its linear flow range is between 0.15 l/s (2.4 GPM) and 0.35 l/s (5.5 GPM) approximately. The water flow rate specified for the heat pump in this experiment falls into the range of the linear flow. The flow meter is installed between the circulation pump and the water inlet of the heat pump. There are two ball valves located up-stream and down-stream of the flow meter. And a bypass pipe runs parallel to the flow meter. In case of the mal-function or a re-calibration is needed, the flow meter can be dismounted readily. Calibration data and regression equations are given in Appendix B. Since the output signal of the flow meter is fairly sensitive to the inevitably unstable power supply, the average voltage output has been adopted in the calibration. The estimated uncertainty is ±2.8% (Wadivkar 1997).

8.3.6. Inlet and Outlet Water Temperatures

The water temperatures are measured at the inlet and outlet of the heat pump by two sheathed type T thermocouple probes. They are OMEGA model TMQSS-125G-6 quick disconnect thermocouple probes with miniature connectors. The probes are embedded into the headers of the source side heat exchanger. The analog output signal of the thermocouple probes are received by the Fluke Data Logger. Calibration data and

regression equations are given in Appendix B. The estimated uncertainty is ±0.5 °C (±0.9 °F) based on the calibration data.

8.3.7. Power Consumption

A watt transducer is put in place to measure power input to the heat pump. The watt transducer is built and calibrated by Ohio Semitronics, Inc. Since the power consumption of the heat pump is around 1,000 Watts, the current flowing into the heat pump will be less than 5 Amp. Hence, no current transformer (current sensing doughnut) is needed to scale down the current to an acceptable level of the watt transducer. The watt transducer has a sensing range of 0–300 VAC and 0–6.25 Amp, provides an analog output proportional to time-averaged instantaneous power. The output signal is calibrated to 1 mA=1kW. The signal is sent to the Fluke Data Logger and then saved by a personal computer. The watt transducer has an accuracy of ±1.0% of reading (Austin 1998).

8.3.8. Data Acquisition and Logging

The analog output signals from all of the sensors are received by a Fluke Hydra data logger. One data logger has a building block of 20 channels. The NetDAQ system can be plug into the existing network to send data directly to a PC.

Signals from all the sensors are actually analog DC voltages configured on the different output scales for each measurement. The signals sent to the data logger from each sensor are:

1–2) return/supply air dry bulb temperatures (analog voltage)

3) return air dew point temperature (analog voltage)

4) air flow rate (analog voltage)

5–6) entering/leaving water temperatures (analog voltage)

7) water flow rate (analog voltage)

8) power consumption (analog voltage)

For this experiment, an isolated network has been set up. The isolated network consists of only NetDAQ instrument and host computer. When a scan is triggered, the instrument scans the analog channels and calculates the computed channels. It stores the resulting time-stamped data in a scan record. The data logger obtains scan records from the instruments and logs the data into files of the computer. Each scan record written in the data file consists of a timestamp, values from all configured analog channels and computed channels.

8.4. Experimental Uncertainty

The uncertainties for individual measurements have been presented previously. The calculation of propagated uncertainties shall follow closely to that of the water-to-water heat pump experiment. For the sake of brevity, the methodology is not described in detail

in this chapter. The overall uncertainties are presented in Section 8.8.1 for heating mode and Section 8.9.1 for cooling mode respectively.

8.5. The Manufacturer's Catalog Data for the Heat Pump

The heat pump in this experiment is a model GT 018 made by FHP Manufacturing (http://www.fhp-mfg.com/). The catalog data are available in FHP published catalog set and the FHP web site as well. The catalog data for both the cooling mode and heating mode are re-organized and presented in both IP and SI units in Table 8.1 through Table 8.4.

Further investigation of the catalog data reveals a few doubtful data points. Based on psychrometrics analysis, the relative humidity of the air leaving the heat pump can be calculated from the dry bulb temperature, wet bulb temperature of the air entering the heat pump and corresponding total and sensible capacities given in the catalog data. The result of this calculation is also presented in Table 8.1 and Table 8.2 with the questionable points underlined. The points with relative humidity higher than 100% are physically unrealistic. To allow the parameter estimation from a rational basis, these points have been deleted from the data set.

Table 8.1. FHP GT018 Catalog Data for Cooling Mode (IP Units)

No.	Load Side						Source Side			Power (kW)
	Entering DB Temp (°F)	Entering WB Temp (°F)	Flow Rate (CFM)	Total Cooling Capacity (Mbtu/Hr)	Sensible Cooling Capacity (Mbtu/Hr)	RH_LVG	EWT (°F)	Flow Rate (GPM)	Heat Rejection (MBtu/Hr)	
1	75.0	61.0	550.0	18.3	13.9	82.63%	50.0	4.0	20.7	0.7

2	80.0	61.0	550.0	18.3	16.7	80.41%	50.0	4.0	20.7	0.7
3	85.0	61.0	550.0	18.3	18.3	67.71%	50.0	4.0	20.7	0.7
4	75.0	64.0	550.0	19.1	13.0	93.53%	50.0	4.0	21.6	0.7
5	80.0	64.0	550.0	19.1	16.5	98.69%	50.0	4.0	21.6	0.7
6	85.0	64.0	550.0	19.1	18.3	86.56%	50.0	4.0	21.6	0.7
7	75.0	67.0	550.0	20.0	12.0	102.97%	50.0	4.0	22.6	0.7
8	80.0	67.0	550.0	20.0	15.6	110.07%	50.0	4.0	22.6	0.7
9	85.0	67.0	550.0	20.0	18.0	103.61%	50.0	4.0	22.6	0.7
10	75.0	70.0	550.0	21.0	10.0	102.55%	50.0	4.0	23.6	0.8
11	80.0	70.0	550.0	21.0	13.8	110.77%	50.0	4.0	23.6	0.8
12	85.0	70.0	550.0	21.0	17.9	123.48%	50.0	4.0	23.6	0.8
13	80.0	73.0	550.0	21.9	11.8	109.65%	50.0	4.0	24.5	0.8
14	85.0	73.0	550.0	21.9	16.1	123.86%	50.0	4.0	24.5	0.8
15	75.0	61.0	550.0	17.4	13.2	80.13%	60.0	4.0	20.0	0.8
16	80.0	61.0	550.0	17.4	15.8	76.76%	60.0	4.0	20.0	0.8
17	85.0	61.0	550.0	17.4	17.4	64.10%	60.0	4.0	20.0	0.8
18	75.0	64.0	550.0	18.2	12.4	91.16%	60.0	4.0	20.9	0.8
19	80.0	64.0	550.0	18.2	15.7	94.42%	60.0	4.0	20.9	0.8
20	85.0	64.0	550.0	18.2	17.4	82.08%	60.0	4.0	20.9	0.8
21	75.0	67.0	550.0	19.1	11.4	100.86%	60.0	4.0	21.8	0.8
22	80.0	67.0	550.0	19.1	14.9	105.87%	60.0	4.0	21.8	0.8
23	85.0	67.0	550.0	19.1	17.2	98.54%	60.0	4.0	21.8	0.8
24	75.0	70.0	550.0	20.0	9.5	101.40%	60.0	4.0	22.8	0.8
25	80.0	70.0	550.0	20.0	13.1	107.57%	60.0	4.0	22.8	0.8
26	85.0	70.0	550.0	20.0	17.1	117.57%	60.0	4.0	22.8	0.8
27	80.0	73.0	550.0	20.8	11.2	107.50%	60.0	4.0	23.7	0.8
28	85.0	73.0	550.0	20.8	15.3	119.05%	60.0	4.0	23.7	0.8
29	75.0	61.0	550.0	16.5	12.5	77.66%	70.0	4.0	19.4	0.9
30	80.0	61.0	550.0	16.5	15.0	73.22%	70.0	4.0	19.4	0.9
31	85.0	61.0	550.0	16.5	16.5	60.60%	70.0	4.0	19.4	0.9
32	75.0	64.0	550.0	17.3	11.7	88.77%	70.0	4.0	20.2	0.9
33	80.0	64.0	550.0	17.3	14.9	90.24%	70.0	4.0	20.2	0.9
34	85.0	64.0	550.0	17.3	16.5	77.74%	70.0	4.0	20.2	0.9
35	75.0	67.0	550.0	18.1	10.8	98.71%	70.0	4.0	21.1	0.9
36	80.0	67.0	550.0	18.1	14.1	101.73%	70.0	4.0	21.1	0.9
37	85.0	67.0	550.0	18.1	16.3	93.60%	70.0	4.0	21.1	0.9
38	75.0	70.0	550.0	18.9	9.0	100.20%	70.0	4.0	22.0	0.9
39	80.0	70.0	550.0	18.9	12.4	104.37%	70.0	4.0	22.0	0.9
40	85.0	70.0	550.0	18.9	16.2	111.82%	70.0	4.0	22.0	0.9
41	80.0	73.0	550.0	19.7	10.6	105.30%	70.0	4.0	22.9	0.9
42	85.0	73.0	550.0	19.7	14.5	114.31%	70.0	4.0	22.9	0.9
43	75.0	61.0	550.0	14.7	11.2	73.07%	85.0	4.0	18.1	1.0
44	80.0	61.0	550.0	14.7	13.4	66.86%	85.0	4.0	18.1	1.0
45	85.0	61.0	550.0	14.7	14.7	54.42%	85.0	4.0	18.1	1.0
46	75.0	64.0	550.0	15.4	10.5	84.34%	85.0	4.0	18.9	1.0
47	80.0	64.0	550.0	15.4	13.3	82.72%	85.0	4.0	18.9	1.0
48	85.0	64.0	550.0	15.4	14.7	70.06%	85.0	4.0	18.9	1.0
49	75.0	67.0	550.0	16.1	9.6	94.66%	85.0	4.0	19.7	1.0

50	80.0	67.0	550.0	16.1	12.6	94.20%	85.0	4.0	19.7	1.0
51	85.0	67.0	550.0	16.1	14.5	84.79%	85.0	4.0	19.7	1.0
52	75.0	70.0	550.0	16.9	8.0	97.85%	85.0	4.0	20.5	1.1
53	80.0	70.0	550.0	16.9	11.1	98.46%	85.0	4.0	20.5	1.1
54	85.0	70.0	550.0	16.9	14.4	101.56%	85.0	4.0	20.5	1.1
55	80.0	73.0	550.0	17.6	9.5	101.17%	85.0	4.0	21.3	1.1
56	85.0	73.0	550.0	17.6	13.0	105.73%	85.0	4.0	21.3	1.1
57	75.0	61.0	550.0	13.3	10.1	69.69%	100.0	4.0	17.2	1.1
58	80.0	61.0	550.0	13.3	12.2	62.30%	100.0	4.0	17.2	1.1
59	85.0	61.0	550.0	13.3	13.3	50.06%	100.0	4.0	17.2	1.1
60	75.0	64.0	550.0	14.0	9.5	81.02%	100.0	4.0	17.9	1.2
61	80.0	64.0	550.0	14.0	12.0	77.32%	100.0	4.0	17.9	1.2
62	85.0	64.0	550.0	14.0	13.3	64.64%	100.0	4.0	17.9	1.2
63	75.0	67.0	550.0	14.6	8.7	91.60%	100.0	4.0	18.6	1.2
64	80.0	67.0	550.0	14.6	11.4	88.74%	100.0	4.0	18.6	1.2
65	85.0	67.0	550.0	14.6	13.2	78.55%	100.0	4.0	18.6	1.2
66	75.0	70.0	550.0	15.3	7.3	96.00%	100.0	4.0	19.4	1.2
67	80.0	70.0	550.0	15.3	10.1	94.06%	100.0	4.0	19.4	1.2
68	85.0	70.0	550.0	15.3	13.1	94.26%	100.0	4.0	19.4	1.2
69	80.0	73.0	550.0	16.0	8.6	98.03%	100.0	4.0	20.1	1.2
70	85.0	73.0	550.0	16.0	11.8	99.51%	100.0	4.0	20.1	1.2

Table 8.2. FHP GT018 Catalog Data for Cooling Mode (SI Units)

No.	Load Side						Source Side			Power (kW)
	Entering DB Temp (°C)	Entering WB Temp (°C)	Flow Rate (m^3/S)	Total Cooling Capacity (kW)	Sensible Cooling Capacity (kW)	RH_LVG	EWT (°C)	Flow Rate (L/S)	Heat Rejection (kW)	
1	23.9	16.1	0.26	5.4	4.1	82.63%	10.0	0.25	6.1	0.7
2	26.7	16.1	0.26	5.4	4.9	80.41%	10.0	0.25	6.1	0.7
3	29.4	16.1	0.26	5.4	5.4	67.71%	10.0	0.25	6.1	0.7
4	23.9	17.8	0.26	5.6	3.8	93.53%	10.0	0.25	6.3	0.7
5	26.7	17.8	0.26	5.6	4.8	98.69%	10.0	0.25	6.3	0.7
6	29.4	17.8	0.26	5.6	5.4	86.56%	10.0	0.25	6.3	0.7
7	23.9	19.4	0.26	5.9	3.5	102.97%	10.0	0.25	6.6	0.7
8	26.7	19.4	0.26	5.9	4.6	110.07%	10.0	0.25	6.6	0.7
9	29.4	19.4	0.26	5.9	5.3	103.61%	10.0	0.25	6.6	0.7
10	23.9	21.1	0.26	6.1	2.9	102.55%	10.0	0.25	6.9	0.8
11	26.7	21.1	0.26	6.1	4.0	110.77%	10.0	0.25	6.9	0.8
12	29.4	21.1	0.26	6.1	5.3	123.48%	10.0	0.25	6.9	0.8
13	26.7	22.8	0.26	6.4	3.4	109.65%	10.0	0.25	7.2	0.8
14	29.4	22.8	0.26	6.4	4.7	123.86%	10.0	0.25	7.2	0.8
15	23.9	16.1	0.26	5.1	3.9	80.13%	15.6	0.25	5.9	0.8
16	26.7	16.1	0.26	5.1	4.6	76.76%	15.6	0.25	5.9	0.8
17	29.4	16.1	0.26	5.1	5.1	64.10%	15.6	0.25	5.9	0.8
18	23.9	17.8	0.26	5.3	3.6	91.16%	15.6	0.25	6.1	0.8
19	26.7	17.8	0.26	5.3	4.6	94.42%	15.6	0.25	6.1	0.8

20	29.4	17.8	0.26	5.3	5.1	82.08%	15.6	0.25	6.1	0.8
21	23.9	19.4	0.26	5.6	3.3	100.86%	15.6	0.25	6.4	0.8
22	26.7	19.4	0.26	5.6	4.4	105.87%	15.6	0.25	6.4	0.8
23	29.4	19.4	0.26	5.6	5.0	98.54%	15.6	0.25	6.4	0.8
24	23.9	21.1	0.26	5.8	2.8	101.40%	15.6	0.25	6.7	0.8
25	26.7	21.1	0.26	5.8	3.8	107.57%	15.6	0.25	6.7	0.8
26	29.4	21.1	0.26	5.8	5.0	117.57%	15.6	0.25	6.7	0.8
27	26.7	22.8	0.26	6.1	3.3	107.50%	15.6	0.25	7.0	0.8
28	29.4	22.8	0.26	6.1	4.5	119.05%	15.6	0.25	7.0	0.8
29	23.9	16.1	0.26	4.8	3.7	77.66%	21.1	0.25	5.7	0.9
30	26.7	16.1	0.26	4.8	4.4	73.22%	21.1	0.25	5.7	0.9
31	29.4	16.1	0.26	4.8	4.8	60.60%	21.1	0.25	5.7	0.9
32	23.9	17.8	0.26	5.1	3.4	88.77%	21.1	0.25	5.9	0.9
33	26.7	17.8	0.26	5.1	4.4	90.24%	21.1	0.25	5.9	0.9
34	29.4	17.8	0.26	5.1	4.8	77.74%	21.1	0.25	5.9	0.9
35	23.9	19.4	0.26	5.3	3.2	98.71%	21.1	0.25	6.2	0.9
36	26.7	19.4	0.26	5.3	4.1	101.73%	21.1	0.25	6.2	0.9
37	29.4	19.4	0.26	5.3	4.8	93.60%	21.1	0.25	6.2	0.9
38	23.9	21.1	0.26	5.5	2.6	100.20%	21.1	0.25	6.4	0.9
39	26.7	21.1	0.26	5.5	3.6	104.37%	21.1	0.25	6.4	0.9
40	29.4	21.1	0.26	5.5	4.7	111.82%	21.1	0.25	6.4	0.9
41	26.7	22.8	0.26	5.8	3.1	105.30%	21.1	0.25	6.7	0.9
42	29.4	22.8	0.26	5.8	4.3	114.31%	21.1	0.25	6.7	0.9
43	23.9	16.1	0.26	4.3	3.3	73.07%	29.4	0.25	5.3	1.0
44	26.7	16.1	0.26	4.3	3.9	66.86%	29.4	0.25	5.3	1.0
45	29.4	16.1	0.26	4.3	4.3	54.42%	29.4	0.25	5.3	1.0
46	23.9	17.8	0.26	4.5	3.1	84.34%	29.4	0.25	5.5	1.0
47	26.7	17.8	0.26	4.5	3.9	82.72%	29.4	0.25	5.5	1.0
48	29.4	17.8	0.26	4.5	4.3	70.06%	29.4	0.25	5.5	1.0
49	23.9	19.4	0.26	4.7	2.8	94.66%	29.4	0.25	5.8	1.0
50	26.7	19.4	0.26	4.7	3.7	94.20%	29.4	0.25	5.8	1.0
51	29.4	19.4	0.26	4.7	4.3	84.79%	29.4	0.25	5.8	1.0
52	23.9	21.1	0.26	4.9	2.4	97.85%	29.4	0.25	6.0	1.1
53	26.7	21.1	0.26	4.9	3.3	98.46%	29.4	0.25	6.0	1.1
54	29.4	21.1	0.26	4.9	4.2	101.56%	29.4	0.25	6.0	1.1
55	26.7	22.8	0.26	5.2	2.8	101.17%	29.4	0.25	6.2	1.1
56	29.4	22.8	0.26	5.2	3.8	105.73%	29.4	0.25	6.2	1.1
57	23.9	16.1	0.26	3.9	3.0	69.69%	37.8	0.25	5.0	1.1
58	26.7	16.1	0.26	3.9	3.6	62.30%	37.8	0.25	5.0	1.1
59	29.4	16.1	0.26	3.9	3.9	50.06%	37.8	0.25	5.0	1.1
60	23.9	17.8	0.26	4.1	2.8	81.02%	37.8	0.25	5.2	1.2
61	26.7	17.8	0.26	4.1	3.5	77.32%	37.8	0.25	5.2	1.2
62	29.4	17.8	0.26	4.1	3.9	64.64%	37.8	0.25	5.2	1.2
63	23.9	19.4	0.26	4.3	2.6	91.60%	37.8	0.25	5.5	1.2
64	26.7	19.4	0.26	4.3	3.3	88.74%	37.8	0.25	5.5	1.2
65	29.4	19.4	0.26	4.3	3.9	78.55%	37.8	0.25	5.5	1.2
66	23.9	21.1	0.26	4.5	2.1	96.00%	37.8	0.25	5.7	1.2
67	26.7	21.1	0.26	4.5	2.9	94.06%	37.8	0.25	5.7	1.2

68	29.4	21.1	0.26	4.5	3.8	94.26%	37.8	0.25	5.7	1.2
69	26.7	22.8	0.26	4.7	2.5	98.03%	37.8	0.25	5.9	1.2
70	29.4	22.8	0.26	4.7	3.4	99.51%	37.8	0.25	5.9	1.2

Table 8.3. GT018 Catalog Data for Heating Mode (IP Units)

No.	Load Side			Source Side			Power (kW)
	Entering DB Temp (°F)	Flow Rate (CFM)	Heating Capacity (MBtuh)	EWT (°F)	Flow Rate (GPM)	Heat Absorption (MBtuh)	
1	60.0	550.0	15.9	50.0	4.0	12.5	0.986
2	70.0	550.0	15.1	50.0	4.0	11.7	1.005
3	80.0	550.0	14.1	50.0	4.0	10.6	1.026
4	60.0	550.0	17.9	60.0	4.0	14.4	1.022
5	70.0	550.0	17.0	60.0	4.0	13.5	1.041
6	80.0	550.0	15.9	60.0	4.0	12.3	1.063
7	60.0	550.0	19.9	70.0	4.0	16.3	1.056
8	70.0	550.0	18.9	70.0	4.0	15.2	1.076
9	80.0	550.0	17.7	70.0	4.0	14.0	1.098
10	60.0	550.0	22.0	80.0	4.0	18.2	1.090
11	70.0	550.0	20.8	80.0	4.0	17.0	1.111
12	80.0	550.0	19.5	80.0	4.0	15.6	1.134

Table 8.4. GT018 Catalog Data for Heating Mode (SI Units)

No.	Load Side			Source Side			Power (kW)
	Entering DB Temp (°C)	Flow Rate (m^3/S)	Heating Capacity (kW)	EWT (°C)	Flow Rate (L/S)	Heat Absorption (kW)	
1	15.6	0.26	4.7	10.0	0.25	3.7	0.986
2	21.1	0.26	4.4	10.0	0.25	3.4	1.005
3	26.7	0.26	4.1	10.0	0.25	3.1	1.026
4	15.6	0.26	5.3	15.6	0.25	4.2	1.022
5	21.1	0.26	5.0	15.6	0.25	3.9	1.041
6	26.7	0.26	4.7	15.6	0.25	3.6	1.063
7	15.6	0.26	5.8	21.1	0.25	4.8	1.056
8	21.1	0.26	5.5	21.1	0.25	4.5	1.076
9	26.7	0.26	5.2	21.1	0.25	4.1	1.098
10	15.6	0.26	6.4	26.7	0.25	5.3	1.090
11	21.1	0.26	6.1	26.7	0.25	5.0	1.111
12	26.7	0.26	5.7	26.7	0.25	4.6	1.134

8.6. Parameter Estimation and a Comparison Between Model Prediction and Catalog Data

The catalog data were used to fit coefficients for the water-to-air heat pump model described in Chapter 5, with the modifications described in Section 6.X. Since this heat pump utilizes a rotary compressor, the rotary compressor model described in Section 6.X is used. The parameters selected for the rotary compressor model have been estimated simultaneously with the other parameters and the results are shown in Table 8.5 and Table 8.6.

Table 8.5. Parameter Estimation Results for the FHP Water-to-Air Heat Pump Model GT018 – Cooling Mode

Parameter	Estimated Value
Displacement V_d	9.294×10^{-4} m^3/s (118.14 ft^3/hr)
Discharge pressure drop ΔP	65.838 kPa (9.55 psia)
Load side heat exchanger total heat transfer coefficient $(UA)_{tot}$	0.509 kW/°C (964.47 Btu/(hr-°F))
Load side heat exchanger air side heat transfer coefficient $h_{co}A_o$	0.5776 kW/°C (1094.5 Btu/(hr-°F))
Source side heat exchanger heat transfer coefficient UA_S	0.609 kW/°C (1153.96 Btu/(hr-°F))
Efficiency η	0.817
Constant part of the electro-mechanical power losses W_{loss}	0.313 kW (1067.96 Btu/hr)
Superheat ΔT_{sh}	7.528 °C (13.55 °F)

Table 8.6. Parameter Estimation Results for the FHP Water-to-Air Heat Pump Model GT018 – Heating Mode

Parameter	Estimated Value
Displacement V_d	9.419×10^{-4} m^3/s (119.73 ft^3/hr)
Discharge pressure drop ΔP	48.99 kPa (7.11 psia)
Load side heat exchanger heat transfer coefficient UA_L	0.182 kW/°C (344.86 Btu/(hr-°F))
Source side heat exchanger heat transfer coefficient UA_S	16.841kW/°C (31910.93 Btu/(hr-°F))
Efficiency η	0.404
Constant part of the electro-mechanical power losses W_{loss}	0.700 kW (2388.26 Btu/hr)
Superheat ΔT_{sh}	20.133 °C (36.24 °F)

Comparisons of the predicted and catalog total cooling capacity, sensible cooling capacity, latent cooling capacity, heat rejection and power consumption for the cooling mode are shown in Figure 8.5 through Figure 8.9. Summary of the RMS errors is presented in Table 8.7. The RMS error of latent cooling capacity is presented as the absolute deviation between model prediction and catalog data because percentage differences become meaningless when the latent capacity goes to zero.

A review of Figure 8.5 through Figure 8.9 and Table 8.7 shows that the model prediction compares favorably to the catalog data except for the latent cooling capacity. The RMS error between model prediction and catalog data for the total cooling capacity is 7.2%. Those of heat rejection and power consumption are 6.6% and 4.9% respectively. However, the errors associated with the splitting of the total cooling capacity into sensible and latent parts are noticeably much larger. The error of latent heat transfer rate depicted in Figure 8.7 shows some undesirable deviations.

As discussed in Chapter 5, the model accuracy in the split of the total cooling capacity into sensible and latent parts are not as satisfactory as that of total cooling capacity itself. What makes this case more unpredictable is the fact that the reliability of the catalog data is a little questionable as discussed previously in Section 8.5. It is not reasonable to expect that the heat pump model could furnish high accuracy prediction if no physically reasonable basis for the catalog data can be found.

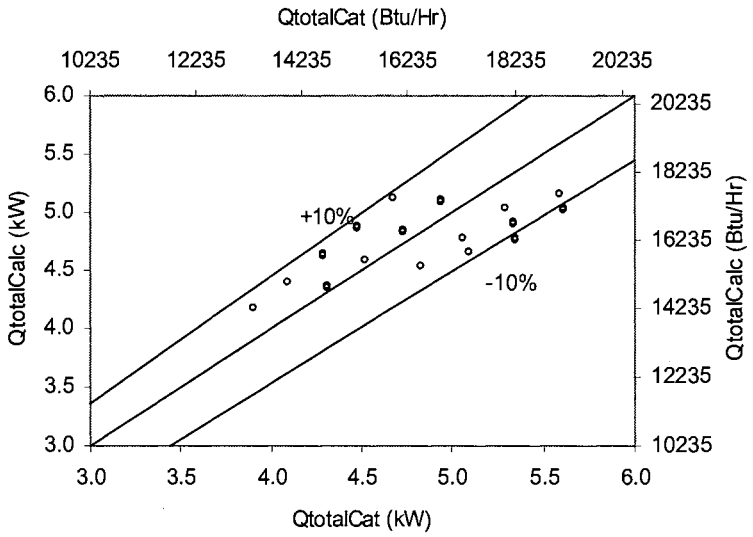

Figure 8.5. Calculated total cooling capacity vs catalog total cooling capacity

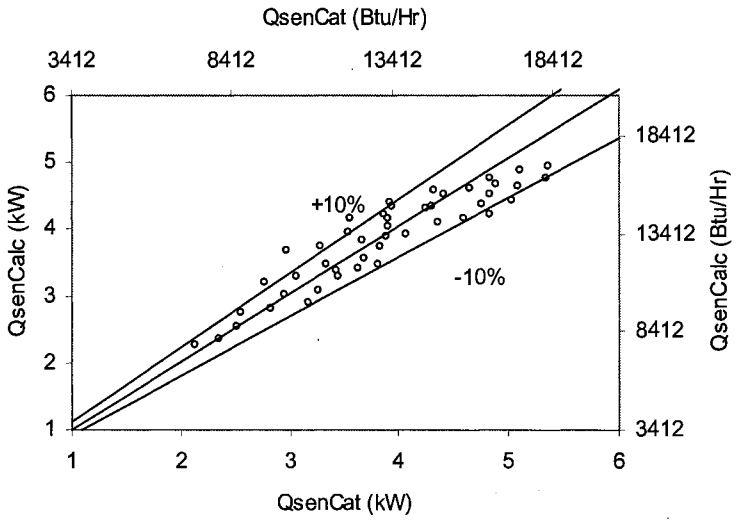

Figure 8.6. Calculated sensible cooling capacity vs catalog sensible cooling Capacity

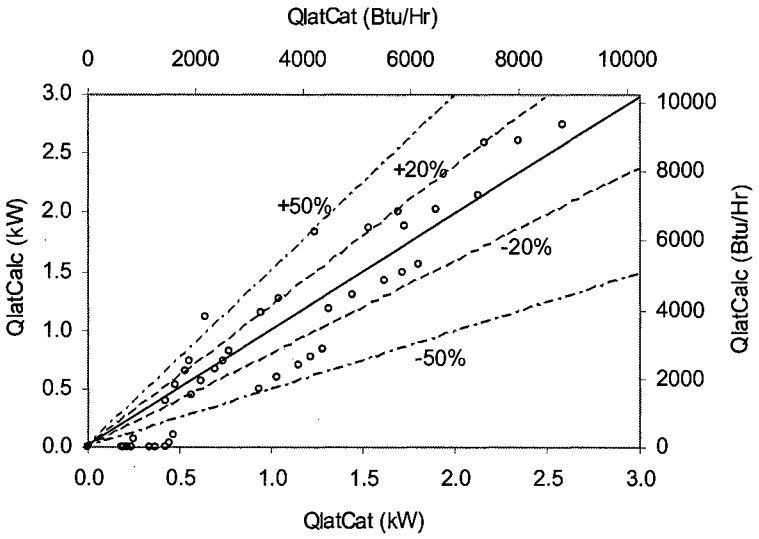

Figure 8.7. Calculated latent cooling capacity vs catalog latent cooling capacity

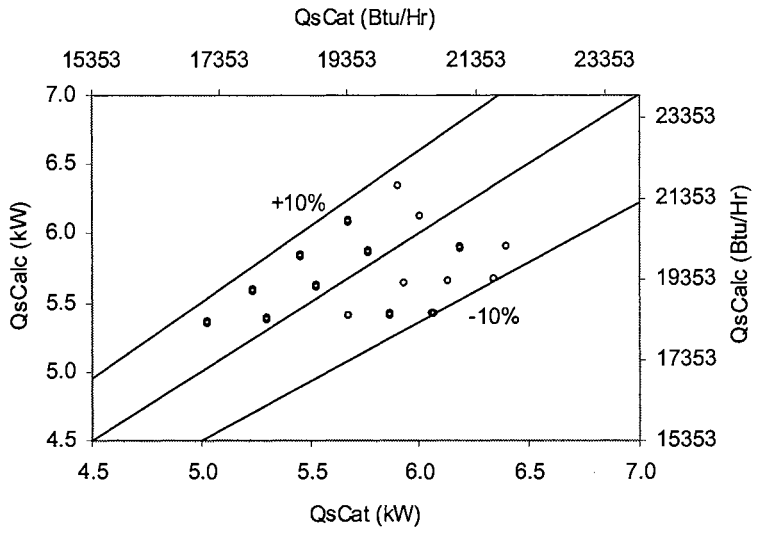

Figure 8.8. Calculated heat rejection vs catalog heat rejection

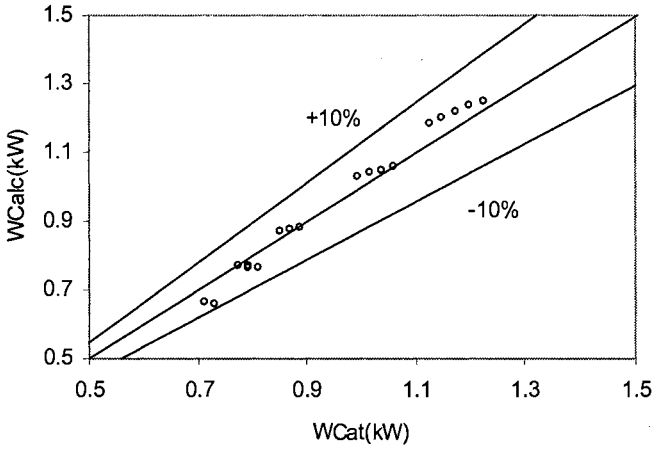

Figure 8.9. Calculated power vs catalog power

Table 8.7. RMS Errors of the Simulations for the Catalog Data

Nominal Capacity		Number of Points	RMS				
(W)	(Btu/hr)		Total	Sensible	Latent	Heat Rejection	Power
5,041 (Cooling)	17,200 (Cooling)	46	7.16 %	8.32 %	0.27 kW (921 Btu/Hr)	6.55%	4.86 %

Comparisons of the predicted and catalog heating capacity, heat extraction and power consumption for the heating mode are shown in Figure 8.10 through Figure 8.12. Summary of the RMS errors is presented in Table 8.8. A review of Figure 8.10 through Figure 8.12 and Table 8.8 shows that the model prediction compares favorably to the catalog data. The highest RMS error of about 5% is with heat extraction.

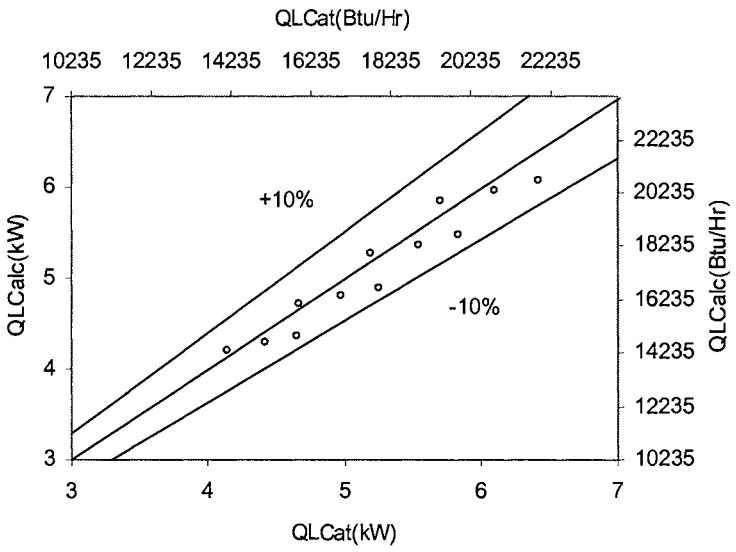

Figure 8.10. Calculated heating capacity vs catalog heating capacity

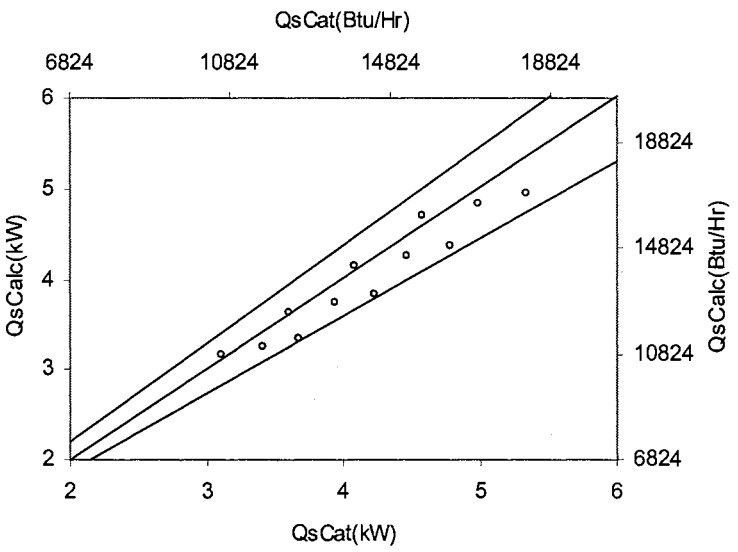

Figure 8.11. Calculated extracted heating vs catalog extracted capacity

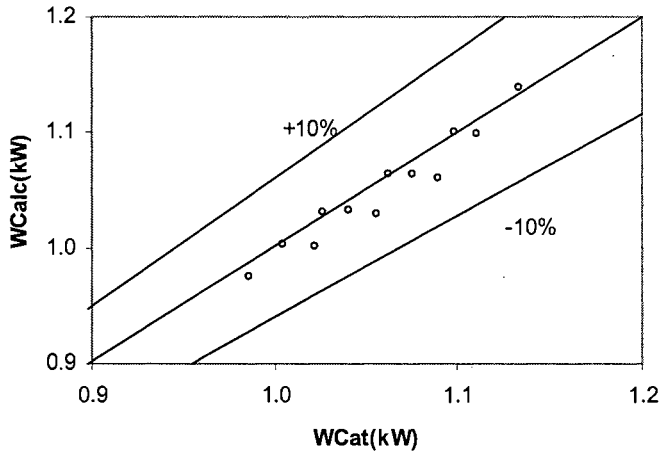

Figure 8.12. Calculated power vs catalog power

Table 8.8. RMS Errors of the Simulations for the Catalog Data

Nominal Capacity		Number of Points	RMS		
(W)	(Btu/hr)		Heating Capacity	Heat Extracted	Power
4,778 (Heating)	16,300 (Heating)	12	4.29 %	5.03 %	1.39 %

8.7. Model Uncertainty

As with the uncertainty of the water-to-water heat pump model, the uncertainty in the water-to-air heat pump model is due to two factors: 1) uncertainty in the catalog data and 2) uncertainties in the model that are reflected in the fact that the model doesn't exactly match the catalog data.

The model is based on the manufacturers' catalog data. The ARI standard allowable tolerance is ±5% from the catalog data for the water-to-air heat pump. Thus, there is also about ±5% inherent uncertainty. However, as already noted, the ARI standard only applies to one single specified point, other points may exhibit further deviation. As discussed earlier, this seems even more likely when correction factors are utilized.

In addition, the model is not able to furnish perfect fidelity to the catalog data. The uncertainty associated with parameter estimation modeling approach is discussed in Section 7.8. For the sake of brevity, only the results are described in this section. The normal distribution of the errors of the parameter estimation can be calculated based on the mean of the errors and their variance. For the catalog data in this case, the mean of errors μ, and the standard deviation σ, as an estimation of the variance for cooling mode are given in Table 8.9. Those of heating mode are given in Table 8.10.

Table 8.9. Mean of Errors and Standard Deviation (Cooling)

	μ	σ
Total Cooling Capacity	-0.065	0.363
Sensible Cooling Capacity	-0.008	0.327
Latent Cooling Capacity	-0.057	0.276
Heat Rejection	-0.07	0.395
Power	-0.005	0.041

Table 8.10. Mean of Errors and Standard Deviation (Heating)

	Heating Capacity	Heat Extraction	Power
μ	-0.149	-0.140	-0.009
σ	0.256	0.240	0.016

As with the water-to-water heat pump model, model uncertainties are given for 95% confidence. The uncertainties of total cooling capacity, sensible cooling capacity, latent cooling capacity, heat rejection and power consumption for cooling mode are presented in Table 8.11. The uncertainties of heating capacity, heat extraction and power consumption for heating mode is presented in Table 8.12. The relative uncertainties in Tables 8.11 and 8.12 are based on the typical heat transfer rates and power consumption in the experimental data.

Table 8.11. Estimated Model Uncertainty Based on Normal Distribution (Cooling Mode)

	Uncertainty	
Total Cooling Capacity	±0.71 kW (2,427 Btu/Hr)	±16.4%
Sensible Cooling Capacity	±0.64 kW (2,187 Btu/Hr)	±15.6%
Latent Cooling Capacity	±0.54 kW (1,842 Btu/Hr)	±52.4 %
Heat Extraction	±0.77 kW (2,641 Btu/Hr)	±14.7%
Power	±0.08 kW (274 Btu/Hr)	±8.9%

Table 8.12. Estimated Model Uncertainty Based on Normal Distribution (Heating Mode)

Heating Capacity	±0.50 kW (1,712 Btu/Hr)	±11.4%
Heat Extraction	±0.47 kW (1,605 Btu/Hr)	±12.7%
Power	±0.03 kW (107 Btu/Hr)	±2.76%

The errors associated with catalog data and parameter estimation model are then compounded by adding in quadrature to find the overall uncertainty of the model prediction. The total uncertainties are shown in Table 8.13 and Table 8.14. The minimum uncertainties in Table 8.13 and 8.14 are based on ±5% deviation specified in ARI standard. As already noted, the 5% deviation only applies to one single specified point, points other than the ARI standard specified point may exhibit greater deviation. It is also noted that the model uncertainty discussed above is limited to the operation ranges of inlet temperatures and flow rates in the catalog. If the inlet temperatures and flow rates are considerably away from the catalog specified range, the model uncertainty is expected to be higher than what we have estimated.

Table 8.13. Total Model Uncertainty (Cooling Mode)

Total Cooling Capacity	≥17.1%
Sensible Cooling Capacity	≥16.4%
Latent Cooling Capacity	≥52.6%
Heat Extraction	≥15.5%
Power	≥10.2%

Table 8.14. Total Model Uncertainty (Heating Mode)

Heating Capacity	≥12.4%
Heat Extraction	≥13.6%
Power	≥5.71%

8.8. Experiment in Heating Mode

Due to the limitation of this experiment apparatus, the load/source side fluid flow rates are both kept fixed at 505 CFM (23.8 L/S) and 4.3 GPM (0.27 L/S) respectively. The time-varying load/source side entering and leaving fluid temperatures and power consumption are plotted below in Figure 8.14 through Figure 8.16. The plots show that the heat pump was operating in a comparatively stable manner for about twelve hours, although the last five hours represent the most stable operation period.

8.8.1. Experimental Uncertainty

The time period between 1.00AM and 6.00AM on March 2, 2002 is selected for comparison, as the heat pump was running under fairly stable conditions. The average measured temperatures and power consumption are given in Table 8.15. The uncertainties of load side heat transfer, source side heat transfer and power consumption are calculated accordingly as discussed in the Section 7.5. The results are shown in Table 8.16.

Table 8.15. Average Temperature Differences and Power Consumption used to Compute the Relative Uncertainties

Load Side Avg ΔT	Source Side Avg ΔT	Avg Power
27.5 °F (15.3 °C)	5.9 °F (3.3 °C)	1.1 kW

Table 8.16. Experimental Uncertainties of Heat Transfer Rate and Power Consumption

Load Side Heat Transfer Rate	Source Side Heat Transfer Rate	Power
±4.7%	±21.6%	±1.0%

8.8.2. Energy Imbalance

As a check on the reasonableness of the experimental measurements, it is also desirable to assess the energy imbalance of the experimental data of the water-to-air heat pump. The measured imbalance is plotted in Figure 8.13.

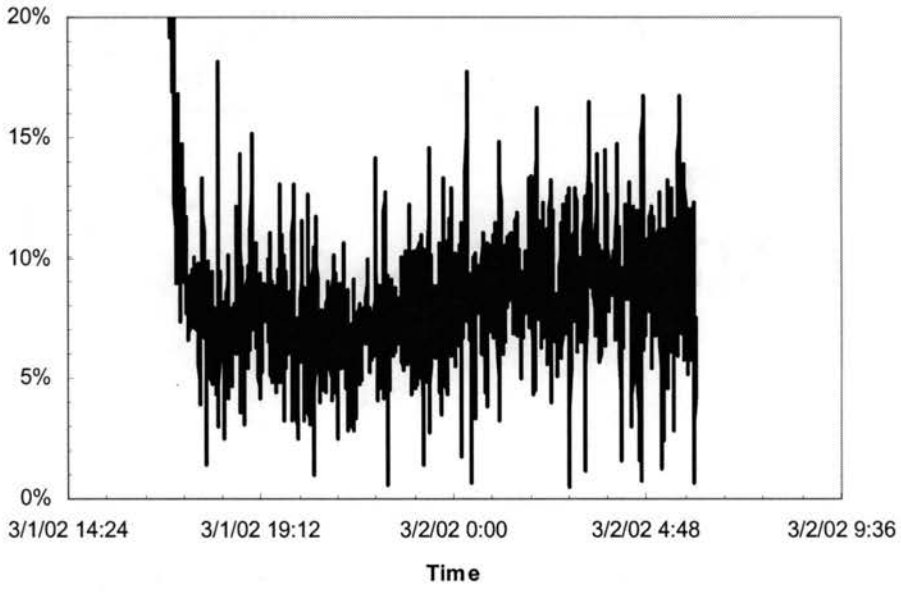

Figure 8.13. Heat pump energy balance (heating)

For the selected analysis period (1.00AM and 6.00AM), the average load side heat transfer rate, average source side heat transfer rate and average power consumption with their uncertainties are presented in Table 8.17. Table 8.17 shows that the energy

imbalance as the residual by subtracting source heat transfer and power consumption from load heat transfer is between -1.4 kW (-4,777 Btu/Hr) and 0.6 kW (2,047 Btu/Hr) when the uncertainty of the instrumentation is included. It could range from 0% to as high as 31.9% of the load side heat transfer rate. Thus, the energy imbalance plotted in Figure 8.13 for the selected time block falls into the band of estimated uncertainty.

Table 8.17. Energy Imbalance with Estimated Uncertainties

Load Heating Capacity	Source Heat of Extraction	Power Consumption
4.39 ± 0.21 kW (14978 ± 716 Btu/Hr)	3.69 ± 0.80 kW (12590 ± 2729 Btu/Hr)	1.1 ± 0.011 kW
Imbalance = Load Heating Capacity - Source Heat of Extraction - Power		
-0.4 ± 1.0 kW or -1.4 ≤ imbalance ≤ 0.6 kW (-1365 ± 3412 Btu/Hr or -4777 ≤ imbalance ≤ 2047 Btu/Hr)		

8.8.3. A Comparison of Model Prediction to the Experimental Data

The comparison between the predicted and experimental heat pump leaving fluid temperatures and power consumption for heating mode is presented in Figures 8.14-8.16. The model has been evaluated using the measured entering fluid temperatures for both load and source sides. Then the predicted leaving fluid temperatures have been compared with the measured temperatures. A review of the model predictions and measured leaving fluid temperatures/power consumption in Figure 8.14 through Figure 8.16 shows good agreement. The resulting errors in heat transfer rates are quantified below.

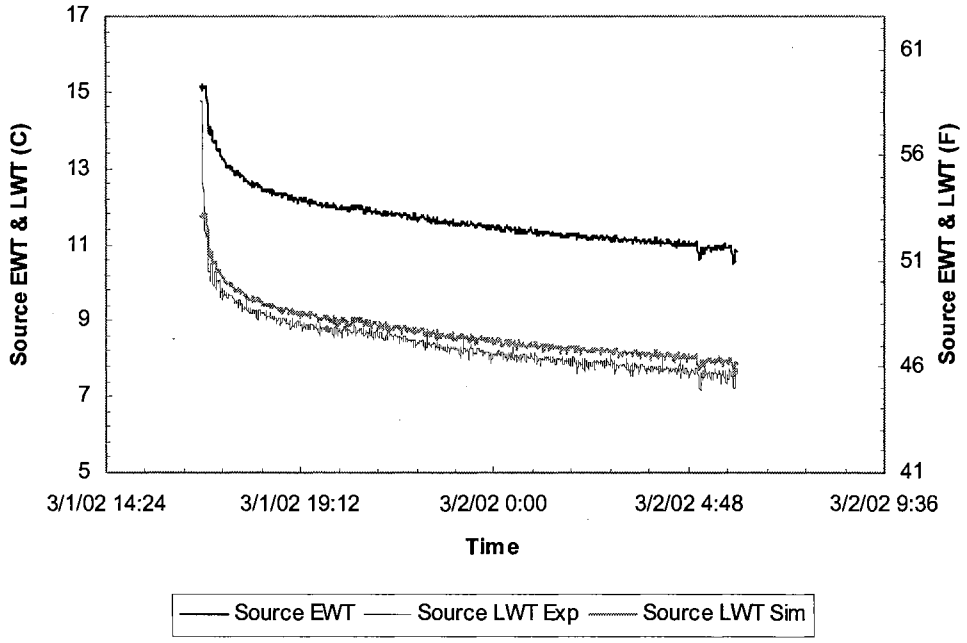

Figure 8.14. Heat pump model validation in heating mode: source side entering/leaving water temp

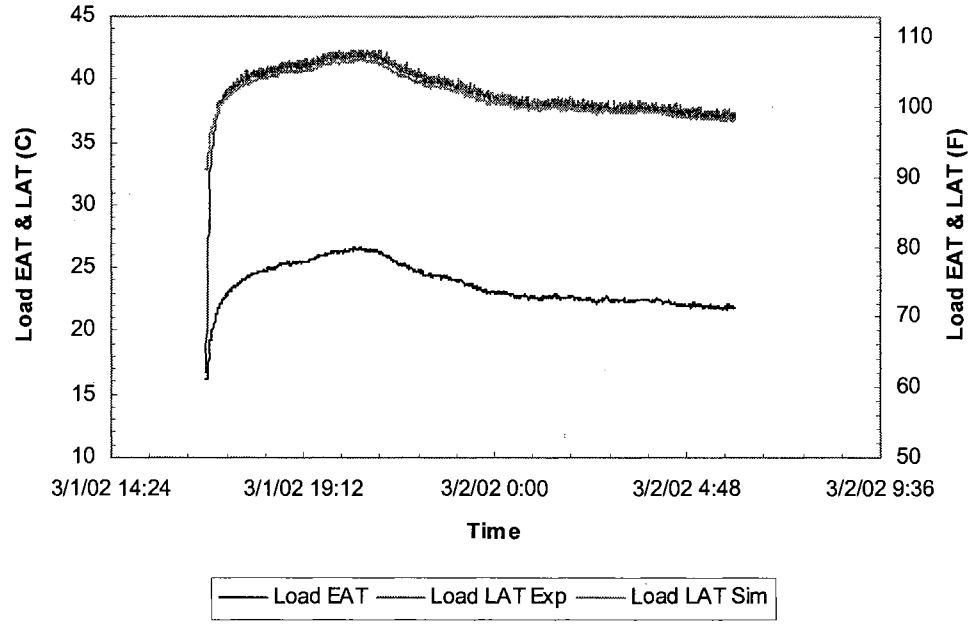

Figure 8.15. Heat pump model validation in heating mode: load side entering/leaving air temp

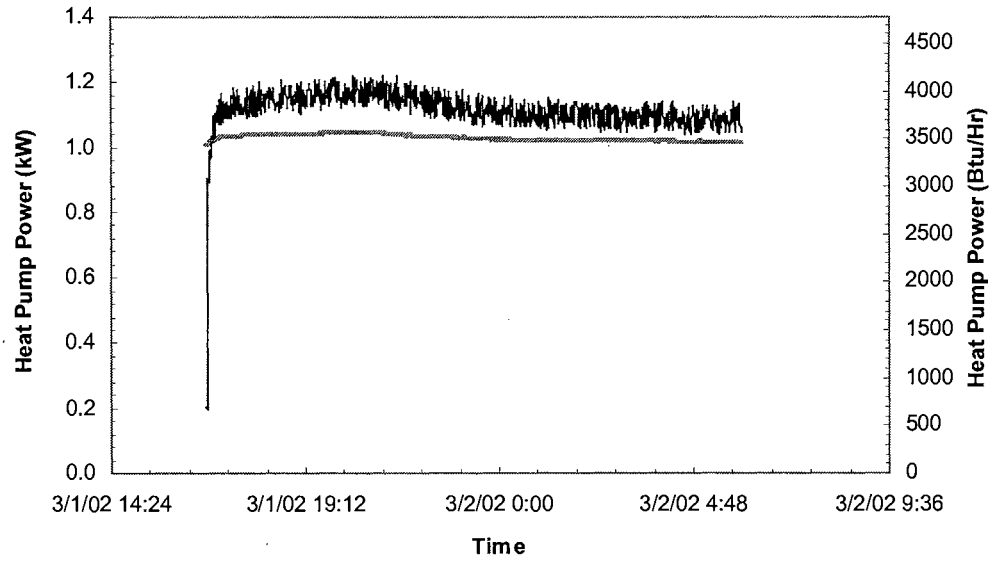

Figure 8.16. Heat pump model validation in heating mode: power consumption

As discussed in Section 8.7, the estimated uncertainties of model prediction are ±12.4% for heating capacity, ±13.6% for heat extraction, and ±5.71% for power consumption. The estimated average uncertainties of experimental data in heating mode are ±4.7% for heating capacity, ±21.6% for heat of extraction and ±1.0% for power consumption. Thus, deviations between model predictions and experimental data of ±17.1% for heating capacity, ±35.2% for heat of extraction and ±6.71% for power consumption, respectively may be accounted for by the uncertainty analysis.

Figures 8.17 through Figure 8.19 show the percentage error between model predictions and experimental measurements for the data in heating mode. Each plot also shows the amount of error that can be explained by the uncertainty analysis, if the catalog data are assumed to have an uncertainty of ±5%. For the most part, except during the initial transients, the model predictions match the experimental results within the bands

of estimated uncertainty. The errors associated with power consumption are a little larger than the estimated uncertainty during certain time period. Since the heat pump in the experiment has been used for a fairly long time, it is possible that there could be some degradation on the heat pump performance. The average load side heat transfer rate, average source side heat transfer rate and average power consumption of the model simulation and experimental data for the selected time period are given in Table 8.18.

Table 8.18. Average Heat Transfer Rates and Power Consumption

	Experiment	Model	Deviation
Load side heat transfer rate	4.39 kW (14978 Btu/Hr)	4.37 kW (14910 Btu/Hr)	-0.02 kW (68 Btu/Hr)
Source side heat transfer rate	3.69 kW (12590 Btu/Hr)	3.35 kW (11430 Btu/Hr)	-0.34 kW (1160 Btu/Hr)
Power	1.1 kW	1.0 kW	-0.1 kW

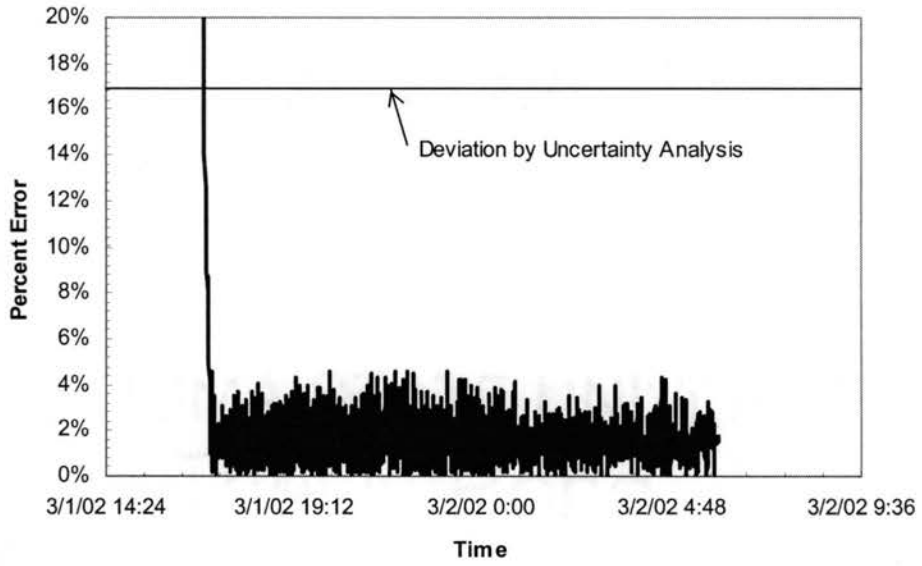

Figure 8.17. Heat pump model validation in heating mode: heating capacity percentage error between model and experiment

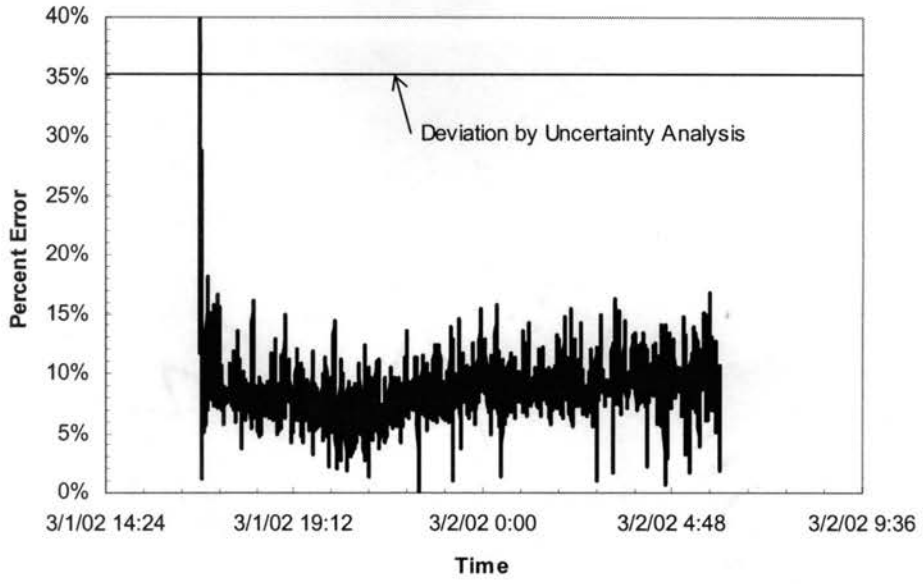

Figure 8.18. Heat pump model validation in heating mode: heating extraction percentage error between model and experiment

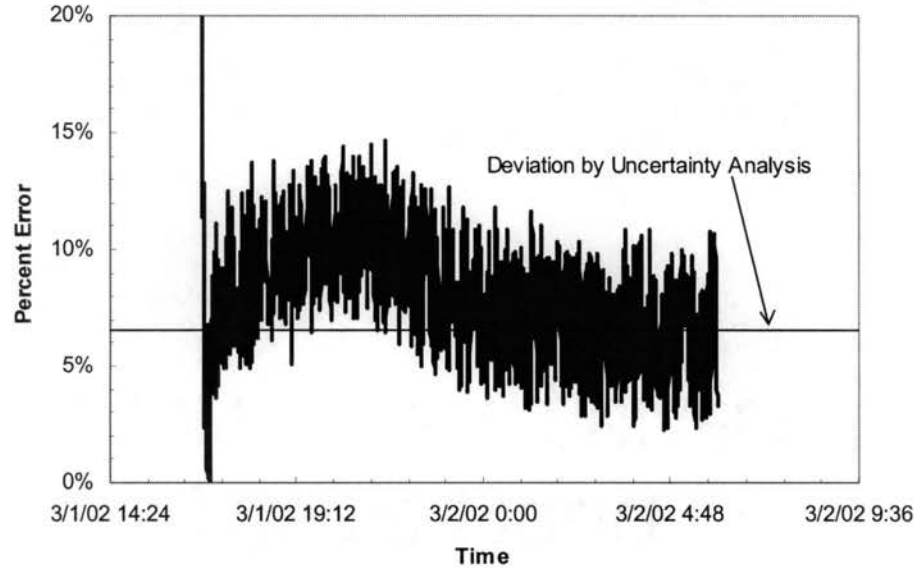

Figure 8.19. Heat pump model validation in heating mode: power consumption percentage error between model and experiment

8.9. Experiment in Cooling Mode

Since the latent cooling capacity is found by measuring the weight of the condensate, the experimental data for cooling mode cannot be collected continuously as those of the heating mode. Some time blocks with relatively stable data points were selected and the condensate from the heat pump within these selected time blocks was measured. Time-averaged values shall be used for the other measurements.

8.9.1. Experimental Uncertainty

Since the operation is switched from heating mode to cooling mode and temperature difference may change considerably, it is desirable to investigate the experimental uncertainty again. The uncertainties of load side sensible heat transfer, latent heat transfer rate and source side heat transfer are calculated accordingly as discussed in the Section 7.5. The results are shown in Table 8.19 to Table 8.21. The uncertainty of watt transducer is 1.0% of the reading.

Table 8.19. Uncertainty of Load Side Sensible Heat Transfer Rate

No	Load Side ΔT		Experimental Uncertainty
	(°C)	(°F)	
1	11.1	19.9	±5.4%
2	10.8	19.5	±5.5%
3	11.2	20.2	±5.4%
4	11.2	20.2	±5.4%
5	11.9	21.5	±5.2%
6	11.7	21.1	±5.2%
7	12.0	21.6	±5.2%

8	12.0	21.6	±5.2%
9	12.3	22.1	±5.1%
10	12.3	22.1	±5.1%
11	12.9	23.2	±5.0%
12	12.6	22.6	±5.1%
13	13.1	23.7	±5.0%
14	13.3	23.9	±5.0%
15	13.2	23.8	±5.0%

Table 8.20. Uncertainty of Latent Heat Transfer Rate

No	Latent H. T. Rate (kW)	Experimental Uncertainty
1	0.68	±7.4%
2	0.70	±7.1%
3	0.79	±6.3%
4	0.77	±6.5%
5	0.82	±6.1%
6	0.87	±5.7%
7	1.11	±4.5%
8	1.15	±4.3%
9	1.30	±3.8%
10	1.31	±3.8%
11	1.09	±4.6%
12	1.10	±4.5%
13	1.19	±4.2%
14	1.24	±4.0%
15	1.26	±4.0%

Table 8.21. Uncertainty of Source Side Heat Transfer Rate

No	Source Side ΔT		Experimental Uncertainty
	(°C)	(°F)	
1	4.0	7.1	±18.1%
2	3.9	7.1	±18.2%
3	4.1	7.4	±17.5%
4	4.1	7.3	±17.7%
5	4.3	7.7	±16.8%
6	4.3	7.7	±16.8%
7	4.6	8.2	±15.7%

8	4.6	8.3	±15.7%
9	4.7	8.5	±15.2%
10	4.8	8.6	±15.1%
11	4.7	8.5	±15.2%
12	4.7	8.5	±15.3%
13	4.9	8.8	±14.8%
14	4.9	8.8	±14.7%
15	4.9	8.9	±14.6%

8.9.2. Energy Imbalance

As a check on the reasonableness of the experimental measurements, it is also desirable to assess the energy imbalance of the data for cooling mode. The imbalance is shown in Table 8.22.

Table 8.22. Heat Pump Energy Imbalance

	Total Cooling (kW)	Sensible Cooling (kW)	Latent Cooling (kW)	Heat Rejection (kW)	Power (kW)	Imbalance
1	3.84	3.16	0.68	4.47	0.94	6.49%
2	3.80	3.10	0.70	4.44	0.95	6.53%
3	4.01	3.21	0.79	4.63	0.94	6.46%
4	3.98	3.21	0.77	4.59	0.94	6.71%
5	4.23	3.41	0.82	4.82	0.93	6.59%
6	4.23	3.36	0.87	4.83	0.93	6.40%
7	4.55	3.44	1.11	5.16	0.94	6.01%
8	4.58	3.43	1.15	5.18	0.96	6.50%
9	4.81	3.51	1.30	5.36	0.95	6.94%
10	4.82	3.51	1.31	5.37	0.96	7.09%
11	4.77	3.68	1.09	5.33	0.98	7.30%
12	4.70	3.60	1.10	5.31	0.97	6.35%
13	4.95	3.76	1.19	5.48	0.98	7.59%
14	5.03	3.79	1.24	5.52	0.98	8.15%
15	5.05	3.79	1.26	5.56	0.98	7.79%

Table 8.23 shows the effect of experimental uncertainties on the energy imbalance of point #1 in Table 8.22. The imbalance, which is the residual by subtracting load side

heat transfer and power consumption from source side heat transfer, is between -1.35 kW (-4,606 Btu/Hr) and 0.73 kW (2,491 Btu/Hr) when the uncertainty of the instrumentation is included. It could range from 0% to as high as 35.2% of the load side heat transfer rate. The energy imbalance shown in Table 8.22 falls into the band of estimated uncertainty, even without accounting for the uncertainty of the latent heat transfer.

Table 8.23. Energy Imbalance with Estimated Uncertainties (Data Point #1)

Source Heat Rejection	Load Sensible H. T.	Load Latent H. T.	Power
4.47 ± 0.81 kW (15251 ± 2764 Btu/Hr)	3.16 ± 0.17 kW (10781 ± 580 Btu/Hr)	0.68 ± 0.05 kW (2320 ± 170 Btu/Hr)	0.94 ± 0.01 kW
Imbalance = Source Heat Rejection - Load Sensible H. T. - Load Latent H. T. - Power			
-0.31 ± 1.04 kW or -1.35 ≤ imbalance ≤ 0.73 kW (-1058 ± 3548 Btu/Hr or -4606 ≤ imbalance ≤ 2491 Btu/Hr)			

8.9.3. Parameter Estimation Based on Experimental Data

It is discussed in Section 8.5 that, quite a few data points in the manufacturer's catalog are physically unrealistic. Parameter estimation and model implementation based on the catalog data shows a greater than acceptable error associated with split of total heat transfer rate. To investigate the discrepancy between the real measurements in the experiment and the catalog data, it might be helpful to use the experimental data to fit the parameters for the water-to-air heat pump model. The estimated parameter values are shown in Table 8.24. The model accuracy against the experimental measurements using the estimated parameters based on the experimental data have assessed. The results are shown in Table 8.25.

Table 8.24. Parameter Estimation Results for the FHP Water-to-Air Heat Pump Model GT018 –Cooling Mode

Parameter	Estimated Value
Displacement V_d	0.001162 m^3/s (147.71 ft^3/hr)
Discharge pressure drop ΔP	81.05 kPa (11.76 psia)
Load side heat exchanger total heat transfer coefficient $(UA)_{tot}$	0.2031 kW/°C (384.84 Btu/(hr-°F))
Load side heat exchanger air side heat transfer coefficient $h_{c,o}A_o$	0.2345 kW/°C (444.34 Btu/(hr-°F))
Source side heat exchanger heat transfer coefficient UA_S	0.7834 kW/°C (1484.41 Btu/(hr-°F))
Efficiency η	0.9677
Constant part of the electro-mechanical power losses W_{loss}	0.328 kW (1119.48 Btu/hr)
Superheat ΔT_{sh}	7.50 °C (13.51 °F)

The parameter estimation results based on experimental data presented in Table 8.24 may be compared to those based on the catalog data presented in Table 8.5. The most remarkable differences are noticed for the total heat transfer coefficient and external heat transfer coefficient of the load side heat exchanger. Given the number of physically impossible data points in the catalog data (Table 8.1 and Table 8.2), and given the relatively high RMS error in the latent cooling capacities predicted with parameters estimated from catalog data, it is not surprising that the parameters which control the sensible/latent split would be significantly different when estimated with experimental data.

The estimated parameters are used to predict the performance with the same inputs as the experimental data. Comparisons of the predicted and experimental total cooling capacity, sensible cooling capacity, latent cooling capacity, heat rejection and power consumption are shown below in Figure 8.20 through Figure 8.24. Summary of the RMS

errors is presented in Table 8.25. A review of Figure 8.20 through Figure 8.24 and Table 8.25 shows a significant improvement on the model accuracy compared to that of the catalog data, especially for the latent cooling capacity.

Table 8.25. RMS Errors of the Simulations for the Experimental Data

Number of Points	RMS				
	Total Cooling Capacity	Sensible Cooling Capacity	Latent Cooling Capacity	Heat Rejection	Power
15	1.82 %	2.23 %	0.08 kW (273 Btu/Hr)	7.80%	1.59 %

8.9.4. A Comparison of Model Prediction to the Experimental Data

The model has been evaluated using the measured entering fluid temperatures for both load and source sides as inputs. Two sets of parameters, one based on the manufacturer's catalog data and the other based on the experimental data, are used in the model to compare their influence on the model accuracy against the experimental data. The predicted leaving fluid temperatures have been compared with the measured temperatures. The model predictions against experimental data with both sets of parameters are plotted in Figures 8.20 to 8.24. A review of Figures 8.20 to 8.24 shows some significant improvement in the model accuracy with parameters based on the experimental data over the accuracy with parameters based on the catalog data. The greatest improvement is obtained for the latent cooling capacity. There may be two reasons accounting for the improvement: first, as discussed earlier, the accuracy of the catalog data is fairly questionable according to the psychrometric analysis. The model can be expected to predict incorrect results. In contrast, the experiment data show a very

reasonable behavior of the coil cooling and dehumidification, and the parameter estimation discussed above shows that a good agreement between model and experimental data can be obtained. Second, it is also possible that degradation of the heat pump performance may lead to a considerable deviation between the experimental measurements and catalog data. In this case, the model using parameters estimated with experimental data should show much better agreement with the experimental data than that using parameters estimated with catalog data.

For the heat rejection, it is noticed that the model accuracy with parameters based on experimental data is a little lower than that with parameters based on catalog data. Presumably, the fact that the experimental data are not consistent with the model assumption of no heat losses may be the cause of this phenomenon.

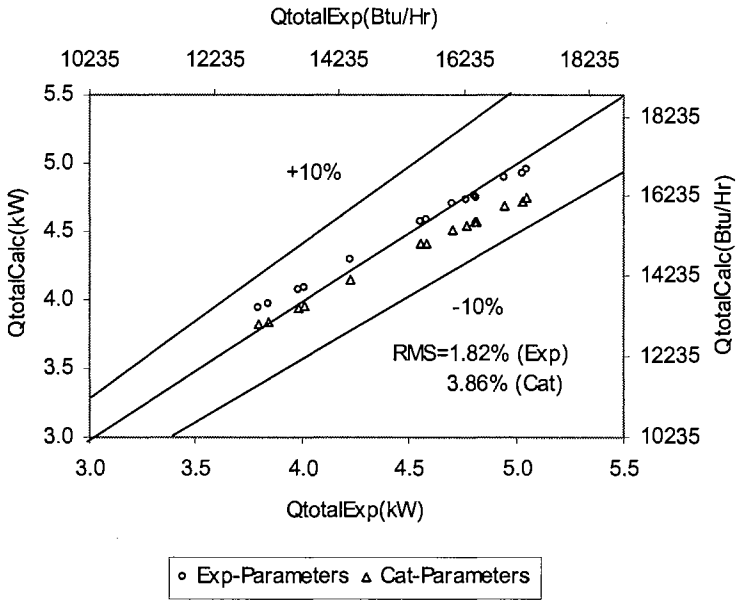

Figure 8.20. Calculated total cooling capacity vs experimental total cooling capacity

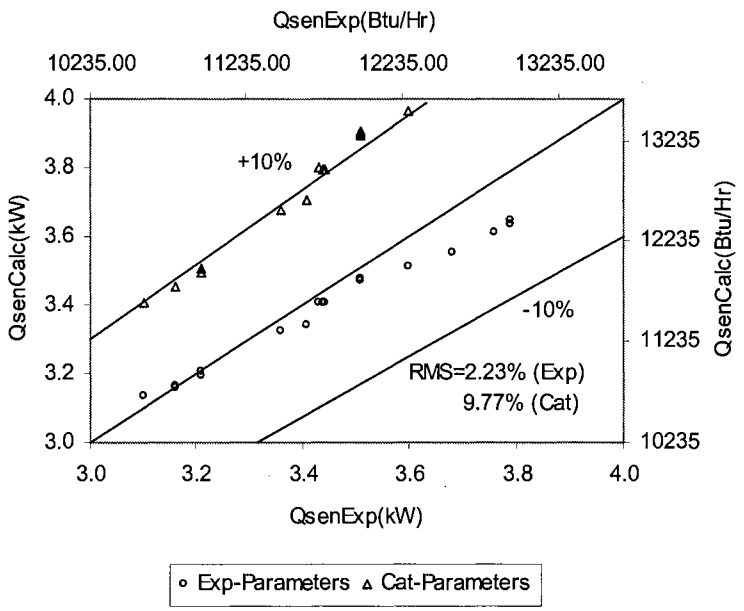

Figure 8.21. Calculated sensible cooling capacity vs experimental sensible cooling capacity

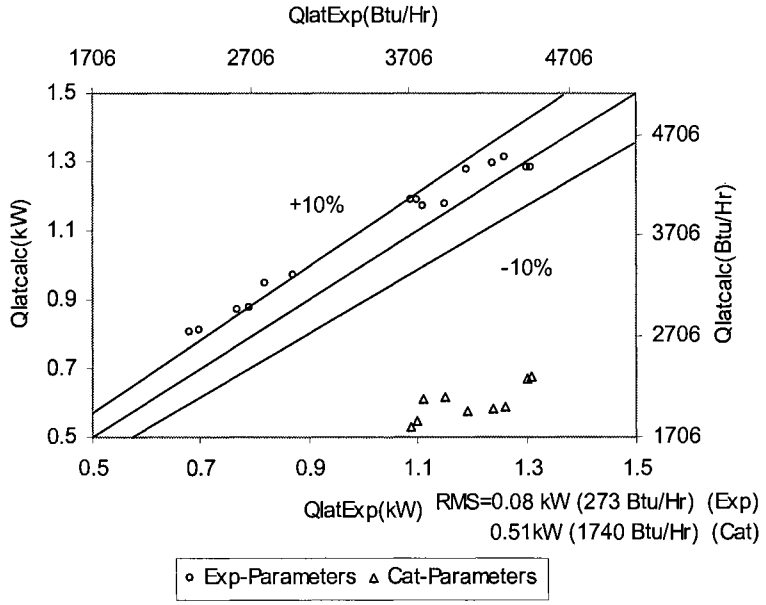

Figure 8.22. Calculated latent cooling capacity vs experimental latent cooling capacity

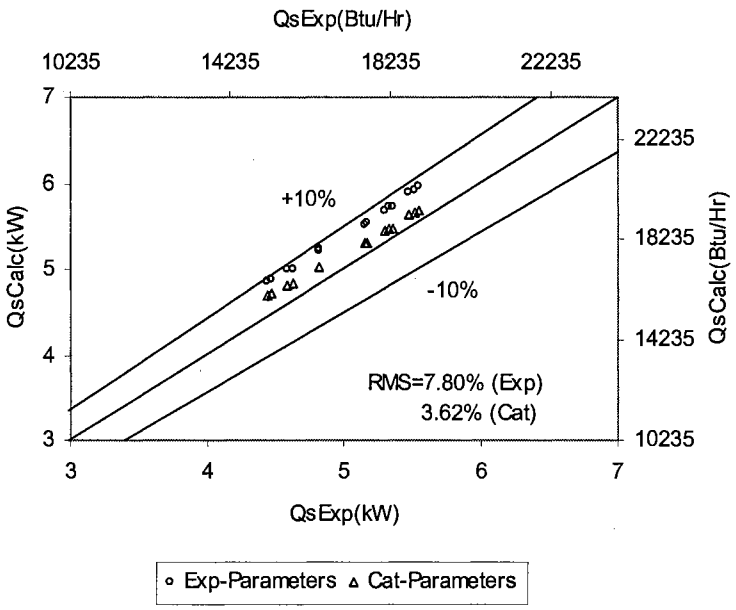

Figure 8.23. Calculated heat rejection vs experimental heat rejection

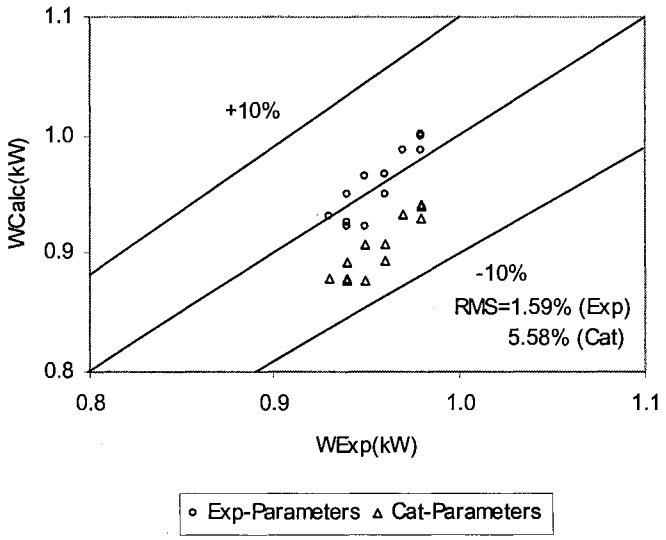

Figure 8.24. Calculated power consumption vs experimental power consumption

8.10. Summary

The model predictions match the experimental data in the bands of estimated uncertainty for sensible heat transfer, latent heat transfer, source side heat transfer and power consumption. Good agreement between the predicted and the measured heat pump heating/total cooling capacity and power consumption is obtained. Relatively high errors for sensible and latent cooling capacities have been observed. There may be three major reasons: first, the accuracy of the sensible and latent capacity as a result of the split of total cooling capacity is not as good as that of the total capacity itself in the heat pump model described in Chapter 5; secondly, the reliability of the catalog data for the sensible and latent capacities is questionable as discussed previously in this chapter, thus the parameters estimated based on the catalog data may result in a considerable error in model prediction. The model prediction accuracy could be significantly improved if a complete and reliable set of experimental data were available. Thirdly, as it is noticed in the experimental data, the latent cooling capacity constitutes about twenty percent of the total cooling capacity only. A significant change for the latent cooling capacity will result in a negligible change in the total cooling capacity. Therefore, a balance of the energy flows does not insure accurate prediction of the latent capacity.

9. Conclusions and Recommendations

9.1. Conclusions

This chapter summarizes the conclusions that can be drawn from the previous chapters. Detailed conclusions are given for each aspect of the work in chapters 4-8 respectively.

Water source heat pumps have been used in building and environmental applications for decades. During this time, modeling of water source heat pumps and other similar vapor compression heating and air-conditioning equipment has received extensive attention. Most of the heat pump models developed previously, which are classified as 'deterministic' models in this thesis, are targeted at the design of the heat pump itself for improved performance. Only the models based on pure mathematical regression (classified as 'equation-fit' models in this thesis) are widely accepted in the building energy calculation programs due to their minimal computational time and information requirements. Though 'equation-fit' models work effectively for many applications, they sometimes have low accuracy and are particularly problematic when the model is operating outside of the range of the manufacturer's catalog data. Furthermore, it is difficult to extend these models when different working fluids are used.

This study has dealt with the modeling of water-to-water and water-to-air heat pumps in building energy calculation programs to overcome the drawbacks of the 'deterministic' and 'equation-fit' models. The challenges associated with the modeling of

water source heat pumps for energy calculation are three-fold. First, HVAC system design engineers typically have access to the manufacturers' catalog data only. It is not feasible for them to obtain detailed information such as heat pump configuration, component dimensions, internal measurements and other parameters that are required by 'deterministic' models. Second, during any system simulation, it is likely that the model inputs may go beyond the catalog data. Even though the ultimate outcome is that the solution will be adjusted to bring the inputs within reasonable limits, it is helpful to have a model that does not catastrophically fail when the inputs are too high or too low. Third, the annual simulation of building and its accompanying thermal systems is normally needed for at least one year, or perhaps as long as twenty years. Each day during the simulation period could be divided into many time steps (i.e. one hour). There may be numerous loops within every time step. Thus, computational speed becomes important and detailed deterministic models would often require too much computational time. This thesis presents parameter estimation based models that address the challenges facing the HVAC system design engineer.

Chapter 4 of this thesis has described the development and validation of a parameter estimation based water-to-water heat pump model for use in energy calculation programs. A parameter estimation modeling approach has been used to simulate the performance of reciprocating vapor compression water-to-water heat pumps. The model has been validated by comparing simulation results to the manufacturers' catalog data. The model's performance compares favorably against the most detailed 'deterministic' model previously published, while not consuming an inordinate amount of computiaonal time.

As compared to 'equation-fit' models, the model retains the physically-based representation of the heat pump, which allows some extrapolation beyond the catalog data. It also perform significantly better than the equation-fit model when a limited number of operating points are utilized for estimation of parameters or coefficients.

Chapter 5 of this thesis presents the development and validation of a parameter estimation based water-to-air heat pump model. An extension of the water-to-water heat pump model, it is complicated by modeling of the direct expansion cooling coil. Difficulties were encountered in modeling partially wet coil conditions with limited information available from the catalog data. This problem has been solved by the approximation of using the fully wet coil external convection heat transfer coefficient to predict all coil conditions. The model predicts sensible and latent capacities acceptably well when the coil approaches the completely dry condition.

Chapter 6 discusses three important extensions to the heat pump models – scroll compressors, rotary compressors and glycol/water mixtures. Scroll compressors and rotary compressors are two frequently used alternatives to reciprocating compressors. A five-parameter scroll compressor model has been developed to replace the reciprocating compressor model used in the water-to-water heat pump model described in Chapter 4. For a heat pump with a scroll compressor, use of the scroll compressor model (instead of a hypothetical reciprocating compressor model) was shown to significantly improve the overall heat pump model performance. A four-parameter rotary compressor model was also developed. The rotary compressor model is, in the end, a simplified version of the

reciprocating compressor model. However, it makes more physical sense than the reciprocating compressor model if the modeled heat pump is really equipped with a rotary compressor. It requires less time for parameter estimation for rotary compressor model than reciprocating compressor model

One of the advantages of the parameter estimation based model over the equation-fit model is that it has the possibility of being adapted to different heat transfer fluids by adjusting the heat exchanger *UA*. Since antifreeze solutions are commonly used with ground source heat pump system, a procedure for adjusting the model parameters to account for the change in working fluids has been developed. This procedure was checked against correction factors provided by one manufacturer and found to give reasonable results. Further experimental work is needed to validate the procedure.

Chapter 7 and Chapter 8 in this thesis discuss the field validations of the water-to-water and water-to-air heat pump models using existing experimental apparatus. These experiments give the opportunity to compare the model prediction to the 'real' experimental measurements, other than what is available in the manufacturers' catalogs. For the water-to-water heat pump, results show that model predicts performance acceptably close for building energy calculation purposes. Generally, the percentage errors between model prediction and experimental data are less than 9% for load side heat transfer rate, 20% for the side heat transfer rate, and 12% for the power consumption. For the water-to-air heat pump experiment, the deviations are also acceptably small (less than 10%) except for the latent cooling capacity. Since quite a few physical unrealistic data

points have been found in the catalog, and relatively high RMS error is obtained in the latent cooling capacities predicted with parameters estimated from catalog data, it is not surprising that the accuracy of the model using parameter estimated from catalog data is relatively low. The model using parameters estimated with experimental data shows much better agreement with the experimental data than that using parameters estimated with catalog data. The comparison shows that the deviations between model simulation and experimental data generally fall into the bands of uncertainties associated with both model and experiment.

9.2. Recommendations

Although the models presented in this thesis are a considerable improvement in the modeling of heat pumps for building energy calculation, further work would be useful.

1. Monitored field data have been used to validate the water-to-water and water-to-air heat pump models. Unfortunately, in both of the experiments, there is no way to control the fluid flow rates and temperatures. It is not possible to get the flow rates and inlet temperatures matched with the data points published in the manufacturers' catalogs, nor is possible to vary them systematically. Therefore, a direct comparison cannot be established between the catalog data and experimental measurements. To quantify the discrepancy between catalog data and actual performance data, and to validate the model performance over a range of conditions, it is highly desirable to have a laboratory-based heat pump test loop where flow rates and inlet temperatures can be controlled on both sides

of the heat pump. A comparison between the actual measurements and the catalog data may be helpful for estimating the model uncertainty based on the deviations of the 'real' performance from the catalog data.

2. In the water-to-water heat pump experiment, no data are available for heat pump operating with pure water on both load and source sides since antifreeze has to be used for freeze protection on the load side. Although the heat pump model has been modified to meet the needs of antifreeze applications, it is still desirable to have an experiment on the heat pump operating with pure water, which may furnish more information to assess the antifreeze adjustment procedure. Again, this would be facilitated by a laboratory-based heat pump test loop.

3. In the water-to-air heat pump experiment, the latent heat transfer was measured only on the basis of the condensation rate with an uncertainty of ±0.05 kW. In a laboratory test loop, this measurement might be made more accurately and could be checked against the humidification flow rate and the change of humidity ratio in the air stream.

4. All cooling mode experiments have high sensible heat factors that range from 0.73 to 0.82. It would be desirable to obtain higher incoming humidity ratio. To achieve a high air humidity ratio, additional humidification capacity is needed. In order to test the full range of the heat pump latent cooling, it would be

desirable to have a humidification capacity of 32 gallons/day (121 kg/day). Two humidifiers, each with a rate capacity of 10 gallons/day (38 kg/day) were used. However, under actual operating conditions, they only put out about 6.3 gallons/day (24 kg/day). Therefore, some further investigation may be necessary to increase the humidification capacity to 32 gallons/day (121 kg/day).

5. While extensively used in many applications such as ground source heat pump systems for providing freeze protection, antifreeze adversely impacts heat transfer performance. The procedure developed for modeling heat pump performance with antifreeze could only be checked against some correction factors provided by one manufacturer. It would be highly desirable to validate the model with laboratory data, where varying concentration of the antifreeze could be used and where inlet conditions to both sides of the heat pump could be controlled.

6. It is also desirable to measure the internal conditions of the heat pump such as suction and discharge pressures, superheat, subcooling, condensing and evaporating temperatures. Some comparisons may be implemented between the intermediate variables of the parameter estimation based heat pump models and observed measurements. These comparisons may provide further insight into the performance of the parameter estimation based heat pump models.

7. Numerous errors in the catalog data are apparently caused by manufacturers' procedure (believed to be based on equation-fit models) for generating non-measured catalog data. As an alternative, the parameter estimation based models developed in this thesis might be utilized by manufacturers to generate the catalog data.

REFERENCES

Akers, W. W., H. A. Deans, O. K. Crosser. 1959. Condensing Heat Transfer within Horizontal Tubes. *Chemical Engineering Progress Symposium Series*, No. 29, Vol. 55, pp. 171- 176.

Allen, J. J., J. F. Hamilton. 1983. Steady-State Reciprocating Water Chiller Models. *ASHRAE Transactions*, 89(2A), pp. 398-407.

Archetti, F., G. P. Szego. 1980. Global Optimization Algorithms. *Nonlinear Optimization: Theory and Algorithm*. Boston: Birkhauser.

ARI. 1987. ARI Standard 410-87, Forced-Circulation Air-Cooling and Air-Heating Coils. Arlington, VA: Air-Conditioning and Refrigeration Institute.

ARI. 1998. ARI Standard 320-98, Water-Source Heat Pumps. Arlington, VA: Air-Conditioning and Refrigeration Institute.

ARI. 1999. ARI Standard 540-99, Positive Displacement Refrigerant Compressors and Compressor Units. Arlington, VA: Air-Conditioning and Refrigeration Institute.

ASHRAE. 2000 ASHRAE Handbook – 2000 HVAC Systems and Equipment. Atlanta: American Society of Heating, Refrigerating, and Air-Conditioning Engineering, Inc.

ASHRAE. 1996. *Psychrometrics: Theory and Practice*. Atlanta: American Society of Heating, Refrigerating, and Air-Conditioning Engineering, Inc.

ASHRAE. 2001. ASHRAE Handbook – 2001 Fundamentals. Atlanta: American Society of Heating, Refrigerating, and Air-Conditioning Engineering, Inc.

Austin III, W.A. 1998. Development of an In Situ System for Measuring Ground Thermal Properties. M.S. Thesis.

Barratt, T. R., E. J. Murzinski. 1987. Rotary Compressor Design Evolution for Heat Pump Application. *ASHRAE Transactions*, 93(1), pp. 1139-1146.

Born, D. W. Inhibited Glycols for Corrosion and Freeze Protection in Water-Based Heating and Cooling Systems. *ASHRAE Transactions*, 95(2), pp. 969-975.

Bourdouxhe, J-P H., M. Grodent, J J. Lebrun, C. Saavedra, K. L. Silva. 1994. A Toolkit for Primary HVAC System Energy Calculation—Part 2: Reciprocating Chiller Models. *ASHRAE Transactions*, 100(2), pp. 774-786.

Bourdouxhe J P, M. Grodent, J. Lebrun. 1998. *Reference Guide for Dynamic Models of HVAC Equipment*. Atlanta: ASHRAE.

Braun, J. E., S.A. Klein, J. W. Mitchell. 1989. Effectiveness Models for Cooling Towers and Cooling Coils. *ASHRAE Transactions*, 95(2), pp. 164-174.

Brandemuehl, M. J., S. Gabel, I. Andresen. 1993. *HVAC 2 Toolkit : a Toolkit for Secondary HVAC System Energy Calculations*. Atlanta: ASHRAE.

Brown, J. S., P. A. Domanski. 2000. Semi-Theoretical Simulation Model for a Transcritical Carbon Dioxide Mobile A/C System. *SAE 2000 World Congress. Proceedings. Society of Automotive Engineers, Inc. (ASE). SAE Technical Paper Series 2000-01-0985. March 6-9, 2000, Detroit, MI.* Society of Automotive Engineers, Inc., Warrendale, PA.

Bush, J. and J. Elson. 1988. Scroll Compressor Design Criteria for Residential Air Conditioning and Heat Pump Applications. *Proceedings of the 1988 International Compressor Engineering Conference (1), Office of Publications, Purdue University, West Lafayette, IN.*, pp. 83-97.

Cane, R. L. D., D. A. Forgas. 1991. Modeling of Ground-Source Heat Pump Performance. *ASHRAE Transactions*, 97(1), pp. 909-925.

Cecchini, C., D. Marchal. 1991. A Simulation Model of Refrigerant and Air-conditioning Equipment Based On Experimental Data. *ASHRAE Transactions*, 97(2), pp. 388-393.

Chen Y., N. Halm, E. A. Groll, J. E. Braun. 2000. A Comprehensive Model of Scroll Compressors, Part I: Compression Process Modeling. *Proceedings of the 2000 International Compressor Engineering Conference at Purdue. Purdue University, West Lafayette, IN.*, pp. 715-724.

Chen Y., N. Halm, E. A. Groll, J. E. Braun. 2000. A Comprehensive Model of Scroll Compressors, Part II: Overall Scroll Compressor Modeling. *Proceedings of the 2000 International Compressor Engineering Conference at Purdue. Purdue University, West Lafayette, IN.*, pp. 725-734.

Chapman, A. J. 1974. *Heat Transfer. Third Edition*. New York: Macmillan Publishing Co., Inc.

Chapra, S. C., R. P. Canale. 1985. *Numerical Methods for Engineers: with Personal Computer Applications*. New York: McGraw-Hill.

Chi, J., D. Didion. 1982. A Simulation Model of the Transient Performance of a Heat Pump. *International Journal of Refrigeration*, 5(3), pp. 176-184.

Chu, I., T. Shiga, K. Ishijima, M. Sakaino. 1978. Analysis of the Rolling-Piston-Type Rotary Compressor. *Proceedings of 1978 Purdue University Compressor Technology Conference*, pp. 219-225.

Chwalowski, M., D. A. Didion, P. A. Domanski. 1989. Verification of Evaporator Computer Models and Analysis of Performance of an Evaporator Coil. *ASHRAE Transactions*, 95(1), pp. 1229-1236.

Clark, D. R. 1985. Dynamic Model for HVAC System Components. *ASHRAE Transactions*, 91(1B), pp. 737-751.

Crawford, R. R., D. B. Shirey. 1987. Dynamic Modeling of a Residential Heat Pump from Actual System Performance Data. *ASHRAE Transactions*, 93(2), pp. 1179-1190.

Dabiri, A. E., C. K. Rice. 1981. A Compressor Simulation Model with Corrections for the Level of Suction Gas Superheat. *ASHRAE Transactions*, 87(2), pp. 771-780.

Dabiri, A. E., 1982. A Steady State Computer Simulation Model for Air-to-Air Heat Pumps. *ASHRAE Transactions*, 88(2), pp. 973-987.

Damasceno, G. S., V. W. Goldschmidt. 1987. An Update of the August 1986 User's Guide of the Heat Pump Performance Model HN. Ray W. Herrick Laboratories Report No. HL 87-37p, Purdue University, West Lafayette, IN.

Damasceno, G. S., S. P. Rooke, V. W. Goldschmidt. 1990. Comparison of Three Steady-state Heat Pump Computer Models. *ASHRAE Transactions*, 96(2), pp. 191-204.

DeRoo, A. M. L., B. W. Lee. 1997. Inhibited Ethylene and Propylene Glycols for Corrosion and Freeze Protection in Water-Based HVAC Systems. *ASHRAE Transactions*, 103(2), pp. 446-455.

Didion, D. A. and W. J. Mulroy. 1983. A laboratory investigation of refrigerant migration in a split-unit air conditioner. NBSIR 83-2756. Washington, D.C.: National Bureau of Standards.

Domanski, P. A., D. A. Didion. 1983. Computer Modeling of the Vapor Compression Cycle with Constant Flow Area Expansion Device. Report No. NBS BSS 155, NBS.

Domanski, P. A., D. A. Didion. 1984. Mathematical Model of an Air-to-Air Heat Pump Equipped with a Capillary Tube. *International Journal of Refrigeration*, 7(4), pp. 249-255.

Domanski, P. A., D. A. Didion. 1985. Simulation of a Heat Pump Operating with a Nonazeotropic Mixture. *ASHRAE Transactions*, 91(2B), pp. 1368-1382.

Domanski, P. A. 1991. Simulation of an Evaporator with Nonuniform One-Dimensional Air Distribution. *ASHRAE Transactions*, 97(1), pp. 793-802.

Domanski, P. A., M. O. McLinden. 1992. A simplified cycle simulation model for the performance rating of refrigerants and refrigerant mixtures. *International Journal of Refrigeration*, 15(2): 81-88.

Domanski, P. A., W. J. Mulroy, D. A. Didion. 1994. Glide Matching With Binary and Ternary Zeotropic Refrigerant Mixtures. Part 2. A Computer Simulation. *International Journal of Refrigeration*, 17(4), pp. 226-230.

Domanski, P. A. 2000. Cycle-11_UA Simulation Model. *National Institute of Standards and Technology*, http://www.bfrl.nist.gov/863/Cycle-11.pdf.

Edwards, J. A., P. Safemazandarani, R. R. Johnson, Y. Mohammadzadeh. 1988. Performance Test of a Direct Expansion Heat Pump System. *ASHRAE Transactions*, 94(1), pp. 318-329.

Elmahdy, A. H., G. P. Mitalas. 1977. A Simple Model for Cooling and Dehumidifying Coils for Use in Calculating Energy Requirements for Buildings. *ASHRAE Transactions*, 83(2), pp. 103-116.

Elson, J., G. Hundy, K. Monnier. 1990. Scroll Compressor Design and Application Characteristics for Air Conditioning, Heat Pumps, and Refrigeration Applications. *Proceedings of the Institute of Refrigeration (London)*, 2.1-2.10.

Etemad, S., J. Nieter. 1989. Design Optimization of the Scroll Compressor. *International Journal of Refrigeration*, 12(5), pp. 146-150.

Ferguson, J. 1997. A Full Scale Room for the Experimental Study of Interior Building Convective Heat Transfer. M.S. Thesis.

Fischer, S. K., C. K. Rice. 1981. A Steady-state Computer Design Model for Air-to-Air Heat Pumps. Report No. ORNL/CON-80. Oak Ridge, TN: Oak Ridge National Laboratory.

Fischer, S. K., C. K. Rice. 1983. The Oak Ridge Heat Pump Models: 1. A Steady-state Computer Design Model for Air-to-Air Heat Pumps. Report No. ORNL/CON-80/R1. Oak Ridge, TN: Oak Ridge National Laboratory.

Fischer, S. K., C. K. Rice, W. L. Jackson. 1988. The Oak Ridge Heat Pump Design Model: Mark III Version Program Documentation. Report No. ORNL/TM-10192. Oak Ridge, TN: Oak Ridge National Laboratory.

Flake, B. A., J. W. Mitchell, W. A. Beckman. 1997. Parameter Estimation for Multiresponse Nonlinear Chilled-Water Plant Models. *ASHRAE Transactions*, 103(1), pp. 470-485.

Forsyth, B. I., R. W. Besant. 1988. The Performance of a Run-Around Heat Recovery System using Aqueous Glycol as a Coupling Liquid. *ASHRAE Transactions*, 94(2), pp. 532-545.

Fukushima T., K. Takao, K. Kawashima. 1987. Mathematical Model of a Rotary Vane Type Compressor. *ASHRAE Transactions*, 93(2), pp. 228-246.

Ganesh, R. 1987. A microcomputer model for the performance simulation of cooling and heating coils with application to HVAC systems. Ph.D. Dissertation, Department of Mechanical and Aerospace Engineering, University of Missouri-Rolla.

Ganesh, R., H. J. Sauer, Jr., R. H. Howell. 1989. Part-Load Simulations of Simple Air-Conditioning Systems Using a New Coil Model. *ASHRAE Transactions*, 95(1), pp 300-311.

Godwin, D. S. 1998. Latent Capacity of Unitary Equipment. *ASHRAE Transactions*, 104(2), pp 763-772.

Goodman,W. 1938, 1939. Performance of Coils for Dehumidifying Air. *Heating, Piping and Air Conditioning*. Vol. 10 (1938) and Vol. 11 (1939).

Gordon, J. M. and K. C. Ng. 1994. Thermodynamic Modeling of Reciprocating Chillers. *Journal of Applied Physics*, 75(6), pp 2769-74.

Gordon, J. M. and K. C. Ng. 1995. Predictive and Diagnostic Aspects of a Universal Thermodynamic Model for Chillers. *International Journal of Heat and Mass Transfer*, 38(5), pp 807-818.

Gravesen, J., Christian Henriksen. 2001. The Geometry of the Scroll Compressor. *Society of Industrial and Applied Mathematics*, 43(1), pp. 113-126.

Greyvenstein, G. P. 1988. A Computer Simulation Model for the Design and Optimization of Heat Pumps and Refrigeration Systems. *South African Journal of Science*, 84(June), pp 494-502.

Gyberg, F., S. Nissen. 1984. A Simulation Model for Fixed Vane Rotary Compressor using Real Gas Properties. *Proceedings of the Purdue Compressor Technology Conference, Proceedings of the 1984 International Compressor Engineering Conference at Purdue*, pp. 33-39.

Hamilton, J. F., J. L. Miller. 1990. A Simulation Program for Modeling an Air-conditioning System. *ASHRAE Transactions*, 96(1), pp. 213-221.

Hassab, M. A., W. A. Kamal, 1988. An Improved Model for the Design of Plain Tube Air cooling and dehumidifying coils. *ASHRAE Transactions*, 94(2), pp. 792-812.

Henderson, H. I., K. Rengarajan. 1996. A Model to Predict the Latent Capacity of Air Conditioners and Heat Pumps at Part-Load Conditions with Constant Fan Operation. *ASHRAE Transactions*, 102(1), pp. 266-274.

Hirsch, S. R. 1973. On the Relation of Compressor Theory to Practice. *ASHRAE Journal*, Vol. 15, pp. 37-41.

Holloway, B. 2000. Personal Communications.

Holzapfel, K., V. Bruno, V. Recchi. 1992. Experimental Analysis of a Water-to-Water Heat Pump with Variable Speed Scroll Compressor. *Proceedings of the International Compressor Engineering Conference/Proceedings of the 1992 International Compressor Engineering Conference at Purdue.* pp. 1529-1538.

Huang, Y. M. 1999. The Performance and Fluid Properties of a Rotary Compressor. *American Society of Mechanical Engineer, Pressure Vessels and Piping Division (Publication) PVP*, V396. pp. 99-104.

Ikegawa, M., E. Sato, K. Tojo, A. Arai, N. Arai. 1984. Scroll Compressor with Self-adjusting Back-pressure Mechanism. *ASHRAE Transactions*, 90(2A), pp. 314-326.

Kamal, W. A., M. A. Hassab. 1986. Heat and Mass Transfer Characteristics of Air Cooling and dehumidifying Coils. *Heat Transfer in Air Conditioning and Refrigeration Equipment. ASME Publication* HTD-Vol. 57, No. 1, pp. 13-80

Kavanaugh S. P., J. G. Woodhouse, J. R. Carter. 1991. Test Results of Water-to-Air Heat Pumps with High Cooling Efficiency for Ground-Coupled Applications. *ASHRAE Transactions*, 97(1), pp. 895-901.

Kays, W. M., A. L. London. 1984. Compact Heat Exchangers. 3rd Edition. New York: McGraw-Hill.

Kern, D. Q. 1950. Process Heat Transfer. New York: McGraw-Hill.

Khan, A. Y. 1994. Heat and Mass Transfer Performance Analysis of Cooling Coils at Part-Load Operating Conditions. *ASHRAE Transactions*, 100(1), pp. 54-62.

Kondo, M., M. Ozu, M. Watanabe. 1975. New High-Performance Rotary Compressors. *Toshiba Review (International Edition)*, 100(11-12), pp. 93-96.

Krakow, K. I., S. Lin. 1983. A Computer Model for the Simulation of Multiple Source Heat Pump Performance. *ASHRAE Transactions*, 89(2A), pp. 590-600.

Krause, P. E., C. W. Bullard. 1996. Cycling and Quasi-Steady Behavior of a Refrigerator. *ASHRAE Transactions*, 102(1), pp. 1061-1070.

Kuester, J., J. H. Mize. 1973. *Optimization Techniques With Fortran*. Chapter 9. New York: McGraw-Hill.

LeBrun, J., J.-P. Bourdouxhe, M. Grodent. 1999. *HVAC 1 Toolkit : a Toolkit for Primary HVAC System Energy Calculations*. Atlanta: ASHRAE.

Lehmkuhl, H. F. 1967. Rotary Compressor 1 to 25 Horsepower Design and Performance. *ASHRAE Publication: Positive Displacement Compressor*, pp. 20-26.

LeRoy, J. T. 1997. Capacity and Power Demand of Unitary Air Conditioners and Heat Pumps under Extreme Temperature and Humidity Conditions. Master's Thesis, Ray W. Herrick Laboratories, Purdue University, West Lafayette, Ind.

LeRoy, J. T., E. A. Groll, J. E. Braun. 1998. Computer Model Predictions of Dehumidification Performance of Unitary Air Conditioners and Heat Pumps Under Extreme Operating Conditions. *ASHRAE Transactions*, 104(2), pp. 773-788.

MacArthur, J. W. 1983. Theoretical Analysis of the Dynamic Interactions of Vapor Compression Heat Pumps. *Energy Conversion and Management*, 24(10), pp. 49-66.

MacArthur, J. W. 1984. Transient Heat Pump Behaviour: A Theoretical Investigation. *International Journal of Refrigeration*, 7(2), pp. 123-132.

MacArthur, J. W. 1984. Analytical Representation of the Transient Energy Interactions in vapor Compression Heat Pumps. *ASHRAE Transactions*, 90(1B), pp. 982-996.

Marques, M. E., P. A. Domanski. 1998. Potential Coefficient of Performance Improvements Due to Glide Matching With R-470C. *International Refrigeration Conference at Purdue, 7th. Proceedings. July 14-17, 1998.* West Lafayette, IN.

McClave, J. T., F. H. Dietrich II. 1994. *Statistics*. Macmillan College Publishing Company, Inc.

McElgin, J., D. C. Wiley. 1940. Calculation of Coil Surface Areas for Air Cooling and Dehumidification. *Heating, Piping and Air Conditioning*, 12(1), pp. 195-201.

McLinden, M. O., R. Radermacher. 1987. Methods for Comparing the Performance of Pure and Mixed Refrigerants in the Vapor Compression Cycle. *International Journal of Refrigeration*, Vol. 10, pp. 318-329.

McQuiston, F. C. 1975. Fin Efficiency with Combined Heat and Mass Transfer. *ASHRAE Transactions*, 81(1), pp. 350-355.

McQuiston, F. C. 1978. Heat, Mass and Momentum Transfer Data for Five Plate-Fin-Tube Heat Transfer Surfaces. ASHRAE Transactions, 84(1), pp. 266-293.

McQuiston, F. C., J. D. Parker, J. D. Spitler. 2001. *Heating, Ventilating, and Air Conditioning Analysis and Design*. New York : Wiley.

Merkel, F. 1925. "Verdunstungskuhlung." VDI Forschungsarbeiten, No. 275, Berlin.

Miller, W. A. 1985. The laboratory Evaluation of the Heating Mode Part-Load Operation of an Air-to-Air Heat Pump. *ASHRAE Transactions*, 91(2B), pp. 524-530.

Mirth, D. R., S. Ramadhyani, D. C. Hittle. 1993. Thermal Performance of Chilled-Water Cooling Coils Operating at Low Water Velocities. *ASHRAE Transactions*, 99(1), pp. 43-53.

Mirth, D. R., S. Ramadhyani, D. C. Hittle. 1993. Comparison of Methods of Modeling the Air-Side Heat and Mass Transfer in Chilled-Water Cooling Coils. *ASHRAE Transactions*, 99(2), pp. 285-299.

Morishita, E., M. Sugihara, T. Inaba, T. Nakamura. 1984. Scroll Compressor Analytical Model. *Proceedings of the Purdue Compressor Technology Conference/Proceedings of the 1984 International Compressor Engineering Conference – At Purdue.* pp. 487-495.

Morisot, O., D. Marchio, P. Stabat. 2002. Simplified Model for the Operation of Chilled Water Cooling Coils Under NonNominal Conditions. *International Journal of HVAC&R*, 8(2), pp. 135-158.

Morissette, B. J. D. Sheppard. 1993. Evaluation of Anitfreeze Solution for Use in Ice Builders. *Canadian Agricultural Engineering*, 35(4), pp. 261-267.

Mullen, C. E., B. D. Bridges, K. J. Porter, G. W. Hahn, C. W. Bullard. 1998. Development and Validation of a Room Air-Conditioning Simulation Model. *ASHRAE Transactions*, 104(2), pp. 389-397.

Newton, H. 2001. Personal Communications.

Nguyen, H., V. W. Goldschmidt. 1986. A User's Guide to the Heat Pump Performance Model HN. Herrick Laboratories Report No. Hl 86-27p, Purdue University, West Lafayette, IN.

O'Neal, D. L., S. Katipamula. 1991. Performance Degradation During on-off Cycling of Single-speed Air Conditioners and Heat Pumps - Model Development and Analysis. *ASHRAE Transactions*, 97(2), pp. 316-323.

Ooi, K. T., T. N. Wong. 1997. A Computer Simulation of a Rotary Compressor for Household Refrigerators. *Applied Thermal Engineering*, Vol. 17, No. 1 pp. 65-78.

Oskarsson, S. P., K. I. Krakow, S. Lin. 1990. Evaporator Models for Operation with Dry, Wet, and Frosted Finned Surfaces Part 2: Evaporator Models and Verification. *ASHRAE Transactions*, 96(1), pp. 381-392.

Ouazia B., W. K. Snelson. 1994. Predicting System Performance of Alternative Refrigerants using a Water-Water Heat Pump. *ASHRAE Transactions*, 100(2), pp. 140-147.

Padhy, S. K. 1994. Dynamic Analysis of a Rotary Compressor. *Journal of Mechanical Design*, Vol. 116. pp. 639-646.

Padhy S. K., S. N. Dwivedi. 1994. Heat Transfer Analysis of a Rolling-Piston Rotary Compressor. *International Journal Refrigeration*, Vol. 17, No. 6, pp. 400-410.

Panchal, C. B., D. M. France, K. J. Bell. 1992. Experimental Investigation of Single-Phasse, Condensation, and Flow Boiling Heat Transfer for a Spirally Fluted Tube. *Heat Transfer Engineering*, 13(1), pp. 42-52.

Parent, D. 1989. Testing and Modeling of a Water-to-Air Heat Pump Operating with a Nonazeotropic Refrigerant Mixture. *ASHRAE Transactions*, 95(2), pp. 405-410.

Parise, J. A. R. 1986. Simulation of Vapor-compression Heat Pumps. *Simulation*, 46(2), pp. 71-76.

Parreira, E. P., J. A. R. Parise. 1993. Performance Analysis of Capacity Control Devices for Heat Pump Reciprocating Compressors. *Heat Recovery Systems & CHP*, 13(5), pp. 451-461.

Pierre, Bo. 1955. S. F. Review Vol. 2, Number 1. Published by A. B. Svenska, Flaktabriken, Stockholm, Sweden.

Popovic, P., H. N. Shapiro. 1995. A Semi-empirical Method for Modeling a Reciprocating Compressor in Refrigeration System. *ASHRAE Transactions*, 101(2), pp. 367-382.

Popovic, P., H. N. Shapiro. 2000. Personal Communication.

Purvis, E. 1987. Scroll Compressor Technology. *Heat Pump Conference*, New Orleans.

Qu, Z., X. Li, S. Li. 1998. Analytical Modeling of Thermodynamic Process for Scroll Compressor with Back Pressure Optimization. *Journal of Xi'An Jiaotong University*. Vol. 32, n. 7, pp. 51-55.

Rabehl, R. J., J. W. Mitchell, W. A. Beckman. 1999. Parameter Estimation and the Use of Catalog Data in Modeling Heat Exchangers and Coils. *International Journal of Heating, Ventilating, and Air-Conditioning Research*, 99(1), pp. 3-17.

Ragazzi, F., C. O. Perdersen. 1991. Modular-Based Computer Simulation of an Air-Cooled Condenser. Air Conditioning and Refrigeration Center TR-07, University of Illinois, Urbana, IL.

Rees, S. J. 2002. Personal Communication.

Rice, C. K. 2000. Personal Communication.

Saavedra, C. 1993. Contribution to Modeling of Heating and Refrigeration Equipments. Ph.D. thesis. University of Liege, Belgium.

Safemazandarani, P., J. A. Edwards, R. R. Johnson, Y. Mohammad-zadeh. 1990. Mathematical Modeling of a Direct Expansion Ground-coupled Heat Pump System. *ASHRAE Transactions*, 96(1), pp. 583-589.

Sami, S. M., J. Schnotale, J. G. Smale. 1992. Prediction of the Heat Transfer Characteristics of R-22/R-152a/R-114and R-22/R-152a/R-124. *ASHRAE Transactions*, 98(2), pp. 51-58.

Senshu, T., A. Arai, K. Oguni, F. Harada. 1985. Annual Energy-Saving Effect of Capacity-Modulated Air Conditioner Equipped with Inverter Driven Scroll Compressor. *ASHRAE Transactions*, 91(2B), pp. 1569-1583.

Shapiro, H. N. 2000. Personal Communication.

Shelton, S. V., E. D. Weber. 1991. Modeling and Optimization of Commercial Building Chiller/Cooling Tower Systems. *ASHRAE Transaction*, 97(2), pp. 1209-1216.

Stefanuk, N. B. M. 1990. Modeling and Simulation of a Water-to-Water Heat Pump Incorporating Superheat Control. M.A.Sc. Thesis, University of Waterloo, Ontario, Canada.

Stefanuk, N. B. M., J. D. Aplevich, M. Renksizbulut. 1992. Modeling and Simulation of a Superheat-controlled Water-to-Water Heat Pump. *ASHRAE Transactions*, 98(2), pp. 172-184.

Stoecker, W. F., Editor. 1975. *Procedures for Simulating the Performance of Components and Systems for Energy Calculations*, 3rd edition. Atlanta: ASHRAE.

Stoecker, W. F., J. W. Jones. 1982. *Refrigeration and Air Conditioning*, 2nd ed. New York: McGraw-Hill.

Stoecker, W. F. 1989. *Design of Thermal Systems*. 3rd ed. New York: McGraw-Hill.

Sutherland, J. W. 1983. Analysis of Mechanical-Draught Counterflow Air/Water Cooling Towers. *Journal of Heat Transfer*, Vol. 105, pp. 576-583.

Takebayashi, M., K. Sekigami, I. Tsubono, H. Kohsokabe, K. Suefuji, K. Inaba. 1994. Performance Improvement of a Variable-speed Controlled Scroll Compressor for Household Air Conditioners. *ASHRAE Transactions*, 100(1), pp. 471-475.

Takeshita, S. 1997. Simulation and Modeling of an A/C Rotary Vane Compressor. *SAE Special Publications, Proceedings of the 1997 International Congress and Exposition,* pp. 83-93.

Thomas, R. M. 1992. Humidity Sensors in Heating, Ventilating and Air Conditioning (HVAC) Systems. *ASHRAE Transactions*, 98(2), pp. 529-539.

Threlkeld, J. L. 1962. *Thermal Environmental Engineering*. Englewood Cliffs, New Jersey: Prentice-Hall.

Tree, D. and B. Weiss. 1986. Two time constant modeling approach for residential heat pumps. *Proceedings of Progress in the Design and Construction of Refrigeration Systems, Purdue University, International Institute of Refrigeration*, pp. 215-222.

Tsubono, I., M. Takebayashi, I. Hayase, K. Inaba, K. Sekiguchi, A. Shimada. 1998. New Back-pressure Control System Improving the Aannual Performance of Scroll Compressors. *ASHRAE Transactions*, 104(1A), pp. 410-417.

Wadivkar, O. 1997. An Experimental and Numerical Study of the Thermal Performance of a Bridge Deck De-Icing System. M.S. Thesis.

Wakabayashi, H., J. Yuuda, T. Aizawa, M. Yamamura. 1982. Analysis of Performance in a Rotary Compressor. *Proceedings of 1982 Purdue University Compressor Technology Conference*, pp. 140-147.

Webb, R. L. 1980. Air-Side Heat Transfer in Finned Tube Heat Exchangers. *Heat Transfer Engineering*, 1(3), pp. 33-49.

Wedekind, G. L., B. Bhatt, and B. Beck. 1978. A System Mean Void Fraction Model for Predicting Various Transient Phenomena Associated with Two-phase Evaporating and Condensing Flows. *International Journal of Multiphase Flow*, Vol. 4, pp. 97-114

Welsby, P., S. Devotta, P. J. Diggory. 1988. Steady- and Dynamic-state Simulations of Heat-pump. Part I: literature review. *Applied Energy*, 31, pp. 189-203.

Welsby, P., M. Pezzani, S. Devotta, P. J. Diggory, J. J. Guy. 1988. Steady- and Dynamic-state Simulations of Heat-pump. Part II: Modeling of a Motor Driven Water-to-Water Heat Pump. *Applied Energy*, 31, pp. 239-262.

Wilson, E. E. 1915. A Basis for Rational Design of Heat Transfer Apparatus. *ASME Transactions*, Vol. 37, pp. 47-70.

Winandy, E., C. Saavedra, J. Lebrun. 2002. Experimental Analysis and Simplified Modeling of a Hermetic Scroll Refrigeration Compressor. *Applied Thermal Engineering*, Vol. 22, n. 2, pp. 107-120.

Yanagisawa, T., T. Shimizu, M. Fukuta, H. Suzuki. 1990. Mathematical Model of Rotary Compressor to Simulate its Transient Behavior. *Proceedings of the 1990 International Compressor Engineering Conference*, pp. 222-227.

Yanagisawa, T., M. Fukuta, H. Suzuki. 1990. Mathematical Modeling of Transient Behavior of a Refrigerating Rotary Compressor. *Transactions of the Japan Society of Mechanical Engineers*, Part B, Vol. 56, No. 526, pp. 1696-1701.

Yaqub, M., S. M. Zubair, S. H. Khan. 1995. Second-law-based Thermodynamic Analysis of Hot-gas By-pass Capacity-control Schemes for Refrigeration and Air-conditioning Systems. *Energy*, 20(6), pp. 483-493.

Yasuda, H., S. Touber, C. H. M. Machielsen. 1983. Simulation Model of a Vapor Compression Refrigeration System. *ASHRAE Transactions*, 89(2A), pp. 408-425.

Yasuda, H., T. Senshu, S. Kuroda, A. Atsumi, K. Oguni. 1990. Heat Pump Performance under Frosting: Part 2 - Simulation of Heat Pump Cycle Characteristics under Frosting Conditions. *ASHRAE Transactions*, 96(1), pp. 330-336.

Zeng, Y. Y., R. W. Besant, K. S. Rezkallah. 1992. The Effect of Temperature-Dependent Properties on the Performance of Run-Around Heat Recovery Systems using Aqueous-Glycol Coupling Fluids. *ASHRAE Transactions*, 98(1), pp.551-562.

Zivi, S. M. 1964. Estimation of Steady-state Steam Void Fraction by Means of the Principle of the Minimum Entropy Production. *Journal of Heat Transfer*, Vol. 86, pp. 247-252.

APPENDIX A

Sensitivity Analysis of the Water-to-Water Heat Pump Model

There are errors associated with the output of the heat pump model such as cooling capacity or heating capacity as a result of the uncertainty of the estimated parameter values. Therefore, a series of sensitivity analyses are performed to assess the influence of a number of parameters that cannot be determined exactly, but estimated with some uncertainty on the predicted capacity of the heat pump model. In this investigation, heat pump A used for the water-to-water heat pump model validation in Chapter 4 has been chosen to do the sensitivity analysis.

A.1. Sensitivity to the Heat Transfer Coefficient of Load Side Heat Exchanger

The sensitivity of the predicted cooling capacity to the heat transfer coefficient of load side heat exchanger is shown in Figures A.1 and A.2. Figure A.1 is a plot for point #1, which is the first point of the specification data. Figure A.2 is a plot for point #81, which is the last point of the specification data. The 100% heat transfer coefficient has been chosen as the reference point, whose value was estimated using the manufacturer's catalog data. Then the heat transfer coefficient has been reduced gradually at the step of 10%. A review of the plots shows that the cooling capacity asymptotically approaches the maximum value, which is the capacity for 100% heat transfer coefficient value. This implies that the estimated heat transfer coefficient value is approximately the least value necessary to achieve the specified capacity of the heat pump. A greater heat transfer coefficient than this value, or in other words, a bigger heat exchanger won't help to enhance the cooling capacity of the heat pump considerably. Apparently, when the heat transfer coefficient of the load side heat exchanger approaches the 100% value, the

cooling capacity is less sensitive to the heat transfer coefficient than it is to a much smaller value.

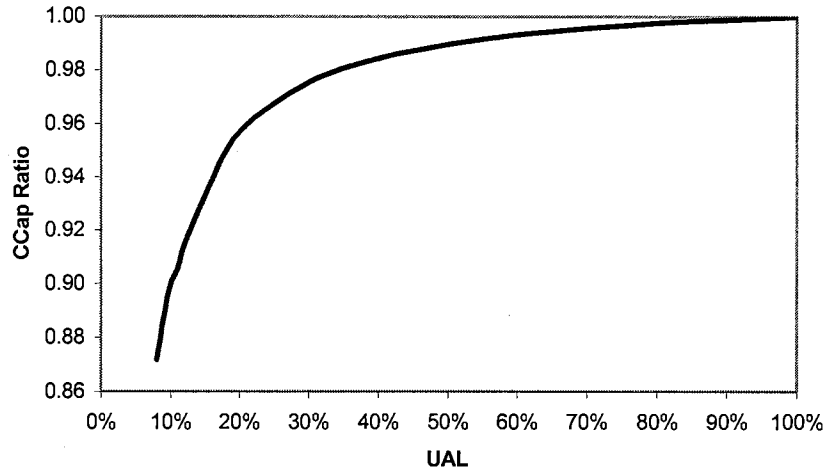

Figure A.1. Cooling capacity correction factor vs. degradation of heat transfer coefficient of load side heat exchanger – catalog data point #1

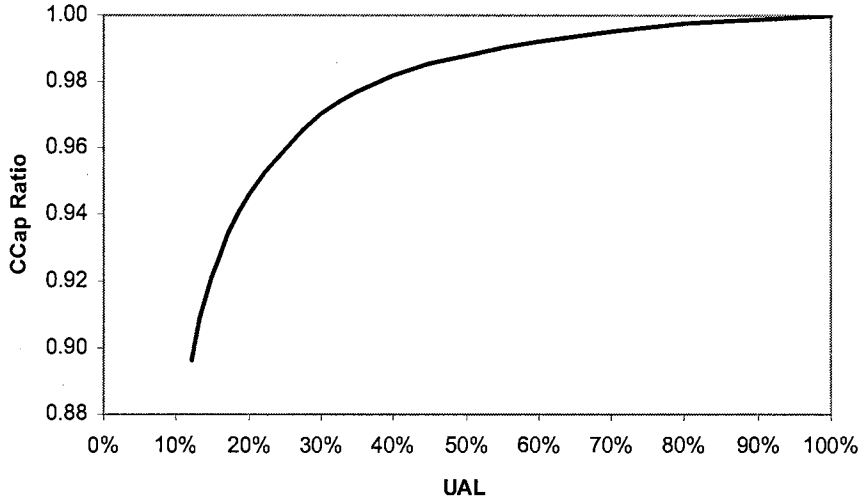

Figure A.2. Cooling capacity correction factor vs. degradation of heat transfer coefficient of load side heat exchanger – catalog data point #81

A.2. Sensitivity to the Heat Transfer Coefficient of Source Side Heat Exchanger

The sensitivity of the predicted cooling capacity to the heat transfer coefficient of source side heat exchanger is shown in Figures A.3 and A.4. Figure A.3 is a plot for point #1, which is the first point of the specification data. Figure A.4 is a plot for point #81, which is the last point of the specification data. The 100% heat transfer coefficient has been chosen as the reference point, whose value was estimated using the manufacturer's catalog data. Then the heat transfer coefficient has been reduced gradually at the step of 10%. A review of the plots shows that the cooling capacity asymptotically approaches the maximum value, which is the capacity for 100% heat transfer coefficient. This behavior can be explained similarly by what has been discussed for the load side heat transfer coefficient.

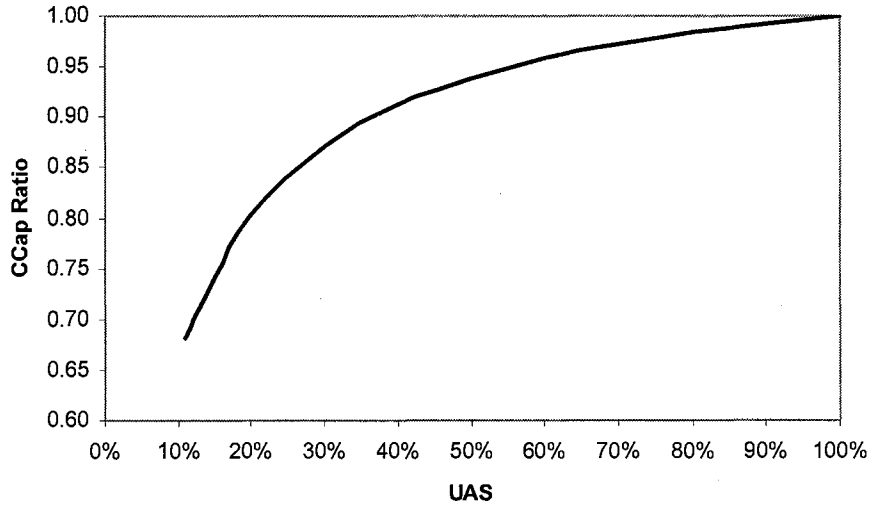

Figure A.3. Cooling capacity correction factor vs. degradation of heat transfer coefficient of source side heat exchanger – catalog data point #1

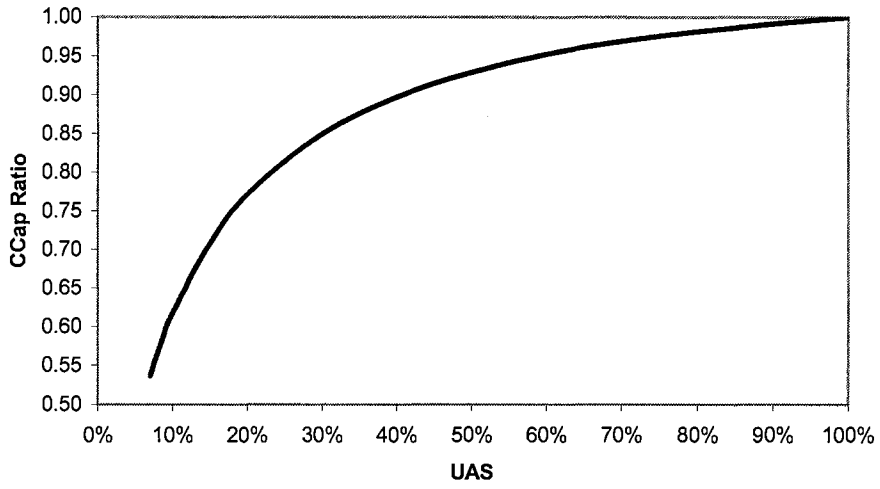

Figure A.4. Cooling capacity correction factor vs. degradation of heat transfer coefficient of source side heat exchanger – catalog data point #81

A.3. Sensitivity to the Compressor Piston Displacement

The sensitivity of the predicted cooling capacity to the compressor piston displacement is shown in Figures A.5 and A.6. Figure A.5 is a plot for point #1, which is the first point of the specification data. Figure A.6 is a plot for point #81, which is the last point of the specification data. The 100% piston displacement has been chosen as the reference point, whose value was estimated using the manufacturer's catalog data. Then the piston displacement has been reduced and increased gradually at the step of 10%. A review of the plots shows that the cooling capacity asymptotically approaches a maximum value, which may be far greater than that with the estimated compressor piston displacement. This implies that the cooling capacity is more sensitive to the piston displacement at the estimated value than the heat transfer coefficients.

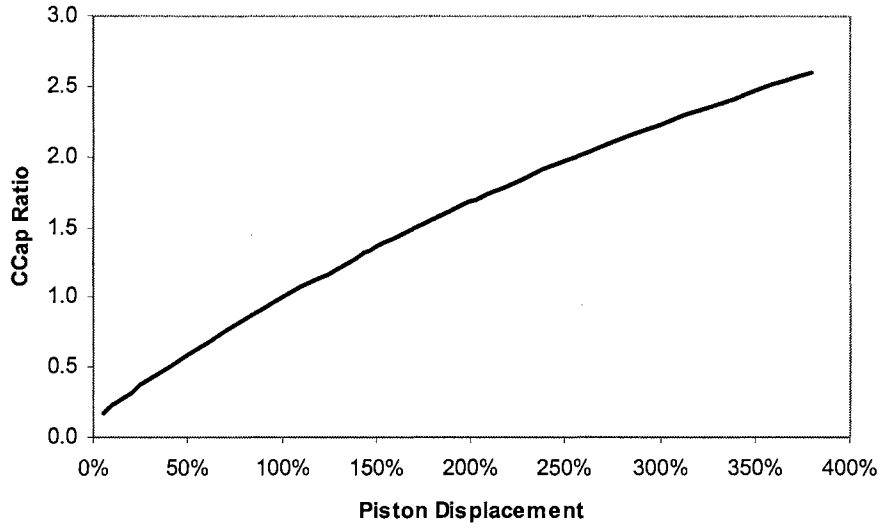

Figure A.5. Cooling capacity correction factor vs. hypothetical variation of compressor piston displacement – catalog data point #1

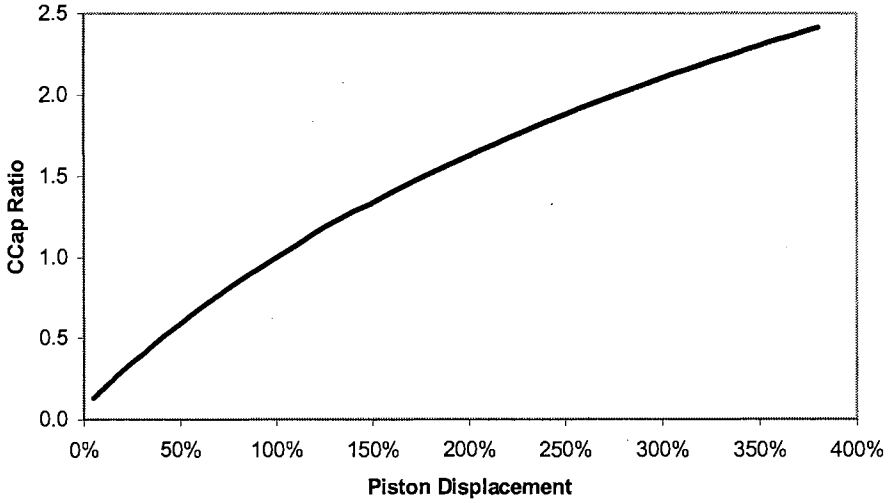

Figure A.6. Cooling capacity correction factor vs. hypothetical variation of compressor piston displacement – catalog data point #81

A.4. Sensitivity to the Compressor Clearance Factor

The clearance factor is another important feature of the compressor design. Obviously, the bigger the clearance factor, the less the cooling capacity is. Since the clearance factor has been defined as a percentage value, the plots of sensitivity of the cooling capacity to the value of the clearance factor in Figures A.7 and A.8 are a little different from the plots for other parameters discussed above. To the author's best knowledge, the clearance factor of the reciprocating compressor with a normal design is no greater than 10%. Hence, the calculation of the sensitivity of the cooling capacity to the clearance factor is only performed between 2% and 9%. This range may be adequately wide to cover the clearance factor values for most of the reciprocating compressors used in the heat pump technology. A review of the plots shows that the relationship between the cooling capacity and clearance factor is nearly linear.

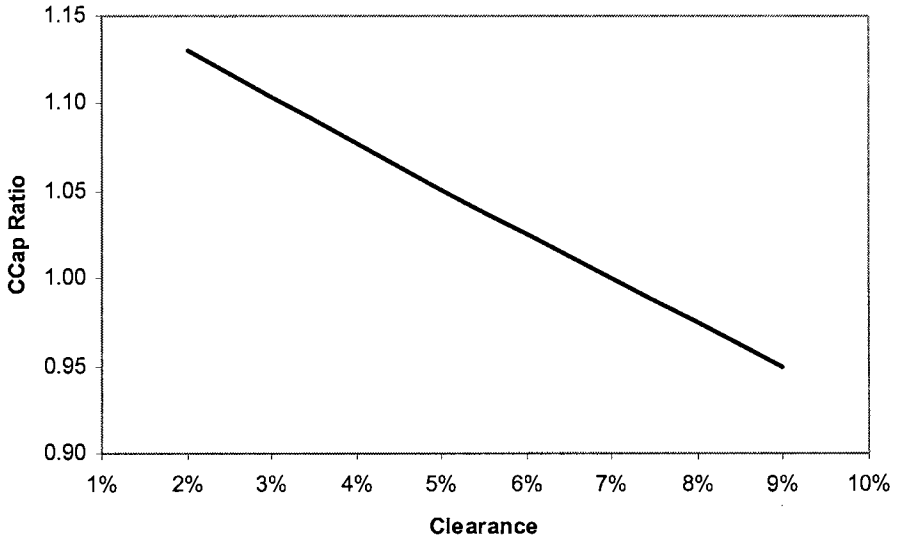

Figure A.7. Cooling capacity correction factor vs. hypothetical variation of compressor clearance factor – catalog data point #1

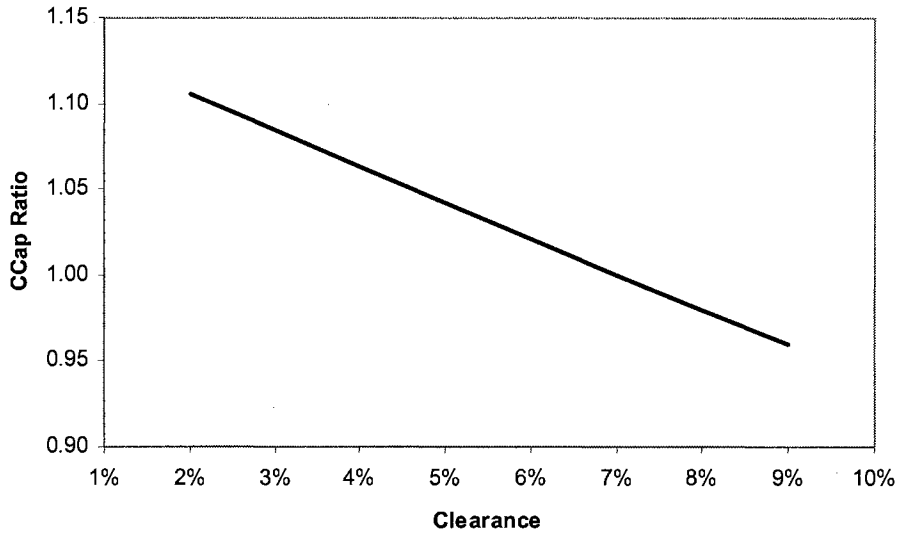

Figure A.8. Cooling capacity correction factor vs. hypothetical variation of compressor clearance factor – catalog data point #81

A.5. Sensitivity to the Suction & Discharge Pressure Drop

The last parameter selected for the sensitivity analysis is the pressure drop across the suction and discharge valves. Obviously, the bigger the pressure drop, the less the cooling capacity is. The sensitivity of the predicted cooling capacity to the pressure drop is shown in Figures A.9 and A.10. Figure A.9 is a plot for point #1, which is the first point of the specification data. Figure A.10 is a plot for point #81, which is the last point of the specification data. The 100% pressure drop has been chosen as the reference point, whose value was estimated using the manufacturer's catalog data. Then the pressure drop has been reduced and increased gradually at the step of 10%. A review of the plots shows that the relationship between the cooling capacity and pressure drop is approximately linear.

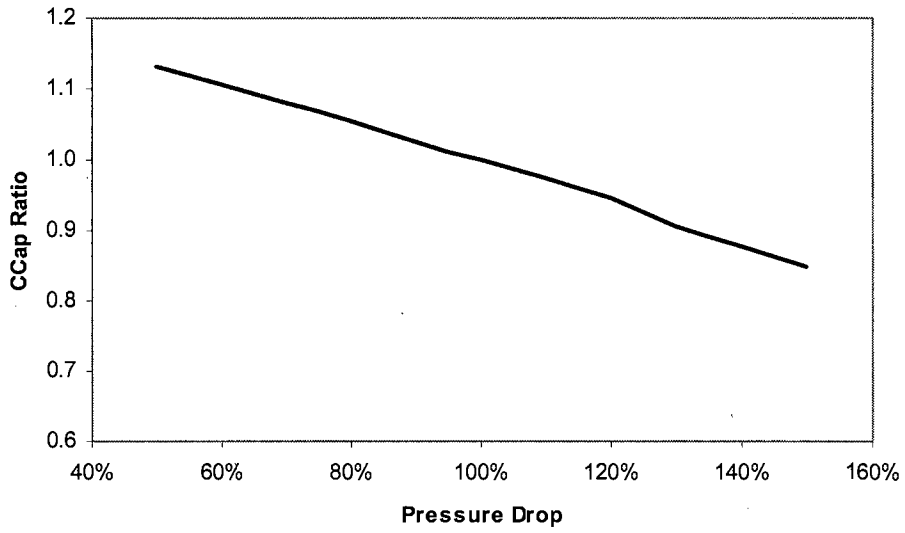

Figure A.9. Cooling capacity correction factor vs. hypothetical variation of suction & discharge pressure drop – catalog data point #1

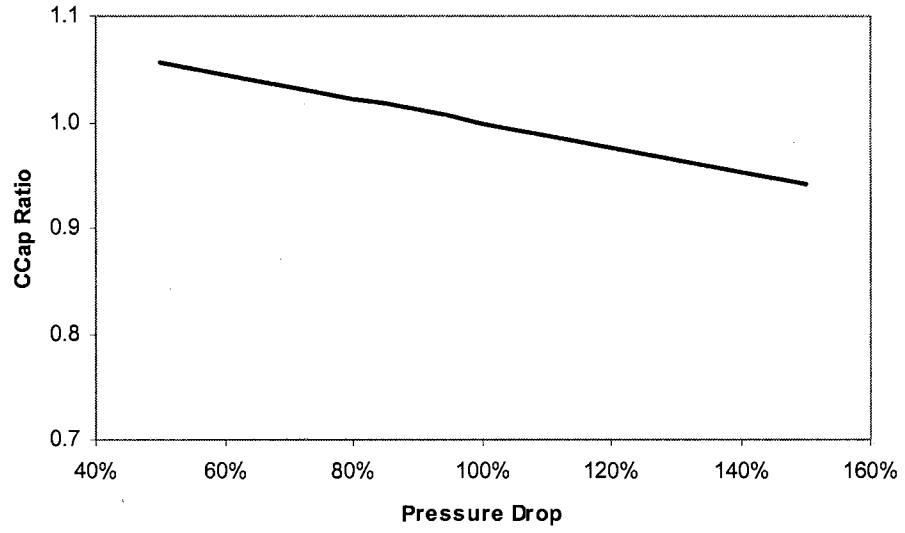

Figure A.10. Cooling capacity correction factor vs. hypothetical variation of suction & discharge pressure drop – catalog data point #81

APPENDIX B

Calibration of the Instrumentation for the Water-to-Air Heat Pump Experiment

This appendix presents the calibration of the experimental devices and uncertainty analysis for the validation of the water-to-air heat pump model.

B.1. Calibration of Experimental Devices

For any experimental apparatus, the uncertainty always exists for all the measurements. When the measurements are used to calculate the derived parameters, the errors are usually compounded and amplified. Therefore, a meticulous calibration of the sensors and data acquisition equipment is necessary to minimize the uncertainties. For this experiment, five types of experimental data are procured: normal temperature (°C or °F), mass flow rate (kg/s or lbm/hr), dew point temperature (°C or °F), pressure difference (kPa or PSI) and input power (watts or Btu/Hr). Each device has been calibrated independently.

B.1.1. Normal Temperature Devices

There are two thermocouple probes, two groups of exposed thermocouples used to measure the normal temperatures. Each device serves a separate and specific purpose. One of the thermocouple probes is used to measure the entering water temperature of the heat pump, the other thermocouple probes is used to measure the leaving water temperature of the heat pump. The exposed thermocouple groups measure the return and supply air dry bulb temperatures of the heat pump.

B.1.1.1. Exposed Junction Thermocouple

The exposed junction thermocouple is a type-T thermocouple, which measures the return and supply air dry bulb temperatures of the heat pump. The uncertainty is about ±0.3 °C (±0.54 °F) based on the calibration data. Type-T thermocouples are made of copper versus constantan and the valid temperature range is between 0 °C (32 °F) and 371.1 °C (700 °F). Since the variation of the air temperatures in the HVAC application and the return and supply air temperatures of the building in this case fall into a considerable narrow range, the thermocouples have been calibrated at three points: 0.7 °C (33.3 °F), 15.8 °C (60.4 °F) and 26.9 °C (80.4 °F). The output voltage of the thermocouple is received by the Fluke data logger. And then the temperature converted internally by the data logger is saved in an ASCII file. An average value is calculated for three different points respectively. The fitted equations have been found for each thermocouple using linear regression analysis tool in Excel.

B.1.1.2. Thermocouple Probe

The experimental apparatus uses two thermocouple probes to measure the entering and leaving water temperatures of the heat pump. They are stainless steel OMEGA TMQSS-125G-6 quick disconnect thermocouple probes with miniature connectors. It is a type-T thermocouple, 0.125" sheath diameter and 6 " sheath length. The probes have an accuracy of ±0.5 °C (±0.9 °F) based on the calibration data. The thermocouple probe is also calibrated with the same approach as the exposed joint thermocouple. The fitted

equations have been found for each thermocouple probe using linear regression analysis tool in Excel.

B.1.2. Flow Meter

The OMEGA FTB-100 and 200 series turbine meters are volumetric measuring flow meters. The flowing fluid engages the vaned rotor causing it to rotate at an angular velocity proportional to the liquid flow rate. The flow meter pickup senses the motion of the rotor and converts it to a pulsing electrical signal which is of a discrete, digital nature. The pickup generates a relatively high magnetic field and produces a high level sinusoidal output. Thus the angular velocity of the rotor results in the generation of an electrical signal (AC sine wave type). Summation of the pulsing electrical signals relates directly to total flow. Frequency of the signals relates directly to the flow rate. The vaned rotor is the only moving part of the flow meter. OMEGA FTB-105 turbine meter has a sealed ball bearing design that gives the widest linear flow range. Its low mass rotor allows for rapid dynamic response, and therefore it can be used in pulsating flow applications. The estimated uncertainty is ±2.8% (Wadivkar 1997).

The output signal from the FTB-105 flowmeter is received by the OMEGA FLSC-28 High Accuracy Integral Signal Conditioner. The input circuitry of the FLSC-28 Signal Conditioner has been designed to condition the low level turbine meter signals while rejecting unwanted noise and spurious signals. A signal threshold control is provided which allows the user to set the input sensitivity above the ambient noise level, thereby

eliminating any false signal on the output. The FLSC-28 provides a 0-5V output that runs off user supplied 10-40 V dc power supply.

The calibration of the flow meter was accomplished by the 'bucket and stop watch method'. The tap water traveled through the flow meter and drain into a big chest. When the reading on the data logger stabilized at the desired value, the flow was diverted into a bucket until it was filled up. The time consumed to fill the bucket was measured using a stop watch. Then the water collected in the bucket was weighted on an electronic scale. Meanwhile, the voltage output from the flow meter was recorded at one-second intervals. A simple average of these reading in terms of Vdc was calculated to minimize the error. This average voltage corresponded to the flow rate that calculated as the weight of the water in the bucket divided by the time consumed.

The maximum and minimum flow rates have to be dependent on the adjustability of the tap water. Fortunately, the desired flow rates fell into the adjustable range of the tap water. It was noticed that the nominal flow rate of the condenser water is around 4 GPM (0.2524 L/S). Hence, to verify the extrapolation ability of the heat pump model, some water flow rates 1 to 2 GPM (0.0631 to 0.1262 L/S) lower and higher than the nominal flow rate are desirable. According to the operator's manual of the flow meter, the linear flow rate extends from 2.5 to 29 GPM (0.15775 to 1.8299 L/S) for Model FTB-105, which is much wider than the desired range. The available signal conditioner (FLSC-28) provides a 0-5V output that runs off user supplied 10-40 V dc power supply.

B.2. Humidity Instrument

B.2.1. Background for the Selection of Dew Point Sensor

A laboratory evaluation of humidity sensors for use in HVAC systems was presented by Thomas (1992). Among the sensors investigated, dew point sensor generally demonstrated the superiority over the others in a few respects.

Sensors to measure the humidity of the air entering and leaving cooling coils are required in the determination of coil loads and supply air quality. Three different humidity sensors were tested, one that measures dew point and two that measure relative humidity. The sensors were tested in an environmental chamber under various typical conditions. The outcome of the tests showed the most accurate instrument for field tests was the dew point sensor.

The dew point sensor showed a 1.6% overall average percent error form the standard for both the cooling coil inlet and outlet calculated absolute humidity in an environmental chamber. The standard deviation of the sensor was 0.75% for coil inlet and 1.7% for outlet measurements. The author then selected the dew point sensor as the most accurate sensor evaluated for its response time in an operating fan/cooling coil setup.

The relative humidity sensor is economical and accurate for compartment ambient humidity measuring requirements. However, the accuracy of relative humidity sensor

used to measure the load of cooling coil is questionable. Since the sensors are subjected to high air velocity and/or dirty environment, they are easily contaminated with dirt and grease, which leads to inaccurate humidity values. In addition, the sensor does not provide any indication of loss of accuracy when it becomes contaminated.

Three sensors were selected for the study, one dew point and two relative humidity instruments. The dew point instrument selected for testing was a low cost chilled mirror dew point transmitter. One of the relatively humidity sensor is of the capacitance type using a polymer dielectric as the sensing element. The other relative humidity sensor is a processed plastic wafer made up of chemically treated styrene copolymer, which has an electrically conducting surface layer that is integral with non-conducting substrate. Changes in relative humidity cause the surface resistivity to vary.

Table B.24 shows a comparison of the calculated accuracy and the chamber test accuracy results. The manufacturers' published accuracy was converted into absolute humidity. And the results of the chamber test were presented using two error analysis methods: the average deviation and the standard deviation (RMS). From the table, it is easily concluded that dew point sensors perform at the manufacturers' stated accuracy. The relative humidity sensors go much worse than the manufacturers' stated accuracies.

Table B.24. Calculated Latent Load and Absolute Humidity Accuracy (Thomas, 1992)

Instrument Type	Percent Error Calculated Accuracy		Absolute Humidity Chamber Test Results	
	Coil Inlet	Outlet	Coil Inlet	Outlet
Dew Point	4.2	4.2	2.3/3.8	5.4/4.5
Capacitive	4.4	2.2	11.5/11.2	-/7.4
Resistive	2.8	1.5	27.8/24.5	15.9/18.1

The author's conclusions were that the dew point sensor is the best choice of the three sensors tested for calculating cooling coil latent load. It is a field-oriented, primary measuring device designed for high velocity ductwork measurements. Based on the selected set of conditions, the latent heat constituted 10% of the total heat. The author found the dew point sensor's expected overall latent load accuracy is around 42%. And the overall sensible load accuracy is 6%. Combing the latent and sensible heat, the total load accuracy is about 8%.

B.2.2. An Introduction of the Chilled Mirror Dew Point Hygrometer

The chilled mirror hygrometer indicates the temperature at which H_2O changes from a gas to liquid (dew point) or from gas to solid (frost point). In the hygrometer, a surface (usually of gold, palladium, platinum, or electroplated nickel) is cooled (thermoelectrically, mechanically, or chemically) until dew begins to condense out. Adiabatic cooling, caused by the sudden expansion of a gas-water vapor mixture, will produce condensate if the dew point is reached. In practice, the sample is compressed, then suddenly expanded to atmospheric pressure, and the surface condensation is detected optically, photoelectrically or by nuclear techniques. The condensate surface is

maintained electronically in vapor pressure equilibrium with the surrounding gas. The measured surface temperature is then the dew point temperature.

The condensate type or chilled mirror dew point hygrometer is an accurate and reliable instrument with a wide humidity range. When the primary criterion of the measurement is accuracy, a chilled mirror will give the most satisfactory result. The largest source of error in a condensate hygrometer stems from the difficulty in measuring condensate surface temperature accurately. Chilled mirror are as accurate as the thermometry used to measure the temperature of the mirror. Typical industrial versions of the instrument are accurate to ±0.5 °C (±0.9 °F) over wide temperature spans. With proper attention to the condensate surface temperature measuring system, errors can be reduced to about 0.2 °C (0.36 °F). Condensation type hygrometers can be made surprising compact using solid state optics and thermoelectric cooling.

Applications for the chilled mirror are extensive. They have found use in meteorology, environmental monitoring, dry operations, storage operations, trace elements in process gases, HVAC climate control, heat-treating furnaces, process gases in semiconductor manufacturing, laboratory standards, clean rooms, compressed air, greenhouses, research and development, emissions testing, glove box atmospheres, food-processing applications and others.

B.2.3. Omega Chilled Mirror Dew Point Transmitter

The RHCM-20-3-100F is one of the OMGA RHCM series chilled mirror dew point transmitters. The sensor is capable of providing long-term repeatability and reliable performance for process control and energy management. The RHCM sensors are designed to be either pipe or duct mounted for process control in HVAC/Energy management applications. Field calibration is not required and the ambient temperature effects, hysteresis, and calibration drift with age are all virtually eliminated.

The RHCM series offer a wide range of user specified power inputs including 24 Vdc, 24 Vac, 115 Vac and 230 Vac, for many applications. The user specified outputs include 100½ platinum RTD (4-wire) or 4 to 20 mA, which can be scaled over three different temperature ranges of 0 to 100°F, 0 to 50°C and -40 to 140°F. Either output can be directly connected to a panel meter, controller or data acquisition system. The accuracy of RHCM-20 duct mount is ±1.0 °F (±0.556 °C).

B.2.4. Error Analysis of the Relative Humidity Sensor and Dew Point Transmitter

To determine the psychrometric properties, it is necessary to know the water vapor saturation pressure. It's given in the following Table B.25 using polynomial regression analysis on data obtained from ASHRAE research. In some other cases, the saturation pressure is given and it is required to calculate backward to obtain the temperature

corresponding to the pressure. The calculation of temperature is shown in Table B.26 derived from the regression analysis analogously.

Table B.25. Calculation of Water-Vapor Saturation Pressure That is Dependent on the Temperature within Various Temperature Ranges

$\alpha = AT^2 + BT + C + DT^{-1}$, T in K

$P_{ws} = 1000e^{\alpha}$, P_{ws} in Pa

	Temperature (K)				
	213.15≤T<273.15	**273.15≤T<322.15**	**322.15≤T<373.15**	**373.15≤T<423.15**	**423.15≤T<473.15**
A	-0.7297593707E-5	0.1255001965E-4	0.1246732157E-4	0.1204507646-4	0.1069730183-4
B	0.5397420727E-2	-0.1923595289E-1	-0.1915465806E-1	-0.1866650553E-1	-0.1698965754E-1
C	0.2069880620E2	0.2705101899E2	0.2702388315E2	0.2683629403E2	0.2614073298E2
D	-0.6042275128E4	-0.6344011577E4	-0.6340941639E4	-0.6316972063E4	-0.6220781230E4

Table B.26. Calculation of Temperature That is Dependent on Water Vapor Saturation Pressure within Various Temperature Ranges

$T = E\beta^4 + F\beta^3 + G\beta^2 + H\beta + K$, T in K

$\beta = \ln(P_{ws})$, P_{ws} in Pa

	Temperature (K)				
	1≤P<611	**611≤P<12350**	**12350≤P<101420**	**101420≤P<476207**	**476207≤P<1555099**
E	0.1004926534E-2	0.5031062503E-2	0.1209512517E-4	0.2467291016E-1	0.2748402484E-4
F	0.1392917633E-2	-0.8826779380E-1	-0.3545542105	-0.9367112883	-0.1068661307E1
G	0.2815151574	0.1243688446E1	0.2125893734E3	0.1514142334E2	0.1742964962E2
H	0.7311621119E1	0.3388534296E1	-0.2050301050E2	-0.9882417501E2	-0.1161208532E3
K	0.2125893734E3	0.2150077993E3	0.2718585432E3	0.4995092948E3	0.5472618120E3

B.2.5. Error Analysis of Relatively Humidity Sensor

For water-to-air heat pumps in cooling mode, the cooling capacity consists of sensible and latent heat removal. Since the moisture removal corresponding to the latent heat is measured using either relative or absolute humidity, the accuracy of the humidity sensor is significant for the calculation of latent cooling capacity thereby. Hence, it is essential to pay a close attention to the manufacturers' published accuracies of the humidity sensors and find out their affect on the error of the cooling capacity calculated. The discussion of deviation of the cooling capacity based on different humidity

measurements using a variety of accuracy of the humidity sensor has been divided into two parts: the first part is for the relative humidity sensor and the second part is for the dew point sensor. Meanwhile, this discussion is also extended to more than one single manufacturers' catalog data.

It is noticed that the manufacturers' catalog data is typically listed by a series of the dry bulb and wet bulb temperatures of the inlet air, instead of the humidity ratio.

Therefore, the first step is to calculated the ideal value of the relative humidity of the inlet air:

Given: Dry Bulb Temperature t_{db}, Wet Bulb Temperature t_{wb}.

Find: Relative Humidity ϕ.

Equations used in sequence:

$$\alpha = AT_{db}^2 + BT_{db} + C + DT_{db}^{-1},\ T \text{ in K} \tag{B.1}$$

$$P_{ws} = 1000e^{\alpha},\ P_{ws} \text{ in Pa} \tag{B.2}$$

$$W_s^* = 0.62198\frac{P_{ws}(t_{wb})}{P - P_{ws}(t_{wb})} \tag{B.3}$$

$$W = \frac{(2501 - 2.381t_{wb})W_s^* - C_{pa}(t_{db} - t_{wb})}{2501 + 1.805t_{db} - 4.186t_{wb}} \tag{B.4}$$

$$P_w = \frac{PW}{W + 0.62918} \tag{B.5}$$

$$\phi = \frac{P_w}{P_{ws}} \tag{B.6}$$

Where α = natural log of saturation vapor pressure over pure water

T_{db} = absolute dry bulb temperature, °K

P_{ws} = pressure of saturated pure water, kPa

W_s^* = humidity ratio of moist air at saturation at thermodynamic wet bulb temperature, kg/kg dry air or lbm/lbm dry air

t_{wb} = wet bulb temperature, °C or °F

W = humidity ratio of moist air, mass of water per unit mass of dry air, kg/kg dry air or lbm/lbm dry air

C_{pa} = air specific heat, kJ/kg-°C or Btu/lbm-°F

t_{db} = dry bulb temperature, °C or °F

P_w = water vapor partial pressure, kPa or psia

P = total pressure of moist air, kPa or psia

ϕ = relative humidity.

The relative humidity calculated is the best measurement we expect from the sensor. However, the actual measurement will not so ideal as we have mentioned before, the accuracy of the sensor will lead to the error of the measured value up to around 5% according to the manufacturers' publication. Table B.27 presents the relative humidity calculated and the worst measurements probable for those operating points using one heat pump manufacturer's specification sheet.

Table B.27. Relative Humidity Error Analysis for Entering States

Entering DB temp		Entering WB temp		RH_ENT	H		RH+2%	H		RH-2%	H	
(F)	(C)	(F)	(C)	CAT	(KJ/KG)	(Btu/lb)		(KJ/KG)	(Btu/lb)		(KJ/KG)	(Btu/lb)
75.000	23.889	61.000	16.111	44.62%	44.95	19.33	46.62%	45.89	19.73	42.62%	43.99	18.91
80.000	26.667	61.000	16.111	32.63%	44.87	19.29	34.63%	45.97	19.77	30.63%	43.73	18.80
85.000	29.444	61.000	16.111	23.35%	44.80	19.26	25.35%	46.14	19.84	21.35%	43.51	18.71
75.000	23.889	64.000	17.778	55.18%	49.99	21.49	57.18%	50.96	21.91	53.18%	49.04	21.09
80.000	26.667	64.000	17.778	41.59%	49.90	21.46	43.59%	51.04	21.94	39.59%	48.78	20.97
85.000	29.444	64.000	17.778	30.97%	49.82	21.42	32.97%	51.16	22.00	28.97%	48.52	20.86
75.000	23.889	67.000	19.444	66.40%	55.38	23.81	68.40%	56.34	24.22	64.40%	54.41	23.39
80.000	26.667	67.000	19.444	51.10%	55.28	23.77	53.10%	56.42	24.26	49.10%	54.15	23.28
85.000	29.444	67.000	19.444	39.06%	55.19	23.73	41.06%	56.55	24.31	37.06%	53.88	23.17
75.000	23.889	70.000	21.111	78.35%	61.15	26.29	80.35%	62.10	26.70	76.35%	60.16	25.87
80.000	26.667	70.000	21.111	61.23%	61.05	26.25	63.23%	62.18	26.73	59.23%	59.89	25.75
85.000	29.444	70.000	21.111	47.68%	60.95	26.20	49.68%	62.30	26.79	45.68%	59.62	25.63
80.000	26.667	73.000	22.778	72.01%	67.24	28.91	74.01%	68.38	29.40	70.01%	66.08	28.41
85.000	29.444	73.000	22.778	56.85%	67.12	28.86	58.85%	68.51	29.46	54.85%	65.81	28.29
75.000	23.889	61.000	16.111	44.62%	44.95	19.33	46.62%	45.89	19.73	42.62%	43.99	18.91
80.000	26.667	61.000	16.111	32.63%	44.87	19.29	34.63%	45.97	19.77	30.63%	43.73	18.80
85.000	29.444	61.000	16.111	23.35%	44.80	19.26	25.35%	46.14	19.84	21.35%	43.51	18.71
75.000	23.889	64.000	17.778	55.18%	49.99	21.49	57.18%	50.96	21.91	53.18%	49.04	21.09
80.000	26.667	64.000	17.778	41.59%	49.90	21.46	43.59%	51.04	21.94	39.59%	48.78	20.97
85.000	29.444	64.000	17.778	30.97%	49.82	21.42	32.97%	51.16	22.00	28.97%	48.52	20.86
75.000	23.889	67.000	19.444	66.40%	55.38	23.81	68.40%	56.34	24.22	64.40%	54.41	23.39
80.000	26.667	67.000	19.444	51.10%	55.28	23.77	53.10%	56.42	24.26	49.10%	54.15	23.28
85.000	29.444	67.000	19.444	39.06%	55.19	23.73	41.06%	56.55	24.31	37.06%	53.88	23.17
75.000	23.889	70.000	21.111	78.35%	61.15	26.29	80.35%	62.10	26.70	76.35%	60.16	25.87
75.000	23.889	70.000	21.111	78.35%	61.15	26.29	80.35%	62.10	26.70	76.35%	60.16	25.87
80.000	26.667	70.000	21.111	61.23%	61.05	26.25	63.23%	62.18	26.73	59.23%	59.89	25.75
75.000	23.889	73.000	22.778	91.07%	67.35	28.96	93.07%	68.34	29.38	89.07%	66.39	28.54
80.000	26.667	73.000	22.778	72.01%	67.24	28.91	74.01%	68.38	29.40	70.01%	66.08	28.41
85.000	29.444	61.000	16.111	23.35%	44.80	19.26	25.35%	46.14	19.84	21.35%	43.51	18.71
75.000	23.889	61.000	16.111	44.62%	44.95	19.33	46.62%	45.89	19.73	42.62%	43.99	18.91
80.000	26.667	61.000	16.111	32.63%	44.87	19.29	34.63%	45.97	19.77	30.63%	43.73	18.80
85.000	29.444	64.000	17.778	30.97%	49.82	21.42	32.97%	51.16	22.00	28.97%	48.52	20.86
75.000	23.889	64.000	17.778	55.18%	49.99	21.49	57.18%	50.96	21.91	53.18%	49.04	21.09
80.000	26.667	64.000	17.778	41.59%	49.90	21.46	43.59%	51.04	21.94	39.59%	48.78	20.97
85.000	29.444	67.000	19.444	39.06%	55.19	23.73	41.06%	56.55	24.31	37.06%	53.88	23.17
75.000	23.889	67.000	19.444	66.40%	55.38	23.81	68.40%	56.34	24.22	64.40%	54.41	23.39
80.000	26.667	67.000	19.444	51.10%	55.28	23.77	53.10%	56.42	24.26	49.10%	54.15	23.28
85.000	29.444	70.000	21.111	47.68%	60.95	26.20	49.68%	62.30	26.79	45.68%	59.62	25.63
75.000	23.889	70.000	21.111	78.35%	61.15	26.29	80.35%	62.10	26.70	76.35%	60.16	25.87
80.000	26.667	70.000	21.111	61.23%	61.05	26.25	63.23%	62.18	26.73	59.23%	59.89	25.75
75.000	23.889	73.000	22.778	91.07%	67.35	28.96	93.07%	68.34	29.38	89.07%	66.39	28.54
80.000	26.667	73.000	22.778	72.01%	67.24	28.91	74.01%	68.38	29.40	70.01%	66.08	28.41
85.000	29.444	61.000	16.111	23.35%	44.80	19.26	25.35%	46.14	19.84	21.35%	43.51	18.71
75.000	23.889	61.000	16.111	44.62%	44.95	19.33	46.62%	45.89	19.73	42.62%	43.99	18.91

80.000	26.667	61.000	16.111	32.63%	44.87	19.29	34.63%	45.97	19.77	30.63%	43.73	18.80
85.000	29.444	64.000	17.778	30.97%	49.82	21.42	32.97%	51.16	22.00	28.97%	48.52	20.86
75.000	23.889	64.000	17.778	55.18%	49.99	21.49	57.18%	50.96	21.91	53.18%	49.04	21.09
80.000	26.667	64.000	17.778	41.59%	49.90	21.46	43.59%	51.04	21.94	39.59%	48.78	20.97
85.000	29.444	67.000	19.444	39.06%	55.19	23.73	41.06%	56.55	24.31	37.06%	53.88	23.17
75.000	23.889	67.000	19.444	66.40%	55.38	23.81	68.40%	56.34	24.22	64.40%	54.41	23.39
80.000	26.667	67.000	19.444	51.10%	55.28	23.77	53.10%	56.42	24.26	49.10%	54.15	23.28
85.000	29.444	70.000	21.111	47.68%	60.95	26.20	49.68%	62.30	26.79	45.68%	59.62	25.63
75.000	23.889	70.000	21.111	78.35%	61.15	26.29	80.35%	62.10	26.70	76.35%	60.16	25.87
80.000	26.667	70.000	21.111	61.23%	61.05	26.25	63.23%	62.18	26.73	59.23%	59.89	25.75
75.000	23.889	73.000	22.778	91.07%	67.35	28.96	93.07%	68.34	29.38	89.07%	66.39	28.54
80.000	26.667	73.000	22.778	72.01%	67.24	28.91	74.01%	68.38	29.40	70.01%	66.08	28.41
85.000	29.444	61.000	16.111	23.35%	44.80	19.26	25.35%	46.14	19.84	21.35%	43.51	18.71
75.000	23.889	61.000	16.111	44.62%	44.95	19.33	46.62%	45.89	19.73	42.62%	43.99	18.91
80.000	26.667	61.000	16.111	32.63%	44.87	19.29	34.63%	45.97	19.77	30.63%	43.73	18.80
85.000	29.444	64.000	17.778	30.97%	49.82	21.42	32.97%	51.16	22.00	28.97%	48.52	20.86
75.000	23.889	64.000	17.778	55.18%	49.99	21.49	57.18%	50.96	21.91	53.18%	49.04	21.09
80.000	26.667	64.000	17.778	41.59%	49.90	21.46	43.59%	51.04	21.94	39.59%	48.78	20.97
85.000	29.444	67.000	19.444	39.06%	55.19	23.73	41.06%	56.55	24.31	37.06%	53.88	23.17
75.000	23.889	67.000	19.444	66.40%	55.38	23.81	68.40%	56.34	24.22	64.40%	54.41	23.39
80.000	26.667	67.000	19.444	51.10%	55.28	23.77	53.10%	56.42	24.26	49.10%	54.15	23.28
85.000	29.444	70.000	21.111	47.68%	60.95	26.20	49.68%	62.30	26.79	45.68%	59.62	25.63
75.000	23.889	70.000	21.111	78.35%	61.15	26.29	80.35%	62.10	26.70	76.35%	60.16	25.87
80.000	26.667	70.000	21.111	61.23%	61.05	26.25	63.23%	62.18	26.73	59.23%	59.89	25.75
75.000	23.889	73.000	22.778	91.07%	67.35	28.96	93.07%	68.34	29.38	89.07%	66.39	28.54
80.000	26.667	73.000	22.778	72.01%	67.24	28.91	74.01%	68.38	29.40	70.01%	66.08	28.41

The second step is to calculate the inlet air enthalpy from the given dry bulb and wet bulb temperatures in the manufacturers' catalog data:

Given: Dry Bulb Temperature t_{db}, Wet Bulb Temperature t_{wb}.

Find: Enthalpy h.

Equations used in sequence:

$$\alpha = AT_{db}^2 + BT_{db} + C + DT_{db}^{-1},\ T \text{ in K} \tag{B.7}$$

$$P_{ws} = 1000e^{\alpha},\ P_{ws} \text{ in Pa} \tag{B.8}$$

$$W_s^* = 0.62198 \frac{P_{ws}(t_{wb})}{P - P_{ws}(t_{wb})} \tag{B.9}$$

$$W = \frac{(2501 - 2.381 t_{wb}) W_s^* - C_{pa}(t_{db} - t_{wb})}{2501 + 1.805 t_{db} - 4.186 t_{wb}} \tag{B.10}$$

$$h = C_{pa} \times t_{db} + W(2501 + 1.805 t_{db}) \tag{B.11}$$

where α = natural log of saturation vapor pressure over pure water

T_{db} = absolute dry bulb temperature, °K

P_{ws} = pressure of saturated pure water, kPa

W_s^* = humidity ratio of moist air at saturation at thermodynamic wet bulb temperature, kg/kg dry air or lbm/lbm dry air

t_{wb} = wet bulb temperature, °C or °F

W = humidity ratio of moist air, mass of water per unit mass of dry air, kg/kg dry air or lbm/lbm dry air

C_{pa} = air specific heat, kJ/kg-°C or Btu/lbm-°F

t_{db} = dry bulb temperature, °C or °F

h = enthalpy of moist air, kJ/kg dry air or Btu/lbm dry air

The enthalpy calculated is based on the ideal dry bulb and wet bulb temperatures in the catalog data that is corresponding to the best measurement of humidity ratio of the inlet air. However, since the inevitable error occurs for the relatively humidity measured, there could be a deviation for the enthalpy calculated based on the measured humidity from the ideal value. The greatest deviation happens when the error of humidity is the

worst. The step for the calculation of enthalpy when the dry bulb temperature and relative humidity are given is as follows:

Given: Dry Bulb Temperature t_{db}, Relative Humidity ϕ.

Find: Enthalpy h.

Equations used in sequence:

$$\alpha = AT_{db}^2 + BT_{db} + C + DT_{db}^{-1},\ T \text{ in K} \tag{B.12}$$

$$P_{ws} = 1000e^{\alpha},\ P_{ws} \text{ in Pa} \tag{B.13}$$

$$P_w = \phi \times P_{ws} \tag{B.14}$$

$$W = 0.62918 \times \frac{P_w}{P - P_w} \tag{B.15}$$

$$h = C_{pa} \times t_{db} + W\left(2501 + 1.805 t_{db}\right) \tag{B.16}$$

where α = natural log of saturation vapor pressure over pure water

T_{db} = absolute dry bulb temperature, °K

P_{ws} = pressure of saturated pure water, kPa

P_w = water vapor partial pressure, kPa or psia

ϕ = relative humidity.

W = humidity ratio of moist air, mass of water per unit mass of dry air, kg/kg dry air or lbm/lbm dry air

P = total pressure of moist air, kPa or psia

C_{pa} = air specific heat, kJ/kg-°C or Btu/lbm-°F

t_{db} = dry bulb temperature, °C or °F

h = enthalpy of moist air, kJ/kg dry air or Btu/lbm dry air

Table B.28 presents the enthalpy calculated using the heat pump manufacturer's specification sheet. In the same table, the enthalpy calculated based on the worst probable error of relative humidity measured is shown.

The total and sensible cooling capacities are listed in the specification sheet. Together with the enthalpy and dry bulb temperature of inlet air have been discussed previously, the leaving air enthalpy and dry bulb temperature can be calculated. When the enthalpy and dry bulb temperature are obtained, the relatively humidity of the moist air is calculated as follows:

Given: Dry Bulb Temperature t_{db}, Enthalpy h.

Find: Relative Humidity ϕ.

Equations used in sequence:

$$\alpha = AT_{db}^2 + BT_{db} + C + DT_{db}^{-1},\ T \text{ in K} \tag{B.17}$$

$$P_{ws} = 1000e^{\alpha},\ P_{ws} \text{ in Pa} \tag{B.18}$$

$$W = \frac{h - C_{pa} \cdot t_{db}}{2501 + 1.805 t_{db}} \tag{B.19}$$

$$P_w = \frac{PW}{W + 0.62918} \tag{B.20}$$

$$\phi = \frac{P_w}{P_{ws}} \tag{B.21}$$

where α = natural log of saturation vapor pressure over pure water

T_{db} = absolute dry bulb temperature, °K

P_{ws} = pressure of saturated pure water, kPa

W = humidity ratio of moist air, mass of water per unit mass of dry air, kg/kg dry air or lbm/lbm dry air

C_{pa} = air specific heat, kJ/kg-°C or Btu/lbm-°F

t_{db} = dry bulb temperature, °C or °F

P_w = water vapor partial pressure, kPa or psia

P = total pressure of moist air, kPa or psia

ϕ = relative humidity.

Analogously, the relative humidity calculated is the best measurement we expect from the sensor. However, the actual measurement will not so ideal as we have mentioned before, the accuracy of the sensor will lead to the error of the measured value up to around 5% according to the manufacturers' publication. Table B.28 presents the relative humidity calculated and the worst measurements probable for those operating points using the heat pump manufacturer's specification sheet.

Table B.28. Relative Humidity Error Analysis for Leaving States

LVG DB		H		RH_LVG	RH+2%	H		RH-2%	H	
C	F	(KJ/KG)	(Btu/Hr)	CAT		(KJ/KG)	(Btu/Hr)		(KJ/KG)	(Btu/Hr)

12.421	54.358	34.756	14.94	98.29%	100.00%	35.15	15.11	96.29%	34.23	14.72
12.378	54.281	34.627	14.89	98.20%	100.00%	35.04	15.07	96.20%	34.12	14.67
12.206	53.972	34.196	14.70	98.19%	100.00%	34.61	14.88	96.19%	33.70	14.49
12.078	53.740	33.851	14.55	98.07%	100.00%	34.29	14.74	96.07%	33.39	14.36
12.936	55.285	36.050	15.50	98.26%	100.00%	36.47	15.68	96.26%	35.51	15.27
13.258	55.864	36.563	15.72	96.97%	98.97%	37.06	15.93	94.97%	36.08	15.51
13.116	55.609	36.261	15.59	97.22%	99.22%	36.74	15.80	95.22%	35.73	15.36
12.636	54.744	35.231	15.15	98.01%	100.01%	35.70	15.35	96.01%	34.76	14.95
13.279	55.902	36.912	15.87	98.18%	100.18%	37.40	16.08	96.18%	36.38	15.64
13.601	56.482	37.331	16.05	96.50%	98.50%	37.83	16.26	94.50%	36.96	15.89
13.455	56.219	37.007	15.91	96.71%	98.71%	37.50	16.12	94.71%	36.58	15.73
12.979	55.362	36.309	15.61	98.88%	100.00%	36.58	15.73	96.88%	35.86	15.42
13.622	56.520	37.775	16.24	98.06%	100.00%	38.26	16.45	96.06%	37.26	16.02
13.987	57.177	38.176	16.41	95.87%	97.87%	38.69	16.64	93.87%	37.70	16.21
13.828	56.891	37.831	16.27	96.15%	98.15%	38.32	16.48	94.15%	37.29	16.03
13.322	55.980	36.999	15.91	98.08%	100.00%	37.47	16.11	96.08%	36.49	15.69
13.794	56.829	38.206	16.43	97.98%	100.00%	38.71	16.65	95.98%	37.71	16.21
14.185	57.532	38.620	16.60	95.58%	97.58%	39.14	16.83	93.58%	38.21	16.43
14.021	57.239	38.249	16.45	95.81%	97.81%	38.76	16.66	93.81%	37.79	16.25
13.494	56.289	37.473	16.11	98.19%	100.00%	37.92	16.30	96.19%	36.93	15.88
13.966	57.138	38.680	16.63	98.06%	100.00%	39.17	16.84	96.06%	38.15	16.40
14.390	57.903	39.077	16.80	95.26%	97.26%	39.61	17.03	93.26%	38.48	16.55
14.223	57.602	38.711	16.64	95.55%	97.55%	39.22	16.86	93.55%	38.31	16.47
13.665	56.598	37.947	16.32	98.30%	100.00%	38.37	16.50	96.30%	37.37	16.07
14.137	57.447	39.155	16.83	98.14%	100.00%	39.63	17.04	96.14%	38.60	16.60
14.601	58.281	39.551	17.01	94.94%	96.94%	40.07	17.23	92.94%	39.03	16.78
14.433	57.980	39.181	16.85	95.23%	97.23%	39.70	17.07	93.23%	38.59	16.59
13.837	56.907	38.422	16.52	98.39%	100.00%	38.83	16.69	96.39%	37.82	16.26
14.438	57.988	40.060	17.22	98.52%	100.00%	40.45	17.39	96.52%	39.66	17.05
14.438	57.988	39.931	17.17	98.03%	100.00%	40.45	17.39	96.03%	39.40	16.94
14.309	57.756	39.629	17.04	98.20%	100.00%	40.10	17.24	96.20%	39.06	16.79
14.223	57.602	39.413	16.95	98.25%	100.00%	39.87	17.14	96.25%	38.83	16.69
14.910	58.837	41.440	17.82	98.86%	100.00%	41.75	17.95	96.86%	40.94	17.60
14.910	58.837	41.354	17.78	98.54%	100.00%	41.75	17.95	96.54%	40.94	17.60
14.824	58.683	41.052	17.65	98.30%	100.00%	41.51	17.85	96.30%	40.43	17.38
14.738	58.528	40.837	17.56	98.37%	100.00%	41.27	17.75	96.37%	40.20	17.28

Due to the inevitable error for the relatively humidity measured, there could be a deviation for the enthalpy calculated based on the measured humidity from the ideal value. The greatest deviation happens when the error of humidity is the worst. The step for the calculation of enthalpy when the dry bulb temperature and relative humidity is given is same as it is discussed previously.

Obviously, the total cooling capacity is the difference between the enthalpies of the inlet and outlet air. If we subtract the sensible cooling from the total cooling, the remainder is latent cooling capacity. When derived total and latent cooling capacities are obtained, they may be compared with the catalog data. The deviation of the derived capacity from the catalog capacity that supposed to be the ideal value is presented in Table B.29 through Table B.31.

Table B.29. Accuracy of RH Meter ±1%
Heat Pump: Make Trane, # of Points 36

	ENT-/LVG-			ENT+/LVG-		
	Max.	Min.	RMS	Max.	Min.	RMS
Total CC	2.20%	1.60%	1.85%	6.10%	3.70%	4.83%
Latent CC	15.20%	5.20%	8.28%	40.80%	11.60%	22.03%
	ENT-/LVG+			ENT+/LVG+		
	Max.	Min.	RMS	Max.	Min.	RMS
Total CC	6.20%	3.70%	4.85%	2.20%	1.60%	1.83%
Latent CC	42.0%	11.80%	22.12%	14.50%	4.90%	8.20%

Table B.30. Accuracy of RH Meter ±2%
Heat Pump: Make Trane, # of Points 36

	ENT-/LVG-			ENT+/LVG-		
	Max.	Min.	RMS	Max.	Min.	RMS
Total CC	5.10%	3.00%	3.67%	12.40%	7.50%	9.73%
Latent CC	33.80%	9.70%	16.52%	81.00%	23.60%	44.25%
	ENT-/LVG+			ENT+/LVG+		
	Max.	Min.	RMS	Max.	Min.	RMS
Total CC	11.20%	7.30%	9.38%	6.00%	3.30%	4.01%
Latent CC	72.40%	23.20%	42.24%	40.80%	10.40%	18.50%

Table B.31. Accuracy of RH Meter ±2.5%
Heat Pump: Make Trane, # of Points 36

	ENT-/LVG-			ENT+/LVG-		
	Max.	Min.	RMS	Max.	Min.	RMS
Total CC	5.40%	4.00%	4.61%	15.10%	9.20%	12.09%
Latent CC	37.00%	12.80%	20.61%	103.00%	29.10%	55.17%
	ENT-/LVG+			ENT+/LVG+		
	Max.	Min.	RMS	Max.	Min.	RMS
Total CC	13.20%	8.60%	11.31%	8.00%	4.30%	5.45%
Latent CC	85.90%	27.40%	50.73%	54.70%	14.50%	25.26%

B.2.5. Error Analysis of Dew Point Sensor

If the dew point sensor is used to measure the humidity of the air instead of the relative humidity sensor, the first step is to calculated the ideal value of the dew point of the inlet air:

Given: Dry Bulb Temperature t_{db}, Wet Bulb Temperature t_{wb}.

Find: Dew Point temperature t_d.

Equations used in sequence:

$$\alpha = AT_{db}^2 + BT_{db} + C + DT_{db}^{-1},\ T \text{ in K} \tag{B.22}$$

$$P_{ws} = 1000e^{\alpha},\ P_{ws} \text{ in Pa} \tag{B.23}$$

$$W_s^* = 0.62198\frac{P_{ws}(t_{wb})}{P - P_{ws}(t_{wb})} \tag{B.24}$$

$$W = \frac{(2501 - 2.381t_{wb})W_s^* - C_{pa}(t_{db} - t_{wb})}{2501 + 1.805t_{db} - 4.186t_{wb}} \tag{B.25}$$

$$P_w = \frac{PW}{W + 0.62918} \tag{B.26}$$

$$\beta = \ln(P_w) \tag{B.27}$$

$$T_d = E\beta^4 + F\beta^3 + G\beta^2 + H\beta + K \tag{B.28}$$

where α = natural log of saturation vapor pressure over pure water

T_{db} = absolute dry bulb temperature, °K

P_{ws} = pressure of saturated pure water, kPa

W_s^* = humidity ratio of moist air at saturation at thermodynamic wet bulb temperature, kg/kg dry air or lbm/lbm dry air

t_{wb} = wet bulb temperature, °C or °F

W = humidity ratio of moist air, mass of water per unit mass of dry air, kg/kg dry air or lbm/lbm dry air

C_{pa} = air specific heat, kJ/kg-°C or Btu/lbm-°F

t_{db} = dry bulb temperature, °C or °F

P_w = water vapor partial pressure, kPa or psia

P = total pressure of moist air, kPa or psia

β = natural log of saturation vapor pressure over pure water

T_d = absolute dew point temperature, °K

The second step is to calculate the inlet air enthalpy from the given dry bulb and wet bulb temperatures in the manufacturers' catalog data, which is same as the step for relative humidity sensor.

The enthalpy calculated is based on the ideal dry bulb and wet bulb temperatures in the catalog data that is corresponding to the best measurement of humidity ratio of the inlet air. However, since the inevitable error occurs for the dew point measured, there could be a deviation for the enthalpy calculated based on the measured dew point from the ideal value. The greatest deviation happens when the error of dew point is the worst. The step for the calculation of enthalpy when the dry bulb temperature and dew point are given is as follows:

Given: Dry Bulb Temperature $t_{db,}$ Dew Point temperature $t_{d.}$

Find: Enthalpy h.

Equations used in sequence:

$$\alpha = AT_d^2 + BT_d + C + DT_d^{-1},\ T \text{ in K} \tag{B.29}$$

$$P_w = 1000e^{\alpha},\ P_w \text{ in Pa} \tag{B.30}$$

$$W = 0.62198\frac{P_w}{P - P_w} \tag{B.31}$$

$$h = C_{pa} \times t_{db} + W\left(2501 + 1.805t_{db}\right) \tag{B.32}$$

where α = natural log of saturation vapor pressure over pure water

T_d = absolute dew point temperature, °K

P_w = water vapor partial pressure, kPa or psia

P = total pressure of moist air, kPa or psia

W = humidity ratio of moist air, mass of water per unit mass of dry air,

kg/kg dry air or lbm/lbm dry air

C_{pa} = air specific heat, kJ/kg-°C or Btu/lbm-°F

t_{db} = dry bulb temperature, °C or °F

h = enthalpy of moist air, kJ/kg dry air or Btu/lbm dry air

Table B.32 presents the enthalpy calculated using the heat pump manufacturer's specification sheet. In the same table, the enthalpy calculated based on the worst probable error of relative humidity measured is shown.

Table B.32. Dew Point Error Analysis for Entering States(FHP)

Entering DB temp		Entering WB temp		Dewpoint		H		Td+0.56	Td+1	H		Td-0.56	Td-1	H	
(F)	(C)	(F)	(C)	(C)	(F)	(KJ/KG)	(Btu/Hr)	(C)	(F)	(KJ/KG)	(Btu/Hr)	(C)	(F)	(KJ/KG)	(Btu/Hr)
75	23.889	61	16.111	11.117	52.011	44.95	19.33	11.677	53.011	45.751	19.67	10.557	51.011	44.173	18.99
80	26.667	61	16.111	8.915	48.047	44.87	19.29	9.475	49.047	45.575	19.60	8.355	47.047	44.191	19.00
85	29.444	61	16.111	6.382	43.488	44.80	19.26	6.942	44.488	45.398	19.52	5.822	42.488	44.212	19.01
75	23.889	64	17.778	14.358	57.845	49.99	21.49	14.918	58.845	50.961	21.91	13.798	56.845	49.046	21.09
80	26.667	64	17.778	12.555	54.600	49.90	21.46	13.115	55.600	50.778	21.83	11.995	53.600	49.055	21.09
85	29.444	64	17.778	10.544	50.980	49.82	21.42	11.104	51.980	50.596	21.75	9.984	49.980	49.065	21.10
75	23.889	61	16.111	11.117	52.011	44.95	19.33	11.677	53.011	45.751	19.67	10.557	51.011	44.173	18.99
80	26.667	61	16.111	8.915	48.047	44.87	19.29	9.475	49.047	45.575	19.60	8.355	47.047	44.191	19.00
85	29.444	61	16.111	6.382	43.488	44.80	19.26	6.942	44.488	45.398	19.52	5.822	42.488	44.212	19.01
75	23.889	64	17.778	14.358	57.845	49.99	21.49	14.918	58.845	50.961	21.91	13.798	56.845	49.046	21.09
80	26.667	64	17.778	12.555	54.600	49.90	21.46	13.115	55.600	50.778	21.83	11.995	53.600	49.055	21.09
85	29.444	64	17.778	10.544	50.980	49.82	21.42	11.104	51.980	50.596	21.75	9.984	49.980	49.065	21.10
85	29.444	67	19.444	14.074	57.333	55.19	23.73	14.634	58.333	56.150	24.14	13.514	56.333	54.260	23.33
85	29.444	61	16.111	6.382	43.488	44.80	19.26	6.942	44.488	45.398	19.52	5.822	42.488	44.212	19.01
80	26.667	61	16.111	8.915	48.047	44.87	19.29	9.475	49.047	45.575	19.60	8.355	47.047	44.191	19.00
85	29.444	64	17.778	10.544	50.980	49.82	21.42	11.104	51.980	50.596	21.75	9.984	49.980	49.065	21.10
85	29.444	67	19.444	14.074	57.333	55.19	23.73	14.634	58.333	56.150	24.14	13.514	56.333	54.260	23.33
85	29.444	70	21.111	17.184	62.932	60.95	26.20	17.744	63.932	62.099	26.70	16.624	61.932	59.832	25.72
85	29.444	61	16.111	6.382	43.488	44.80	19.26	6.942	44.488	45.398	19.52	5.822	42.488	44.212	19.01
75	23.889	61	16.111	11.117	52.011	44.95	19.33	11.677	53.011	45.751	19.67	10.557	51.011	44.173	18.99
80	26.667	61	16.111	8.915	48.047	44.87	19.29	9.475	49.047	45.575	19.60	8.355	47.047	44.191	19.00
85	29.444	64	17.778	10.544	50.980	49.82	21.42	11.104	51.980	50.596	21.75	9.984	49.980	49.065	21.10
80	26.667	64	17.778	12.555	54.600	49.90	21.46	13.115	55.600	50.778	21.83	11.995	53.600	49.055	21.09
85	29.444	67	19.444	14.074	57.333	55.19	23.73	14.634	58.333	56.150	24.14	13.514	56.333	54.260	23.33
85	29.444	70	21.111	17.184	62.932	60.95	26.20	17.744	63.932	62.099	26.70	16.624	61.932	59.832	25.72

85	29.444	61	16.111	6.382	43.488	44.80	19.26	6.942	44.488	45.398	19.52	5.822	42.488	44.173	18.99
75	23.889	61	16.111	11.117	52.011	44.95	19.33	11.677	53.011	45.751	19.67	10.557	51.011	44.191	19.00
80	26.667	61	16.111	8.915	48.047	44.87	19.29	9.475	49.047	45.575	19.60	8.355	47.047	49.065	21.10
85	29.444	64	17.778	10.544	50.980	49.82	21.42	11.104	51.980	50.596	21.75	9.984	49.980	49.046	21.09
80	26.667	64	17.778	12.555	54.600	49.90	21.46	13.115	55.600	50.778	21.83	11.995	53.600	54.260	23.33
85	29.444	67	19.444	14.074	57.333	55.19	23.73	14.634	58.333	56.150	24.14	13.514	56.333	54.261	23.33
85	29.444	70	21.111	17.184	62.932	60.95	26.20	17.744	63.932	62.099	26.70	16.624	61.932	59.853	25.73

The total and sensible cooling capacities are listed in the specification sheet. Together with the enthalpy and dry bulb temperature of inlet air have been discussed previously, the leaving air enthalpy and dry bulb temperature can be calculated. When the enthalpy and dry bulb temperature are obtained, the dew point temperature of the moist air is calculated as follows:

Given: Dry Bulb Temperature t_{db}, Enthalpy h.

Find: Dew Point temperature t_d.

Equations used in sequence:

$$\alpha = AT_{db}^2 + BT_{db} + C + DT_{db}^{-1},\ T \text{ in K} \tag{B.33}$$

$$P_{ws} = 1000e^{\alpha},\ P_{ws} \text{ in Pa} \tag{B.34}$$

$$W = \frac{h - C_{pa} \cdot t_{db}}{2501 + 1.805 t_{db}} \tag{B.35}$$

$$P_w = \frac{PW}{W + 0.62918} \tag{B.36}$$

$$\beta = \ln(P_w) \tag{B.37}$$

$$T_d = E\beta^4 + F\beta^3 + G\beta^2 + H\beta + K \tag{B.38}$$

where α = natural log of saturation vapor pressure over pure water

T_{db} = absolute dry bulb temperature, °K

P_{ws} = pressure of saturated pure water, kPa

P_w = water vapor partial pressure, kPa or psia

P = total pressure of moist air, kPa or psia

W = humidity ratio of moist air, mass of water per unit mass of dry air, kg/kg dry air or lbm/lbm dry air

β = natural log of saturation vapor pressure over pure water

T_d = absolute dew point temperature, °K

Analogously, the dew point temperature calculated is the best measurement we expect from the sensor. However, the actual measurement will not so ideal as we have mentioned before, the accuracy of the sensor will lead to the error of the measured value up to around 1 °F (0.56 °C) according to the manufacturers' publication. Table B.33 presents the dew point calculated and the worst measurements probable for those operating points using the heat pump manufacturer's specification sheet.

Table B.33. Dew Point Error Analysis for Leaving States (FHP)

LVG DB		H		Dewpoint		Td+0.56	Td+1	H		Td-0.56	Td-1	H	
(C)	(F)	(KJ/KG)	(Btu/Hr)	(C)	(F)	(C)	(F)	(KJ/KG)	(Btu/Hr)	(C)	(F)	(KJ/KG)	(Btu/Hr)
10.881	51.585	27.770	11.940	8.045	46.481	8.605	47.481	28.429	12.223	7.485	45.481	27.132	11.666
11.060	51.909	27.693	11.906	7.820	46.076	8.380	47.076	28.344	12.186	7.260	45.076	27.064	11.636
12.351	54.231	27.616	11.874	6.556	43.801	7.116	44.801	28.218	12.132	5.996	42.801	27.034	11.623
11.719	53.095	31.976	13.748	10.710	51.279	11.270	52.279	32.752	14.082	10.150	50.279	31.225	13.425
11.218	52.192	31.891	13.712	11.020	51.836	11.580	52.836	32.682	14.052	10.460	50.836	31.127	13.383
12.310	54.159	31.806	13.675	10.134	50.241	10.694	51.241	32.556	13.998	9.574	49.241	31.081	13.363
11.511	52.719	28.601	12.297	8.208	46.775	8.768	47.775	29.267	12.583	7.648	45.775	27.956	12.020
11.816	53.269	28.524	12.264	7.874	46.174	8.434	47.174	29.177	12.545	7.314	45.174	27.892	11.992

13.178	55.721	28.448	12.231	6.548	43.787	7.108	44.787	29.050	12.490	5.988	42.787	27.866	11.981
12.308	54.155	32.849	14.123	10.909	51.636	11.469	52.636	33.635	14.461	10.349	50.636	32.089	13.797
11.966	53.538	32.763	14.087	11.098	51.977	11.658	52.977	33.557	14.428	10.538	50.977	31.994	13.756
13.140	55.652	32.678	14.050	10.154	50.277	10.714	51.277	33.430	14.373	9.594	49.277	31.952	13.738
13.373	56.071	37.243	16.013	13.147	55.665	13.707	56.665	38.142	16.399	12.587	54.665	36.373	15.639
17.715	63.887	29.305	12.600	2.549	36.588	3.109	37.588	29.775	12.802	1.989	35.588	28.851	12.405
11.253	52.256	29.381	12.633	9.076	48.337	9.636	49.337	30.084	12.935	8.516	47.337	28.702	12.340
18.471	65.248	33.576	14.436	6.312	43.362	6.872	44.362	34.172	14.692	5.752	42.362	33.000	14.189
19.343	66.817	38.184	16.417	9.527	49.149	10.087	50.149	38.910	16.729	8.967	48.149	37.481	16.115
21.022	69.840	43.166	18.559	11.909	53.437	12.469	54.437	44.005	18.920	11.349	52.437	42.353	18.210
18.971	66.148	30.964	13.313	3.011	37.419	3.571	38.419	31.449	13.521	2.451	36.419	30.497	13.112
11.323	52.382	31.117	13.379	10.373	50.671	10.933	51.671	31.878	13.706	9.813	49.671	30.382	13.063
12.904	55.227	31.040	13.346	9.059	48.305	9.619	49.305	31.743	13.648	8.499	47.305	30.361	13.054
19.646	67.363	35.316	15.184	6.826	44.287	7.386	45.287	35.932	15.449	6.266	43.287	34.721	14.928
12.872	55.169	35.401	15.221	12.283	54.109	12.843	55.109	36.255	15.588	11.723	53.109	34.576	14.866
20.425	68.765	40.005	17.200	10.081	50.146	10.641	51.146	40.756	17.523	9.521	49.146	39.278	16.887
21.925	71.465	45.070	19.378	12.562	54.612	13.122	55.612	45.943	19.753	12.002	53.612	44.225	19.015
19.956	67.921	32.265	13.872	3.363	38.053	3.923	39.053	32.761	14.086	2.803	37.053	31.787	13.667
12.506	54.510	32.418	13.938	10.444	50.799	11.004	51.799	33.182	14.267	9.884	49.799	31.679	13.620
14.198	57.557	32.341	13.905	9.045	48.282	9.605	49.282	33.043	14.207	8.485	47.282	31.661	13.613
20.568	69.023	36.680	15.771	7.216	44.989	7.776	45.989	37.311	16.042	6.656	43.989	36.070	15.508
14.169	57.505	36.766	15.807	12.310	54.158	12.870	55.158	37.622	16.176	11.750	53.158	35.939	15.452
21.273	70.292	41.434	17.814	10.504	50.907	11.064	51.907	42.206	18.147	9.944	49.907	40.688	17.494
22.632	72.737	46.564	20.020	13.058	55.504	13.618	56.504	47.465	20.408	12.498	54.504	45.694	19.646

Due to the inevitable error for the dew point measured, there could be a deviation for the enthalpy calculated based on the measured dew point from the ideal value. The greatest deviation happens when the error of dew point is the worst. The step for the calculation of enthalpy when the dry bulb temperature and dew point is given is same as it is discussed previously.

Obviously, the total cooling capacity is the difference between the enthalpies of the inlet and outlet air. If we subtract the sensible cooling from the total cooling, the remainder is latent cooling capacity. When derived total and latent cooling capacities are obtained, they may be compared with the catalog data. The deviation of the derived

capacity from the catalog capacity that supposed to be the ideal value is presented in Table B.34.

Table B.34. Accuracy of Dew Point Transmitter ±1 °F (±0.56 °C) Heat Pump: Make FHP, # of Points 75

	ENT-/LVG-			ENT+/LVG-		
	Max.	Min.	RMS	Max.	Min.	RMS
Total CC	1.7%	0.004%	0.876%	14.1%	6.818%	9.503%
Latent CC	4.8%	1.66%	3.072%	266.7%	21.1%	85.5%
	ENT-/LVG+			ENT+/LVG+		
	Max.	Min.	RMS	Max.	Min.	RMS
Total CC	13.9%	6.798%	9.483%	1.8%	0%	0.896%
Latent CC	93.7%	21%	35.4%	3.59%	3.34%	3.12%

B.3. Watt Transducer

The watt transducer measures the amount of power transfer to the heat pump including the compressor and blower. The watt transducer is calibrated by the manufacturer and has a seal of warranty on the casing ensuring calibration. The watt transducer has a sensing range of 0-20 kW and provides an analog output proportional to time-averaged instantaneous power with an accuracy of ±1.0% of reading (Austin 1998). The output signal is calibrated to 1 mA=1kW. The signal is sent to the Fluke Data Logger and then a personal computer. The total power input to the heat pump is saved in the computer and can be displayed as a real time plot in an MS Excel format.

VITA 2

Hui Jin

Candidate for the Degree of

Doctor of Philosophy

Thesis: PARAMETER ESTIMATION BASED MODELS OF WATER SOURCE HEAT PUMPS

Major Field: Mechanical Engineering

Biographical:

Education: Received Bachelor of Science and Master of Science degrees in Mechanical Engineering at Shanghai Jiaotong University, Shanghai, China, in July 1992 and February 1995, respectively. Completed the requirements for Doctor of Philosophy with a major in Mechanical Engineering from Oklahoma State University, Stillwater, Oklahoma, December 2002.

Experience: Employed as Research Assistant at the School of Mechanical & Aerospace Engineering, Oklahoma State University, Stillwater, Oklahoma from January 1999 to present; Design Engineer at Carrier Corporation, Shanghai, China from April 1995 to April 1998.

Professional Memberships: American Society of Heating, Refrigerating and Air-Conditioning Engineers (ASHRAE), International Building Performance Simulation Association (IBPSA).